POLITECNICO
MILANO 1863

School of Industrial and Information Engineering

M.Sc. in Energy Engineering for Renewables and Environmental Sustainability

Electric Vehicle Charge Scheduling for Residential Neighbourhoods and Commercial Buildings

Supervisor: Prof. Ola Jabali

Co-Supervisor: Prof. Jorge Mendoza Gimenez (HEC Montréal)

Thesis by:

Ibrahim El Khoudari

Academic Year: 2020-2021

Acknowledgments

First and foremost, I would like to express my profound gratefulness to my thesis supervisor, ***Prof. Ola Jabali****, for her continuous support and constructive feedback throughout the research period. Starting from her coursework, her technical and analytical advice and her proper guidance were significant to get this research accomplished.*

I feel special being an Energy Engineering student at ***Politecnico di Milano*** *one of the leading institutions worldwide, which highly contributed to fulfilling my technical knowledge and graduate experience. I want to thank all my colleagues for being a source of inspiration and motivation.*

Finally, I would like to dedicate my success to my beloved family and friends for their enormous and endless support, especially my parents, and without them moving forward would have been impossible.

Table of Contents

Acknowledgments i
Table of Contents ii
List of Figures v
List of Tables xii
Abstract xiv
Sommario xv
Extended Abstract xvi
1 INTRODUCTION 1
1.1 CHALLENGES AND OPPORTUNITIES 3
1.2 SMART CHARGING POTENTIAL 4
1.3 THESIS OUTLINE 5
2 STATE OF THE ART 7
2.1 ELECTRIC VEHICLE DEPLOYMENT: TRENDS, OPPORTUNITIES, AND BARRIERS 7
2.2 ELECTRIC VEHICLE TECHNOLOGIES 11
2.2.1 Battery Electric Vehicle (BEV): 11
2.2.2 Hybrid Electric Vehicle (HEV): 13
2.2.3 Plug-In Hybrid Electric Vehicle (PHEV): 13
2.2.4 Fuel Cell Electric Vehicle (FCEV): 14
2.3 BATTERY ELECTRIC VEHICLE COMPONENTS 15
2.3.1 Batteries 15
2.3.2 Battery Management System 17
2.3.3 Electric Motors 18
2.3.4 Power Electronics Unit 18
2.4 CHARGING INFRASTRUCTURE 19
2.4.1 Available Charging Systems 20
2.4.1.1 Battery Swapping 20
2.4.1.2 Inductive charging 21
2.4.1.3 Conductive charging 21

2.4.2 Charging Power Levels 23
2.4.3 Charging Clusters 23
2.5 SMART CHARGING 25
2.5.1 Smart Charging Strategies 25
2.5.1.1 Time-of-use- pricing without automated control: 25
2.5.1.2 Dynamic pricing with automated control: 25
2.5.1.3 Basic controlled (on/off): 25
2.5.1.4 Unidirectional controlled charging (V1G): 26
2.5.1.5 Bidirectional controlled charging (V2G, V2H, V2B): 26
2.5.2 Smart Charging Related Works 28
3 BATTERY CHARGING PROCESS 31
3.1 CONSTANT CURRENT-CONSTANT VOLTAGE CHARGING SCHEME 31
3.2 CHARGIN LOSSES 34
3.3 CONSTANT CURRENT-CONSTANT VOLTAGE CHARGING PROCESS SIMULATION 37
3.3.1 Charging Simulation for a Lithium-Ion Battery Cell used in Commercial Electric Vehicles. 37
3.3.2 Charging Simulation for a Lithium-Ion Battery Cell Used in Passenger Electric Vehicles ... 40
3.4 VARIABLE-CURRENT CHARGING SCHEMES 43
4 THE COMMERCIAL AND INDUSTRIAL PROBLEM MODEL 46
4.1 COMMERCIAL AND INDUSTRIAL PROBLEM DESCRIPTION 47
4.2 MATHEMATICAL FORMULATION OF THE COMMERCIAL PROBLEM 50
4.3 SIMPLE EXAMPLE WITH MULTIPLE OPTIMAL SOLUTIONS 56
5 THE RESIDENTIAL NEIGHBOURHOOD PROBLEM MODEL 62
5.1 RESIDENTIAL NEIGHBOURHOOD PROBLEM DESCRIPTION 65
5.2 PEAK SHAVING MODEL FORMULATION 66
5.3 CHARGING COST REDUCTION MODEL FORMULATION 71
5.4 SIMPLE EXAMPLE OF SEVERAL OPTIMAL SOLUTIONS 78
6 RESULTS, DISCUSSIONS, AND MANAGERIAL INSIGHTS 87
6.1 RESULTS OF THE COMMERCIAL AND INDUSTRIAL PROBLEM 88
6.1.1 Base Case Scenario Description 89
6.1.2 Base Case Results 90
6.1.3 Multi-Criteria Analysis for The Commercial Charging Problem 92
6.1.4 Impacts of the Clustered Charging Technology 96

6.1.5 Effects of the FRD Charges 100
6.1.6 Impact of Grid's Power Limit 104
6.1.7 Effects of Charging Interruptions 106
6.2 RESULTS OF THE RESIDENTIAL NEIGHBOURHOOD PROBLEM 109
6.2.1 Base Case Scenario Description 112
6.2.2 Base Case Results 112
6.2.3 Effects of Smart Pricing Strategies 116
6.2.4 Impacts of Charging Interruptions 118
6.2.5 Effects of the Grid Power Restrictions 121
6.2.6 Impacts of EV Penetration Level 124
6.2.7 Significance of The Peak Shaving Model 128
7 CONCLUSIONS 132
8 BIBLIOGRAPHY 135

List of Figures

Figure 1: Transport sector CO2 emissions by mode in the Sustainable Development Scenario, 2000-2030. 1

Figure 2: Electric car deployment in selected countries, 2013-2018 2

Figure 3: Global electric car sales and market share, 2013-18 8

Figure 4: Barriers to BEV adoption. 9

Figure 5: A shortlist of the impacts of EVs on the power grid, environment, and economy. 10

Figure 6: A McKinsey analysis of Lithium-ion battery cost evolution, assuming learning effects and technology breakthrough 11

Figure 7: Different powertrain technologies in detail. 12

Figure 8: BEV configuration. The battery's DC-AC power conversion to power the motor. 12

Figure 9: Principle of ICE series hybrid vehicles. 13

Figure 10: FCEV configuration. Oxygen from air and hydrogen from the cylinders react in fuel cells to produce electricity that runs the motor. Only water is produced as a by-product which is released into the environment. 14

Figure 11: Electrification evolution. 14

Figure 12: EV block diagram. 15

Figure 13: The schematic diagram of the manufacturing process of battery packs for EVs. 17

Figure 14: Example of unbalanced cells. 18

Figure 15: EV power flow block diagram. 19

Figure 16: Basic components of a battery charger. 19

Figure 17: Electric powertrains: Charging infrastructure archetypes. 20

Figure 18: Inductive charging. 21

Figure 19: EVSE arrangement for onboard AC slow charging. 21

Figure 20: EVSE arrangement for off-board DC Fast Charger(DCFC). 22

Figure 21: Off-board and on-board chargers for an electrical vehicle (EV). 22

Figure 22: CSO-controlled power management. 24

Figure 23: EV charging and PV integration in a house using a V2H smart charging scheme. 26

Figure 24: Advanced forms of smart charging. 27

Figure 25: Constant Current-Constant Voltage charging scheme. 31

Figure 26: CC-CV charging scheme. The horizontal axis shows the time; the vertical axis is not in scale to simultaneously illustrate the behavior of current, voltage, and state of charge. The CC phase (t < ts) is obtained explicitly from Eq. (2). The CV phase (t > ts) is obtained as a numerical solution of the differential Eqs. (4)-(6). 33

Figure 27: System components overview with the electric measurement system. 35

Figure 28: A comparison of the discretized CC-CV process of a 3.6V-38Ah lithium-Ion battery cell with different current values in the CC phase: (a) A single-phase EVSE of 7.36 kW power capacity (b) A three-phase EVSE of 11 kW power capacity 38

Figure 29: The CC-CV charging scheme approximation for a 3.6V-38Ah Lithium-Ion battery cell by a linear piecewise: (a) Using a 7.36 kW single-phase EVSE, (b) Using an 11 kW three-phase EVSE 39

Figure 30: The discretized CC-CV process of different Lithium-Ion battery cells using the same power supply of a 7.36 kW capacity. (a) 3.6V-34Ah Lithium-Ion battery cell of a Nissan leaf EV (Nissan, 2017), (b) 3.6V-40Ah Lithium-Ion battery cell of a BMW i3 EV (BMW, 2018), and (c) 3.6V-36Ah Lithium-Ion battery cell of a Toyota RAV4 EV (Toyota, 2013). 41

Figure 31: The approximated linear piecewise of the discretized CC-CV process for different Lithium-Ion battery cells using the same power supply of a 7.36 (kW) capacity. (a) 3.6V-34Ah battery cell of a Nissan leaf EV (Nissan, 2017), (b) 3.6V-40Ah battery cell of a BMW i3 EV (BMW, 2018), and (c) 3.6V-36Ah battery cell of a Toyota RAV4 EV (Toyota, 2013). 42

Figure 32: Summary of various charging methods.....44

Figure 33: A Simplified scheme of a smart charging system's clustered infrastructure in the depot 49

Figure 34: The SoC evolution with time during the charging process of EVs "1", "2" and "3" using: (a) 3 single-socket chargers each having a 7.36 kW power capacity, (b) a double-socket charger and a single-socket charger both having a 7.36 kW power capacity, (c) a triple-socket charger of 11 kW power capacity. 57

Figure 35: The power consumption profile of the building when using three different charging infrastructure cases and the electricity prices variation with time. 60

Figure 36: The building's electricity bill as a result of three different charging infrastructure scenarios. 61

Figure 37: rolec-wallpod-EV-homesmart (Driving Electric, n.d.). 63

Figure 38: Charging station equipment and activities (Mal et al., 2013). 63

Figure 39: (a) Charge status screen. (b) Charge profile screen (Mal et al., 2013). 64

Figure 40: A comparison of the electricity bills of all the houses obtained in the PSM and the CCRM. 83

Figure 41: The power retrieved by all the houses in the neighbourhood: (a) optimal solution of the PSM, (b) optimal solution of the CCRM with % slack distribution algorithm, (c) optimal solution of the CCRM with even slack distribution algorithm. 84

Figure 42: The charging schedule of all the EVs in the neighbourhood: (a) optimal solution of the PSM, (b) optimal solution of the CCRM with % slack distribution algorithm, (c) optimal solution of the CCRM with even slack distribution algorithm. 85

Figure 43: The total electricity bill and the peak power demand for all the charging behaviours of the commercial base case. 91

Figure 44: The FRD charges and energy cost contributions in the total electricity bill of the building for all the instances. 92

Figure 45: Peak power demand variation based on the different charging clusters used for all charging behaviors. 97

Figure 46: The total electricity bill of the building for all the instances using different charging technologies. 98

Figure 47: The percentage contributions of the FRD fees and energy costs in the electricity bill of different test instances using multiple charging techniques. 99

Figure 48: A comparison between the peak power demand in the instances of high FRD charges and the ones with low FRD charges using different charging technology. 100

Figure 49: The total electricity bill of the building for different test instances using multiple charging technologies under the low and high FRD charges scenario. 103

Figure 50: The charging energy cost for different test instances using multiple charging technologies under the low and high FRD charges scenario. 104

Figure 51: The peak power demands of the building for different test instances after applying a grid's power limit. 105

Figure 52: A comparison of the building's total electricity bill in different test instances under the effects of the grid's power limit. 106

Figure 53: A comparison of the charging energy cost in different test instances under the effects of the grid's power limit. 106

Figure 54: A comparison of the peak power demand in different test instances using the multiple charging technologies: (a) refers to the scenario of $N = 1$, (b) refers to the scenario of $N = 0$. 107

Figure 55: A comparison of the building's total electricity bill in different test instances using multiple charging technologies under two scenarios: (a) One charging interruption, (b) zero charging interruptions. 108

Figure 56: Comparison between the run time of the optimization models using the “CCRM-E” and the “CCRM-%” approaches under both scenarios of the base case and Two-price. 116

Figure 57: Comparison between the percentages of houses in the neighbourhood with no changes, reduction, or increase in their energy bills under the base case and 2-prices scenarios. 117

Figure 58: Comparison between the average reduction rates and the reduction increase percentages of the houses with the maximum and minimum rates under both the base case and 2-prices scenarios. 117

Figure 59: The runtime analysis of the optimization models following the “CCRM-%” and the “CCRM-E” under different charging interruption scenarios compared to the base case. 118

Figure 60: The peak power demands obtained by the PSM for two different charging interruption scenarios and compared to the base case one. 119

Figure 61: The percentage distribution of the houses in the neighbourhood based on the reduction rate in their energy bills for different charging interruption scenarios compared to the base case. 120

Figure 62: The average, maximum, and minimum reduction rates and the maximum increase rate in electricity bills among all houses in the entire neighbourhood under the base case and two different charging interruption scenarios. 121

Figure 63: The runtime comparison of the optimization model following the “CCRM-%” and the “CCRM-E” between different scenarios of power grid restrictions compared to the base case in all test instances. 122

Figure 64: The peak power demands obtained by the PSM for two different scenarios of various power grid restrictions compared to the base case one. 122

Figure 65: The percentage distribution of all the houses in the neighbourhood in all test instances based on the reduction rate in their energy bills for different scenarios, each of a different power restriction value per house compared to the base case. 123

Figure 66: The average, maximum, and minimum reduction rates and the maximum increase rate in the electricity bills among all houses in the entire neighbourhood under the base case and three other scenarios, each of different power grid limit values. 124

Figure 67: Comparison of the PSM and the TSREV-CSP model's total runtime between different scenarios of EV penetration levels compared to the base case in all test instances. 125

Figure 68: Comparison between the peak power demand of the neighbourhood and the peak power demand of EV users only in the same neighbourhood obtained by the PSM for three scenarios of different EV sizes compared to the base case one. 126

Figure 69: The percentage distribution of all the houses in the neighbourhood in all test instances based on the reduction rate in their energy bills for different cases EV users' percentages compared to the base case. 127

Figure 70: The average, maximum, and minimum reduction rates and the maximum increase rate in the electricity bills among all houses in the entire neighbourhood under the base case and three other scenarios, each of a different percentage of EV users in the same neighbourhood. 127

Figure 71: Comparison of the overall runtime of the optimization models between the TSREV-CSP and the Cost model. 129

Figure 72: Comparison between the peak power demand obtained by the PSM and that obtained by the "Cost" model in the same neighbourhood under different scenarios. 130

Figure 73: The percentage distribution of all the houses in the neighbourhood in all test instances based on the reduction rate in their energy bills for different cases of the grid's power limit compared to the base case and using both models of the TSREV-CSP and "Cost". 131

Figure 74: The average reduction and the maximum increase rates in the electricity bills of all houses in the entire neighbourhood obtained from the optimization models of the “Cost” and TSREV-CSP under the base case and different scenarios each of various grid’s power limit values. 131

List of Tables

Table 1: “Norwegian EV policy time period of introduction.” 3

Table 2: “Explanations and sources of barriers.” 4

Table 3: Common battery types, their basic construction components, advantages, and disadvantages. 16

Table 4: Electrical ratings of different EVS charge methods in Europe. 23

Table 5: Annual relative peak power reduction under a different scenario. 28

Table 6: Charging losses of building components. 35

Table 7: Battery losses (%) as a function of the battery state-of-charge (SOC) and the AC values. 36

Table 8: PEU Charging Losses (%) as a function of the battery’s SOC and AC value. 36

Table 9: Causes, effects, and influences of Lithium-ion anode ageing. 43

Table 10: Summary of different batteries' responses to variable charging. 45

Table 11: Route parameters for the simple numerical example 56

Table 12: Design parameters associated with the breakpoints of the linear approximation of the charging process 56

Table 13: The power consumption for three optimal solutions of different cluster types 58

Table 14: The design specifications and route parameters for the simple numerical example 79

Table 15: The design parameters associated with the linear approximation breakpoints of the charging process of different vehicles' models 79

Table 16: Optimal solution of the PSM 80

Table 17: Optimal solution of the CCRM using the percentage weighted algorithm for calculating the complementary slack parameters. 81

Table 18: Optimal solution of the CCRM using the even distribution algorithm for estimating the complementary slackness parameters. 82

Table 19: The nine main instances of the commercial and industrial scenario. 88

Table 20: The results of all instances in the base case scenario. 90

Table 21: The solution time of all the tests of the commercial charging problem under the five main scenarios. 94

Table 22: The Optimality gap of all the tests of the commercial charging problem under the five main scenarios. 95

Table 23: The peak power demand in (kW) using different types of clusters. 96

Table 24: The cost analysis of the different charging technologies and their effect on the total energy cost and its contributions. 98

Table 25: The total electricity bill of the building, the percentage contribution of the FRD fees in the total cost, and the energy cost reduction rate for different test instances using multiple charging technologies under the low and high FRD charges scenario. 101

Table 26: The main instances of the residential neighbourhood problem. 110

Table 27: Technical specifications of different EVs of residential users. 111

Table 28: The parameters corresponding to the breakpoints that are approximated for the charging process of a Lithium-ion battery cell for each EV model. 111

Table 29: The results obtained for the base case scenario, including peak power demand of, run time, and final gap comparisons. 113

Table 30: Cost analysis and a comparison between the results of the CCRM's even and percentage approaches in the base scenario. 114

Abstract

The advent of electric vehicles (EVs) promises to be a game-changer for the world's shift to sustainability. EV deployment has been accelerating in the past decade due to many factors, and it is expected to increase in the future at an exponential pace. However, the higher the EV penetration level, the higher power demand is imposed on the power system, which increases the risk of frequency unbalance at the grid. Moreover, the main challenge ahead lies in improving the range and reducing the cost of the currently available technologies, especially the charging costs. This thesis aims to provide a sort of solution to minimize the impact of EV charging on the power grid by providing smart charging models and proposing new smart charging technologies for two scenarios of namely, a residential neighbourhood scenario and a commercial building scenario. We formulate a cost minimization model that minimizes the electricity bill of a commercial facility by optimizing the charging schedule of its EVs based on the variable electricity prices and using a proposed technology of three-phase charging clusters. In addition, we formulate another model for a residential neighbourhood of two optimization stages; The first is based on the peak shaving concept of reducing the impact of high power demand due to enormous EV penetration from an energy supplier standpoint. The second subsequent stage aims to reduce the houses' electricity bills obtained by the first stage in the entire neighbourhood. After performing extensive experiments of different scenarios for both models, we find that the commercial model proves the advantages of high power charging clusters having charging points up to 4 to replace the single-phase single-socket chargers. Similarly, the results of the residential scenario show the high feasibility level of the proposed model in reducing the peak power demand to its minimum values compared to using only cost minimization models. It also proves that the two-stage model can satisfy at least 90% of the houses in a particular neighbourhood with a cost reduction rate that could reach 20% in some cases.

Keywords: Electric Vehicles, Electric Freight Vehicles, Residential Neighbourhoods, Commercial and Industrial Facilities, Smart Charging, Smart Pricing, Charging Clusters, Cost Minimization, Peak Power Shaving, Load Shifting, Optimization, Mixed Integer Linear Programming.

Sommario

L'avvento dei veicoli elettrici (EV) promette di essere un game-changer per il passaggio del mondo alla sostenibilità. La diffusione dei veicoli elettrici è stata accelerata nell'ultimo decennio a causa di molti fattori e si prevede che aumenterà in futuro ad un ritmo esponenziale. Tuttavia, più alto è il livello di penetrazione dei veicoli elettrici, più alta è la domanda di energia che viene imposta al sistema elettrico, il che aumenta il rischio di squilibrio di frequenza nella rete. Inoltre, la sfida principale è quella di migliorare l'autonomia e ridurre il costo delle tecnologie attualmente disponibili, specialmente i costi di ricarica. Questa tesi mira a fornire una sorta di soluzione per ridurre l'impatto della ricarica dei veicoli elettrici sulla rete elettrica, fornendo modelli di ricarica intelligente e proponendo nuove tecnologie di ricarica intelligente per due scenari, ovvero uno scenario di quartiere residenziale e uno scenario di edificio commerciale. Formuliamo un modello di minimizzazione dei costi che minimizza la bolletta elettrica di una struttura commerciale ottimizzando il programma di ricarica dei suoi veicoli elettrici basato sui prezzi variabili dell'elettricità e utilizzando una tecnologia proposta di cluster di ricarica trifase. Inoltre, formuliamo un altro modello per un quartiere residenziale di due livelli di ottimizzazione dove il primo è basato sul concetto di peak shaving per ridurre l'impatto dell'alta domanda di energia dovuta all'enorme penetrazione dei veicoli elettrici dal punto di vista del fornitore di energia. Mentre la seconda fase successiva mira a ridurre le bollette elettriche delle case ottenute dalla prima fase in tutto il quartiere. Dopo aver eseguito ampi esperimenti di diversi scenari per entrambi i modelli, troviamo che il modello commerciale dimostra i vantaggi dei cluster di ricarica ad alta potenza con punti di ricarica fino a 4 per sostituire i caricabatterie monofase a presa singola. Allo stesso modo, i risultati dello scenario residenziale mostrano l'alto livello di fattibilità del modello proposto nel ridurre la domanda di potenza di picco ai suoi valori minimi rispetto all'utilizzo di soli modelli di minimizzazione dei costi. Si dimostra anche che il modello a due fasi può soddisfare almeno il 90% delle case in un certo quartiere con un tasso di riduzione dei costi che potrebbe raggiungere il 20% in alcuni casi.

Parole chiave: Veicoli elettrici, veicoli elettrici per il trasporto merci, quartieri residenziali, strutture commerciali e industriali, ricarica intelligente, tariffazione intelligente, cluster di ricarica, minimizzazione dei costi, riduzione dei picchi di potenza, spostamento del carico, ottimizzazione, programmazione lineare integrale mista.

Extended Abstract

Introduction

The advent of electric vehicles (EVs) including battery electric vehicles (BEVs) and plug-in hybrid electric vehicles (PHEVs) promises to be a game-changer for the world's shift to sustainability. Nowadays, transport electrification is considered one of the top technological alternatives to mitigate climate change as it contributes significantly to reducing GHG emissions, especially CO_2 emissions and energy dependence on petroleum fuel and other external energy supplies offering the potential to reduce the oil imports and many economic benefits.

The main challenge ahead lies in improving the range and reducing the cost of the currently available technologies, whether it is the price of buying the EV or the charging fees. The energy system is evolving due to a steady increase in electric vehicles on the demand side and local output (mostly from solar panels) on the supply side. Both technologies could bring the energy grid under strain at certain times of the day, especially that EVs require high power for an extended period while charging, even though there is enough capacity on the grid for most of the day.

EV smart charging techniques are highly efficient and promising ways to deal with the surplus production and represent a critical component of the friendly environment and cost-effective EV integration into the power grid. The central concept of smart charging is to shift the charging schedule of EVs towards the Off-peak periods of the day and when electricity cost is at its lowest values to eliminate the risk of a demand spike at the same time of satisfying the vehicle owner's need. Smart charging techniques are based on exchanging data of electricity prices and energy demand and generation levels at a given time between EVs and the smart grid to offer customers lower charging costs when charging their EV on low demand periods of the day.

The smart charging strategies in use could be classified into five main strategies that are as follows: Time-of-use-pricing without automated control, dynamic pricing with automated control, basic controlled (on/off), unidirectional controlled charging (V1G), and bidirectional controlled charging (V2G, V2H, V2B). Such technologies allow EVs to be charged during periods of the day with low energy costs and then supply their access energy to the house/building during periods of high energy prices, which helps in reducing the electricity bill.

We present in this research decentralized charging strategies that give individual EV users a level of decision making in which EV intelligent charging points often communicate a small amount of data with a centralized unit which then sends global coordination to all charging points. We propose two Mixed Integer Linear Programming (MILP) problems that refer to two different EV charge scheduling problems. The first problem is based on a commercial and industrial scenario (CIS) where we create a mathematical model to optimize the charging schedule of medium-duty electric trucks using a clustering technology for the charging infrastructure. This model aims to explore the potential of clustered charging techniques for charging commercial EVs overnight at a minimum cost considering the effects of grid restrictions and charging interruptions.

The second optimization model is a two-stage EV charging problem of a residential scenario. The primary stage seeks to reduce the EV integration impacts on the power grid in a residential neighborhood as the first from a DSO point of view by developing a peak shaving model (PSM). However, the second one aims to minimize the total electricity bill for each housing of EV users in the neighbourhood by creating a charging cost reduction model (CCRM) and analyze the effects of smart pricing, EV penetration levels, and different approaches for the two-stage interface of the optimization model.

Battery Charging Process

EVs are commonly charged under a constant current-constant voltage (CC-CV) approach to minimize the impact of overcharging degradation that can cause permanent damage to EV batteries. CC-CV charging scheme is the most prevalent method for charging Li-ion batteries that are typically used in modern EVs. CC-CV method is developed from combining the two basic charging schemes CC and CV charging methods to increase the charging efficiency and overcome their major downsides such as overcharging or undercharging, battery capacity losses for the CC charging scheme, slow charging, and overheat for the CV charging method. The battery charging behavior under the CC-CV method is illustrated in Fig. 1, consisting of two stages of different characteristics.

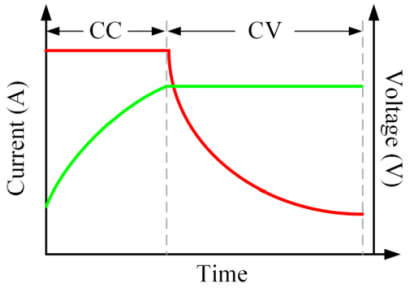

Fig. 1: Constant Current-Constant Voltage charging scheme.

We simulate the CC-CV charging process for four different Lithium-ion battery cells used in four different EV models of different design characteristics by referring to a simplified battery model. The battery charging simulations consider only the charging losses in the EV components as a function of the battery's SoC. The simulations were performed using a Microsoft Excel worksheet, whereas the results visualizations were done in python using the Matplotlib library. The charging simulations refer to the EV charging problem of both the commercial scenario using one type of medium-duty electric freight vehicle and the residential one using three different models of passenger EVs.

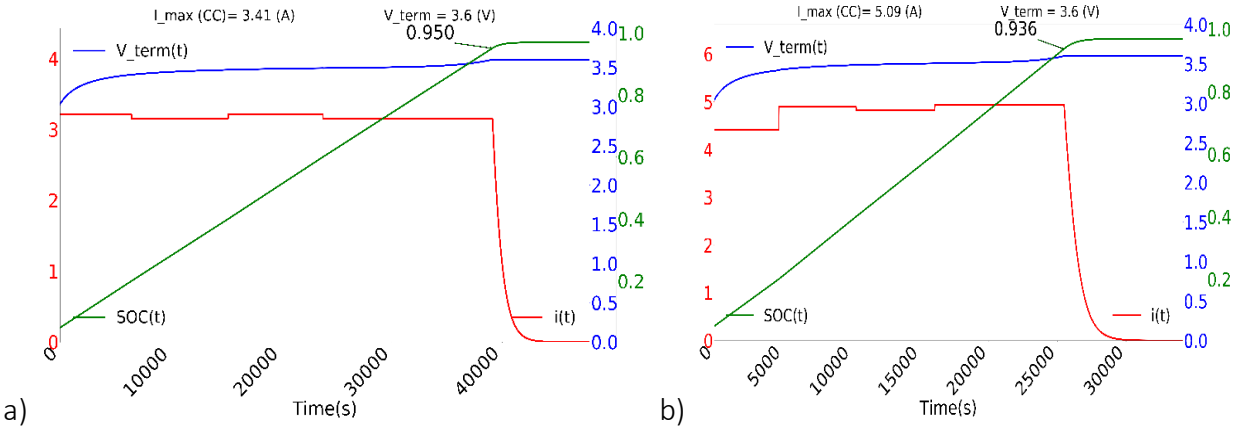

Fig. 2: A comparison of the discretized CC-CV process of a 3.6V-38Ah lithium-Ion battery cell with different current values in the CC phase: (a) A single-phase EVSE of 7.36 kW power capacity (b) A three-phase EVSE of 11 kW power capacity.

Fig. 2 illustrates a comparison of the charging simulation performed for a 3.6V-38Ah Lithium-Ion battery cell that corresponds to a medium-duty electric vehicle having a total energy capacity of 82.8 (kWh) using two I_{cc} values: (a) refers to a 3.4 (A) DC value equivalent to a 0.085C charge rate that corresponds to the single-phase 32 (A) AC power supply of 7.36 (kW) power capacity. (b) corresponds to the usage of a three-phase power supply having a phasor current of 16 (A) a total power capacity of 11 (kW), and it is able to deliver a maximum DC value of 5.09 (A) equivalent to a 0.1275C charge rate. **Fig. 3** illustrates the CC-CV charging process of the three batteries that correspond to three different EV models in discrete time formulation and accounting for the Power Electronics Unit (PEU) percentage losses defined by the parameter q.

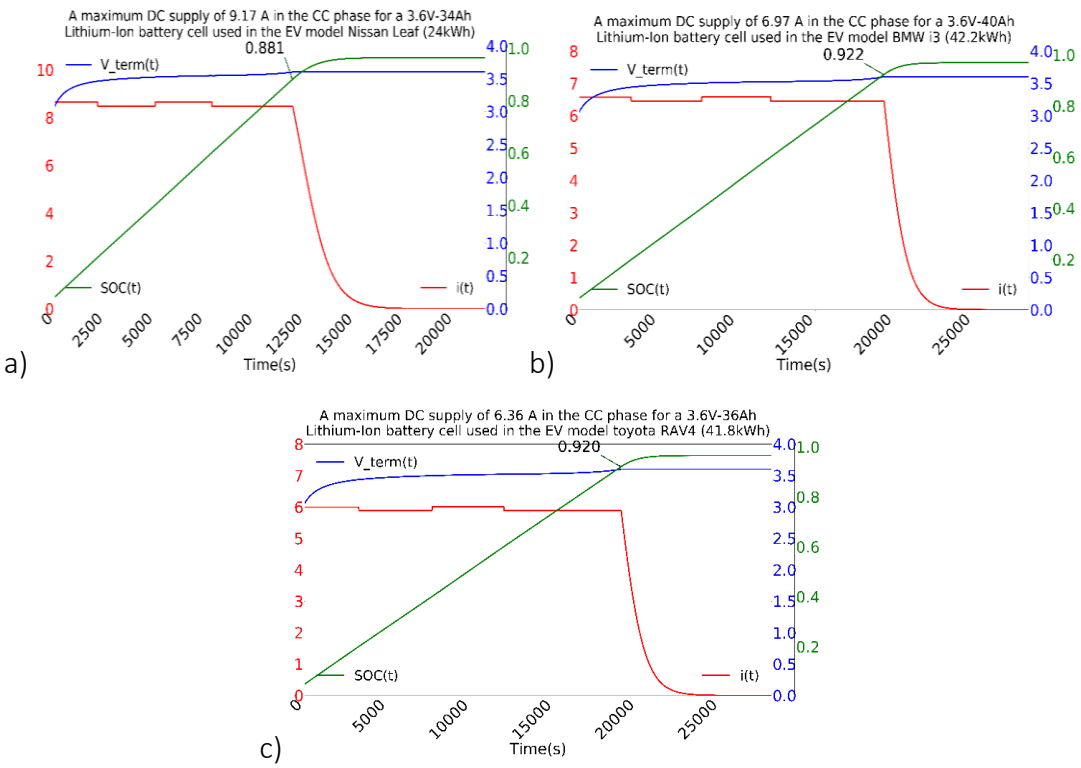

Fig. 3: The discretized CC-CV process of different Lithium-Ion battery cells using the same power supply of a 7.36 kW capacity. (a) 3.6V-34Ah Lithium-Ion battery cell of a Nissan leaf EV, (b) 3.6V-40Ah Lithium-Ion battery cell of a BMW i3 EV, and (c) 3.6V-36Ah Lithium-Ion battery cell of a Toyota RAV4 EV.

The Commercial and Industrial Problem Model

We minimize the total electricity bill of a goods distribution firm by optimizing the overnight charge scheduling of a fleet of electric freight vehicles charged using the conventional smart chargers and new proposed smart charging clusters. The model considers the electricity prices that vary during the day and other battery parameters of each vehicle like the remaining state of charge (SoC), the energy needed to perform tasks in the coming day, and the departure and arrival periods from and to the site for each vehicle. This model is defined over a planning interval of one day, assumed to be a working day. Our planning interval is discretized into a set $T = \{1, \dots, T_{max}\}$ of n_t consecutive periods, each having a duration Δt of 15 minutes (0.25 h) ($t \in T$). The set $V = \{1, \dots, m\}$ represents a fleet of m homogeneous EFVs assumed to be medium-duty electric trucks, each equipped with several lithium-ion battery cells combined to give the required total energy capacity.

The charging system's infrastructure in the depot consists of a set of C dedicated clusters of different power capacities. Each cluster $c \in C$ is a similar example of electric vehicle supply equipment (EVSE) of a specific charging power level and equipped with one or more sockets. One or more than one EV could be plugged simultaneously into the same cluster and share its maximum power such that if only one EV is plugged into the cluster, it benefits from the total power output of the cluster alone, which means a higher charging rate and shorter charging. If any other EV is plugged into the same cluster, then the power would be divided and shared between both EVs but not necessarily evenly distributed. We assume having three types of clusters classified as follows: Type one is a single-phase EVSE having an output voltage of 230 V and a 32 (A) maximum current supply that corresponds to a power capacity G_c (kW) of 7.36 (kW). Type two and three are three-phase EVSE with an output voltage of 400 V, and current capacities per phase of 16 (A) and 32 (A) that are equivalent to 11 (kW) and 22 (kW) power capacities respectively. Fig. 4 shows a simplified configuration of the smart charging system's clustered infrastructure in the depot where the bidirectional arrows represent the direction of data communication among the system's different levels. However, power flow is unidirectional from the grid as a top-level towards EVSEs as the bottom-level and is represented by the unidirectional red arrows.

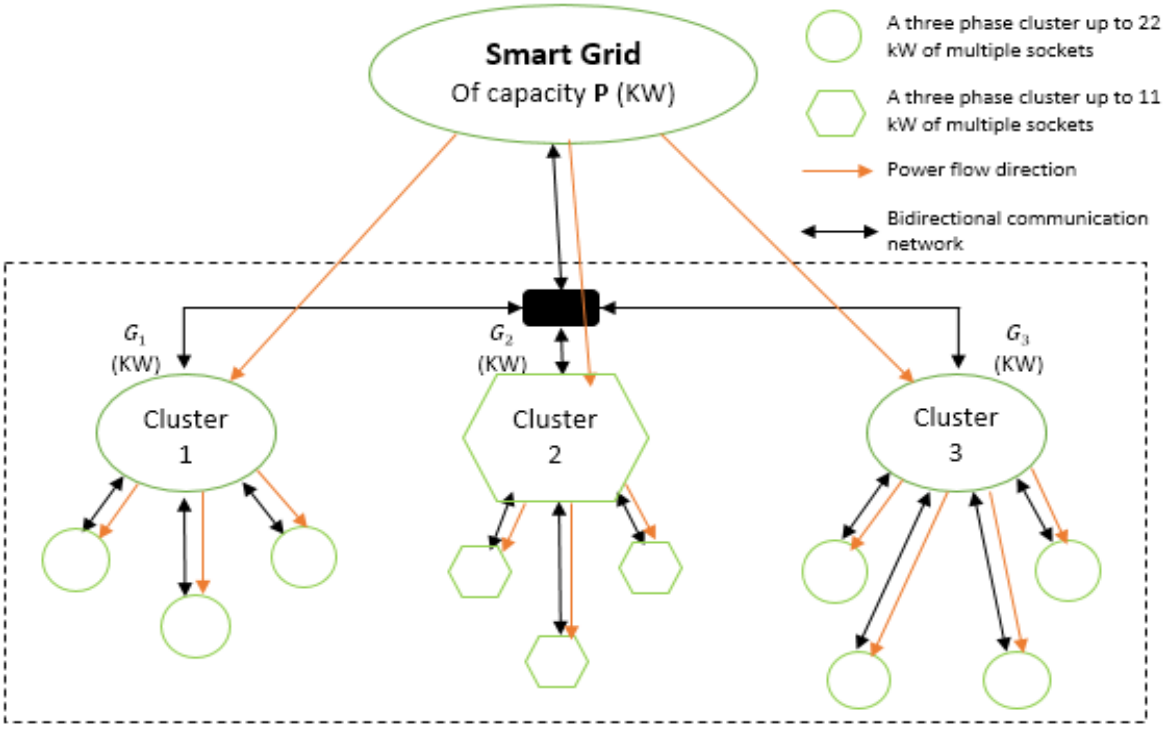

Fig. 4: A Simplified scheme of a smart charging system's clustered infrastructure in the depot

Mathematical Formulation

Six sets of decision variables are required for our formulation. Binary variables $u_{v,c}$ take a value of 1 if vehicle v is connected to cluster c, and take a value of 0 otherwise. Binary variables $z_{t,v}^{c,b}$ that take the value of 1 if EFV v is retrieving current from a charging socket in cluster *c* during period t before departure time from the site between breakpoints $SOC_{b-1,c}^{break}$ and $SOC_{b,c}^{break}$, and take a value of 0 otherwise. While binary variables $y_{t,v}$, take a value of 1 when the charging event of EFV v shifts from ON to OFF between periods $t-1$ and t and take a value of 0 otherwise.

Real and positive variables $i_{t,v,c}$ refer to the charging current applied to EFV v by cluster c during the entire period t. Real and positive variables $soc_{t,v}$ refer to the state of charge of EFV v at the beginning of time t. Finally, Real positive variable s indicates the maximum charging power retrieved from the grid during the planning interval used to determine the FRD charges. To sum up, our problem is presented in the following mathematical model and the mixed-integer linear programming formulation (MILP), respectively:

Sets:

- T: Set of time in the scheduling horizon $(T = \{1, \dots, T^{max}\})$
- V: Set of EFVs. $(v \in V)$
- C: Set of charging clusters. $(c \in C)$
- B_c: Set of breakpoints used in the piecewise linear approximation of the CC-CV charging process using cluster c. $(b \in B_c)$

Parameters:

- l_t: non-flexible consumption profile of the commercial site (non-EFV) at time t. (kW)
- p_t: Electricity price at time t. $(€/kWh)$
- Q: The charge capacity of the battery of the EFV (Ah).
- QE: The energy capacity of the battery of the EFV (kWh).
- L: The onboard power capacity of the EFV (kW).
- $U_{battery}$: The rated voltage of the battery of the vehicle (V).
- N: The maximum number of cuts allowed for the battery of EFV.
- a_v: The arrival time of EFV v to the depot.
- d_v: The departure time of EFV v from the depot.
- e_v: Energy needed for EFV v to travel the next day (KWh).
- SOC_v^{start}: The SoC associated with the first period of the time horizon for each EFV $v \in V$.

- P: The Grid power capacity that could be consumed by the site at any time (kW)
- F: FRD charge $(€/kW)$
- G_c: Maximum power could be withdrawn instantaneously from cluster c. (kW)
- h_c: The number of charging sockets in cluster c.
- $I_{c,b}^{max}$: The maximum current that could be retrieved in the piecewise linear approximation
- of the CC-CV charging process depending on the charging level of cluster c between
- the breakpoints b and $b-1$ for $b \in B_c$, b > 0. (A)
- $I_{c,b}^{min}$: The minimum current that should be retrieved in the piecewise linear approximation
- of the CC-CV charging process depending on the charging level of cluster c between
- the breakpoints b and $b-1$ for $b \in B_c$, b > 0. (A)
- $SOC_{c,b}^{break}$: The state of charge associated with breakpoints $b \in B_c$ in the piecewise linear
- approximation of the CC-CV charging function of cluster c.
- SOC^{max}: The maximum state of charge that any vehicle could reach while charging.
- SOC^{min}: The minimum state of charge that any vehicle could reach during the discharging
- Process.
- q: The average weighted power loss factor during charging.
- Δt: Timestep in (h).

Variables:

- $i_{t,v,c} \geq 0$: The current value is taken by EFV v at time t in cluster c. (A)
- $soc_{t,v} \geq 0$: The state of charge of EFV v at time t.
- $z_{t,v}^{c,b} \in \{0,1\}$: 1 if EFV v uses a cluster c at time t with a state of charge between
- $SOC_{c,b-1}^{break}$ and $SOC_{c,b}^{break}$.
- 0 otherwise.
- $y_{t,v} \in \{0,1\}$: 1 if EFV v stops charging at time period t.
- 0 otherwise
- $u_{v,c} \in \{0,1\}$: 1 if EFV v is plugged into cluster c.
- 0 otherwise
- $s \geq 0$: The maximum charging power withdrawn from the grid along the planned horizon.

Formulation:

$$\text{minimize} \qquad \sum_{t\in T} p_t \Delta t \left(l_t + \sum_{v\in V}\sum_{c\in C} \frac{i_{t,v,c}}{Q} QE \right) + F \cdot s \tag{1}$$

subject to:

$$l_t + \sum_{v\in V}\sum_{c\in C} \frac{i_{t,v,c}}{Q} QE \le s \qquad \forall t \in T \tag{2}$$

$$0 \le s \le P \tag{3}$$

$$\sum_{v\in V} \frac{i_{t,v,c}}{Q} QE \le G_c \qquad \forall\, t \in T, c \in C \tag{4}$$

$$\sum_{t=1}^{a_v-1}\sum_{v\in V}\sum_{c\in C}\sum_{b\in B_c\backslash\{0\}} z_{t,v}^{c,b} + \sum_{t=d_v}^{\boldsymbol{T^{max}}}\sum_{v\in V}\sum_{c\in c}\sum_{b\in B_c\backslash\{0\}} z_{t,v}^{c,b} = 0 \tag{5}$$

$$soc_{1,v} = SOC_v^{start} \qquad \forall v \in V \tag{6}$$

$$soc_{d_{v+1},v} = soc_{d_v,v} - \frac{e_v}{QE} \qquad \forall v \in V \tag{7}$$

$$soc_{d_v,v} = soc_{a_v,v} + \frac{e_v}{QE} \qquad \forall v \in V \tag{8}$$

$$\sum_{t\in T}\sum_{c\in C} \frac{i_{t,v,c}(1-q)\Delta t}{Q} + SOC_v^{start} - SOC^{min} = \frac{e_v}{QE} \qquad \forall v \in V \tag{9}$$

$$soc_{t,v} = soc_{t-1,v} + \sum_{c\in C} \frac{i_{t-1,v,c}(1-q)\Delta t}{Q} \qquad \forall t \in T\backslash\{1, d_v, d_v+1\}, v \in V \tag{10}$$

$$soc_{t+1,v} \le SOC_{c,b}^{break} + 1 - z_{t,v}^{c,b} \quad \forall t \in \{\boldsymbol{a_v}, \dots, d_v - 1\}, v \in V, c \in C, b \in B_c\backslash\{0\} \tag{11}$$

$$soc_{t,v} \geq SOC_{c,b-1}^{break} - 1 + z_{t,v}^{c,b} \quad \forall t \in \{\boldsymbol{a_v}, \dots, d_v\}, v \in V, c \in C, b \in B_c \backslash \{0\} \tag{13}$$

$$SOC^{min} \leq soc_{t,v} \leq SOC^{max} \qquad \forall t \in T, v \in V \tag{14}$$

$$i_{t,v,c} \leq \sum_{b \in B_c \backslash \{0\}} I_{c,b}^{max} z_{t,v}^{c,b} \qquad \forall t \in T, v \in V, c \in C \tag{15}$$

$$i_{t,v,c} \geq \sum_{b \in B_c \backslash \{0\}} I_{c,b}^{min} z_{t,v}^{c,b} \qquad \forall t \in T, v \in V, c \in C \tag{16}$$

$$\sum_{c \in C} \sum_{b \in B_c \backslash \{0\}} z_{t-1,v}^{c,b} - \sum_{c \in C} \sum_{b \in B_c \backslash \{0\}} z_{t,v}^{c,b} \leq y_{t,v} \qquad \forall t \in \{\boldsymbol{a_v} + \boldsymbol{1}, \dots, d_v\}, v \in V \tag{17}$$

$$\sum_{c \in C} \sum_{b \in B_c \backslash \{0\}} z_{t,v}^{c,b} \geq y_{t,v} \qquad \forall t \in T \backslash \{\boldsymbol{a_v} + \boldsymbol{1}, \dots, d_v\}, v \in V \tag{18}$$

$$\sum_{t \in T} y_{t,v} + \sum_{c \in C} \sum_{b \in B_c \backslash \{0\}} z_{T^{max},v}^{c,b} \leq N + 1 \qquad \forall v \in V \tag{19}$$

$$\sum_{c \in C} \sum_{b \in B_c \backslash \{0\}} z_{t,v}^{c,b} \leq 1 \qquad \forall t \in T, v \in V \tag{20}$$

$$\sum_{b \in B_c \backslash \{0\}} z_{t,v}^{c,b} \leq u_{v,c} \qquad \forall t \in T, v \in V, c \in C \tag{21}$$

$$\sum_{c \in C} u_{v,c} \leq 1 \qquad \forall v \in V \tag{22}$$

$$\sum_{v \in V} \sum_{b \in B_c \backslash \{0\}} z_{t,v}^{c,b} \leq h_c \qquad \forall t \in T, c \in C \tag{23}$$

$$\sum_{v \in V} u_{v,c} \leq h_c \qquad \forall c \in C \tag{24}$$

$$i_{t,v,c} \leq \sum_{b \in B_c \setminus \{0\}} \frac{G_c \cdot 1000}{U_{battery}} z_{t,v}^{c,b} \qquad \forall t \in T, v \in V, c \in C \tag{25}$$

$$i_{t,v,c} \leq \sum_{b \in B_c \setminus \{0\}} \frac{L \cdot 1000}{U_{battery}} z_{t,v}^{c,b} \qquad \forall t \in T, v \in V, c \in C \tag{26}$$

$$z_{t,v}^{c,b} \in \{0,1\} \qquad \forall v \in V, t \in T, c \in C, b \in B_c \tag{27}$$

$$y_{t,v} \in \{0,1\} \qquad \forall v \in V, t \in T \tag{28}$$

$$u_{v,c} \in \{0,1\} \qquad \forall v \in V, c \in C \tag{29}$$

The objective function (1) minimizes the total energy costs over the planning horizon. The first term corresponds to the total energy cost of the site that is the cost of electricity p_t $(€/kWh)$ multiplied by another two subterms that are the non-EV normal power demand of the site $\boldsymbol{l_t}$ (kW) multiplied by the period length $\boldsymbol{\Delta t}$ (hours) and the total energy consumed by EFVs for charging their batteries over the planned horizon. The second term in the objective function (1) represents the FRD charges that the whole site is subjected to and is determined by multiplying the fee F (€/kW) by the maximum charging power retrieved from the grid throughout the entire planned interval. EFVs would be scheduled in a way to retrieve power from the grid during the periods when the regular power consumption of the site l_t is relatively lower than its values in other periods.

Simple Example with Multiple Solutions

To help readers comprehend the problem and its mathematical formulation, we generate examples of different optimal solutions for a small instance of the EFV-CCSP. We assume having a time interval of 24 periods that starts from 15:00 with a time step of one hour resulting in a whole night charging problem such that the cost of energy p_t and the non-EV power consumption of the building l_t are given in Table 3. The grid power limit P is set to the value of 200 (kW) that could be neglected for the sake of simplicity, and the FRD fees are set to be 11 (€/kW). We apply the experiments on a set of 3 homogeneous vehicles with an energy capacity of 82.8 (kWh), a charge capacity of 230 (Ah), 360 (V) battery voltage, and a 12 kW onboard charger. The energy needed e_v (kWh), and the arrival and departure periods for each vehicle are given in TABLE 1.

TABLE 1: Route parameters for the simple numerical example

V	distance(km)	$e_v\ (kWh)$	d_v	a_v
1	62	40	17	3
2	65	42	18	2
3	68	44	17	4

There are three types of clusters installed in the depot in which, for every example, all EVs for their charging process use the same type of cluster to analyze better the effects of the cluster's types on the charging behavior of the EFV behavior while performing the overnight charging. For the sake of simplicity, we set only two breakpoints associated with the linear approximation CC-CV charging process of the battery using any cluster type such that $B_c = \{0,1\}$. The values of the maximum current $I_{c,b}^{max}$ and the minimum current $I_{c,b}^{min}$ and the SoC breakpoint $SOC_{c,b}^{break}$ that correspond to the breakpoints specified to each charging type are summarized in TABLE 2.

TABLE 2: Design parameters associated with the breakpoints of the linear approximation of the charging process

B	32 (A) single-phase EVSE			16 (A) three-phase EVSE		
	$SOC_{c,b}^{break}$	$I_{c,b}^{max}$	$I_{c,b}^{min}$	$SOC_{c,b}^{break}$	$I_{c,b}^{max}$	$I_{c,b}^{min}$
0	0.05	0	0	0.05	0	0
1	0.99	20.5	4.1	0.99	30.5	6

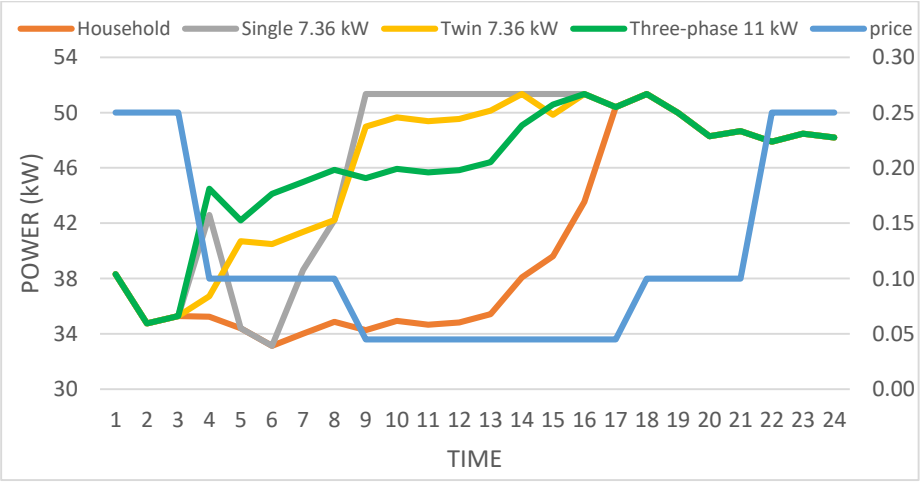

Fig. 5: The power consumption profile of the building when using three different charging infrastructure cases and the electricity prices variation with time.

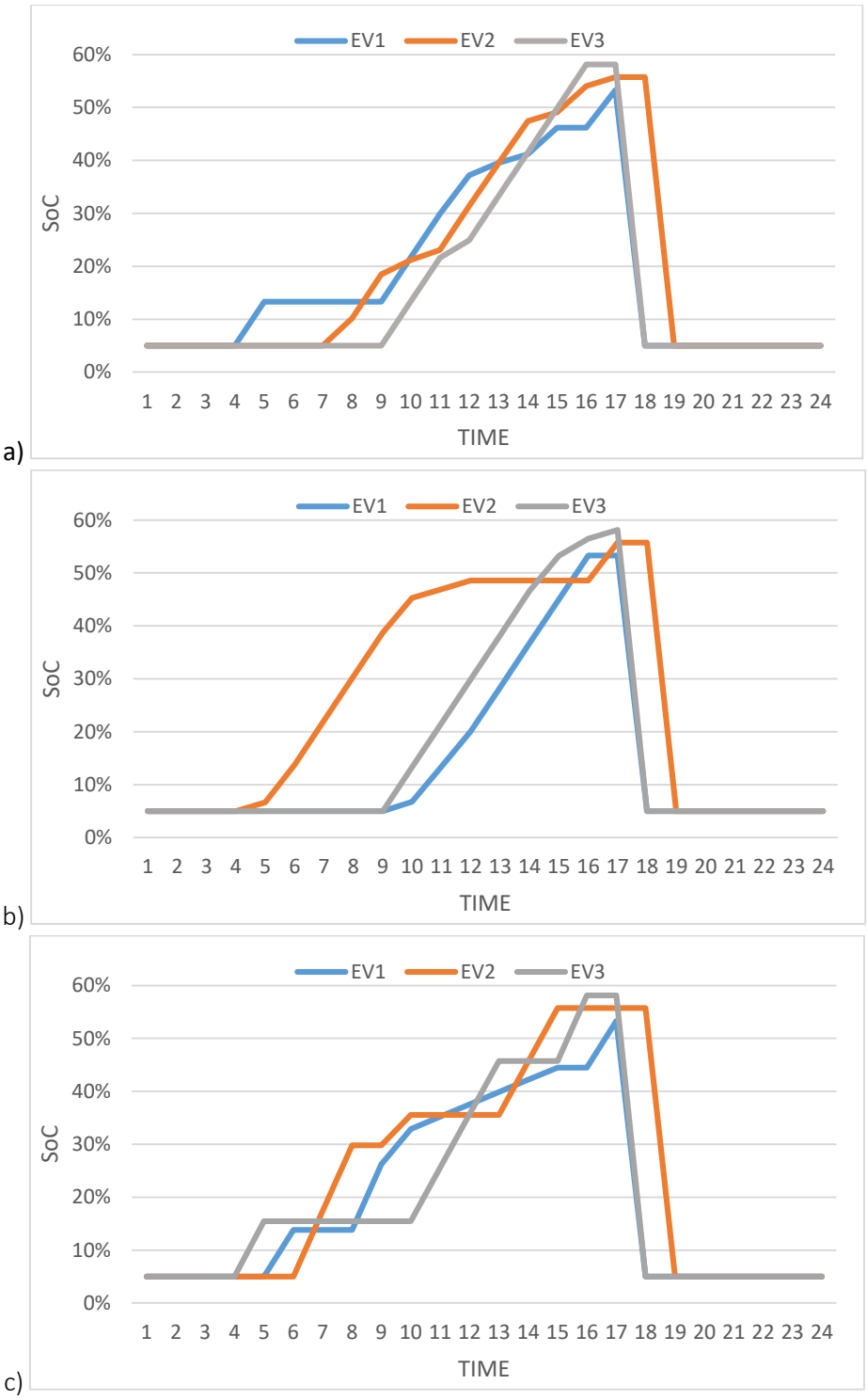

Fig. 6: The SoC evolution with time during the charging process of EVs "1", "2" and "3" using: (a) 3 single-socket chargers each having a 7.36 kW power capacity, (b) a double-socket charger and a single-socket charger both having a 7.36 kW power capacity, (c) a triple-socket charger of 11 kW power capacity.

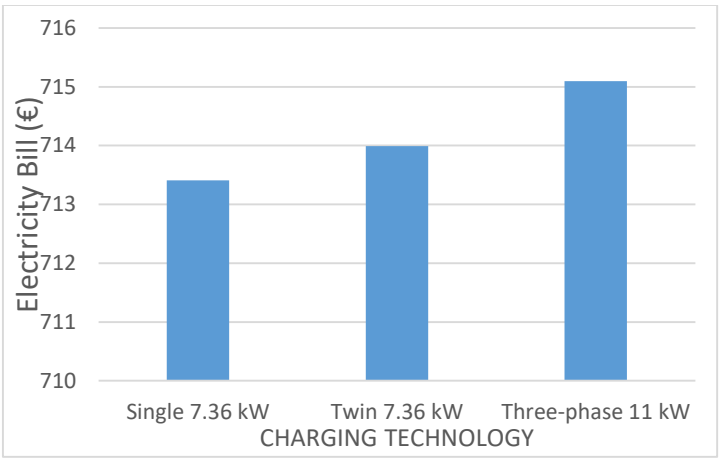

Fig. 7: The building's electricity bill as a result of three different charging infrastructure scenarios.

Three cases are defined as A, B, and C, where A refers to a charging infrastructure composed of single-socket single-phase 32 (A) charging stations such that h_c=1 for all the clusters and characterized by a power capacity of 7.36 kW each. Case B represents a depot equipped with two twin-socket single-phase 32 (A) intelligent chargers with a power capacity of 7.36 kW. Each of the two clusters could deliver a power of 7.36 kW per socket and the same power value combined. Finally, case C is similar to case B, with the difference in having a three-phase 16 (A) smart cluster equipped with 3 charging sockets and delivering a combined power of up to 11 kW. Figures 5, 6, and 7 illustrate the results of the optimal solutions for the example proposed before using the three different charging technologies and show their effect on the charging cost and the power system.

The Residential Neighbourhood Problem Model

This section considers having a DSO that aims to reduce the impact of the daily EVs' charging profile and avoid the spiking electricity demand in a particular neighborhood. To do so, the DSO offers its clients a new smart charging technology consisting of a dedicated smart charging station installed at every house in the neighborhood and is connected through the internet to a smart charging app installed on any smartphone. The mobile app allows communication between EVs and the smart grid and between all EVs in the neighborhood through the smart chargers installed in each house. Logically speaking, this new technology would be accepted by EV users only if it helps them save money and make their EV charging process more accessible and more secure in the sense of ensuring that their EV would be charged with at least the energy needed at the departure time they specify as an input parameter through the mobile app.

TSREV-CSP serves as an exciting charging strategy to satisfy both the DSO and EV users simultaneously for being designed with dual objective functions corresponding to two dependent optimization models. The first model is a peak shaving model (PSM) that allows the DSO to minimize the grid power capacity and normalize the neighborhood's load profile throughout the entire day. Then comes the subsequent charging cost reduction model (CCRM) based on the optimal solution of PSM to minimize the cost of EV charging thanks to the smart pricing strategies.

Our problem is defined over a set *T*= (1,..,T^{max}) the time interval of equidistant periods with a time step Δt of 15 mins (0.25 h). The neighborhood consists of a set *V* of electric vehicles (EVs) that could be charged daily, assuming that each EV *v* corresponds to one house and that every house owns one EV. Each EV $v \in V$ requires to be charged with a given amount of energy e_v (KWh) estimated based on the available energy in the battery and the travel distance as a sum of the route destinations specified by the EV user for the next day. The arrival time a_v to the house and the departure time d_v from the house are given for each EV. The SOC for each vehicle v at the arrival time is defined with the input parameter $SOC_v^{arrival}$. Each EV $v \in V$ is characterized by an energy capacity QE_v (kWh), an output battery voltage $U_v^{battery}$, a charge capacity represented by the parameter Q_v (Ah), and equipped with an onboard charger of a power capacity defined as L_v. We define the state of charge (SOC) of a battery as the amount of charge it contains divided by its charge capacity Q_v. We assume that a level 2 single-phase 230V-32A smart charger with a power capacity of up to 7.3 kW defined by the parameter G is installed. Based on the battery model presented before, we approximate a linear piecewise function for the discretized CC-CV charging process of the batteries, which consists of several breakpoints $q_v + 1$ fitted to the real CC-CV concave charging function of the battery of vehicle v.

Mathematical Formulation of the Peak Shaving Model

Five sets of decision variables are required for the formulation of PSM. Binary variables $z_{t,v}^b$ take a value of 1 if vehicle v is retrieving current while being plugged into the EVSE during period *t* that lies in the time interval between a_v the arrival time to the site and $d_v - 1$ the period before departure time from the site between breakpoints SOC_{b-1}^{break} and SOC_b^{break} And take a value of 0 otherwise. While $y_{t,v}$ are binary variables that depend on the values of $z_{t,v}^b$. They take a value of 1 for any interruption in the charging process of vehicle v between periods $t - 1$ and t and takes a value of 0 otherwise.

Real and positive variables $i_{t,v}$ refer to the charging current applied to vehicle v during the entire period t. Real and positive variables $soc_{t,v}$ refer to the state of charge of vehicle v at the beginning of time t. Finally, Real and positive variable X^{max} that corresponds to the maximum charging power retrieved from the grid by all the neighborhood houses during the planning interval. To sum up, our problem is presented in the following mathematical model and the mixed-integer linear programming formulation (MILP), respectively:

Sets:

- T: The set of time in the scheduling horizon $(T = \{1, \dots, T^{max}\}, (t \in T)$
- V: Set of EVs. $(v \in V)$
- B_v: Set of breakpoints used in the piecewise linear approximation of the CC-CV charging function of the battery of vehicle v. $(b \in B_v)$

Parameters:

- M_t: The neighborhood household total power consumption at time t.
- $l_{t,v}$: non-flexible consumption profile (non-EV) of each house of EV v at time t. (kW)
- Q_v: The charge capacity of the battery of EV v. (Ah)
- QE_v: The energy capacity of the battery of EV v. (kWh)
- L_v: The onboard power capacity of the charger of EV v. (kW)
- N_v: The maximum number of cuts allowed for the battery of EV v.
- a_v: The arrival time of EV v to the house.
- d_v: The departure time of EV v from the house.
- e_v: Energy needed by EV v. (KWh)
- $SOC_v^{arrival}$: The state of charge associated with the arrival time for each EV $v \in V$.
- P_v The Grid power capacity of the house of EV v at any time(kW)
- $U_v^{battery}$: The rated voltage of the battery of EV v. (V)
- l_v^{max} : Power supply limit of the EVSE installed at the house of EV v (Charger specification). (kW)
- $I_{v,b}^{max}$: The maximum current that could be withdrawn in the piecewise linear approximation of the CC-CV charging function of the charger of EV v between the breakpoints b and $b-1$ with $b \in B_v$, $b > 0$. (A)
- $I_{v,b}^{min}$: The minimum current that could be withdrawn in the piecewise linear approximation of the CC-CV charging function of the charger of EV v between the breakpoints b and $b-1$ with $b \in B_v$, $b > 0$. (A)

- $SOC_{v,b}^{break}$: The state of charge associated with breakpoints $b \in B_v$ of the piecewise linear approximation of the CC-CV charging function of the charger of EV v.
- SOC^{max}: The maximum state of charge that any vehicle could reach while charging.
- SOC^{min}: The minimum state of charge that any vehicle could reach during the discharging process while performing its route the next day.
- q: The average weighted power loss factor due to the AC-DC conversion.
- Δt: Timestep in (h).

Variables:

- $i_{t,v} \geq 0$: current withdrawn by EV v at time t. (A)
- $soc_{t,v} \geq 0$: The state of charge of EV v at time t.
- $z_{t,v}^{b} \in \{0,1\}$: 1 if EV v is charging at time t with a state of charge between $SOC_{,b-1}^{break}$ and $SOC_{v,b}^{break}$.
  0 otherwise.
- $y_{t,v} \in \{0,1\}$: 1 if EV v stops charging at time period t.
  0 otherwise
- $\bar{X} \geq 0$: The maximum total household power consumption of the neighbourhood withdrawn from the grid along the planned horizon.

Formulation:

$$\text{minimize} \qquad \text{Maximum power } = \bar{X} \tag{30}$$

subject to:

$$\left(M_t + \sum_{v \in V} \frac{i_{t,v}}{Q_v} QE_v\right) \leq \bar{X} \qquad \forall t \in T \tag{31}$$

$$l_{t,v} + \frac{i_{t,v}}{Q_v} QE_v \leq P_v \qquad \forall\, t \in T, v \in V \tag{32}$$

$$\sum_{t=1}^{a_v - 1} \sum_{v \in V} \sum_{b \in B_v \setminus \{0\}} z_{t,v}^{b} + \sum_{t=d_v}^{T^{max}} \sum_{v \in V} \sum_{b \in B_v \setminus \{0\}} z_{t,v}^{b} = 0 \tag{33}$$

$$soc_{t,v} = SOC_v^{arrival} \qquad \forall v \in V, t \in \{1, \dots, a_v\} \tag{34}$$

$$soc_{d_{v+1},v} = soc_{d_v} - \frac{e_v}{QE_v} \qquad \forall v \in V \tag{35}$$

$$soc_{d_v,v} = soc_{a_v} + \frac{e_v}{QE_v} \qquad \forall v \in V \tag{36}$$

$$\sum_{t \in T} \frac{i_{t,v} \Delta t(1-q)}{Q_v} + SOC_v^{arrival} - SOC^{min} = \frac{e_v}{QE_v} \qquad \forall v \in V \tag{37}$$

$$soc_{t,v} = soc_{t-1,v} + \frac{i_{t-1,v} \Delta t(1-q)}{Q_v} \qquad \forall t \in \mathrm{T}\backslash\{1, d_v, d_v+1\}, v \in V \tag{38}$$

$$soc_{t+1,v} \leq SOC_{v,b}^{break} + 1 - z_{t,v}^b \qquad \forall t \in \{a_v, \dots, d_v - 1\}, v \in V, b \in B_v\backslash\{0\} \tag{39}$$

$$soc_{t,v} \leq SOC_{v,b-1}^{break} - 1 + z_{t,v}^b \qquad \forall t \in \{a_v, \dots, d_v\}, v \in V, b \in B_v\backslash\{0\} \tag{40}$$

$$SOC^{min} \leq soc_{t,v} \leq SOC^{max} \qquad \forall t \in T, v \in V \tag{41}$$

$$i_{t,v} \leq \sum_{b \in B_v\backslash\{0\}} I_{v,b}^{max} z_{t,v}^b \qquad \forall t \in T, v \in V \tag{42}$$

$$i_{t,v} \leq \sum_{b \in B_v\backslash\{0\}} I_{v,b}^{min} z_{t,v}^b \qquad \forall t \in T, v \in V \tag{43}$$

$$\sum_{b \in B_v\backslash\{0\}} z_{t-1,v}^b - \sum_{b \in B_v\backslash\{0\}} z_{t,v}^b \leq y_{t,v} \qquad \forall t \in \{a_v + 1, \dots, d_v\}, v \in V \tag{44}$$

$$\sum_{b \in B_v\backslash\{0\}} z_{\mathrm{t},v}^b \geq y_{\mathrm{t},v} \qquad \forall t \in \mathrm{T}\backslash\{a_v + 1, \dots, d_v\}, v \in V \tag{45}$$

$$\sum_{t \in T} y_{t,v} \leq N_v + 1 \qquad \forall v \in V \tag{46}$$

$$i_{t,v} \leq \frac{l_v^{max}}{U_v^{battery}} \cdot 1000 \cdot \sum_{b \in B_v \setminus \{0\}} z_{t,v}^b \qquad \forall t \in T, v \in V \tag{47}$$

$$i_{t,v} \leq \frac{L_v}{U_v^{battery}} \cdot 1000 \cdot \sum_{b \in B_v \setminus \{0\}} z_{t,v}^b \qquad \forall t \in T, v \in V \tag{48}$$

$$z_{t,v}^b \in \{0,1\} \qquad \forall v \in V, t \in T, b \in B_v \tag{49}$$

$$y_{t,v} \in \{0,1\} \qquad \forall v \in V, t \in T \tag{50}$$

The objective function (30) minimizes the maximum total household power consumption of the neighbourhood withdrawn from the grid along the planning horizon $\bar{X}$ to reduce the impact of the increasing EVs' charging demand. Specifically, $\bar{X}$ represents the maximum value of the sum of the normal power consumption M_t of all the houses in the neighborhood and the power retrieved by all the EVs at any period t over the planned time interval.

Mathematical Formulation of the Charging Cost Reduction Model

The CCRM is a cost minimization model and is a subsequent submodel dependent on the primary optimization model PSM. The CCRM aims to provide EV users a degree of freedom in choosing their charging schedule for electricity bill reduction while not violating the maximum power constraint established in the primary model. This model depends mainly on the results of the PSM such that we generate slack parameters calculated through the difference between the obtained value of $\bar{X}$ and the total power retrieved by all the houses, which is estimated using the output decision variables $\overline{\iota_{t,v}}$ at each time t that represent the charge current applied to each vehicle *v* at time t. This model is used individually for each house in the neighbourhood that owns an EV. We follow two approaches of percentage and even distribution strategies to calculate the slack parameters for each EV.

The parameters $\overline{u_{t,v}}$ correspond to the decision variable of the charge current $\overline{i_{t,v}}$ applied to each vehicle v at time *t* as an output of the first optimization stage performed in PSM. We define $\overline{u_{t,v}}$ (kW) as the power retrieved by vehicle v at time t and is estimated by dividing the product of the charge current $\overline{i_{t,v}}$ (A) and the energy capacity QE_v (kWh) by the total charge capacity Q_v (Ah) for each vehicle *v.* The slack parameters $\overline{s_{t,v}}$ are the additional power allowed to be retrieved by vehicle v at time t compared to $\overline{u_{t,v}}$. The combination of both parameters $\overline{u_{t,v}}$ and $\overline{s_{t,v}}$ represent the grid limit during the charging process of vehicle *v* at any time *t.* Our problem follows the same mathematical model presented in the first stage of the PSM but having some changes in the input parameters and variables. The parameter M_t and the decision variable of the maximum power $\bar{X}$ are removed, and only the following new parameters are added:

- p_t: Electricity price at time t. $(€/kWh)$
- $u_{t,v}$: The power retrieved by EV v at time t as an output from the PSM. (kW)
- $s_{t,v}$**:** The power slack parameter is given to each vehicle v at time t for more flexibility in
- the charge schedule. (kW)

Mathematical Formulation of $\mathbf{CCRM}_v$ $\forall v \in V$:

The mathematical formulation of the $CCRM_v$ is the same as in the model of PSM but having some changes. We replace the objective function (30) with a cost minimization objective function defined in Eq. (51). Moreover, we replace the constraints (31) with Eq. (52), which represent the weighted grid power restrictions applied to each house v individually and composed of the power consumption of EV v obtained from the PSM and the estimated slack parameters based on the peak power output also in the PSM.

$$\text{minimize:} \quad \sum_{t \in t} p_t \Delta t \left(l_{t,v} + \frac{i_{t,v}}{Q_v} QE_v \right) \tag{51}$$

$$\frac{i_{t,v}}{Q_v} QE_v \leq \overline{u_{t,v}} + \overline{s_{t,v}} \qquad \forall\, t \in T \tag{52}$$

The objective function (51) minimizes cost_v the total electricity bill over the planning horizon for each house of vehicle $v \in V$. The $CCRM_v$ is applied individually to each house owning an EV by creating a loop over the set V. cost_v (€) is the product of the energy cost p_t (€/kWh), the duration of time Δt (hours), and the total power retrieved by the house, including both $l_{t,v}$ (kW) the household power and the EV charging power retrieved by house v at every period t then summed up over the planning horizon of set T.

Simple Example with Multiple Solutions

This section aims to help the reader better understand the functionality of the RNS by presenting a small instance with different parameters that give other optimal solutions. We design this example with a time interval of 24 equidistant periods with a time step of one hour. The planning horizon starts from 16:00 and lasts until 15:00 the next day, such that we have a whole night charging problem. We discretize our planning horizon with 24 equidistant periods with period lengths of one hour (i.e., $\delta = 1\ h$), where 16:00 is set to 1 and 15:00 is denoted by 24. We consider having a set of 3 EVs such that each vehicle represents a house in the neighbourhood.

The cost of energy p_t is assumed to be as follows: 0.25 ($€/\mathrm{kWh}$) during the peak hours from periods 1 to 3 and 21 to 24 (12:00-18:00), 0.05 ($€/\mathrm{kWh}$) during the off-peak hours from periods 9 to 17 (00:00-8:00), and 0.15 ($€/\mathrm{kWh}$) during the shoulder hours the rest of day. The total household power consumption parameters M_t (kW) of all the houses in the neighbourhood and the individual household power consumption $l_{t,v}$ (kW) of each house of an EV user *v* are given at every period *t*. The EV's specifications-related parameters and all the routes data for every vehicle $v \in V$ are shown in TABLE 3.

TABLE 3: The design specifications and route parameters for the simple numerical example

V	EV model	Q (Ah)	QE (kWh)	L (kW)	$U^{battery}$ (V)	l^{max} (kW)	P (kW)	$SOC^{arrival}$	N	a	d	e (kWh)
1	BMW i3	120	42.24	11	352	7.36	10	0.05	2	4	22	31.68
2	RAV4	108	41.8	10	386	7.36	10	0.05	2	8	17	31.35
3	NISSAN LEAF	66	24	6.6	360	7.36	6	0.05	2	6	19	18

We set only three breakpoints associated with the linear approximation CC-CV charging process of the battery of each vehicle *v* using a level 2 fast charger of 7.36 (kW) power capacity and a charge current of 32 (A) such that $B_v = \{0,1,2\}$. The values of the maximum current $I_{v,b}^{max}$ and the minimum current $I_{v,b}^{min}$ And the SOC breakpoint $SOC_{v,b}^{break}$ that correspond to the breakpoints specified to each vehicle *v* are summarized in TABLE 4.

TABLE 4: The design parameters associated with the linear approximation breakpoints of the charging process of different vehicles' models.

B_v	EV 1 (BMW i3)			EV 2 (RAV4)			EV 3 (NISSAN LEAF)		
	$SOC_{1,b}^{break}$	$I_{1,b}^{max}$ (A)	$I_{1,b}^{min}$ (A)	$SOC_{2,b}^{break}$	$I_{2,b}^{max}$ (A)	$I_{2,b}^{min}$ (A)	$SOC_{3,b}^{break}$	$I_{3,b}^{max}$ (A)	$I_{3,b}^{min}$ (A)
0	0	0	0	0	0	0	0	0	0
1	0.923	21	2	0.92	19.1	2	0.882	18.5	2
2	0.99	10.5	1	0.99	10	1	0.99	10.5	1

a)

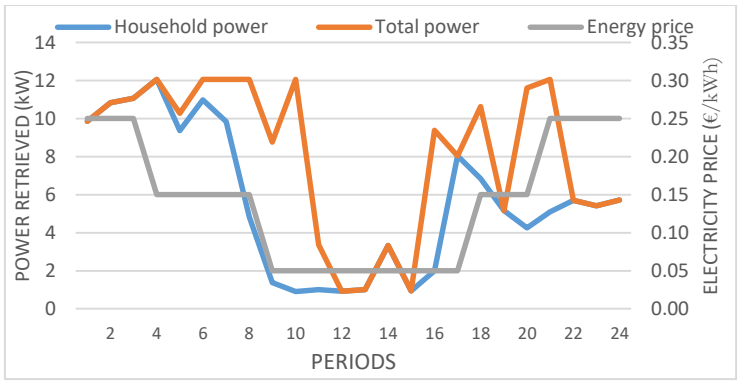

b)

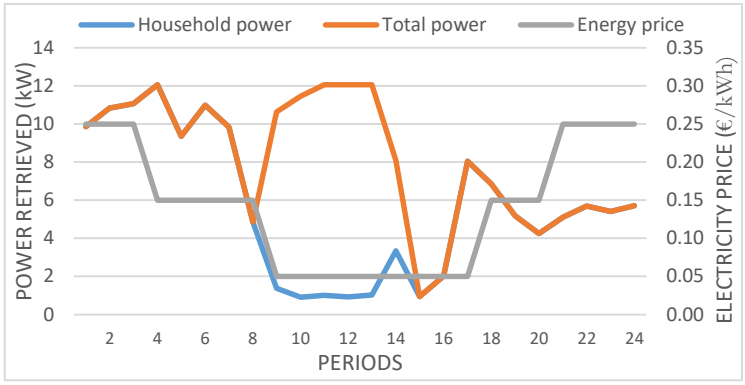

c)

Fig. 8: The power retrieved by all the houses in the neighbourhood: (a) optimal solution of the PSM, (b) optimal solution of the CCRM with % slack distribution algorithm.

Figures 8 and 9 show a comparison of the solution obtained by the CCRM's percentage approach compared to that of the PSM. Fig. 8 presents a comparison between the building's total power consumption and the charging power retrieved by the EVs as obtained by the PSM and both approaches of the CCRM. By comparing the three graphs, we notice the role of the PSM in the peak power reduction as well as the effects of the CCRM in shifting the EV loads. Fig. 9 shows a remarkable decrease in all the houses' electricity bills with at least a 5% reduction.

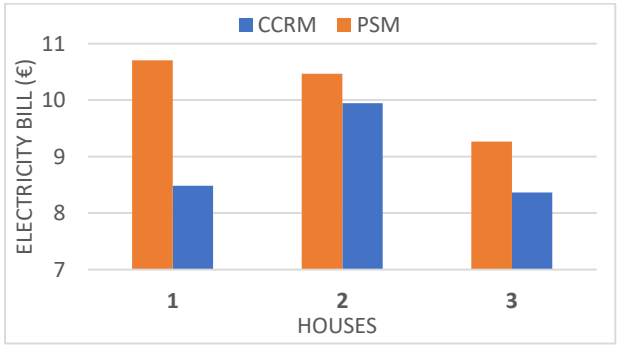

Fig. 9: A comparison of the electricity bills of all the houses obtained in the PSM and the CCRM.

Numerical Experiments and Discussions

This section consists of the experiments we perform for each of the proposed optimization problems of the CIS and RNS. For both problems, we present a base case and show its results. We analyze our models' feasibility by generating extensive experiments of different scenarios. Each scenario is based on changing only one parameter while fixing the others compared to the base case scenario. The base case scenario of the commercial problem consists of nine test instances that are the results of three charging behaviors of a low, medium, and high energy demand along with long, medium, and short charging duration all applied to three fleet sizes of EVs of 8, 12, and 16. Then we perform a multi-criteria analysis that consists of five scenarios represented by high Facility Demand Charges (FRD) of 11 $(€/kW)$, low FRD charges of 0.1 $(€/kW)$, lower grid power restrictions of 110 kW instead of 500 kW, and last two scenarios of one and zero charging interruptions instead of two in the base case.

Figures **10** and **11** represent examples of the results obtained in the commercial building problem. The first shows the peak power demand of the building in the different test instances when applying both the high and low FRD charges. In general, we see that higher power demand is imposed on the grid when applying the low FRD charges using all charging technologies. We notice that the cluster "3S_22kW" of a 22 kW power capacity and consists of 3 charging sockets shows better results of lower power demands for both FRD values than all other technologies. However, **Fig. 11** demonstrates the total electricity bill of the building using different charging technologies in all test instances. It also shows a privilege to the results obtained using cluster "3S_22kW".

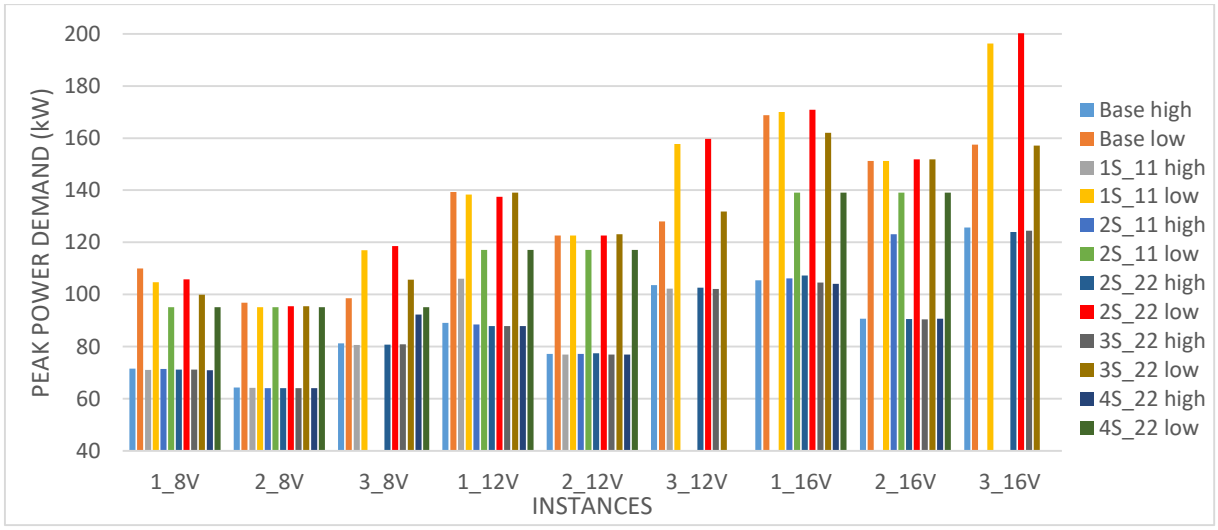

Fig. 10: A comparison between the peak power demand in the instances of high FRD charges and the ones with low FRD charges using different charging technology in the commercial problem.

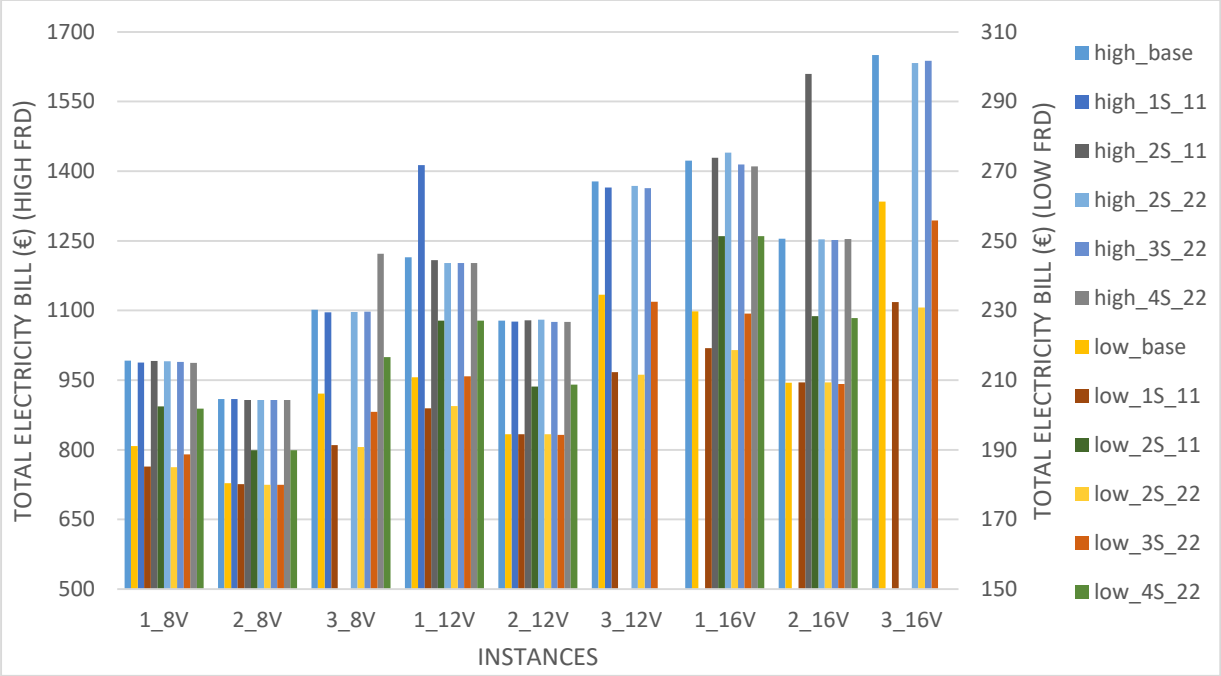

Fig. 11: The total electricity bill of the commercial building for different test instances using multiple charging technologies under the low and high FRD charges scenario

Similarly, we generate the same three test instances for the residential problem but with an additional instance representing a random mix of the other three together. We apply these instances on four different numbers of EVs of 30, 40, 50, and 60 EVs that result in 16 test instances for the base case scenario. Then we perform extensive experiments of different scenarios to check the feasibility of our model. We assume two charging interruptions scenarios of one and two cuts instead of two in the base case, a Smart-Pricing strategy of two different prices per day instead of three in the base case. In addition, we generate three more scenarios with contract power values of 6 kW, 10 kW, and a mix of both when it was 20 kW in the base case.

We assume another three scenarios of different EV-users' percentages in the neighbourhood of 50%, 67%, and 75% instead of 100% in the base case scenario. We repeat the experiments in the base case scenario and the contract power ones using only the CCRM model while neglecting the global grid power limits to check the effects of the PSM on both the individual electricity bill of each house and the peak power demand of the neighbourhood. Finally, we generate a cost minimization model similar to the one in the commercial problem by including the peak power demand in the objective function as a high power demand penalty, and then we compare it with the base case.

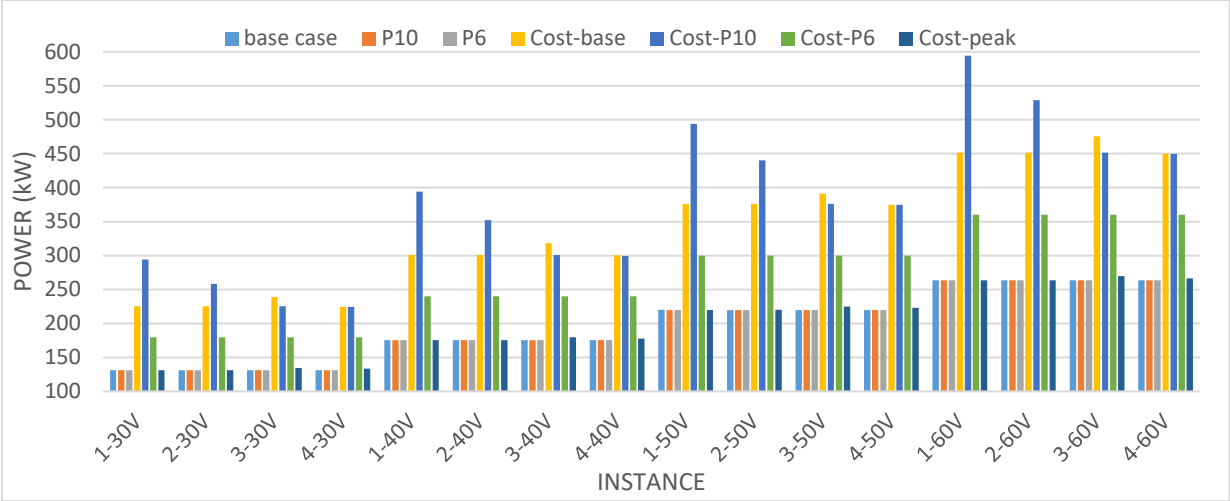

Fig. 12: Comparison between the peak power demand obtained by the PSM and that obtained by the "Cost" model in the same neighbourhood under different scenarios.

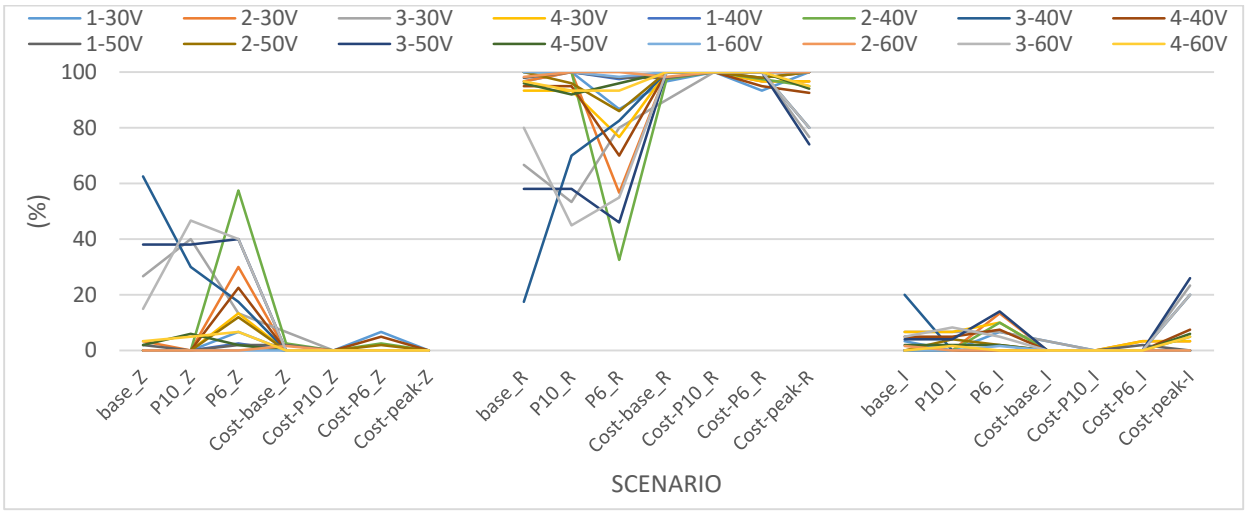

Fig. 13: The percentage distribution of all the houses in the neighbourhood in all test instances based on the reduction rate in their energy bills for different cases of the grid's power limit compared to the base case and using both models of the TSREV-CSP and "Cost".

Figures **12** and **13** show a comparison between the results obtained from the TSREV-CSP and the other two cost-based models, namely a "Cost" and a "Cost-peak", in terms of peak power demand and the percentage distribution of all the houses in the neighbourhood based on their electricity bills reduction rates. We observe that the TSREV-CSP results in the least power demands in all the test instances compared to other models, but the results obtained by the "Cost-peak" are acceptable for showing slight increases in the power demand. However, the cost analysis in **Fig. 13** gives preferences to the results obtained by "Cost" over the other two models. Since the goal is to satisfy both the energy supplier and the EV users, then the TSREV-CSP and the "Cost-peak" models sound more efficient than the "Cost" one.

1 INTRODUCTION

The advent of electric vehicles (EVs), including battery electric vehicles (BEVs) and plug-in hybrid electric vehicles (PHEVs), promises to be a game-changer for the world's shift to sustainability (IRENA, 2019). The transport sector that is primarily relying on conventional internal combustion engine vehicles (ICEVs) is responsible for 24% of the global energy-related CO_2 emissions in which passenger cars, together with road freight vehicles, account for nearly 75% of transport CO_2 emissions, as shown in Figure 1. Because of productivity enhancements, electrification of the transport sector, and expanded use of biofuels, global transportation emissions rose by less than 0.5 percent in 2019 (compared to 1.9 percent annually since 2000) (IEA, 2020).

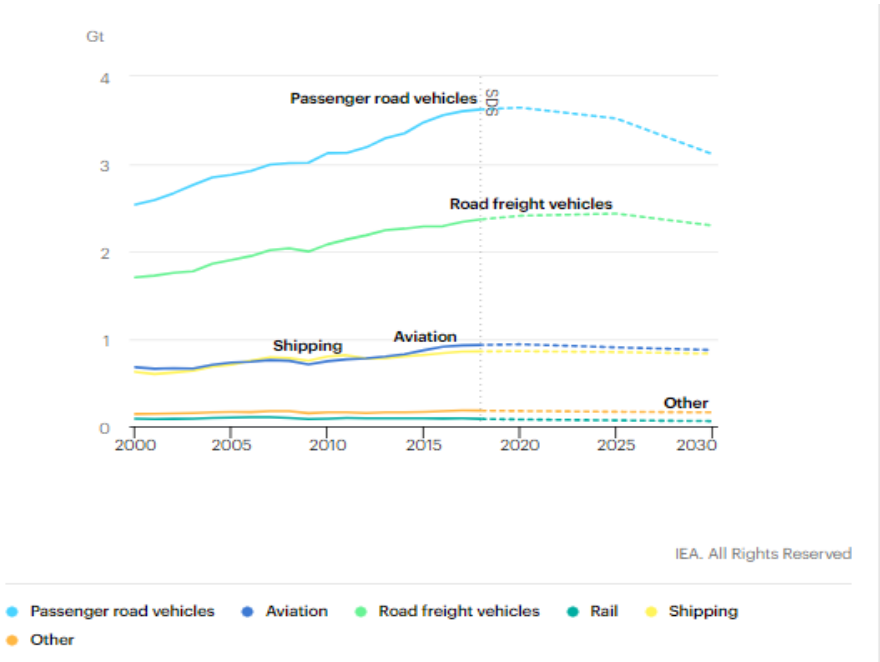

Figure 1: Transport sector CO2 emissions by mode in the Sustainable Development Scenario, 2000-2030.

Source: (IEA, 2020).

Electric vehicles deployment has been accelerating in the past decade thanks to the international policies, governmental incentives in many countries worldwide, and the remarkable improvements in EV technologies that propose electric cars as an attractive substitute for ICEVs (IEA, 2019). **Figure 2** shows that the global stock of electric passenger cars registered an increase of 63% between 2017 and 2018, recording more than 5 million in 2018, where 45% of the total number of EVs is in china.

China has emerged as the leader in EV sales worldwide and is expected to promote more advanced EV technologies and applications in the future (Wu et al., 2021). In comparison, Europe accounted for 24% of the global fleet in the 2nd place and the United States with 22% being the 3rd in the EV sales worldwide. The EV deployment is expected to increase in the future at an exponential pace because EVs are cleaner, more silent, and more economical than ICEVs for having a lower operational cost.

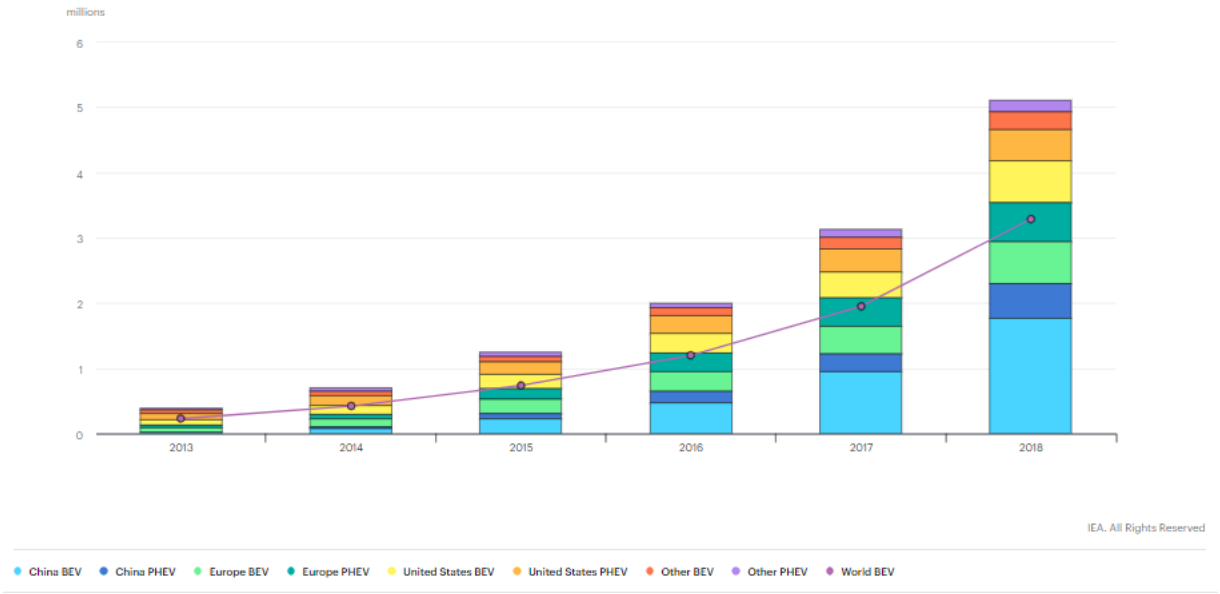

Figure 2: Electric car deployment in selected countries, 2013-2018

Source: (IEA, 2019).

Nowadays, transport electrification is considered one of the top technological alternatives to mitigate climate change as it contributes significantly to reducing GHG emissions, especially CO_2 emissions and energy dependence on petroleum fuel and other external energy supplies (Skerlos & Winebrake, 2010; Van Vliet et al., 2011), offering the potential to reduce the oil imports and many economic benefits (Michalek et al., 2011; Su et al., 2012). Moreover, it raises the electricity production company's tendency to go for cleaner alternatives and renewable energy resources (Chau et al., 1999) to achieve higher environmental objectives (Zhang et al., 2012). For these reasons, many countries have embraced various policies to increase energy conservation and enhance electricity production from renewable energy sources, as in China (She et al., 2017; Wu et al., 2021), the Netherlands (MNP, 2006; Ros et al., 2009), Germany (Loisel et al., 2020), and other European countries (Dudin et al., 2020). Some countries like Norway follow the policy of offering incentives to encourage EV adoption and increase EV sales, as shown in **Table 5**.

Table 5: “Norwegian EV policy time period of introduction.”

Source: (Chaim et al., 2016)

EV policy incentive	Time period of introduction
Exemption from registration tax	1990s
Free public parking	1990s
Toll exemptions	1990s
Value added tax exemption	2001
Bus lane access	2003 (Oslo) and 2005 (Nationwide)
Reduced ferry rates	2009
Public EV charging station construction	2009

1.1 CHALLENGES AND OPPORTUNITIES

Electric vehicles, just like other technologies, represent a solution for many problems and offer plenty of social benefits, but at the same time have their drawbacks that are under consideration in both the public and private realm. Compared to ICEVs, EVs overtake with zero exhaust emissions, higher efficiency, and considerable potential to minimize GHG emissions. However, they aren’t yet highly competitive for their high purchasing cost, and battery technology is still under development resulting in many uncertainties concerning many aspects such as electricity generation and large-scale introduction (Poullikkas, 2015). The main challenge ahead lies in improving the range and reducing the cost of the currently available technologies, whether it is the price of buying the EV or the charging fee (Wang et al., 2021). There are some other issues explained in Table 6 that might represent an obstacle nowadays for some users to adopt an EV, especially for passenger road vehicles.

From an environmental standpoint, the process of replacing ICEVs with EVs makes sense only if those vehicles are powered solely by renewable energy sources (RES) (Helmers et al., 2020). However, RES such as wind and photovoltaic power (PV) differ in output independently of electricity demand, resulting in surplus production or shortages. Consequently, the energy system is evolving due to a steady increase in electric vehicles on the demand side and local output (mostly from solar panels) on the supply side. Both technologies could bring the energy grid under strain at certain times of the day, especially that EVs require high power for an extended period while charging, even though there is enough capacity on the grid for most of the day. One way to deal with grid unbalances is using electric heat pumps to satisfy heat demand, with the heat being stored in substantial thermal stores. Both are examples of demand-side control (DSM) (Van Der Burgt et al., 2015).

Table 6: "Explanations and sources of barriers."

Source: (She et al., 2017)

Barrier type	Item	Possible barrier	Explanation
Financial Barrier	B1	Price	Original price of BEVs without purchase subsidy
	B2	Battery cost	Replacement cost of the battery once the battery reach the end of life
	B3	Poor understanding of fuel cost	Fuel cost refers to electric cost of driving BEVs
	B4	Poor understanding of maintenance cost	Maintenance cost refers to the routine maintenance cost of BEVs, not includes the repair cost caused by accidents
Vehicle performance barrier	B5	Safety	Whether feel safe when driving a BEVs
	B6	Range	Longest driving distance after BEVs fully charged for one time
	B7	Reliability	Quality and stability of whole vehicle
	B8	Battery life	Lifetime of battery considered of degradation
	B9	Charging time	Overall consideration of the time to fully charge a BEV in a quick and slow charging model
	B10	Power	Max speed and accelerating ability of BEVs
Infrastructure barrier	B11	Public infrastructure availability	Numbers and service radius of public charging spots or charging stations
	B12	infrastructure availability at work	Charging condition in workplace including office buildings
	B13	infrastructure availability at home	Charging condition in residence communities
	B14	infrastructure availability on highway	Charging condition in highway service stations

Here comes the dilemma: How could the energy authorities worldwide maintain the annual increase of EV deployment at a higher rate while maintaining a highly efficient power system?

1.2 SMART CHARGING POTENTIAL

EV smart charging techniques are highly efficient and promising ways to deal with the surplus production and represent a critical component of the friendly environment and cost-effective EV integration into the power grid. The central concept of smart charging is to shift the charging schedule of EVs towards the Off-peak periods of the day and when electricity cost is at its lowest values to eliminate the risk of a demand spike at the same time of satisfying the vehicle owner's need. Smart charging is a combination of the three key elements: "Smart pricing, Smart technology, and smart infrastructure," all coupled together to enable small end-users and utilities to leverage the essential flexibility of charging the EVs (Hildermeier et al., 2019a).

When talking about smart charging, we can't ignore the tremendous efforts exerted by many governments worldwide to create the so-called "Smart Cities" with those in Asia and Europe are at the top of the rankings (ASME, n.d.; Eden Strategy Institute & Ltd., n.d.). Smart cities require a modification in their urban system's infrastructure and public services to be more interactive, accessible, practical, and friendly environment by utilizing information and communication technology (ICT) (Pellicer et al., 2013).

Smart charging techniques are based on exchanging data of electricity prices and energy demand and generation levels at a given time between EVs and the smart grid to offer customers lower charging costs when charging their EV on low demand periods of the day. Therefore, smart cities represent the perfect environment for charging EVs intelligently, in which EV users receive real-time information about their energy usage or prices, and they choose when to charge the EV (Harrison & Donnelly, 2011).

1.3 THESIS OUTLINE

The different charging methods for reducing the impact of EV penetration in the power system can be categorized based on the various actors' perspectives, including EV end-users, distribution system operators (DSOs), and transmission system operators (TSOs). Liu et al., (2015) highlighted two main charging strategies: Centralized and decentralized charging strategies. Various studies have been conducted based on centralized charging strategies in which all network data is accessible to a centralized controller, which processes the data and determines the charging rate for each EV. However, centralized strategies were found to have difficulties in accessing the global system information and inaccurate scaling. Thus, we present in this research decentralized charging strategies that give individual EV users a level of decision making in which EV intelligent charging points often communicate a small amount of data with a centralized unit which then sends global coordination to all charging points.

This research is inspired by the practices of the French energy company's projects (EDF, n.d.), the 1st producer of renewable electricity in Europe. We aim to construct and model a controlled overnight charging technique to perform the so-called peak shaving for the power retrieved from the grid along a specified time horizon. Simultaneously, we minimize the EV charging fee for the end-users in two different scenarios: A Commercial & Industrial Scenario (CIS) of clustered charging points and a Residential Neighborhood Scenario (RNS). We test our models on many test instances.

Chapter 2 is the state of the art of models and smart charging technologies that are about similar applications. Besides, it illustrates the technologies of integrating EV charging with RES by showing various Smart Charging techniques and the importance of the existence of intelligent metering and smart grids. It also gives an overview of the different types of EVs available in the market, focusing more on fully electric vehicles known as Battery Electric Vehicles (BEVs) and their components, Battery technologies, EV charging standards, challenges, EV integration impacts on the power system, and future development directions on which our experimental data would be based. Finally, it exhibits a general understanding of the different approaches we followed to build up both optimization models.

In chapter 3, we describe the generic charging process of lithium-ion battery cells and describe the factors affecting it. Then, we simulate the charging profile of lithium that corresponds to different types of chargers used in our research. We apply the simulation to medium-duty commercial and residential passenger EVs.

In chapter 4, the mathematical model of the CIS and the charging technologies are explained, where we provide a general description of the Electric Freight Vehicles Clustered Charge Scheduling Problem (EFV-CCSP) and explain the approaches followed to model the charging process in discrete time. Then we present the EFV-CCSP mathematical formulation followed by descriptions of optimal solutions for a small instance of the problem and an illustration of the results.

In chapter 5, The RNS mathematical model and the charging algorithms are defined. We give a general overview of the Two-Stage Residential Electric Vehicles Charge Scheduling Problem (TSREV-CSP), and we clarify the method used to model the charging mechanism in discrete time for different EV types included in our research. Then, we explain the mathematical model of the first stage defined as a Peak Shaving Model (PSM) that aims to reduce the peak power in the neighborhood. Subsequently, we present the second optimization level that is the Charging Cost Reduction Model (CCRM), and we explain its interface with the PSM that minimizes the electricity bill of all the houses adopting EVs. Finally, we provide a small instance with some numerical results to better understand the charging algorithm.

In chapter 6, illustrates extensive computational results of multiple cases for both models, and we derive managerial insights. We show the base case scenario results and analyze the main observations. We compare the results obtained from the base case scenario and those of all the computational instances for both models of the Commercial and Industrial Scenario (CIS) and the Residential Neighbourhood Scenario (RNS), respectively.

2 STATE OF THE ART

This chapter highlights the main studies on similar EV smart charging applications. In section 2.1, we present the main features of an EV, mentioning some of its opportunities and barriers. Then we describe the different technologies of existing EVs and explain their functionalities briefly in section 2.2. In section 2.3, we show the general architecture of an EV and briefly describe the main components that influence our research. In section 2.4, we present the charging infrastructure systems available worldwide and the most interesting and highly efficient ones. Finally, we focus on some papers and studies that consider smart charging applications and describe their followed methodology to deal with the presented problem in section 2.5.

2.1 ELECTRIC VEHICLE DEPLOYMENT: TRENDS, OPPORTUNITIES, AND BARRIERS

The EV deployment is developing at a rapid pace, and this growth rate is expected to increase more in the future. Many reports and surveys (Aurora, 2018; IEA, 2019) highlight the present situation of EVs in the transport sector and present a forecast of a promising future for vehicle electrification. EV deployment trends are shown in Figure 3 with nearly 1.1 million electric vehicles sold in 2018. The People's Republic of China is the world's most significant electric car industry, and it accounts for roughly half of the total electric car stock (2.3 million units). At the end of 2018, Europe had 1.2 million electric vehicles, and the United States had 1.1 million, with sales increases of 385000 and 361000 electric cars, respectively, from the previous year. The world leader in terms of electric vehicle market share in 2018 remained Norway which accounts for 46% of the global EV market share, more than double Iceland's second-largest market share of 17%.

The EV's potential in dealing with three of the most crucial and universal concerns explains the growing interests in electrifying the transport sector and further developments of E-mobility technologies. The life-cycle air emissions and oil consumption assessments conducted by Michalek et al. (2011) for ICE vehicles, HEVs, PHEVs, and BEVs in the US show the benefits of EVs in reducing both GHG emissions and tail emissions that contribute to global warming, climate change, and other pollutants which affect the people and the environment. EVs also help to minimize the reliance on imported oil due to gasoline demand reduction for being powered being electricity rather than gasoline that results in plenty of environmental benefits.

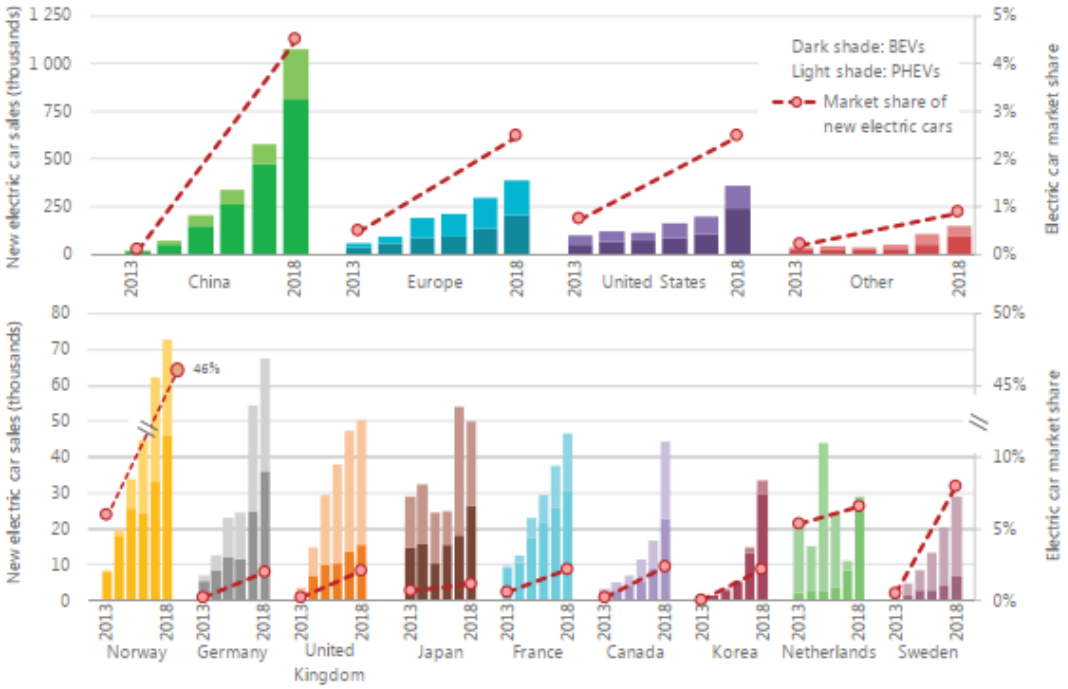

Notes: BEVs = battery electric vehicles; PHEVs = plug-in hybrid electric vehicles. Europe includes Austria, Belgium, Bulgaria, Croatia, Cyprus,[2] Czech Republic, Denmark, Estonia, Finland, France, Germany, Greece, Hungary, Iceland, Ireland, Italy, Latvia, Liechtenstein, Lithuania, Luxembourg, Malta, Netherlands, Norway, Poland, Portugal, Romania, Slovakia, Slovenia, Spain, Sweden, Switzerland, Turkey and United Kingdom. Other includes Australia, Brazil, Chile, India, Japan, Korea, Malaysia, Mexico, New Zealand, South Africa and Thailand.

Sources: IEA analysis based on country submissions, complemented by ACEA (2019); EAFO (2019); EV Volumes (2019); Marklines (2019); OICA (2019).

Figure 3: Global electric car sales and market share, 2013-18

Source: (IEA, 2019)

EVs also provide different ancillary services to support the power system, such as frequency regulation, spinning and non-spinning reserves, and supplemental resources, which are features of the Vehicle-to-Grid (V2G) technology. White and Zhang,(2011) investigate the financial feasibility of using plug-in hybrid electric cars as a grid option and highlight some technical and economic benefits that PHEVs provide using the V2G technologies. This paper concludes that there is considerable financial potential when the V2G service is used for frequency regulation, while there are few financial incentives for individuals when using the V2G service solely for peak reduction. Moreover, the assessment by Bañol Arias et al.,(2020) presents the economic benefits for EV owners participating in the primary frequency regulation (PFR) market, which is responsible for regulating and restoring the grid's frequency to the rated value in case of the power unbalance in the case of higher or lower power demands compared to the power generated. It proposes a heuristic method to optimize the power bid that maximizes the EV owners' benefit.

EVs possess significant onboard energy storage capacities from a few kWh up to several tens of kWh, which imposes a high demand on the power systems, especially with the high EV penetration worldwide and the development of the charging infrastructure, and the introduction of fast and rapid chargers. Kutt et al. (2013) provides an overview of EV charging impacts on the power system and defines these impacts to distribution networks as thermal loading, voltage regulation, harmonic distortion levels, unbalances, losses, and transformers loss of life with focusing more on the harmonic and unbalance effects. This thesis aims to provide a solution to reduce the impact of EV charging on the power grid by providing controlled charging models in different instances.

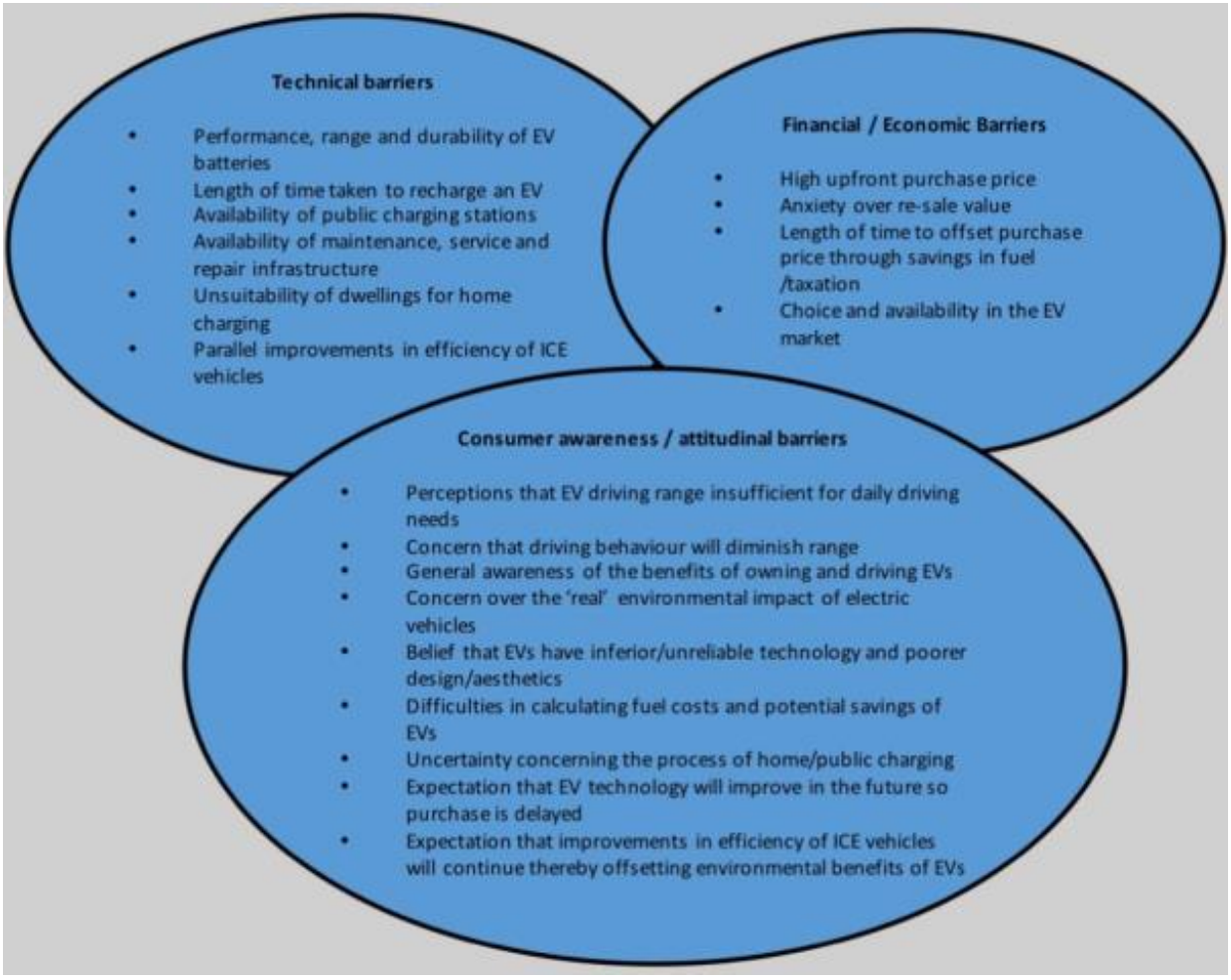

Figure 4: Barriers to BEV adoption.

Source: (Berkeley et al., 2017).

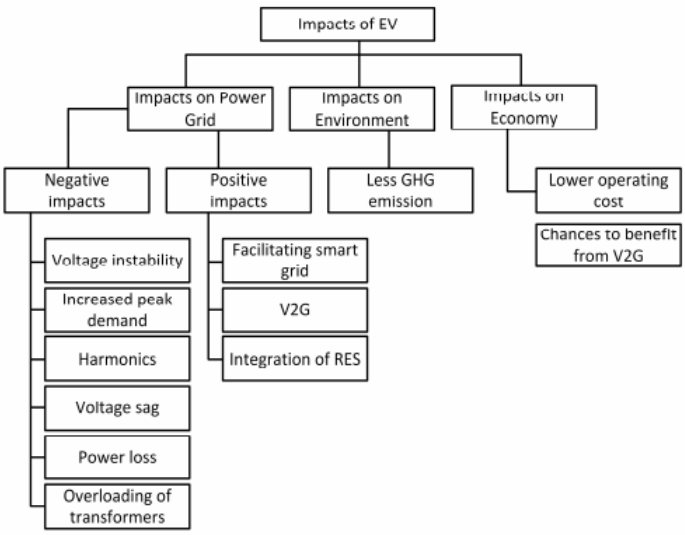

Figure 5: A shortlist of the impacts of EVs on the power grid, environment, and economy.

Source: (Un-Noor et al., 2017)

EV adoption has a long way to go for facing many obstacles and challenges that require further researches. Besides the power system barriers that EV charging is facing, many researchers like (She et al., 2017; Wang et al., 2021) give an overview of the various obstacles and challenges affecting the widespread of battery electric vehicles. The main technological barriers nowadays are the long charging period and the limited range due to the limited Energy capacity (Un-Noor et al., 2017). Berkeley et al. (2017) has classified different barriers to EV adoption into technical obstacles, financial and economic barriers, and consumer awareness and attitudinal barriers, as shown in Figure 4. Similarly, Un-Noor et al. (2017) present a general list of EV impacts on the power grid, the environment, and the economy, as shown in Figure 5. In this thesis, we will be dealing with the barriers related to the uncertainty concerning the process of home/public charging and the difficulties in calculating charging energy costs from a consumer point of view. Moreover, we will address some technical challenges concerning the charging duration for different vehicles and the potential of different types of charging infrastructure for an efficient charging process.

The battery price accounts for a significant portion of the overall cost of BEVs, so lowering it is essential, which helps in reducing the effect of the high purchase price barrier that is one of the major financial barriers against EV adoption. Some surveys and forecasts expect the prices of batteries to drop in the future thanks to the technology development of Lithium-ion batteries, as shown in Figure 6.

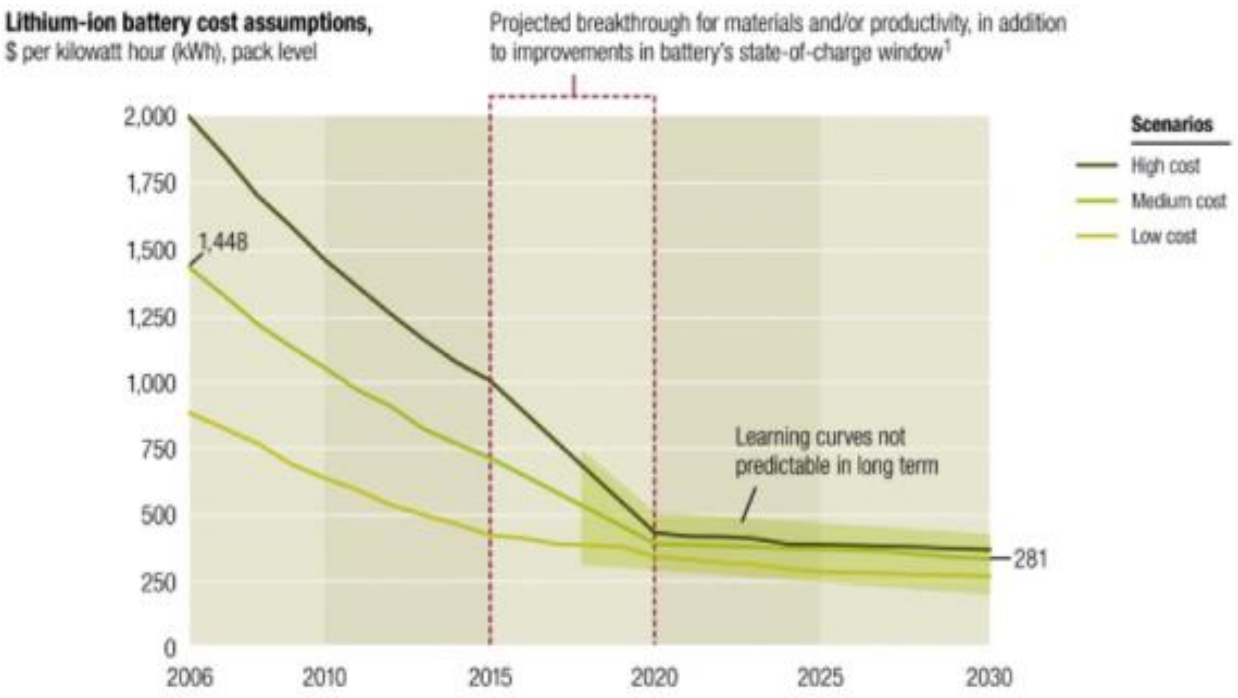

Figure 6: A McKinsey analysis of Lithium-ion battery cost evolution, assuming learning effects and technology breakthrough

Source: (Mahmoudzadeh Andwari et al., 2017).

2.2 ELECTRIC VEHICLE TECHNOLOGIES

Un-Noor et al. (2017) and European Environment Agency,(2019) define four types of EVs based on the energy sources each vehicle is as shown in Figure 7 equipped with and could be categorized as follows:

2.2.1 Battery Electric Vehicle (BEV):

BEVs are electric vehicles that rely solely on the energy contained in their battery packs to power the drivetrain, which makes their range directly proportional to the battery power. Charging the battery pack after it has been drained takes up to 36 hours. BEVs emit no GHG, generate no noise, and are therefore environmentally friendly. Figure 8 presents the basic configuration of BEVs where we see the wheels being propelled by an electric motor(s) that is driven by batteries via a power converter circuit.

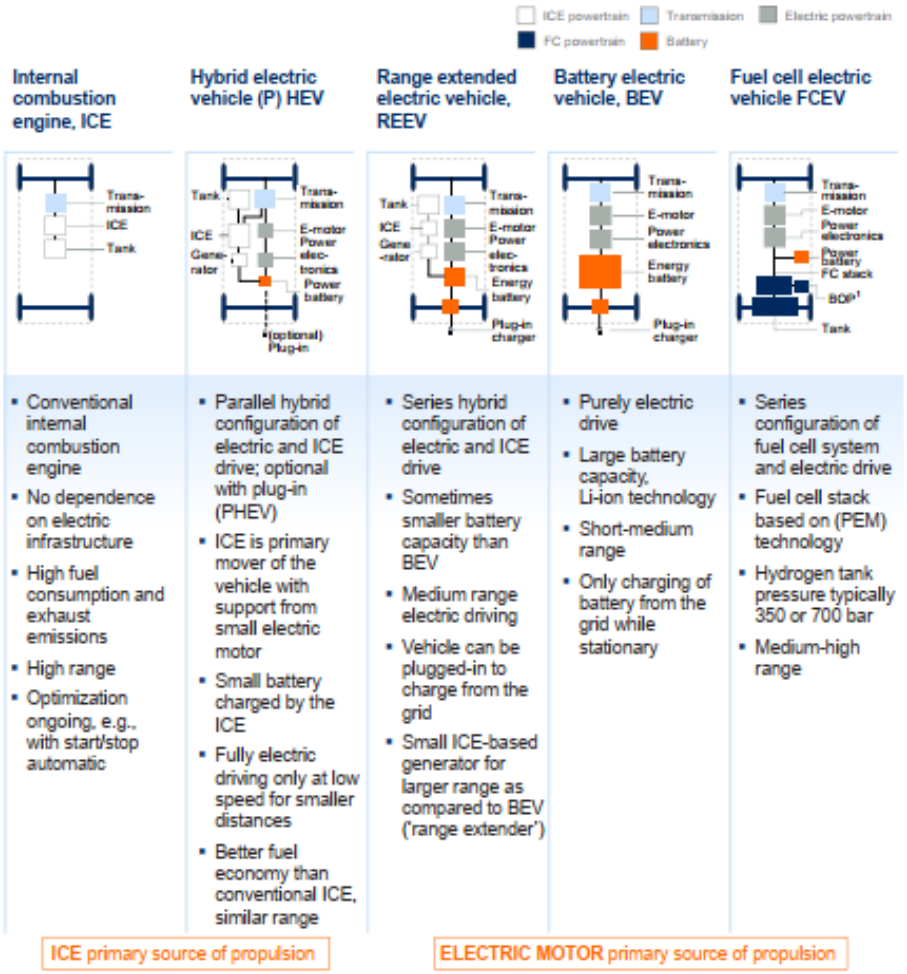

Figure 7: Different powertrain technologies in detail.

Source: (European Environment Agency, 2019)

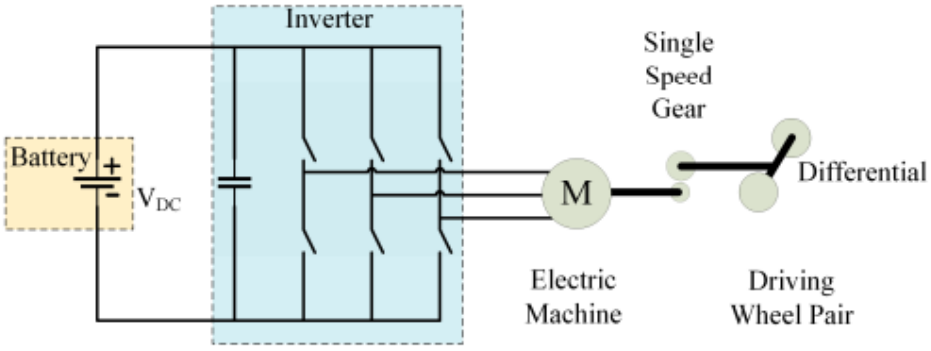

Figure 8: BEV configuration. The battery's DC-AC power conversion to power the motor.

Source: (Un-Noor et al., 2017).

2.2.2 Hybrid Electric Vehicle (HEV):

HEVs are powered by different combinations of an ICE and an electrical power train. The ICE mode is considered as the main driving power while the electric propulsion system is activated only for low power demands, which makes it an interesting technology in low-speed conditions like urban areas. HEVs reduce fuel consumption and GHG and other pollutant emissions because of relying primarily on the electric propulsion system during idling periods leaving the ICE entirely off, and that minimizes the effect of the residues produced from the partial fuel combustion that can damage the exhaust system faster. When more power is needed, the HEV switches to the ICE. However, the two drive trains may also cooperate for better performance. Therefore, HEVs are essentially ICE-powered vehicles that use an electric drive train to increase mileage or improve efficiency. Figure 9 shows an example of one configuration type of HEVs.

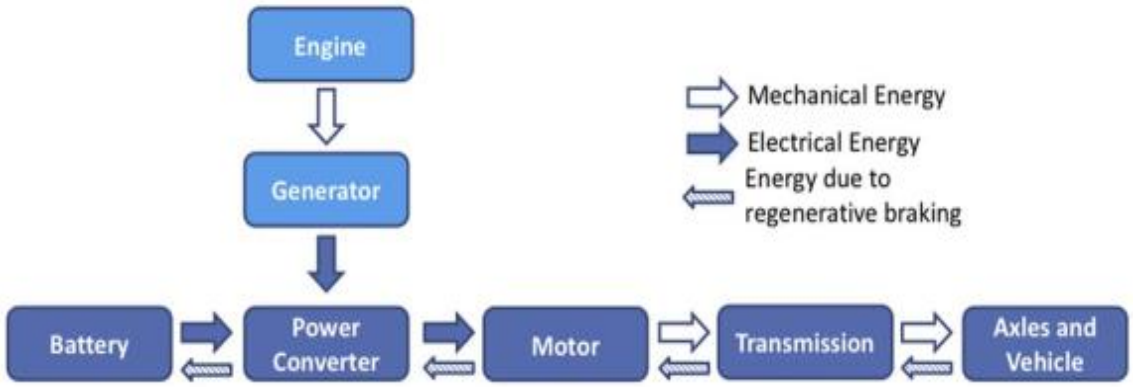

Figure 9: Principle of ICE series hybrid vehicles.

Source: (Mahmoudzadeh Andwari et al., 2017)

2.2.3 Plug-In Hybrid Electric Vehicle (PHEV):

PHEVs represent an example of HEVs equipped with an all-electric range. The main difference, compared to HEVs, is that they can run solely on the energy stored in their battery packs and shift to the ICE mode only when the batteries are low in charge, which makes their gas emissions lower than that of the HEVs. This means that the ICE helps in improving the range and recharges the batteries, and larger batteries are required.

2.2.4 Fuel Cell Electric Vehicle (FCEV):

FCEVs or Fuel Cell Vehicles (FCVs) are powered by the electricity produced from hydrogen fuel combustion with oxygen through a chemical reaction that produces only water and zero carbon emissions. Excess energy is stored in energy storage devices such as batteries and supercapacitors. The major advantage of these vehicles is the refilling time that is almost the same as that of the ICEVs at a gas station. But there are also safety issues if flammable hydrogen leaks from the tanks. A simple configuration of the FCEV is presented in Figure 10.

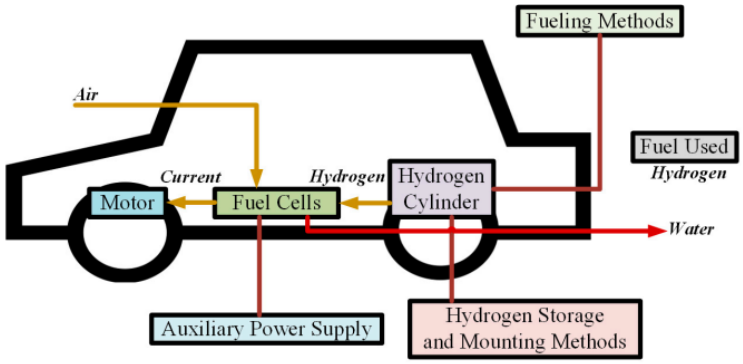

Figure 10: FCEV configuration. Oxygen from air and hydrogen from the cylinders react in fuel cells to produce electricity that runs the motor. Only water is produced as a by-product which is released into the environment.

Source: (Un-Noor et al., 2017)

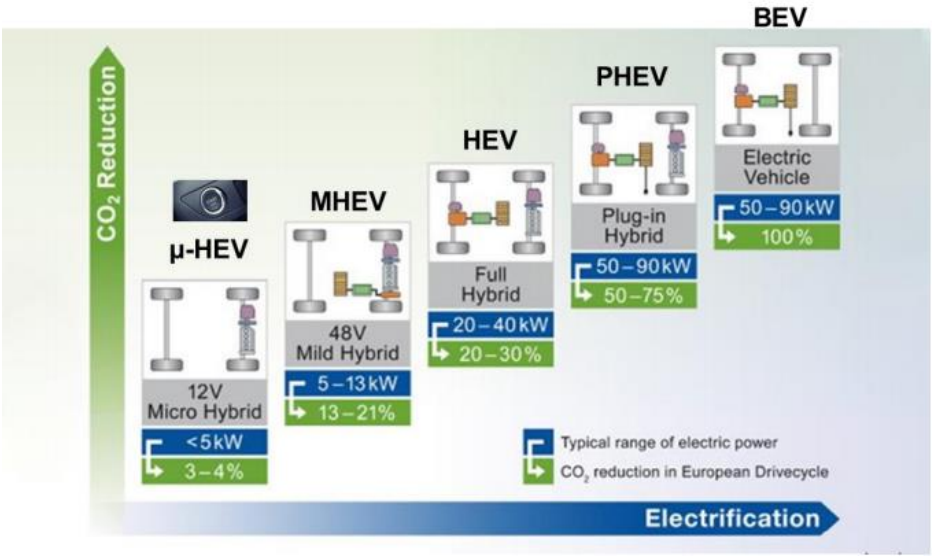

Figure 11: Electrification evolution.

Source: (Oestreicher, 2020)

In this research, we consider having only BEVs for the simulation of our both optimization models because they are generally equipped with larger battery packs of bigger energy capacities that means a higher impact on the power grid. Moreover, BEVs represent a more promising technology for having almost zero noise pollution and no GHG emissions compared to PHEVs, as shown in Figure 11.

2.3 BATTERY ELECTRIC VEHICLE COMPONENTS

The main components of BEVs were well explained by Mahmoudzadeh Andwari et al.,(2017). In Figure 12, the EV components can be classified into a high voltage (HV) battery pack, battery management system (BMS), power electronics unit (PEU), and the electric motor that provides a traction force to the wheels.

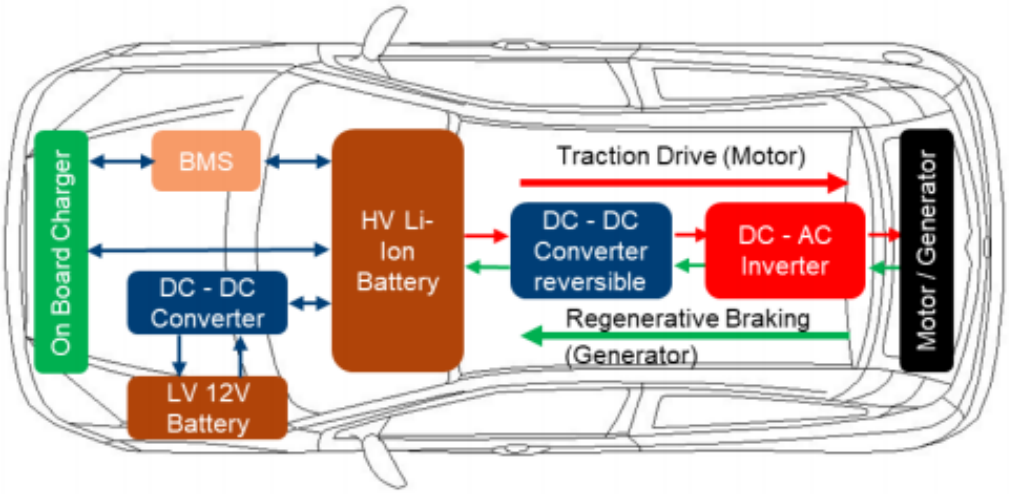

Figure 12: EV block diagram.

Source: (Oestreicher, 2020)

2.3.1 Batteries

Battery packs are made up of several modules that are connected in parallel to produce the required charge capacity and have identical nominal voltage as the battery pack. Each module is made up of identical cells that are bound in series resulting in the nominal voltage. Figure 13 shows the manufacturing process of the battery packs for EVs. For BEVs, the battery is typically sized based on the amount of energy required to reach the required range set by the manufacturer.

Table 7: Common battery types, their basic construction components, advantages, and disadvantages.

Source: (Un-Noor et al., 2017)

Battery Type	Components	Advantage	Disadvantage
Lead-acid	• Negative active material: spongy lead • Positive active material: lead oxide • Electrolyte: diluted sulfuric acid	• Available in production volume • Comparatively low in cost • Mature technology as used for over fifty years	• Cannot discharge more than 20% of its capacity • Has a limited life cycle if operated on a deep rate of SoC • Low energy and power density • Heavier • May need maintenance
Li-Ion (Lithium-Ion)	• Positive electrode: oxidized cobalt material • Negative electrode: • carbon material • Electrolyte: lithium salt solution in an organic solvent	• High energy density, twice of NiMH • Good performance at high temperature • Recyclable • Low memory effect • High specific power • High specific energy • Long battery life, around 1000 cycles	• High cost • Recharging still takes quite a long time, though better than most batteries
Ni-Zn (Nickel-Zinc)	• Positive electrode: • nickel oxyhydroxide • Negative electrode: zinc	• High energy density • High power density • Uses low-cost material • Capable of deep cycle • Friendly to environment • Usable in a wide temperature range from -10 ◦C to 50 ◦C	• Fast growth of dendrite, preventing use in vehicles

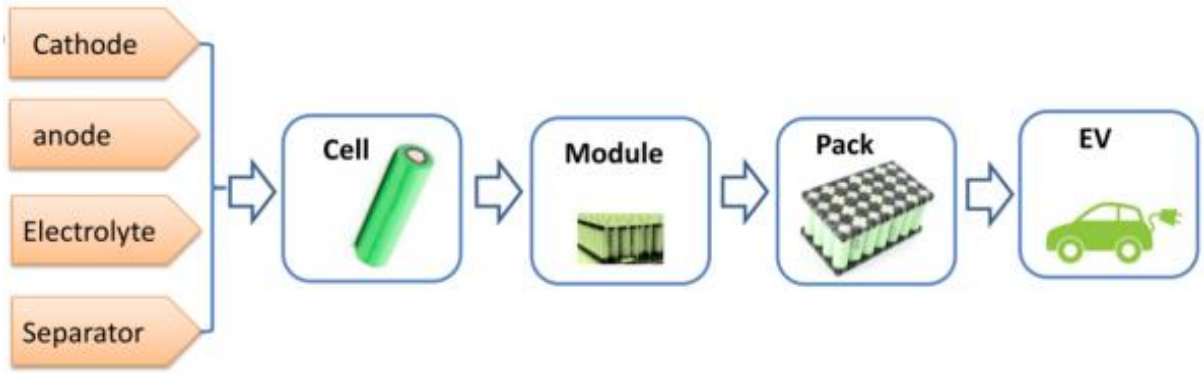

Figure 13: The schematic diagram of the manufacturing process of battery packs for EVs.

Source: (Ding et al., 2019)

Battery packs have been the primary energy source for EVs using various battery technologies characterized by high energy density and high power density. The energy capacity, power density, cycle life, calendar life, cost per kWh, volume, safety, and energy efficiency are the most critical parameters to consider when comparing batteries, according to Mahmoudzadeh Andwari et al.,(2017). Table 7 summarizes the different characteristics of common battery types. In this research, we focus more on the technology of lithium-ion battery cells, where we assume that the considered EVs are made up of packs of several lithium-ion batteries.

2.3.2 Battery Management System

According to Warner,(2014), the battery management system (BMS) is probably the most essential component in the EV because it is in charge of measuring the battery's output and adapting the system to accommodate the consumption and environment. Mahmoudzadeh Andwari et al.,(2017) explain the different components of an EV and highlight two prominent roles of the BMS that ensure an efficient and secure functionality to the battery packs.

The first role is tracking the battery for details such as its State of Health (the battery's capacity to produce its specified output), State of Charge, and Remaining Life Cycle, and communicate it to the onboard systems during both the charging and discharging process. The second role is ensuring a safe, efficient, and non-damaging battery operation by balancing the charge within each cell and extend the stack's lifespan because balancing the charge among all cells is necessary since the cell characteristics vary slightly, as in Figure 14. This might cause overheat for some weak batteries that get fully charged while others are not, and the same happens during the discharging process.

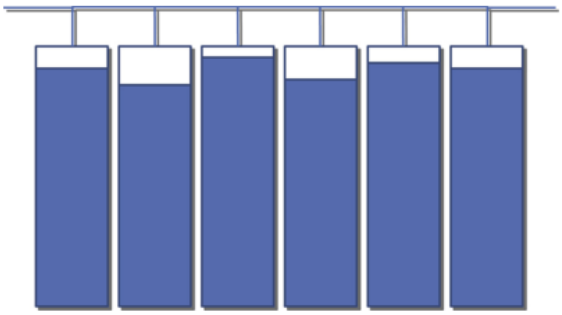

Figure 14: Example of unbalanced cells.

Source: (Warner, 2014)

2.3.3 Electric Motors

There are several benefits of using electric motors over ICEs, like having higher power conversion efficiency in the range of 70% to 90%, besides offering a high torque and power density. Moreover, electric motors are quiet, provide rapid and smooth acceleration, and can be used as generators while braking to recover electricity. Electric motors could be DC or AC motors, each of different types. The regular maintenance of DC motors due to the existence of commutators and brushes that are in touch and vulnerable to wear makes AC motors a better technology for BEVs. Chau et al.,(1999) define three main types of AC motors typically installed in BEVs: Induction, switched reluctance, and permanent magnet (PM) brushless motor.

2.3.4 Power Electronics Unit

The Power Electronics Unit (PEU) consists of power electronics that serve as intermediaries among the other electric components of the EV. Figure 15 shows an EV power flow block diagram where the power supplied by the EVSE is converted inside the PEU from AC to DC using an AC-DC converter (Rectifier) and then stored in the battery packs during charging. Then during the discharge process, the DC power is converted back into AC power using a DC-AC inverter to drive and fed to the AC electric motor while a portion of the power stored in the batteries passes through a DC-DC converter (Buck converter) to reduce its voltage making it suitable for other auxiliaries.

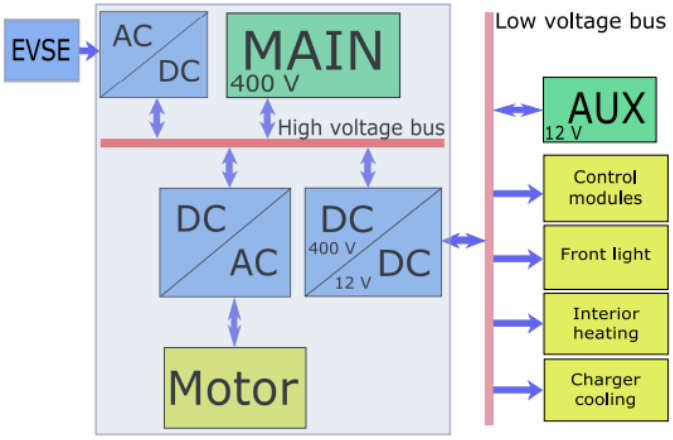

Figure 15: EV power flow block diagram.

Source: (Kieldsen et al., 2016)

2.4 CHARGING INFRASTRUCTURE

A battery charger is a combination of an AC-DC rectifier and a DC-DC converter that are responsible for transferring energy to the rechargeable battery packs after processing and controlling the electric current passing through them. The simple configuration of the basic components of a battery charger is shown in Figure 16, where the battery is plugged into a 3 phase power supply through the charger. Charging EVs is a bit more complicated when it comes to real-time applications, and that's because of the different types of EVs and various types of chargers. EV charging is done by either an onboard charger or an off-board charger with a unidirectional or bidirectional power flow. European Environment Agency,(2019), Shareef et al.,(2016), and Yilmaz & Krein,(2013) categorize the charging infrastructure system based on the mode of energy transfer, charging power level, electrical current, and other standards like plugs and connectors.

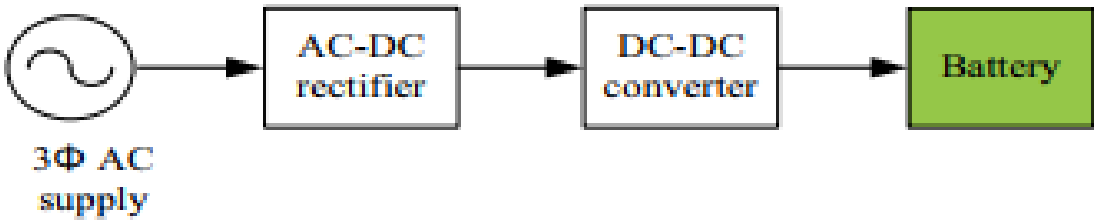

Figure 16: Basic components of a battery charger.

Source: (Shareef et al., 2016)

2.4.1 Available Charging Systems

The types of charging systems are determined based on the way of transferring energy from the power supply into the battery packs. The different types of charging systems are illustrated in Figure 17, which shows their main characteristics, charging duration, suitable applications, and current availability in the European market. These types are Battery swapping, inductive (wireless) charging, conductive (wired) charging.

	Energy source				
	GASOLINE/DIESEL	HYDROGEN	BATTERY		
					
	Fueling gasoline or diesel at a petrol station	**Fueling hydrogen at a hydrogen refueling station**	**"Wired" charging using a plug**	**Battery swapping**	**Induction charging**
Description	Conventional gasoline or diesel refueling	Hydrogen refueling (similar to natural gas refueling)	Plugging in to a charging station using a cable and plug	Replacing a battery for a fully charged one at a special swapping station	Battery in the car is charged by wireless induction charging
Time needed[1]	5 min	5 min	4-8 hrs (slow) 20-30 min (fast)	5 min	~2-8 hrs[2]
Suitable for which power-trains	▪ ICE ▪ HEV ▪ PHEV ▪ REEV (gasoline)	▪ FCEV ▪ REEV (hydrogen)	▪ PHEV ▪ BEV suitable for plug-in charging	▪ Special BEVs suitable for battery swapping	▪ Special BEVs suitable for induction charging
Example car	▪ All ICEs	▪ Hyundai ix35 (FCEV)	▪ Renault Zoe (BEV)	▪ Special model of Renault Fluence	▪ N/A (few pilot cars)
Current availability in Europe	Widely available: ~131,000 stations	Very limited: ~80 stations	Limited availability: >20,000 (slow) >1,000 (fast)	Very limited ~50 stations	Not available (few pilots in progress)

Figure 17: Electric powertrains: Charging infrastructure archetypes.
Source: (European Environment Agency, 2019)

2.4.1.1 Battery Swapping

Battery swapping is based on replacing the discharged EV battery with a fully charged one at a special swapping station. Swapping the EV battery takes a few minutes and preserves long battery life. However, this charging system is still very limited in terms of availability and acceptance by EV manufacturers (Ahmad et al., 2020).

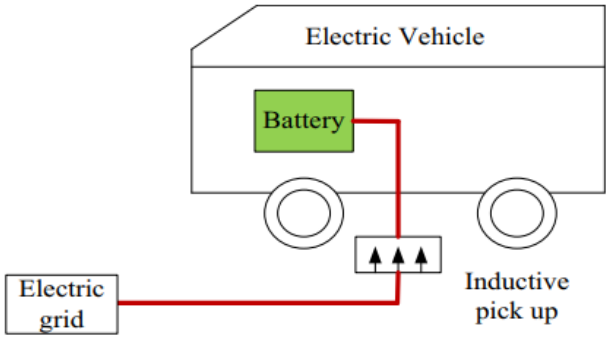

Figure 18: Inductive charging.

Source: (Shareef et al., 2016)

2.4.1.2 Inductive charging

Inductive or wireless charger transfers electric current to the EV battery using an electromagnetic field that is created on a surface underneath the car, as shown in Figure 18. It represents a safer charging technique as no plugs and connectors are required, but it has low efficiency and high power losses and not compatible with most EVs.

2.4.1.3 Conductive charging

Conductive charging is the most common type of charging EVs for its simple configuration and high efficiency. This charging type is based on transferring power into the battery packs through via a physical cord of specific plugs and connectors suitable for each EV type. Wired charging could be an onboard method as shown in Figure 19 or and an off-board method as presented in Figure 20.

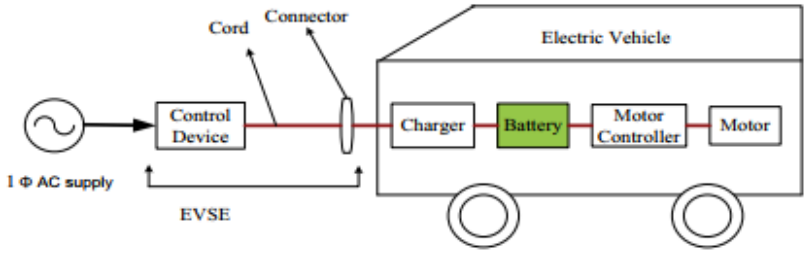

Figure 19: EVSE arrangement for onboard AC slow charging.

Source: (Shareef et al., 2016)

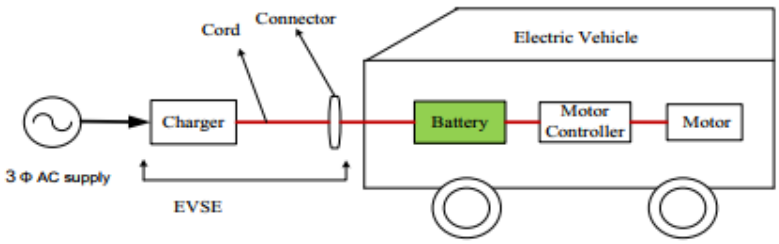

Figure 20: EVSE arrangement for off-board DC Fast Charger(DCFC).

Source: (Shareef et al., 2016)

The main differences between the onboard and off-board chargers could be understood by comparing Figures 19 and 20. When charging using the onboard chargers, the AC EVSE consists of a control device that communicates with the BMS installed in the EV for current control. The AC power conversion takes place inside the vehicle's PEU before being fed into the battery packs, which explains the existence of onboard power limits specified for each EV.

However, off-board chargers that are themselves the EVSE are also responsible for rectifying and converting the AC power into a DC power supply that bypasses the onboard charger and charges the battery packs, as shown in Figure 21. Off-board chargers are more unrestricted in size limitations and power capacities but at the same time more expensive. In our research, we will consider using only conductive onboard chargers for charging both the residential and commercial EVs in the simulation of both models.

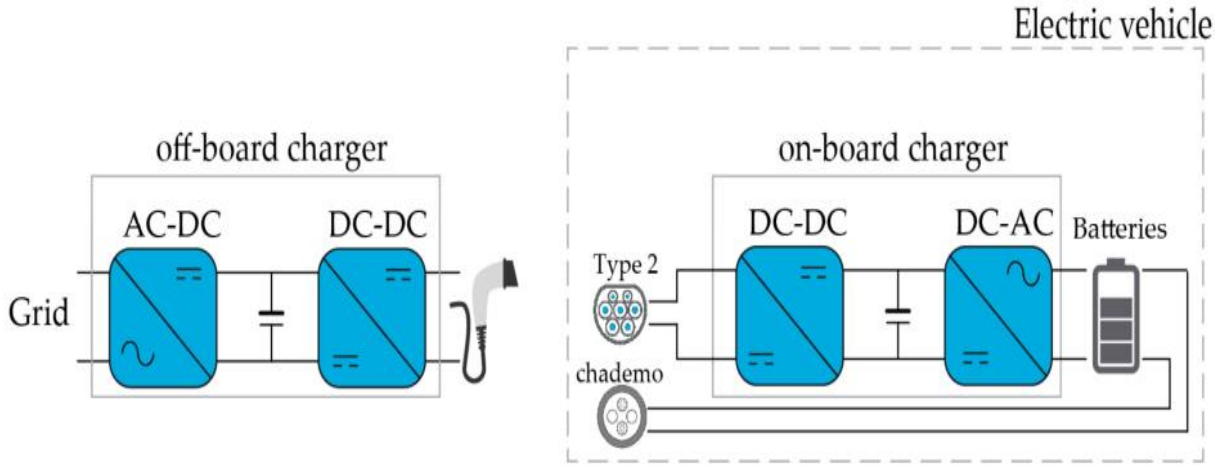

Figure 21: Off-board and on-board chargers for an electrical vehicle (EV).

Source: (Barone et al., 2020)

2.4.2 Charging Power Levels

In this section, we categorize battery chargers according to their output power levels, where normal power or slow charging refers to single-phase AC EV chargers with a power level up to 3.7 kW and a maximum current of 16 A equivalent to the standard domestic sockets. Medium power or quick charging corresponds to dedicated single or three-phase EVSE with a power level up to 22 kW and a charge current up to 32A per phase. Finally, high power or (fast charging) refers to either AC three-phase chargers or DC fast chargers with a charging power superior to 22 kW. This classification is defined by Falvo et al.,(2014), who present the international standards of the charging infrastructure, including the types of chargers, plugs, and connectors available in North America and Europe. Table 8 represents a summary of the EV charging standards in the European case with providing the most relevant applications for each power level.

Table 8: Electrical ratings of different EVS charge methods in Europe.

Source: (Falvo et al., 2014)

Charge Method	Connection	Power [kW]	Max current [A]	Location
Normal power (slow charging)	1-Phase AC connection	3,7	10-16	Domestic
Medium power (quick charging)	AC connection 1- or 3-phase	3,7 - 22	16-32	Semi-Public
High power (fast charging)	3-phase AC connection	> 22	> 32	Public
High power (fast charging)	DC connection	> 22	> 3,225	Public

2.4.3 Charging Clusters

Clustered charging technologies have not been fairly addressed until now as the majority of the researches talk about DC fast chargers and single phase. Charging clusters devices are pretty similar to dual chargers that are currently installed in public car parks, shopping centers, etc. (enel X, n.d.; pod POINT, n.d.-b). Žitnik & Mehle,(2014) and Bedogni et al.,(2015) define the cluster as a collection of public or semi-private EVSE that allows several EVs to be charged simultaneously under a specific power capacity that is optimized for each cluster by the Charging Station Operator (CSO) taking into consideration the grid situation of supply and demand.

The main benefit of using clusters is to exchange data between the clusters themselves, between the cluster and its EVSE, and between the cluster and the smart grid for the aim of reducing power demand at the same time of allowing EVs to retrieve the highest possible power while charging. Žitnik & Mehle,(2014) proposed the smart charging infrastructure shown in Figure 22 for semi-private applications that is made up of:

- The CSO is responsible for controlling the power flow among all equipment after collecting demand and capacities data
- Demand Side Module (DSM) that allows the CSO to manage remotely the charging system
- Master cluster that is connected directly to the DSM and collects data from other slave clusters about the current and power capacities for each EVSE and the power demand required for the plugged EVs based on their battery state of charge.
- Slave clusters that receive signals and charging plans from the cluster master

In this research, we consider having EV clusters for the commercial and industrial scenario only for charging the medium-duty electric freight vehicles, and we analyze the effect of the power capacity and the number of sockets available in each cluster.

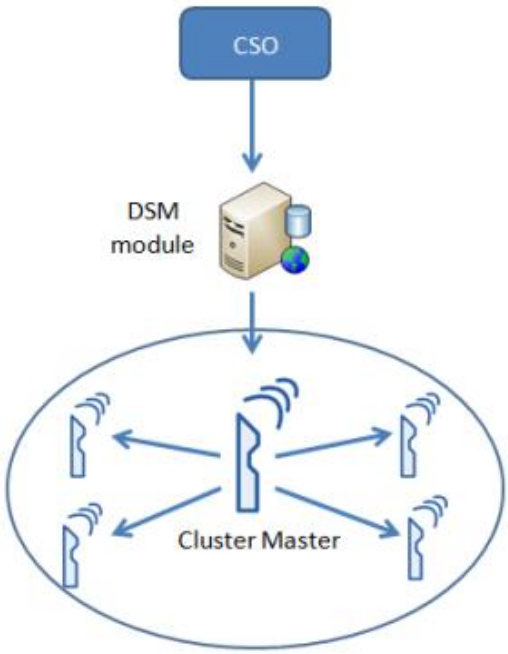

Figure 22: CSO-controlled power management.

Source: (Žitnik & Mehle, 2014)

2.5 SMART CHARGING

2.5.1 Smart Charging Strategies

The concept of smart charging is as simple as a process of facilitating the EV integration in the power system through controlling the demand of both the power grid and the EV users while satisfying the mobility needs. Smart charging lowers the costs of reinforcing power grids and reduces simultaneity peak demand, unlike uncontrolled charging. Hildermeier et al.,(2019) stated, "smart EV charging can integrate increasing amounts of renewable energy resources, increase utilization of the existing network infrastructure, lower the operating cost of EVs, and minimize the need for new investment.". There are plenty of studies that discuss the economic and technical benefits of EV-grid integration.

Some research like Hildermeier et al.,(2019a) and IRENA,(2019) provide a clear definition of smart charging and highlight the benefits it offers to enhance EV adoption and integration. Moreover, they discuss the importance of some forms of energy policies and incentives given to EV users, like "time-of-use pricing" that encourages EV users to shift their charging periods towards off-peak periods to minimize peak power demand. IRENA,(2019) mention five main smart charging strategies that are currently in use and are as follows:

2.5.1.1 Time-of-use- pricing without automated control:

The user himself chooses his charging periods based on the least energy costs during the day by physically plugging or unplugging the EV into the EVSE.

2.5.1.2 Dynamic pricing with automated control:

It's based on reducing the charging energy costs by allowing the EV to be automatically charged during periods of low electricity prices that vary during the day.

2.5.1.3 Basic controlled (on/off):

This strategy is based on the charging scheduling of EVs throughout the day in a way to reduce the peak power demands, but it doesn't include charging current adaptations, so the EV charger always retrieves the rated power value.

2.5.1.4 Unidirectional controlled charging (V1G):

This strategy includes charging rate adjustment for the power consumed depending on the price of electricity, the grid and the charger capacity, and the EV's SOC.

2.5.1.5 Bidirectional controlled charging (V2G, V2H, V2B):

Vehicle-to-Grid (V2G) gives EVs the potential to be considered as ancillary services on periods of peak demand and involves a power flow from EVs towards the grid and vice-versa (Yilmaz & Krein, 2013b). Similarly, Vehicle-to-House (V2H) and Vehicle-to-building (V2B) consider EVs to act as supplement power suppliers to the house or the building and serve as an Energy Storage System (ESS)as in Figure 23.

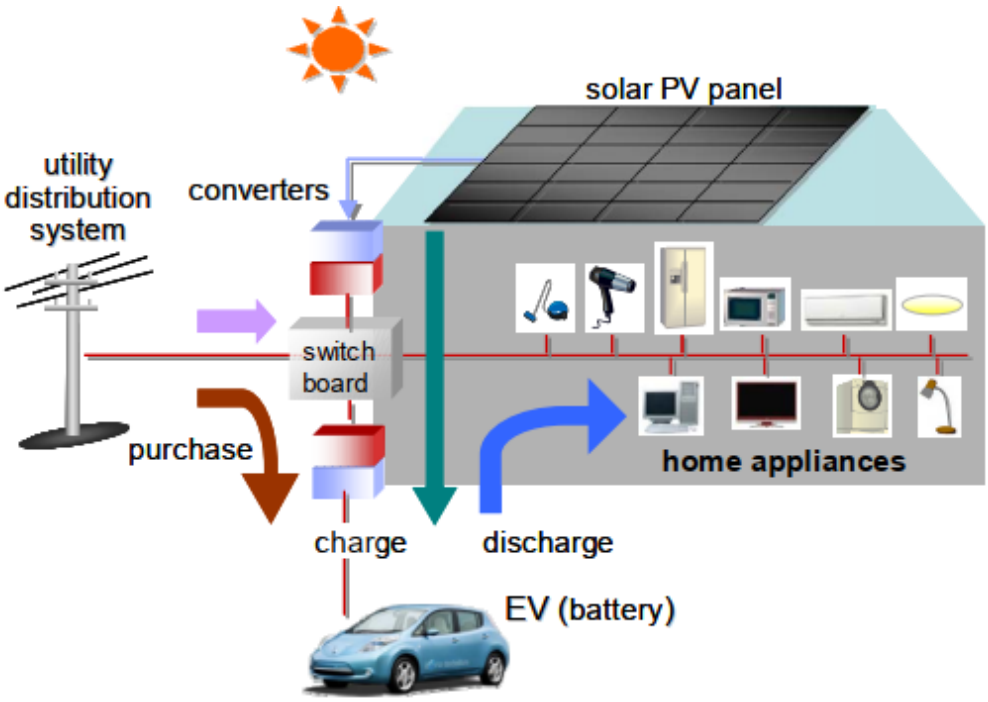

Figure 23: EV charging and PV integration in a house using a V2H smart charging scheme.

Source: (Yoshimi et al., 2012)

Such technologies allow EVs to be charged during periods of the day with low energy costs and then supply their access energy to the house/building during periods of high energy prices, which helps in reducing the electricity bill (C. Liu et al., 2013). Figure 24 illustrates these advanced strategies of smart charging. This research is based on the unidirectional controlled charging strategy of a one-way power flow from grid to EVs based on the lowest energy costs and relatively lower power demands.

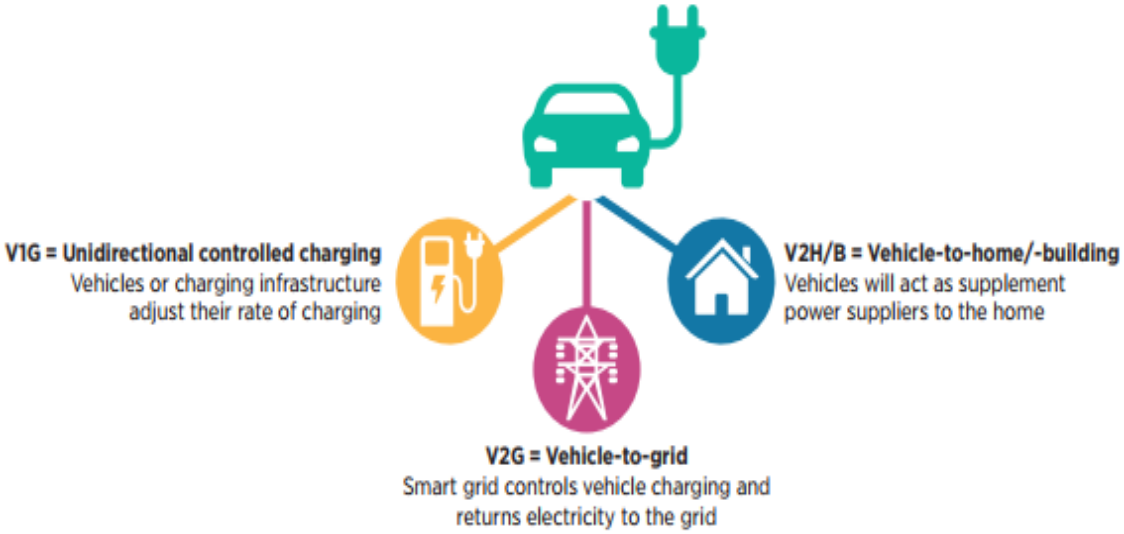

Figure 24: Advanced forms of smart charging.

Source: (IRENA, 2019)

Smart charging strategies offer plenty of benefits over the standard charging method. This fact drives scientists and researchers to invest more in exploring new opportunities. Yilmaz & Krein,(2013b) highlight the differences among both the controlled and uncontrolled charging methods and address the benefits offered by smart charging in different aspects like the reduction of power losses and the enhancement of the power quality.

White & Zhang,(2011) explore the potential of using the V2G service with PHEV mainly for peak reduction and some financial return for EV users. In addition to showing the effect of high V2G participation rates in frequency regulations and market energy saturation. Similarly, Wali et al.,(2019) analyze the cost benefits of a smart charging schedule for V2G applications from an EV-user point of view. Loisel et al.,(2020) examine the opportunity of V2G and G2V schemes for a large-scale deployment of EVs in Germany by 2030 and shows that high EV integration doesn't hamper the system stability and can contribute to higher integration of intermittent renewable energy sources (RES) mainly wind and photovoltaic (PV). The integration of RES into the transport and electricity sectors through the three different bidirectional charging schemes is well explained in (Lund & Kempton, 2008; Mwasilu et al., 2014; Yoshimi et al., 2012).

2.5.2 Smart Charging Related Works

Talking about smart charging means a combination of smart pricing strategies, smart technologies, and smart charging infrastructure. Hildermeier et al.,(2019a) present several smart pricing methods that are implemented in different countries in Europe other than the standard tariff, such as time-of-use (TOU) tariffs based on setting a specific price for different time blocks. Real-time pricing requires a smart meter to monitor the actual power and demand conditions across the grid. Limmer(2019) gives an overview of the dynamic pricing strategy and defines it as a demand response that encourages EV users to shift their charging schedule and power consumption based due to financial incentives. Dynamic pricing involves adapting the electricity price dynamically by the DSO or an operator of charging stations depending on the power supply and demand across the power grid.

Smart charging infrastructure is more expensive and more complicated than conventional EV charging stations (Yilmaz & Krein, 2013b). It requires the installation of a dedicated measurement system and special smart meters that constantly monitor the EV and grid parameters. In addition to a bidirectional communication connection and control to send signals among the grid, charging station, and the BMS installed in the EV. Several studies have been conducted to assess the potential effect of EV charging load on power systems. Some of these studies present smart charging optimization models like Montoya et al.,(2017) that focus on the electric vehicle routing problem with a non-linear charging function to explore cheaper optimal solutions.

Trippe et al.,(2015) and Hoke et al.,(2011) present two charge scheduling optimization models of a charging cost minimization problem, where the first applies the optimization model on a sample of passenger BEVs, and considers the effect of cycle battery aging in the cost objective function. However, the second is applied to PHEV and includes the impact of lithium-ion battery degradation costs in the optimization model. Turker et al.,(2014) solve a cost minimization problem of PEVs in a residential neighbourhood by generating an offline heuristic algorithm and considering two types of energy prices.

Table 9: Annual relative peak power reduction under a different scenario.

Source: (Ghotge et al., 2020)

Nr.	Scenario	Relative peak power reduction (%)
Ref.	Unscheduled charging	0%
1	No EV forecast	16% (↓)
2	Average EV forecast	36% (↓)
3	Robust EV forecast	39% (↓)
Ref.	Perfect forecasting	54% (↓)

Ghotge et al.,(2020) propose an optimization schedule model that minimizes the peak power demand of a solar parking lot used for EV charging. They develop a smart charging strategy based on a Model Predictive Control method to deal with the uncertainty in the arrival and departure periods of the EVs and their energy needs. The research considers a parking lot of 40 parking spaces each equipped with a level 2 EVSE with a rated power of 7.4 (kW) and powered by a roof-mounted solar array over the parking spaces with a total power generation of 120 kW_p. Passenger EVs were considered, including HEVs and BEVs with battery capacities from $8\ (kWh)$ and up to $100\ (kWh)$. The total number of EVs is equal to the number of parking spots with an additional stand-alone battery of $50\ (kWh)$ capacity to store the excess power produced. The simulations were performed over a year time interval under different scenarios where the results are reported in Table 9 that show an additional peak power reduction of up to 54% when applying using a new forecasting strategy of higher accuracy.

Zhang et al.,(2012) present another example of peak reduction optimization models for a quadratic programming problem of EV charge scheduling at a large scale. In (Zhang et al., 2012), multiple case studies of the national power demand of the U.K. are considered with a series of different EV penetration levels from 10% and up to 50% of the total registered cars in the U.K. of about 28.4 million vehicles. Four scenarios were assumed of several charging behaviours of different charging modes considered to be either at home or public stations over a time horizon of 24h, besides performing an error and sensitivity analysis on the optimization model to improve the obtained results. The paper concluded that EV charging load shows high potential in flattening the national power demand curve in the U.K., especially in the EV fast-charging scenarios. Moreover, the increase in EV penetration level from 10% to 50% contributes to a gradual reduction in the power demand profile's fluctuations.

Pelletier et al.,(2018) consider a charge scheduling problem for electric freight vehicles (EFVs) and propose an optimization model to minimize the total charging cost while ensuring the energy needed to perform the routes assigned to each vehicle. This model allows charging to take place only at the depot and takes into consideration several factors like grid restrictions, degradation costs, time-dependent energy costs, and facility-related demand (FRD) charges. The experiments performed were based on a charging infrastructure composed of a reasonable number of DC fast chargers and level-2 AC chargers over a planning horizon of three days.

In (Pelletier et al., 2018), five test instances were generated for different EFV sizes of three, six, and nine and assumed that each EFV would perform two routes per 24-h interval. The results showed that the strategy of splitting long travel routes into several shorter ones contributes to the reduction of the total costs when considering the degradation costs, which goes along with the EV nature of a limited range. Moreover, it showed that an optimization model based on the combination of energy, FRD, and degradation costs reflects positively on the cycle and calendar lifetime of the batteries.

This research proposes two Mixed Integer Linear Programming (MILP) problems that refer to two different EV charge scheduling problems. The first problem is based on a commercial and industrial scenario (CIS) where we create a mathematical model to optimize the charging schedule of medium-duty electric trucks using a clustering technology for the charging infrastructure. This model aims to explore the potential of clustered charging techniques for charging commercial EVs overnight at a minimum cost taking into consideration the effects of grid restrictions and charging interruptions similar to the work done in (Pelletier et al., 2018).

The second optimization model is a two-stage EV charging problem of a residential scenario. The primary stage seeks the reduction of the EV integration impacts on the power grid in a residential neighborhood as the first from a DSO point of view through developing a peak shaving model (PSM). However, the second one aims to minimize the total electricity bill for each housing of EV users in the neighbourhood by creating a charging cost reduction model (CCRM) and analyze the effects of smart pricing, EV penetration levels, and different approaches for the two-stage interface of the optimization model.

3 BATTERY CHARGING PROCESS

EVs are commonly charged under a constant current-constant voltage (CC-CV) approach to minimize the impact of overcharging degradation that can cause permanent damage to EV batteries (Lam, 2011). CC-CV charging scheme is the most prevalent method for charging Li-ion batteries that are typically used in modern EVs (Lin et al., 2019). CC-CV method is developed from the combination of the two basic charging schemes CC and CV charging methods to increase the charging efficiency and overcome their major downsides such as overcharging or undercharging and battery capacity losses for the CC charging scheme and slow charging and overheat for the CV charging method. In section 3.1, we explain the CC-CV charging scheme and the methodology followed to estimate the charging profile of a lithium-ion battery cell. Charging losses are discussed in section 3.2, with the main factors affecting them. Then we simulate the charging profile of a lithium-ion battery cell of some EV models commonly used in commercial and residential applications in section 3.3. Finally, section 3.4 presents an analysis of some variable-current charging schemes generated based on the CC-CV one.

3.1 CONSTANT CURRENT-CONSTANT VOLTAGE CHARGING SCHEME

The battery charging behavior under the CC-CV method is illustrated in **Figure 25**, which consists of two stages of different characteristics. The first stage represents the CC phase, where the charging current I_{cc} is held constant at a preset value based on the power supply while the battery terminal voltage rises until it reaches a predefined maximum value V_{cv} when the second phase, the CV stage, is entered. The CV phase then holds the terminal voltage constant at V_{cv} while the charging current decreases exponentially with time to prevent overcharging and then battery degradation.

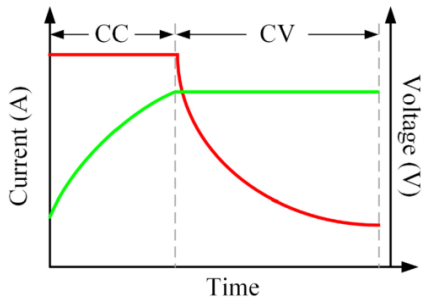

Figure 25: Constant Current-Constant Voltage charging scheme.

source: (Lin et al., 2019)

In general, the CC phase accounts for the major part of the charging process where the SoC of the battery increases linearly with time at the highest rate to reach at least 85% in many cases, then the SoC's rate starts decreasing during the CV charging phase with the exponential reduction of the electrical current till it reaches the cut-off value. The battery behavior models proposed by Tremblay et al.,(2007) and Pelletier et al.,(2017) help us better comprehend the CC-CV charging process and model the charging behavior of the vehicles used in our proposed models. During the CC phase, the battery behavior model requires a monitor of the instantaneous battery terminal voltage V_{term} that is a function of the instantaneous SoC and the charging current. The charging current remains constant during the CC stage and equals to the maximum current I_{cc} specified by the charger's manufacturer as shown in Eq. (1).

$$i(t) = I_{cc} \quad \forall t | V_{term}(t) < V_{cv} \tag{1}$$

The instantaneous SoC of the battery is estimated based on Eq. (2) and defined as the sum of the SoC in the previous period and the SoC variation, which is equal to the ratio of the charging current over the battery charge capacity Q (Ah) multiplied by the infinitesimal time. We assume that the charging current is positive while charging and negative during the discharge process.

$$SoC(t + dt) = SoC(t) + \frac{i(t) \cdot dt}{3600 \cdot Q} \tag{2}$$

Then, we calculate the battery's open-circuit voltage V_{oc} which refers to the battery's terminal voltage in the load-free situation as a function of the instantaneous SoC, the battery's constant voltage E_0, Q (Ah), the polarization resistance K (V/Ah), the exponential zone amplitude A (V), and the exponential zone time constant inverse B (Ah^{-1}) as in Eq. (3). The parameters E_0, K, A, and B are basically taken from (Marra et al., 2012). The combination of Eqs. (1), (2), and (3) produces Eq. (4), which estimates V_{term} till the end of the CC phase with assuming that the internal battery resistance is constant. V_{term} is always greater or equal to V_{oc} during the charging process whereas it's less than or equal to V_{oc} while discharging the battery. When V_{term} reaches the predefined maximum voltage V_{cv}, the CC stage is finished and the battery shifts into the CV charging mode where the voltage is held constant with the simultaneous decrease in the charging current value based on Eq. (5). Unlike the CC phase, the SoC's rate during the CV phase is no more constant and decreases with time simultaneously with the decrease of the charging current. We estimate it instantaneously by solving the differential Eq. (6). The numerical solution of the model proposed by Pelletier et al.,(2017) is illustrated in Figure 26.

$$V_{oc}\big(SoC(t)\big) = E_0 - \frac{K}{SoC(t)} + Aexp\Big(-BQ\big(1 - SoC(t)\big)\Big) \tag{3}$$

$$V_{term}(t) = V_{oc}\big(SoC(t)\big) + R \cdot i(t) \quad \forall t | V_{term}(t) < V_{cv} \tag{4}$$

$$i(t) = \frac{V_{cv} - V_{oc}\big(SoC(t)\big)}{R} \quad \forall t \geq t_s \tag{5}$$

$$\dot{SoC}(\mathrm{t}) = \frac{V_{cv} - V_{oc}\big(SoC(t)\big)}{R \cdot 3600 \cdot Q} \quad \forall t \geq t_s \tag{6}$$

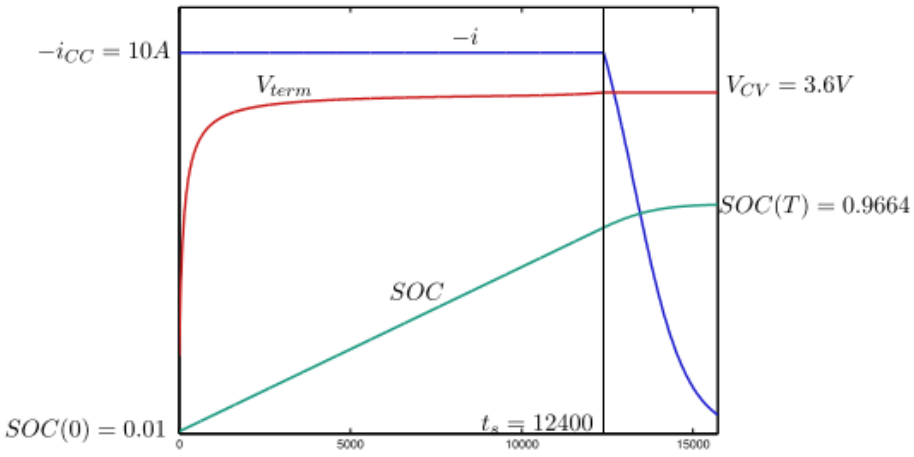

Figure 26: CC-CV charging scheme. The horizontal axis shows the time; the vertical axis is not in scale to simultaneously illustrate the behavior of current, voltage, and state of charge. The CC phase (t < t_s) is obtained explicitly from Eq. (2). The CV phase (t > t_s) is obtained as a numerical solution of the differential Eqs. (4)-(6).

source: (Pelletier et al., 2017)

For the sake of simplicity, we follow the same procedure of the simplified model in Pelletier et al.,(2017) to avoid solving differential equations and integrating current to determine charge rates. Our simplified model is based on discretizing the time horizon into short intervals of equidistant time steps Δt with a length of 10 seconds and under the assumption that the battery's power, terminal voltage, and current remain constant. Thus, the SoC is calculated at the beginning of each time step k according to Eq. (7) and for a given initial SoC and the current value applied during the previous time step that is equal to I_{cc} for the entire CC phase.

$$SoC_{k+1} = SoC_k + \frac{i_k \cdot \Delta t}{3600 \cdot Q} \tag{7}$$

Then we use Eqs. (8) and (9) to determine the open-circuit and the terminal voltage respectively, with the same assumption of constant internal resistance inside the battery. When the CV stage is entered, the electric current value at every time step isn't constant anymore and strictly less than I_{cc} and it is determined according to Eq. (10) as a function of the preset terminal constant voltage and the open-circuit voltage that corresponds to the SoC at the beginning of each time step k.

$$V_{oc}(SoC_k) = E_0 - \frac{K}{SoC_k} + Aexp\big(-BQ(1 - SoC_k)\big) \tag{8}$$

$$V_{term_k} = V_{oc}(SoC_k) + R \cdot i_k \tag{9}$$

$$i_k = \frac{V_{cv} - V_{oc}(SoC_k)}{R} \quad \forall k | V_{term_k} \geq V_{cv} \tag{10}$$

3.2 CHARGIN LOSSES

In real practices, the EV charging process, just like other energy transfer schemes, undergoes efficiency losses distributed among the different components of the charging system and have to be considered. Recent research conducted by Apostolaki-Iosifidou et al.,(2017) measures the charging and discharging losses across the different levels of the EV charging and discharging infrastructure. In this section, we focus only on the charging losses and specifically the current-rate related losses that occur in the PEU. Apostolaki-Iosifidou et al.,(2017) define two main ways of charging losses represented in the building electrical components that consist mainly of Electric Vehicle Supply Equipment (EVSE), circuit breakers panel, and transformer. The other losses are caused by the EV components that include the battery pack, PEU, and Vehicle Smart Link (VSL). The losses were measured on two types of passenger EVs charging in the same building with different charging AC values of 10, 30, and 50 A by installing multiple AC and DC meters across the various components of the electrical system and the EV as shown in Figure 27 besides the building sub-meter to measure the transformer losses.

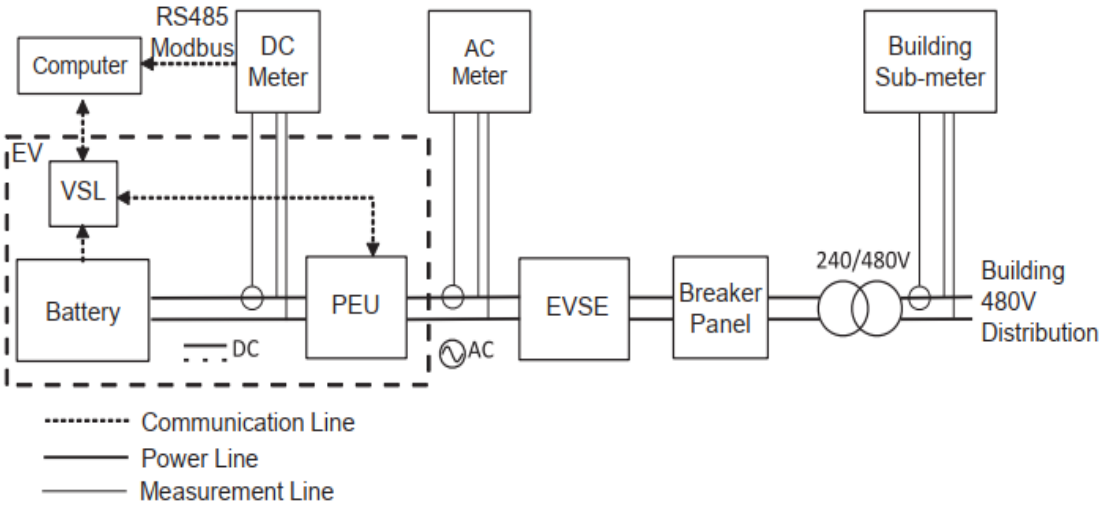

Figure 27: System components overview with the electric measurement system.

Source: (Apostolaki-Iosifidou et al., 2017)

$$l = \frac{P_{in} - P_{out}}{P_{in}} \times 100 \quad (11)$$

The power losses percentage l for each component in the system is calculated according to Eq. (11) where P_{in} and P_{out} correspond to the input and output power of the specified component respectively and based on the current flow direction. The results of the measured losses are presented in Tables 10, 11, and 12.

Table 10: Charging losses of building components.

Source: (Apostolaki-Iosifidou et al., 2017)

Component	AC current (A)	Percentage losses (%)
EVSE	10	0.10
	30	0.32
	42	0.29
Breakers	10	0.00
	30	1.50
	42	1.30
Transformer	10	10.20
	30	7.60
	42	3.33

Table 10 shows the losses measured across the building components at different input AC values of 10, 30, and 42 (A). We can see that the power losses across the transformer account for the major part of the building total losses at all the current values. However, the power losses in the transformer are the highest when charging with a slow charger and are inversely proportional to the current values. In general, the building total power losses are found to be the lowest for fast charging modes.

Table 11: Battery losses (%) as a function of the battery state-of-charge (SOC) and the AC values.

Source: (Apostolaki-Iosifidou et al., 2017)

AC current (A)	SoC			
	20%	40%	60%	80%
10	1.37	1.15	1.28	1.34
30	2.74	3.26	2.50	2.65
50	5.04	4.39	4.33	3.85
70	6.39	7.87	6.27	5.27

Table 12: PEU Charging Losses (%) as a function of the battery's SOC and AC value.

Source: (Apostolaki-Iosifidou et al., 2017)

AC current (A)	SoC			
	20%	40%	60%	80%
10	16.53	2.10	5.30	1.19
30	5.91	7.68	5.73	7.82
50	4.12	5.43	4.64	4.77
70	1.96	2.36	0.88	2.33

Tables 11 and 12 present the results of the charging losses measured across the battery and PEU respectively, as functions of the SoC of the battery and the EVSE input AC. By comparing the two tables, we notice that the power losses trend measured in the PEU at the SoC values 20% and 60% is similar to that of the transformer in Table 10, in the sense that lower power losses decrease with the increase of AC values used with having minor exceptions. On the contrary, the power losses measured in the battery at any SoC increase when using higher charging levels. Talking about the PEU charging losses in Table 12 as a function of the battery's SoC, we find remarkable fluctuations at the low current levels of 10 and 30 (A).

3.3 CONSTANT CURRENT-CONSTANT VOLTAGE CHARGING PROCESS SIMULATION

This section presents CC-CV charging simulations for four different Lithium-ion battery cells used in four different EV models of different design characteristics by referring to the simplified model proposed by Pelletier et al.,(2017) and using the Eqs. (7)-(10) discussed in section 3.1. The battery charging simulations take into consideration only the charging losses in the EV components, as shown in section 3.2 as a function of the battery's SoC. The simulations were performed using a Microsoft Excel worksheet, whereas the results visualizations were done in python using the Matplotlib library. The charging simulations refer to the EV charging problem of both the commercial scenario using one type of medium-duty electric freight vehicle (Mitsubishi Fuso, 2019) and the residential one using three different passenger electric vehicles (BMW, 2018; Nissan, 2017; Toyota, 2013).

3.3.1 Charging Simulation for a Lithium-Ion Battery Cell used in Commercial Electric Vehicles

We simulate the charging process for a 3.6V-38Ah Lithium-Ion battery cell that corresponds to a medium-duty electric vehicle having a total energy capacity of 82.8 (kWh) (Mitsubishi Fuso, 2019) using different current values I_{cc} in the CC phase and a maximum voltage V_{cv} of 3.6 (V) in the CV phase. Figure 28 illustrates a comparison of the charging simulation performed for the previously defined battery cell using two I_{cc} values: (a) refers to a 3.4 (A) DC value equivalent to a 0.085C charge rate that corresponds to the single-phase 32 (A) AC power supply of 7.36 (kW) power capacity. (b) corresponds to the usage of a three-phase power supply having a phasor current of 16 (A) a total power capacity of 11 (kW), and it is able to deliver a maximum DC current of 5.09 (A) equivalent to a 0.1275C charge rate.

Figure 28 shows that the time t_s at which the CV process is entered decreases as the value of I_{cc} increases. Similarly, as the value of I_{cc} increases, the SoC at time t at which the CV phase is entered decreases from 95% in (a) to 93.6% in (b) with current values of 3.6 and 5.09 (A) respectively. By comparing the two charging profiles, we notice that the non-linear part of the charging process that lies in the CV phase gets greater influence and has to be considered, especially when using the fast chargers where the CV stage is entered at a SoC lower than 80% as in (Pelletier et al., 2018). We approximate the discretized CC-CV charging process by a linear piecewise using a set of breakpoints fitted to the real CC-CV concave function and suitable for the evolution of SoC over time as in (Montoya et al., 2017).

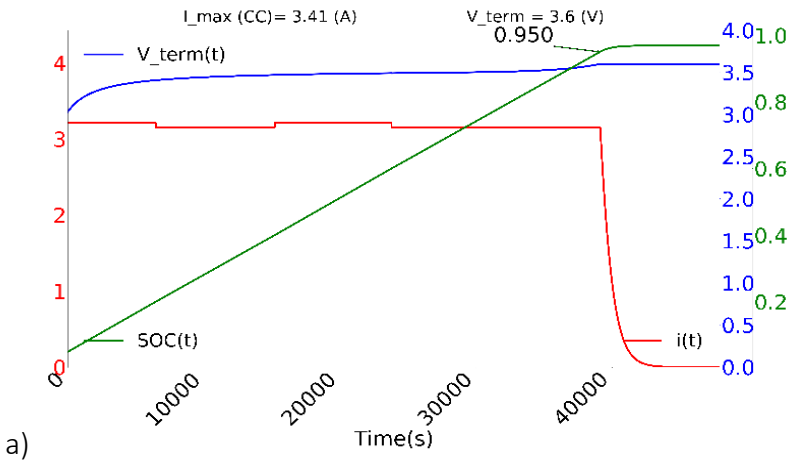

Figure 28: A comparison of the discretized CC-CV process of a 3.6V-38Ah lithium-Ion battery cell with different current values in the CC phase: (a) A single-phase EVSE of 7.36 kW power capacity (b) A three-phase EVSE of 11 kW power capacity

Figure 29 illustrates the approximated linear piecewise of the CC-CV charging process where the SoC increases with time while the battery is charged with multi-level charging rates between different breakpoints. The charge rate C could be defined as the ratio of charging current retrieved between two consecutive breakpoints over the total charge capacity Q and is reported at each breakpoint where we see an apparent declination in the charging rates when the CV stage is entered. The fluctuations in the current profile in the CC-phase are caused by the charging losses. The battery performs almost an entire charging event using one value for the I_{cc} in the CC phase.

For that reason, we replace the variable loss factor that is a function of the input AC values and the battery's SoC with an average weighted loss factor for both charging levels by neglecting the minor differences. We notice that when using the three-phase charger in (b), the linear approximation requires an additional breakpoint in the charging process to keep V_{term} under the predefined threshold compared to the number of breakpoints in (a), which charges with a relatively low current. Even though the CV phase is entered at relatively late SoC in both charging levels, still we set at least three breakpoints for our charging process to prevent the terminal voltage V_{term} from exceeding the design limits.

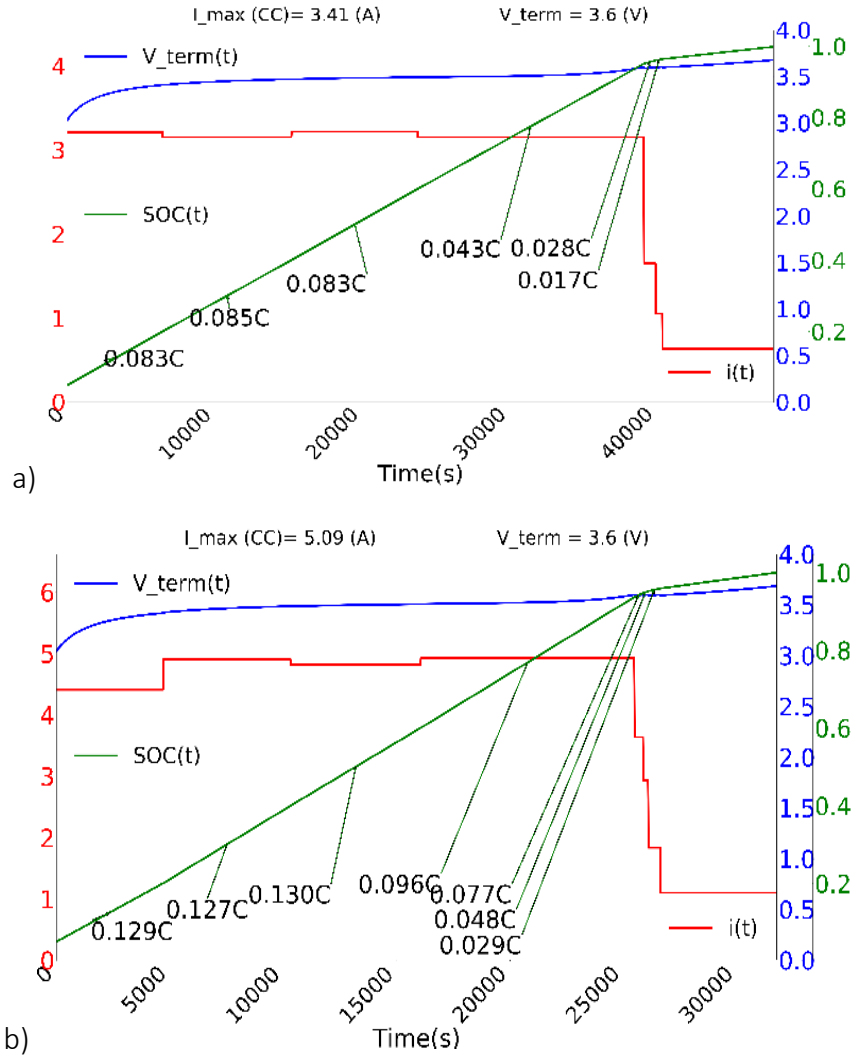

Figure 29: The CC-CV charging scheme approximation for a 3.6V-38Ah Lithium-Ion battery cell by a linear piecewise: (a) Using a 7.36 kW single-phase EVSE, (b) Using an 11 kW three-phase EVSE

3.3.2 Charging Simulation for a Lithium-Ion Battery Cell Used in Passenger Electric Vehicles

This section illustrates a simulation for three different Lithium-Ion battery cells characterized with various charge capacities but sharing the same output voltage. These battery cells correspond to the three BEV models: BMW i3 which uses $3.6V$-$34Ah$ Lithium-Ion battery cells in its battery pack (BMW, 2018), Nissan Leaf equipped with a battery pack made of $3.6V$-$40Ah$ Lithium-Ion battery cells (Nissan, 2017), and Toyota Rav4 that consists of multiple $3.6V$-$36Ah$ Lithium-Ion battery cells in its battery pack assembly (Toyota, 2013).

Similar to what we did in section 3.3.1, we simulate the CC-CV charging process for the three defined batteries using identical EVSE. However, the current values in the CC phase might vary from one battery cell to another because of the onboard charger's power capacity of each EV. Figure 30 illustrates the CC-CV process of the three batteries that correspond to three different EV models in discrete time formulation as in (Pelletier et al., 2017), and also accounting for the PEU percentage losses defined by the parameter q.

We can see that the maximum current $\mathbf{I_{cc}}$ applied to each vehicle in the CC phase is different because of the differences in the onboard charger capacity of each EV. By comparing the three charging profiles, we notice that the charging process of the BMW EV in (b) is too close to that of the Rav4 EV in (c) in terms of the SoC breakpoint and the time at which the CV stage is entered. Unlike that of the Nissan Leaf in (a), where the effect of a higher current value in the CC phase and a smaller battery capacity caused the battery to shift into CV mode 7000 seconds earlier than those in (b) and (c) and at a lower SoC of 88%.

Figure 31 illustrates the linear approximation of the CC-CV charging function for the same batteries used in **Figure 30**. Even that the CV phase for the battery in (a) is entered earlier, having the same number of breakpoints of suitable charge rates made it possible to preserve the terminal voltage. The EV Nissan Leaf experienced higher charge rates for all its breakpoints because it's equipped with a smaller battery pack of lower energy capacity compared to the other two, even that the power supply is lower than 7.36 (kW) because of onboard charger power limitations.

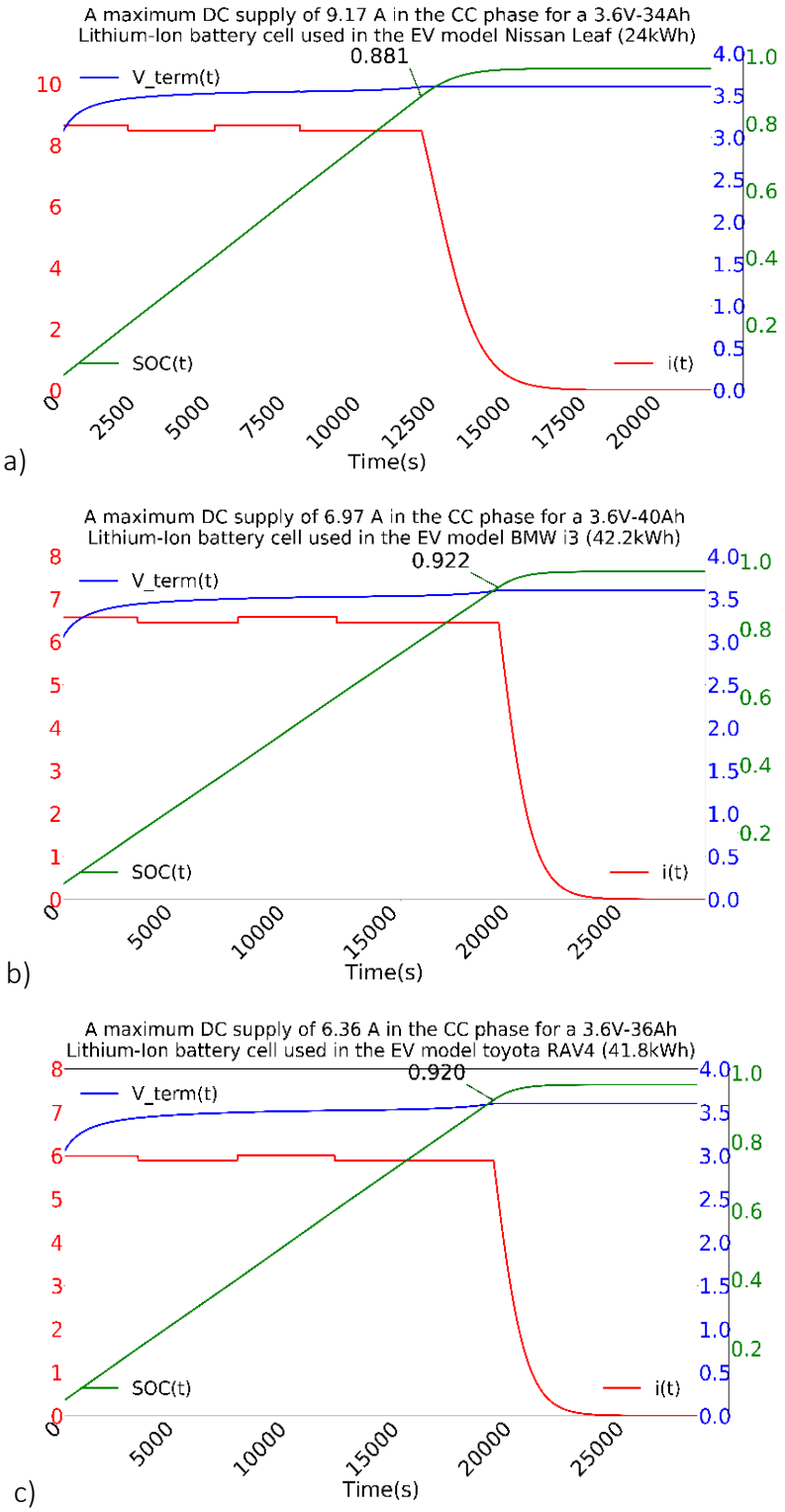

Figure 30: The discretized CC-CV process of different Lithium-Ion battery cells using the same power supply of a 7.36 kW capacity. (a) 3.6V-34Ah Lithium-Ion battery cell of a Nissan leaf EV (Nissan, 2017), (b) 3.6V-40Ah Lithium-Ion battery cell of a BMW i3 EV (BMW, 2018), and (c) 3.6V-36Ah Lithium-Ion battery cell of a Toyota RAV4 EV (Toyota, 2013).

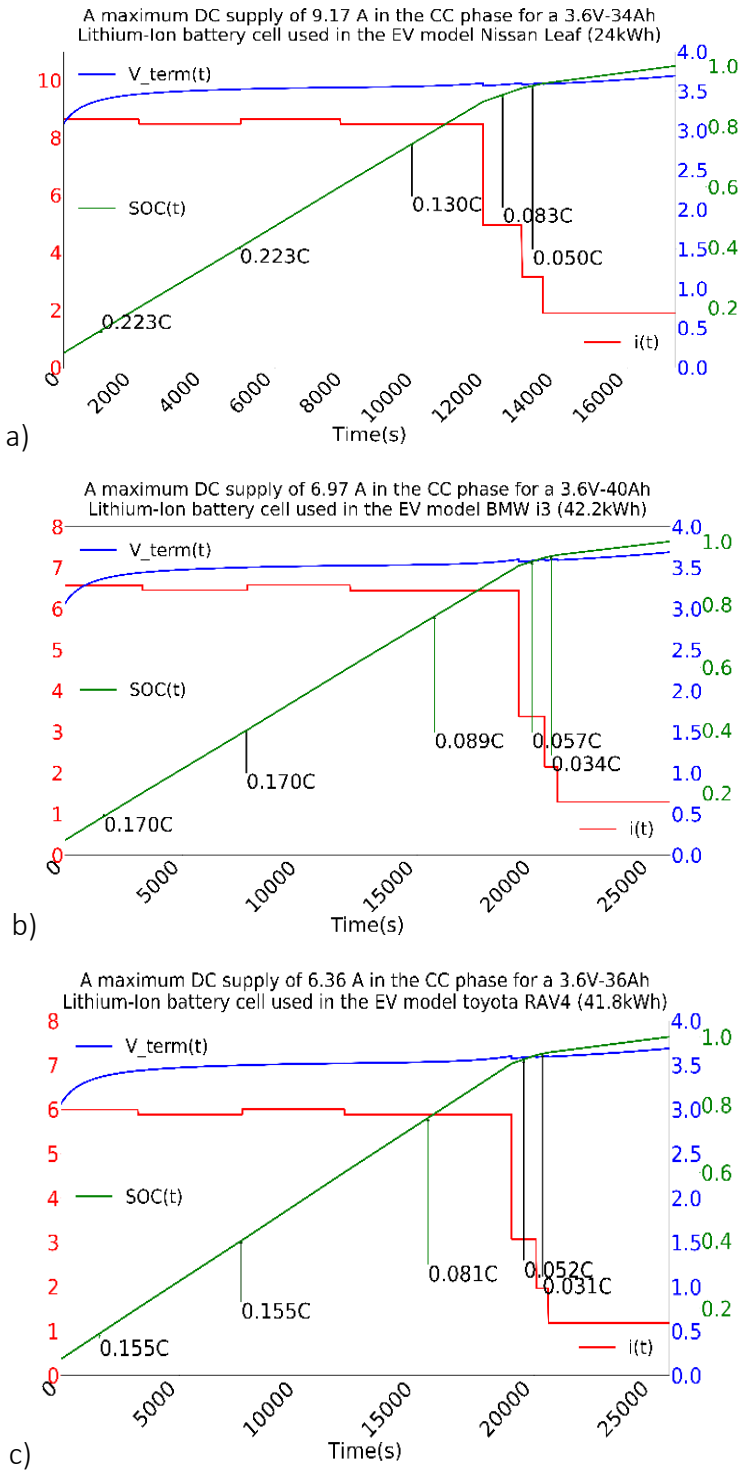

Figure 31: The approximated linear piecewise of the discretized CC-CV process for different Lithium-Ion battery cells using the same power supply of a 7.36 (kW) capacity. (a) 3.6V-34Ah battery cell of a Nissan leaf EV (Nissan, 2017), (b) 3.6V-40Ah battery cell of a BMW i3 EV (BMW, 2018), and (c) 3.6V-36Ah battery cell of a Toyota RAV4 EV (Toyota, 2013).

3.4 VARIABLE-CURRENT CHARGING SCHEMES

Although the CC-CV charging scheme for charging EVs is efficient and widely used nowadays, it still has its share of the side effects on the battery life cycle and ageing effects. The CC-CV charging method has flexibility issues, especially in the CC stage, where it's not possible to adapt the current values in response to the changing batter characteristics (Jiang et al., 2021).

Table 13: Causes, effects, and influences of Lithium-ion anode ageing.

Source: (Vetter et al., 2005)

Cause	Effect	Leads to	Reduced by	Enhanced by
Electrolyte decomposition (→SEI) (Continuous side	Loss of lithium Impedance rise	**Capacity fade** **Power fade**	Stable SEI (additives) Rate decreases with time	High temperatures High SOC (low potential)
Solvent co-intercalation, gas evolution and subsequent cracking formation in particles	Loss of active material (graphite exfoliation) Loss of lithium	Capacity fade	Stable SEI (additives) Carbon pre-treatment	Overcharge
Decrease of accessible surface area due to continuous SEI growth	Impedance rise	**Power fade**	Stable SEI (additives)	High temperatures High SOC (low potential)
Changes in porosity due to volume changes, SEI formation and growth	Impedance rise Overpotentials	Power fade	External pressure Stable SEI (additives)	High cycling rate High SOC (low potential)
Contact loss of active material particles due to volume changes during cycling	Loss of active material	**Capacity fade**	External pressure	High cycling rate High DOD
Decomposition of binder	Loss of lithium Loss of mechanical stability	Capacity fade	Proper binder choice	High SOC (low potential) High temperatures
Current collector corrosion	Overpotentials Impedance rise Inhomogeneous distribution of current and potential	Power fade Enhances other ageing mechanisms	Current collector pre-treatment (?)	Over-discharge Low SOC (high potential)
Metallic lithium plating and subsequent electrolyte decomposition by metallic Li	Loss of lithium (Loss of electrolyte)	Capacity fade (power fade)	Narrow potential window	Low temperature High cycling rates Poor cell balance Geometric misfits

Lin et al.,(2019) state some of the CC-CV issues like higher polarization voltage due to the battery capacity fade, the difficulties in distinguishing among the individual cells because of its independence from the battery model, low charging efficiency due to the high temperature, especially in the CC phase where the current is high for an extended period which affects the battery life cycle and enhances the ageing effects. Table 13 presents an overview of the ageing mechanism and the related causes, effects, and impacts on the battery. By looking at the right column, we can see that the high temperature enhances the ageing mechanism in most cases.

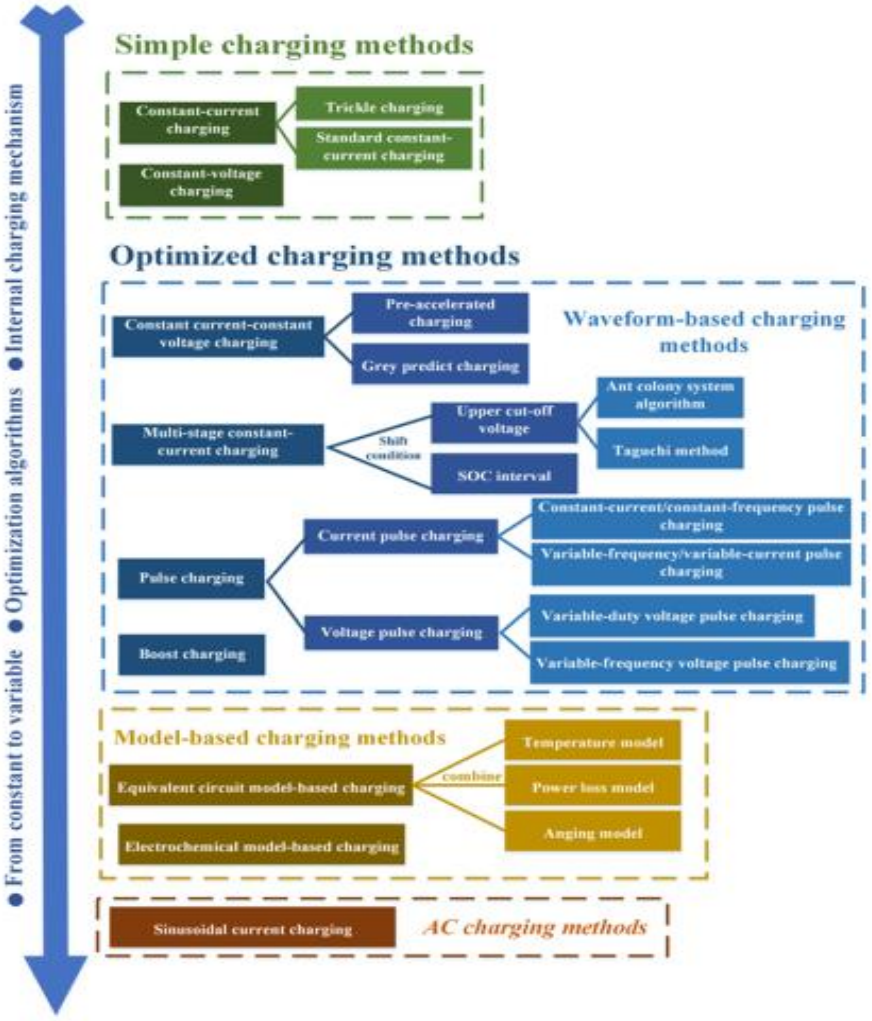

Figure 32: Summary of various charging methods.

Source: (Lin et al., 2019)

The CC-CV charging approach represents a base for many optimized charging models that are summarized in Figure 32. Recent researchers proposed battery models based on an improved CC-CV charging scheme that considers a variable current instead of the constant current in the CC phase. Table 14 presents the summary of the comparison conducted by Krieger et al., 2013 on four battery types using a variable current charging (VCC) method and reported their response on the major aspects. The results show that the LFP, which is one type of Lithium-Ion batteries that is widely used in EV production, has an excellent response in terms of cycle life and no measured effects of variability on lifetime. Moreover, LFP batteries show minimal capacity fade after over 1000 cycles which makes them superior to the other battery types and raises the interest in discovering more in the VCC method.

Table 14: Summary of different batteries' responses to variable charging.

source: (Krieger et al., 2013)

Characteristic	Lead-acid	LCO	LCO-NMC	LFP
Characteristic cycle life	Poor	Good	Very good	Excellent
Effect of variability on lifetime	Decreases lifetime	No measured effect	Neutral or positive effect	No measured effect
Pulse length dependence on charge acceptance	Short pulses better than longer pulses	No measured effect	No measured effect	Short pulses better than longer pulses
Incomplete charge is a stressor	Yes	No	No	No
Charge power fade observed	Yes	Yes	Yes	No

Jiang et al.,(2021) and Cho et al.,(2019) have explored the effect of the VCC method on Lithium-Ion batteries and showed its opportunities. The first presents a VCC strategy that is based on breaking down the charging profile of the battery based on the SoC instead of the terminal voltage as in the CC-CV method. This research consists of several experiments on the same battery type that is charged with both the CC-CV method and the proposed VCC method, and the results showed an interesting reduction in the battery's temperature of about 2.9℃ and charging losses reduction of about 0.5%. Similarly, Cho et al.,(2019) propose a charging algorithm that adjusts the charging current in response to the temperature increase inside the battery to prolong its lifetime and minimize the ageing effects. The charging algorithm is based on the VCC method that is applied on two types of Lithium-Ion cells, the high-capacity, and the high-power ones. The results of the experiment show that the VCC is an efficient method to decelerate the battery ageing mechanism caused by a repeated charging and discharging process.

In our model, we consider a combination of the CC-CV charging method and the VCC method for the EV charging problem in both chapters 4 and 5. We assume a charging scheme that considers the charging current breakpoints estimated using the CC-CV charging method as thresholds for the actual current that the EV will use while charging but using the same SoC breakpoints. In other words, the current breakpoints approximated using the CC-CV charging scheme represent an upper limit to the charging current decision variable. Such a charging scheme gives more flexibility to the optimization model as the charging period isn't as crucial as the charging cost and quality.

4 THE COMMERCIAL AND INDUSTRIAL PROBLEM MODEL

This chapter presents the clustered charging strategy of the commercial and industrial scenario (CIS) and its mathematical model, and it's organized as follows. First, we give a general description of the Electric Freight Vehicles Clustered Charge Scheduling Problem (EFV-CCSP) in Section 4.1. Then we present the EFV-CCSP mathematical formulation in Section 4.2, followed by a simple example of the problem for better understanding and analyzing several optimal solutions of different instances in Section 4.3.

In this model, we consider a commercial firm for distributing goods using a fleet of electric freight vehicles. The aim is to optimize the overnight charge scheduling of these EFVs to minimize the total electricity bill taking into consideration the price of electricity that varies during the day and other parameters of the battery of each vehicle like the remaining state of charge (SoC), the energy needed to perform tasks in the coming day, and the departure and arrival periods from and to the site for each vehicle. To do so, we design an intelligent charging model in which we assume a way of communication between the charging station and the vehicle, between the charging station and the user through a mobile EV charging application between the charging stations and the cluster, between all clusters, between the charging stations themselves, and between the clusters and the power grid.

Like other optimization problems, several assumptions are considered while modeling EFV-CCSP, in which we highlight the most significant ones in this section**.** First, it is assumed that each EFV would be performing only one route during the planning horizon in which the different routes are of different ranges resulting in different energies needed for the EFVs. Second, the energy required per vehicle would be estimated automatically by the mobile charging application based on GPS after specifying the various destinations to be traveled on the following day, considering several factors as in (Schwertner & Macht, 2018). Third, the charging process can take place only in the depot of the commercial site, and that all EFVs can charge only in the day's non-working periods, assuming a daily working period for each EFV to be from 9:30 till 17:00. Finally, we discretize the planning horizon and optimize the resulting problem accordingly, supposing that no charging occurs between the departure and the arrival times from and to the depot.

4.1 COMMERCIAL AND INDUSTRIAL PROBLEM DESCRIPTION

This model is defined over a planning interval of one day, assumed to be a working day. Our planning interval is discretized into a set $T = \{1, \dots, T_{max}\}$ of n_t consecutive periods, each having a duration Δt of 15 minutes (0.25 h) ($t \in T$). The energy cost p_t in Euro per kilowatt-hour (€/kWh) is assumed to be variable along the day any time $t \in T$. The non-EV power consumption represents the site's average power demand where the power retrieved by EFVs while charging is excluded and is denoted by the input parameter l_t Kilowatt (kW).

The set $V = \{1, \dots, m\}$ represents a fleet of m homogeneous EFVs assumed to be medium-duty electric trucks, each equipped with several lithium-ion battery cells combined to give a total energy capacity QE kilowatt-hours (kWh), an output voltage $U_{battery}$ Volts (V) and a total maximum charge capacity represented by the parameter Q ampere-hours (Ah). The maximum charge capacity is equal to the ratio of the total energy capacity QE over the battery voltage $U_{battery}$.

Each EV is equipped with an onboard charger of maximum power capacity defined as $L\ (kW)$. We define the state of charge (SoC) of a battery as the amount of charge it contains divided by its charge capacity Q. The whole power system of the commercial site is subjected to a grid power limit $P\ (kW)$, which's the maximum power that could be retrieved from the grid by the site at any time. The maximum observed power consumption of the building throughout the planning interval is subjected to FRD charges of F (€/kW).

For each vehicle $v \in V$, some input parameters are required to be inserted by the user before starting the optimization process and are as follows. Parameters d_v and a_v represent the departure and arrival time from and to the depot, respectively. The energy needed by vehicle v to complete the route of the next day is defined by e_v (kWh). It's determined by summing up the travel distance of all the destinations specified by the user, then multiplying it by the range (kWh/km) of vehicle v. The SOC of each vehicle v at the beginning of the planning horizon is defined as SOC_v^{start}. Let N be the maximum number of cuts that can occur while charging vehicle v to limit the charging interruption for battery health reasons that result in longer battery life besides avoiding impractical solutions in which vehicles are constantly being moved from one cluster to another. we set a maximum and a minimum value of SOC denoted by the input parameters SOC^{max} and SOC^{min} respectively, for battery health reasons as well.

The charging system's infrastructure in the depot consists of a set of C clusters of different power capacities. Each cluster $c \in C$ is a similar example of electric vehicle supply equipment (EVSE) of a specific charging power level and equipped with one or more sockets and connectors of the same type (pod POINT, n.d., enel X, n.d.). One or more than one EV could be plugged simultaneously into the same cluster and share its maximum power such that if only one EV is plugged into the cluster, it benefits from the total power output of the cluster alone, which means a higher charging rate and shorter charging. If any other EV gets plugged into the same cluster, then the power would be divided and shared between both EVs but not necessarily evenly distributed.

The idea behind grouping the charging stations into several clusters is to optimize the charging levels across all EVSE installed in the depot. Charging stations can exchange data gathered from EFVs that benefit the user from most of the power available on the grid without paying taxes on the power consumption that might exceed the contracted capacity. Besides, clusters with multiple charging sockets mean fewer charging devices by replacing them with only a few more connections. Moreover, most commercial and industrial sites are equipped with a three-phase power system, making it easier for the three-phase AC clusters to be installed with no significant modification of the site's power infrastructure.

A charging level 1 is not considered in our modeling since the smart charging technology requires the installation of EVSE to communicate with the cluster and the grid. Moreover, it is based on connecting the onboard charger into the regular electric socket and takes at least 18 hours to charge the EFV up to only 80%, which would be infeasible with a maximum charging period of 15 hours. On the other hand, The EFVs are equipped with an onboard charger of a 12 (kW) power capacity that makes it economically infeasible to go for an EVSE of a capacity higher than the charger's one. Similarly, off-board DC fast chargers are not considered for their high installation cost and because they are not commonly used for overnight charging but installed in public charging stations and shopping malls for daytime short charging periods.

Our model is designed with several dedicated smart EVSE installed in the depot based on European standards. Each EVSE is assumed to be of a charging mode 3 and acts as a cluster of multiple charging sockets of either single or three-phase charging modes. It is equipped with a Mennekes type-2 connector compatible with all EVs in Europe and other countries (Falvo et al., 2014). We assume having three types of clusters as follows: Type one is a single-phase EVSE having an output voltage of 230 V and a 32 (A) maximum current supply that corresponds to a power capacity G_c (kW) of 7.36 (kW). Type two and three are three-phase EVSE with an output voltage of 400 V, and current capacities per phase of 16 (A) and 32 (A) that are equivalent to 11 (kW) and 22 (kW) power capacities, respectively (Marra et al., 2012).

Parameters h_c refer to the number of charging sockets available in each cluster c. We assume that each EFV v would be connected to only one cluster c during its entire charging process. Figure 33 shows a simplified configuration of the smart charging system's clustered infrastructure in the depot, where the bidirectional arrows represent the direction of data communication among the system's different levels. However, power flow is unidirectional from the grid as a top-level towards EVSEs as the bottom-level and is represented by the unidirectional red arrows.

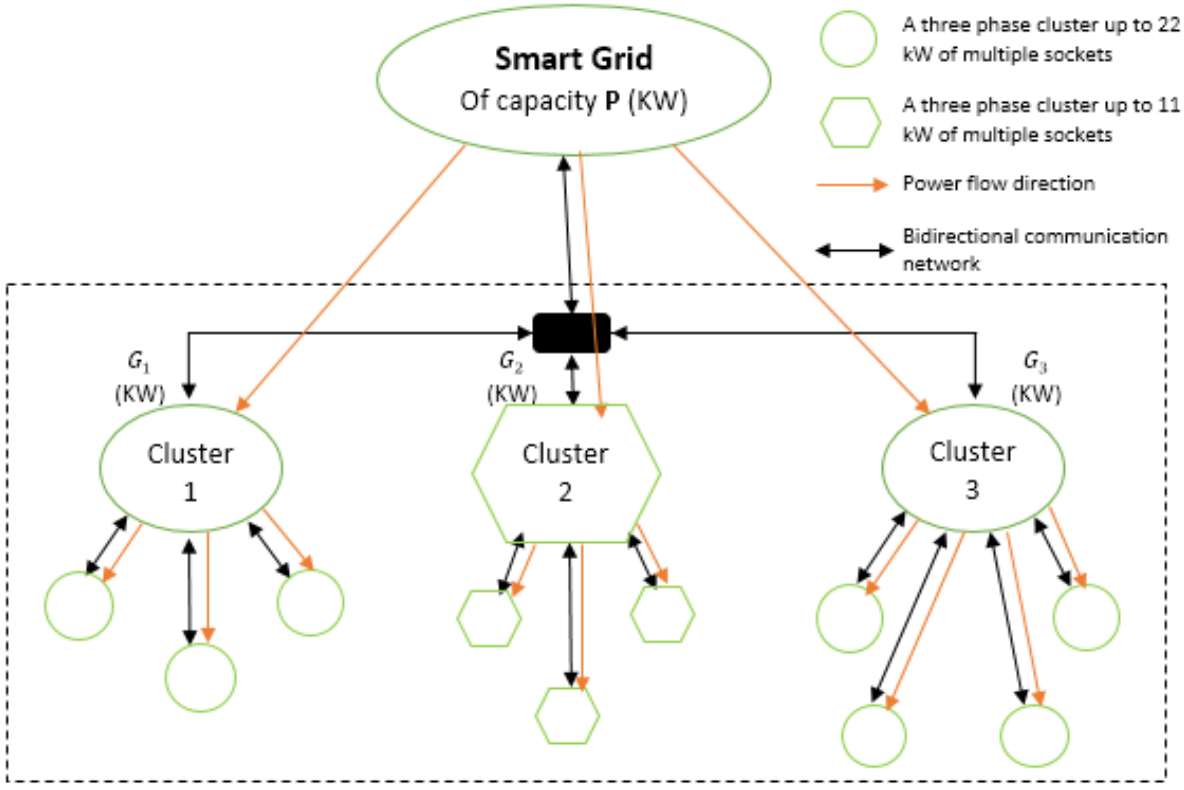

Figure 33: A Simplified scheme of a smart charging system's clustered infrastructure in the depot

By referring to section 3.3.1, we assume that each cluster $c \in C$ has a specific CC-CV charging function approximated by a linear piecewise using $b_c + 1$ breakpoints fitted to the real CC-CV concave function, and it's different for each cluster type depending on its power level. The linear approximation of the charging process using cluster c assumes that the charging current $I_{c,b}^{max}$ between breakpoints b and $b-1$ represents a ceiling to the actual current to be retrieved. B_c is the set of breakpoints corresponding to the charging function of cluster c. Let $SOC_{c,b}^{break}$ be the SoC associated with the breakpoint $b \in B_c$ of the charging function of charger c. Finally, we set a minimum current $I_{c,b}^{min}$ applied to each EFV v between two consecutive breakpoints b and $b-1$ of the charging function of a cluster c for battery protection purposes.

4.2 MATHEMATICAL FORMULATION OF THE COMMERCIAL PROBLEM

Six sets of decision variables are required for the formulation of the EFV-CCSP model. Binary variables $u_{v,c}$ take a value of 1 if vehicle v is connected to cluster c, and take a value of 0 otherwise. It is constant for the entire charging process until EFV v this avoids impractical solutions in which vehicles are constantly being moved from one cluster to another. In addition, binary variables $z_{t,v}^{c,b}$ that take the value of 1 if EFV v is retrieving current from a charging socket in cluster *c* during period t before departure time from the site between breakpoints $SOC_{b-1,c}^{break}$ and $SOC_{b,c}^{break}$ and take a value of 0 otherwise. While binary variables $y_{t,v}$, take a value of 1 when the charging event of EFV v shifts from ON to OFF between periods $t-1$ and t and take a value of 0 otherwise.

Real and positive variables $i_{t,v,c}$ refer to the charging current applied to EFV v by cluster c during the entire period t. Real and positive variables $soc_{t,v}$ refer to the state of charge of EFV v at the beginning of time t. Finally, Real positive variable s indicates the maximum charging power retrieved from the grid during the planning interval used to determine the FRD charges. To sum up, our problem is presented in the following mathematical model and the mixed-integer linear programming formulation (MILP), respectively:

Sets:

- T: Set of time in the scheduling horizon $(T = \{1, \dots, T^{max}\})$
- V: Set of EFVs. $(v \in V)$
- C: Set of charging clusters. $(c \in C)$
- B_c: Set of breakpoints used in the piecewise linear approximation of the CC-CV charging process using cluster c. $(b \in B_c)$

Parameters:

- l_t: non-flexible consumption profile of the commercial site (non-EFV) at time t. (kW)
- p_t: Electricity price at time t. $(€/kWh)$
- Q: The charge capacity of the battery of the EFV (Ah).
- QE: The energy capacity of the battery of the EFV (kWh).
- L: The onboard power capacity of the EFV (kW).
- $U_{battery}$: The rated voltage of the battery of the vehicle (V).
- N: The maximum number of cuts allowed for the battery of EFV.
- a_v: The arrival time of EFV v to the depot.
- d_v: The departure time of EFV v from the depot.

- e_v: Energy needed for EFV v to travel the next day (KWh).
- SOC_v^{start}: The SoC associated with the first period of the time horizon for each EFV $v \in V$.
- P: The Grid power capacity that could be consumed by the site at any time (kW)
- F: FRD charge $(€/kW)$
- G_c: Maximum power could be withdrawn instantaneously from cluster c. (kW)
- h_c: The number of charging sockets in cluster c.
- $I_{c,b}^{max}$: The maximum current that could be retrieved in the piecewise linear approximation
- of the CC-CV charging process depending on the charging level of cluster c between
- the breakpoints b and $b-1$ for $b \in B_c$, b > 0. (A)
- $I_{c,b}^{min}$: The minimum current that should be retrieved in the piecewise linear approximation
- of the CC-CV charging process depending on the charging level of cluster c between
- the breakpoints b and $b-1$ for $b \in B_c$, b > 0. (A)
- $SOC_{c,b}^{break}$: The state of charge associated with breakpoints $b \in B_c$ in the piecewise linear
- approximation of the CC-CV charging function of cluster c.
- SOC^{max}: The maximum state of charge that any vehicle could reach while charging.
- SOC^{min}: The minimum state of charge that any vehicle could reach during the discharging
- Process.
- q: The average weighted power loss factor during charging.
- Δt: Timestep in (h).

Variables:

- $i_{t,v,c} \geq 0$: The current value is taken by EFV v at time t in cluster c. (A)
- $soc_{t,v} \geq 0$: The state of charge of EFV v at time t.
- $z_{t,v}^{c,b} \in \{0,1\}$: 1 if EFV v uses a cluster c at time t with a state of charge between
- $SOC_{c,b-1}^{break}$ and $SOC_{c,b}^{break}$.
- 0 otherwise.
- $y_{t,v} \in \{0,1\}$: 1 if EFV v stops charging at time period t.
- 0 otherwise
- $u_{v,c} \in \{0,1\}$: 1 if EFV v is plugged into cluster c.
- 0 otherwise
- $s \geq 0$: The maximum charging power withdrawn from the grid along the planned horizon.

Formulation:

$$\text{minimize} \qquad \sum_{t\in T} p_t \Delta t \left(l_t + \sum_{v\in V}\sum_{c\in C} \frac{i_{t,v,c}}{Q} QE \right) + F \cdot s \tag{12}$$

subject to:

$$l_t + \sum_{v\in V}\sum_{c\in C} \frac{i_{t,v,c}}{Q} QE \le s \qquad \forall t \in T \tag{13}$$

$$0 \le s \le P \tag{14}$$

$$\sum_{v\in V} \frac{i_{t,v,c}}{Q} QE \le G_c \qquad \forall\, t \in T, c \in C \tag{15}$$

$$\sum_{t=1}^{a_v-1}\sum_{v\in V}\sum_{c\in C}\sum_{b\in B_c\setminus\{0\}} z_{t,v}^{c,b} + \sum_{t=d_v}^{\boldsymbol{T^{max}}}\sum_{v\in V}\sum_{c\in c}\sum_{b\in B_c\setminus\{0\}} z_{t,v}^{c,b} = 0 \tag{16}$$

$$soc_{1,v} = SOC_v^{start} \qquad \forall v \in V \tag{17}$$

$$soc_{d_{v+1},v} = soc_{d_v,v} - \frac{e_v}{QE} \qquad \forall v \in V \tag{18}$$

$$soc_{d_v,v} = soc_{a_v,v} + \frac{e_v}{QE} \qquad \forall v \in V \tag{19}$$

$$\sum_{t\in T}\sum_{c\in C} \frac{i_{t,v,c}(1-q)\Delta t}{Q} + SOC_v^{start} - SOC^{min} = \frac{e_v}{QE} \qquad \forall v \in V \tag{20}$$

$$soc_{t,v} = soc_{t-1,v} + \sum_{c\in C} \frac{i_{t-1,v,c}(1-q)\Delta t}{Q} \qquad \forall t \in T\setminus\{1, d_v, d_v+1\}, v \in V \tag{21}$$

$$soc_{t+1,v} \le SOC_{c,b}^{break} + 1 - z_{t,v}^{c,b} \quad \forall t \in \{\boldsymbol{a_v}, \dots, d_v - 1\}, v \in V, c \in C, b \in B_c\setminus\{0\} \tag{22}$$

$$soc_{t,v} \geq SOC_{c,b-1}^{break} - 1 + z_{t,v}^{c,b} \quad \forall t \in \{\boldsymbol{a_v}, \dots, d_v\}, v \in V, c \in C, b \in B_c \backslash \{0\} \tag{23}$$

$$SOC^{min} \leq soc_{t,v} \leq SOC^{max} \qquad \forall t \in T, v \in V \tag{24}$$

$$i_{t,v,c} \leq \sum_{b \in B_c \backslash \{0\}} I_{c,b}^{max} z_{t,v}^{c,b} \qquad \forall t \in T, v \in V, c \in C \tag{25}$$

$$i_{t,v,c} \geq \sum_{b \in B_c \backslash \{0\}} I_{c,b}^{min} z_{t,v}^{c,b} \qquad \forall t \in T, v \in V, c \in C \tag{26}$$

$$\sum_{c \in C} \sum_{b \in B_c \backslash \{0\}} z_{t-1,v}^{c,b} - \sum_{c \in C} \sum_{b \in B_c \backslash \{0\}} z_{t,v}^{c,b} \leq y_{t,v} \qquad \forall t \in \{\boldsymbol{a_v} + \boldsymbol{1}, \dots, d_v\}, v \in V \tag{27}$$

$$\sum_{c \in C} \sum_{b \in B_c \backslash \{0\}} z_{t,v}^{c,b} \geq y_{t,v} \qquad \forall t \in T \backslash \{\boldsymbol{a_v} + \boldsymbol{1}, \dots, d_v\}, v \in V \tag{28}$$

$$\sum_{t \in T} y_{t,v} + \sum_{c \in C} \sum_{b \in B_c \backslash \{0\}} z_{T^{max},v}^{c,b} \leq N + 1 \qquad \forall v \in V \tag{29}$$

$$\sum_{c \in C} \sum_{b \in B_c \backslash \{0\}} z_{t,v}^{c,b} \leq 1 \qquad \forall t \in T, v \in V \tag{30}$$

$$\sum_{b \in B_c \backslash \{0\}} z_{t,v}^{c,b} \leq u_{v,c} \qquad \forall t \in T, v \in V, c \in C \tag{31}$$

$$\sum_{c \in C} u_{v,c} \leq 1 \qquad \forall v \in V \tag{32}$$

$$\sum_{v \in V} \sum_{b \in B_c \backslash \{0\}} z_{t,v}^{c,b} \leq h_c \qquad \forall t \in T, c \in C \tag{33}$$

$$\sum_{v \in V} u_{v,c} \leq h_c \qquad \forall c \in C \tag{34}$$

$$i_{t,v,c} \leq \sum_{b \in B_c \setminus \{0\}} \frac{G_c \cdot 1000}{U_{battery}} z_{t,v}^{c,b} \qquad \forall t \in T, v \in V, c \in C \tag{35}$$

$$i_{t,v,c} \leq \sum_{b \in B_c \setminus \{0\}} \frac{L \cdot 1000}{U_{battery}} z_{t,v}^{c,b} \qquad \forall t \in T, v \in V, c \in C \tag{36}$$

$$z_{t,v}^{c,b} \in \{0,1\} \qquad \forall v \in V, t \in T, c \in C, b \in B_c \tag{37}$$

$$y_{t,v} \in \{0,1\} \qquad \forall v \in V, t \in T \tag{38}$$

$$u_{v,c} \in \{0,1\} \qquad \forall v \in V, c \in C \tag{39}$$

The objective function (12) minimizes the total energy costs over the planning horizon. The first term corresponds to the total energy cost of the site that is the cost of electricity p_t $(€/kWh)$ multiplied by another two subterms that are the non-EV normal power demand of the site $\boldsymbol{l_t}$ (kW) multiplied by the period length $\boldsymbol{\Delta t}$ (hours) and the total energy consumed by EFVs for charging their batteries over the planned horizon.

By referring to some numerical simulations of the CC-CV process conducted in the battery model proposed by Tremblay et al.,(2007), we noted that the cumulative energy (kWh) recharged in the battery is constantly and linearly increasing with the increase of the SOC during the CC-CV process regardless of the charging current used in the CC phase. As a result, the SOC variation is determined by multiplying the charging current $i_{t,v,c}$ (A) by the period length $\boldsymbol{\Delta t}$ (hours) divided by the battery charge capacity Q (Ah), and we then calculate the corresponding energy recharged in the battery by multiplying the resulting SOC variation by the energy capacity QE (kWh).

The second term in the objective function (12) represents the FRD charges that the whole site is subjected to and is determined by multiplying the fee F (€/kW) by the maximum charging power retrieved from the grid throughout the entire planned interval. EFVs would be scheduled in a way to retrieve power from the grid during the periods when the regular power consumption of the site l_t is relatively lower than its values in other periods.

Constraints (13) calculates the maximum charging power retrieved from the grid throughout the entire planned interval. Constraints (14) ensure that the site's instantaneous total power consumption would never exceed the grid limit *P* at any time t. Constraints (15) set the power limit for each cluster $c \in C$ such that the total power retrieved by all EFVs that are connected to the charging points in cluster c at each t would be less than or equal to its power capacity G_c (kW) at any time. Constraints (16) ensure that no charging events take place while EFVs are performing their routes and $z_{t,v}^{k,b}$ take the value of 0. Constraints (17) associate the SOC at the beginning of the time interval to the predefined SOC corresponding to the arrival time of each vehicle v. Constraints (18) refer to the discharge process of each vehicle upon its departure from the depot at period d_v.

Constraints (19) and (20) ensure that each vehicle would be charged with the exact amount of energy needed e_v (kWh) during its charging process. Constraints (21) calculate the SOC of each EFV v at time t *as* the sum of its SOC and the equivalent SOC of the charge value stored in the battery based on the current retrieved from cluster c in the previous period $t-1$. Constraints (22) and (23) bound the SOC of EFV v between two consecutive periods depending on the specific piecewise linear function of the CC-CV process that corresponds to charger c where the car is connected. Constraints (24) bound the SOC of each vehicle during each period for a longer battery lifecycle.

Constraints (25) and (26) force the charging current applied to an EFV not to exceed or go below the maximum and minimum current values associated with the segment of the CC-CV charger-specific linear piecewise linear function. Constraints (27)-(29) set the restrictions for the maximum number of cuts N allowed for each EFV v along the planning horizon to minimize the effects of battery degradation resulting in longer battery life. Constraints (30) ensure that each vehicle EFV v could retrieve power from only one cluster c at any time. Constraints (31) and (32) assign each vehicle v to only one cluster c for the entire charging process.

Constraints (33) and (34) adjust the number of vehicles that are plugged into cluster c at any time t not to exceed the number of its charging sockets h_c and guarantee that each vehicle v would retrieve power from only one socket in one specific cluster for the entire charging process. Constraints (35) limit the power withdrawn from any socket in cluster c not to exceed its power capacity G_c. Constraints (36) ensure that the power retrieved by EFV v from the charging station of cluster c respects the power capacity of its onboard charger. Constraints (37) and (39) define the domains of the variables that were not appropriately bounded by the other constraints.

4.3 SIMPLE EXAMPLE WITH MULTIPLE OPTIMAL SOLUTIONS

To help readers comprehend the problem and its mathematical formulation, we generate examples of different optimal solutions for a small instance of the EFV-CCSP. We assume having a time interval of 24 periods that starts from 15:00 with a time step of one hour resulting in a whole night charging problem such that the cost of energy p_t and the non-EV power consumption of the building l_t are given in Table 3. The grid power limit P is set to the value of 200 (kW) that could be neglected for the sake of simplicity, and the FRD fees are set to be 11 (€/kW). We apply the experiments on a set of 3 homogeneous vehicles with an energy capacity of 82.8 (kWh), a charge capacity of 230 (Ah), 360 (V) battery voltage, and a 12 kW onboard charger. We assume the SoC for all vehicles equals the minimum SoC of 0.05 and could be charged up to a maximum SoC of 0.99. Let *N* the maximum number of cuts along the entire charging process be equal to 2. The energy needed e_v (kWh), and the arrival and departure periods for each vehicle are given in Table 15.

Table 15: Route parameters for the simple numerical example

V	distance(km)	$e_v\ (kWh)$	d_v	a_v
1	62	40	17	3
2	65	42	18	2
3	68	44	17	4

There are three types of clusters installed in the depot in which, for every example, all EVs for their charging process use the same kind of cluster to analyze better the effects of the cluster's types on the charging behavior of the EFV behavior while performing the overnight charging. For the sake of simplicity, we set only two breakpoints associated with the linear approximation CC-CV charging process of the battery using any cluster type such that $B_c = \{0,1\}$. The values of the maximum current $I_{c,b}^{max}$ and the minimum current $I_{c,b}^{min}$ and the SoC breakpoint $SOC_{c,b}^{break}$ that correspond to the breakpoints specified to each charging type are summarized in Table 16.

Table 16: Design parameters associated with the breakpoints of the linear approximation of the charging process

B	32 (A) single-phase EVSE			16 (A) three-phase EVSE		
	$SOC_{c,b}^{break}$	$I_{c,b}^{max}$	$I_{c,b}^{min}$	$SOC_{c,b}^{break}$	$I_{c,b}^{max}$	$I_{c,b}^{min}$
0	0.05	0	0	0.05	0	0
1	0.99	20.5	4.1	0.99	30.5	6

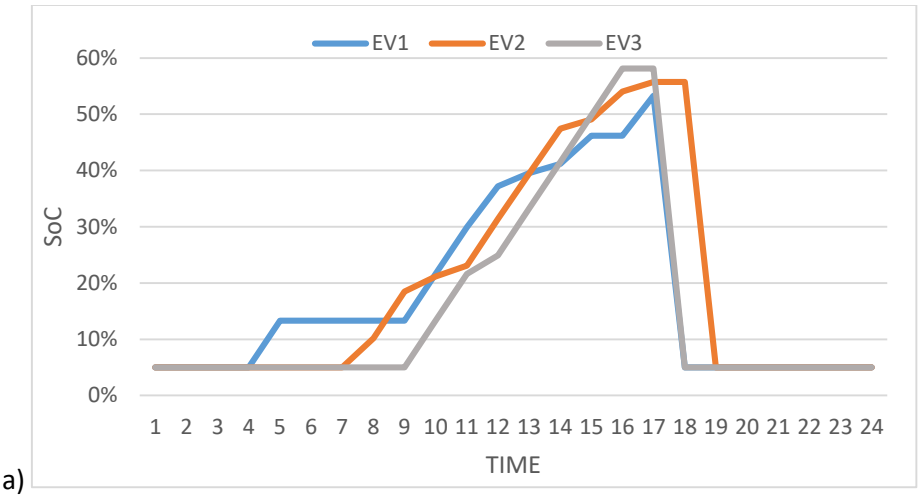

a)

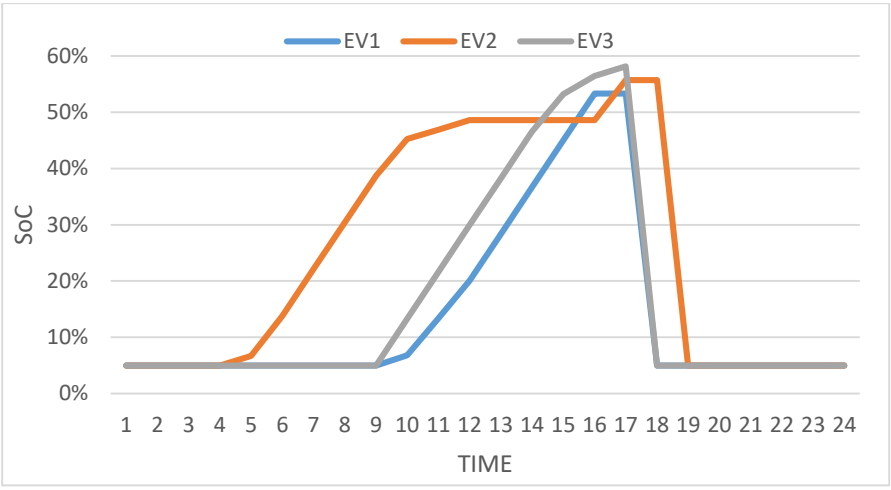

b)

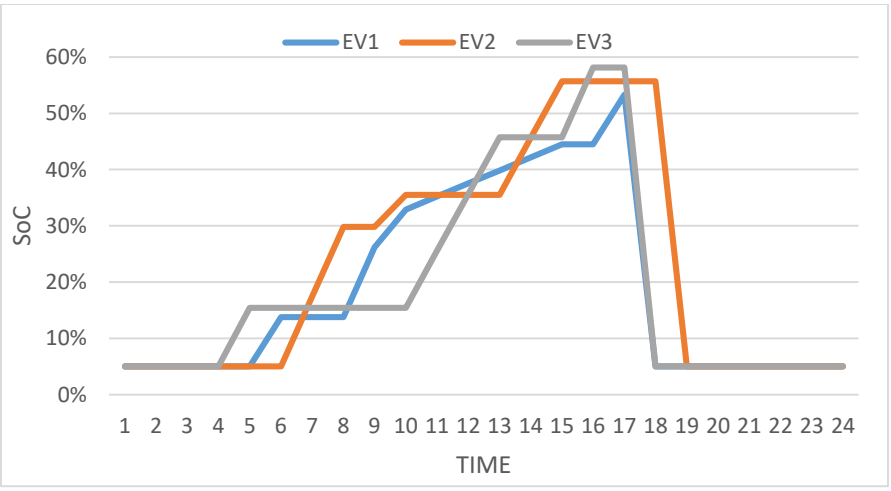

c)

Figure 34: The SoC evolution with time during the charging process of EVs "1", "2" and "3" using: (a) 3 single-socket chargers each having a 7.36 kW power capacity, (b) a double-socket charger and a single-socket charger both having a 7.36 kW power capacity, (c) a triple-socket charger of 11 kW power capacity.

Table 17: The power consumption for three optimal solutions of different cluster types.

Periods (T)	Energy Cost p_t (€/kWh)	Non-EV power retrieved l_t (kW)	EV power consumption (kW)								
			Case 1 Single-phase 32 (A) 3 single-socket EVSE A, B, and C			**Case 2** Single-phase 32 (A) 2 Double-sockets clusters A and B			**Case 3** Three-phase 16 (A) one Triple-sockets cluster A		
			1/A	2/B	3/C	1/A	2/A	3/B	1/A	2/A	3/A
1	0.25	38.31	0	0	0	0	0	0	0	0	0
2	0.25	34.75	0	0	0	0	0	0	0	0	0
3	0.25	35.29	0	0	0	0	0	0	0	0	0
4	0.1	35.25	7.36	0	0	0	1.48	0	0	0	9.25
5	0.1	34.41	0	0	0	0	6.30	0	7.79	0	0
6	0.1	33.14	0	0	0	0	7.36	0	0	10.98	0
7	0.1	34.01	0	4.60	0	0	7.36	0	0	10.98	0
8	0.1	34.87	0	7.36	0	0	7.36	0	10.98	0	0
9	0.045	34.27	7.36	2.36	7.36	1.57	5.79	7.36	5.93	5.07	0
10	0.045	34.93	7.36	1.70	7.36	5.88	1.48	7.36	2.06	0	8.94
11	0.045	34.67	6.42	7.36	2.90	5.88	1.48	7.36	2.06	0	8.94
12	0.045	34.83	2.05	7.11	7.36	7.36	0	7.36	2.06	0	8.94
13	0.045	35.42	1.48	7.10	7.36	7.36	0	7.36	2.06	8.94	0
14	0.045	38.09	4.43	1.48	7.36	7.36	0	5.90	2.06	8.94	0
15	0.045	39.61	0	4.38	7.36	7.36	0	2.88	0	0	10.98
16	0.045	43.55	6.32	1.48	0	0	6.32	1.48	7.80	0	0
17	0.045	50.41	0	0	0	0	0	0	0	0	0
18	0.1	51.35	0	0	0	0	0	0	0	0	0
19	0.1	49.98	0	0	0	0	0	0	0	0	0
20	0.1	48.30	0	0	0	0	0	0	0	0	0
	Net Charged Energy (kWh)		40	42	44	40	42	44	40	42	44
	Gross Charged Energy (kWh)		42.78	44.92	47.06	42.78	44.92	47.06	42.78	44.92	47.06
	excess charged energy (kWh)		0	0	0	0	0	0	0	0	0

Three cases are defined as A, B, and C, where A refers to a charging infrastructure composed of single-socket single-phase 32 (A) charging stations such that h_c=1 for all the clusters and characterized by a power capacity of 7.36 kW each. Case B represents a depot equipped with two twin-socket single-phase 32 (A) intelligent chargers with a power capacity of 7.36 kW each. Each of the two clusters could deliver a power of 7.36 kW per socket and the same power value combined. Finally, case C is similar to case B, with the difference in having a three-phase 16 (A) smart cluster equipped with 3 charging sockets and delivering a combined power of up to 11 kW. Table 17 and figures 34, 35, and 36 illustrate the results of the optimal solutions for the example proposed before using the three different charging technologies and show their effect on the charging cost and the power system.

Figure 34 illustrates the SOC's evolution for each of the three vehicles over the planned horizon in the three different cases where (a), (b), and (c) refer to the previously explained instances of A, B, and C respectively. The effects of using different types of chargers are evident in the deformation of the SoC profile of each EV. We see that the charging behaviors of all EVs in case A are more flexible in which all EVs are charging simultaneously and at different charging rates. However, in case B, EVs 1 and 2 are sharing the same charging cluster of a power capacity up to 7.36 (kW) where we see that EV2 takes advantage of its earlier arrival period than that of EV1 and starts charging at the high charging rates solely for five periods. When EV2 reaches relatively a high SoC, then EV1 starts charging, and the power gets divided among both EVs for only three periods. At period 12, EV2 stops charging, giving a privilege to the empty battery of EV1 that starts charging at the highest charging rate, as shown in Table 17.

However, the charging profile of EV3 shows no significant changes because of using the same charger in case A. Interestingly, the charging profiles of all EVs restore their flexibility due to the upgrade in the power capacity of the cluster used with compared to that in case B. During the entire time interval, we notice that the 11 (kW) cluster allows only two EVs to charge at the same time as in the interval between periods 9 and 14 where EV1 keeps charging at a low rate while EVs 2 and 3 are interchanging with high charging rates.

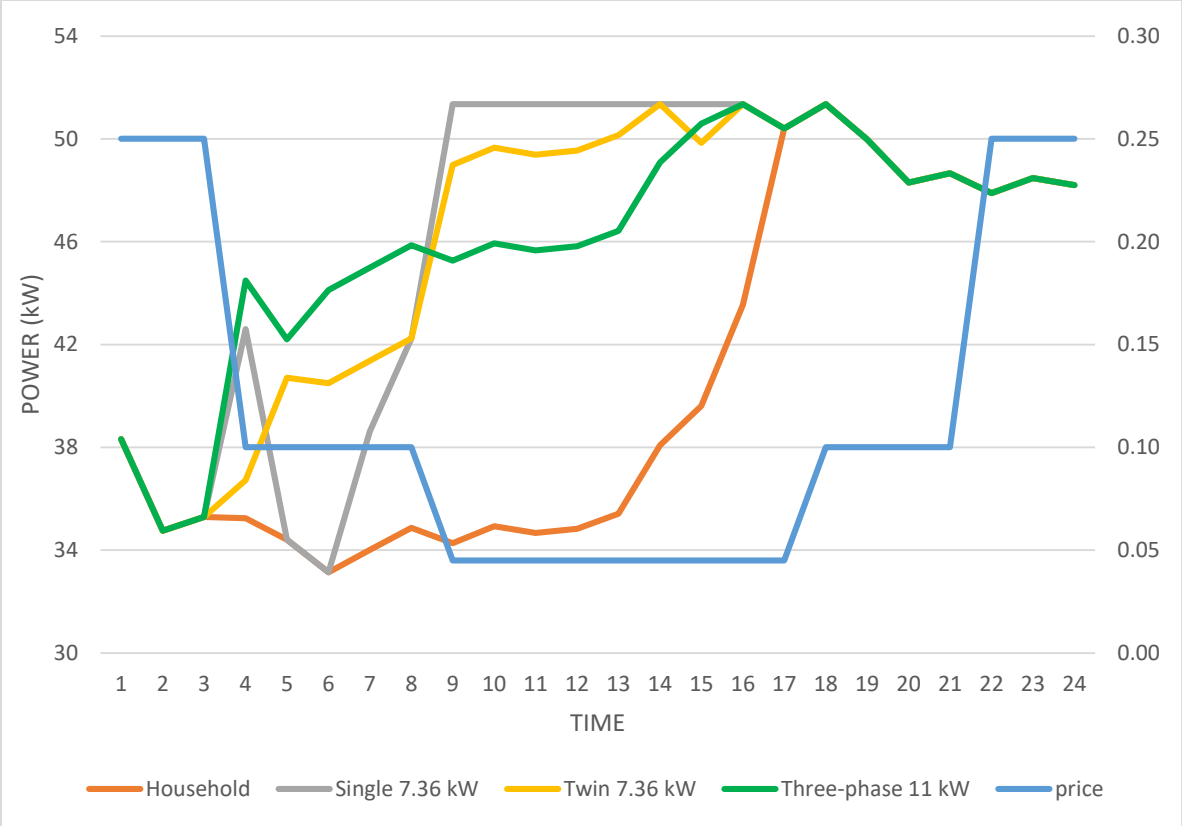

Figure 35: The power consumption profile of the building when using three different charging infrastructure cases and the electricity prices variation with time.

Table 17 and Figure 35 present the power retrieved by each EV individually at every period and the total power retrieved by the building at every point of time respectively. Each color in Table 17 refers to a specific EV where the dark colors refer to the arrival periods of the EVs, whereas the bright ones correspond to the departure periods. We find that the charging schedules in cases B and C are more flexible, where we notice that most EVs take advantage of the high power availability and complete their charge in a lesser time compared to case A. The clusters in cases B and C contribute to a power grid's relief by delivering higher power to the EVs on periods when the normal power demand is low. We can also see that the building's maximum power over all the day is common for all cases. However, this maximum power got registered on nine periods in case A that is three times more than that in case B of three periods and almost five times more compared to that in case C of two periods. The total power consumption profiles using all charging technologies show the effect of the optimization model in charging EVs only during periods of low household power consumption and electricity prices.

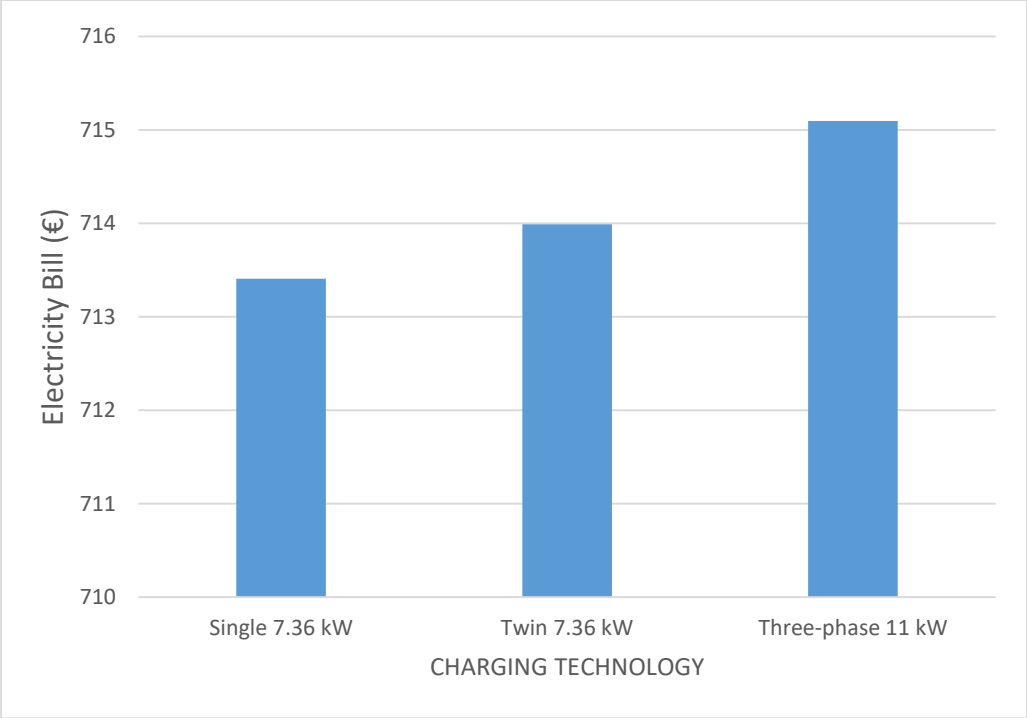

Figure 36: The building's electricity bill as a result of three different charging infrastructure scenarios.

Figure 36 shows the building's total electricity bill for the cases of using different charging technologies. The total electricity bill in case A having a value of about 713.4 (€) appears to be the least among all cases with around 0.6 (€) less than that of case B and around 1.7 (€) lower than the maximum value in case C of approximately 715.1 (€). The results might not be too impressive when comparing the variable cost of the different charging technologies, but we need to bear in mind that we're using half the number of charging points and even less as in case C, which results in lesser installation costs. Moreover, other types of charging clusters could be more efficient, especially in the worst-case charging scenarios, as we will see in chapter 6.

5 THE RESIDENTIAL NEIGHBOURHOOD PROBLEM MODEL

This chapter presents a two-stage optimization modeling for the EV charge scheduling problem of a residential neighborhood scenario (RNS), and it is laid out as follows. Section 5.1 provides a general description of the Two-Stage Residential Electric Vehicle Charge Scheduling Problem (TSREV-CSP) and explains the relationship between the objective functions of both model's stages. We decompose the TSREV-CSP into two distinct models that interact with each other. The following sections 5.2 and 5.3 present the mathematical formulations for the two stages of the TSREV-CSP, the Peak Shaving Model (PSM) and the Charging Cost Reduction Model (CCRM) respectively. Finally, we generate in section 5.4 a simple example and show different optimal solutions for the TSREV-CSP to help readers better understand the tradeoffs.

TSREV-CSP is an example of multi-objective optimization problems where we have multiple end-users of different interests and goals to be achieved such that if each is achieved individually, the other's objectives might be violated. Such a model comes as a solution to intelligently allow all these different objectives to be met at once. TSREV-CSP is based on the same concept in which we have two leading players in the game. On the one hand, the Distribution System Operator (DSO) and indirectly the Transmission System Operator (TSO) that co-exist with a high level of coordination to maintain a safe operation of the transmission system and balance the energy supply and demand to keep the grid frequency and the thermal burden of electrical equipment within defined parameters (Zipf & Most, 2016).

In this section, we consider having a DSO that aims to reduce the impact of the daily EVs' charging profile and avoid the spiking electricity demand in a particular neighborhood. To do so, the DSO offers its clients a new smart charging technology consisting of a dedicated smart charging station installed at every house in the neighbourhood (pod POINT, n.d.-a) and is connected through the internet to a smart charging app installed on any smartphone (ev.energy, n.d.) as shown in Figures 37 and 38. The mobile app allows communication between EVs and the smart grid and between all EVs in the neighborhood through the smart chargers installed in each house. Logically speaking, this new technology would be accepted by EV users only if it helps them save money and make their EV charging process more accessible and more secure in the sense of ensuring that their EV would be charged with at least the energy needed at the departure time they specify as an input parameter through the mobile app.

Figure 37: rolec-wallpod-EV-homesmart (Driving Electric, n.d.).

Figure 38: Charging station equipment and activities (Mal et al., 2013).

TSREV-CSP serves as an exciting charging strategy to satisfy both the DSO and EV users simultaneously for being designed with dual objective functions corresponding to two dependent optimization models. The first model is a peak shaving model (PSM) that allows the DSO to minimize the grid power capacity and normalize the neighborhood's load profile throughout the entire day. Then comes the subsequent charging cost reduction model (CCRM) based on the optimal solution of PSM to minimize the cost of EV charging thanks to the smart pricing strategies.

Like the EFV-CCSP discussed before, the TSREV-CSP is designed for overnight charging, and the charging process for each vehicle would take place only through the EVSE installed in the house. We consider having only one EV for each house of the neighbourhood for the sake of simplicity. We assume that the arrival and departure periods and the energy needed for all EVs are inserted by the EV owners and known before the optimization process. The energy needed by each EV would be calculated in the app upon selecting the travel plan or could be inserted manually as a percentage of the car energy capacity, as shown in Figure 39. Finally, this model is designed in the way of allowing the charging events of all vehicles to take place only at the charging point installed in the house of each EV.

Figure 39: (a) Charge status screen. (b) Charge profile screen (Mal et al., 2013).

5.1 RESIDENTIAL NEIGHBOURHOOD PROBLEM DESCRIPTION

Our problem is solved with two optimization models where the primary model PSM is independent of the cost of electricity and aims to reduce the maximum instantaneous power demand over the entire day. Its optimal solution represents an input parameter for the second optimization stage. Specifically, the PSM is followed by the CCRM that considers the neighborhood's output optimal maximum power limit and the cost of energy as new inputs compared to PSM to minimize each house's electricity bill. The optimal solution in PSM is considered feasible in the CCRM but not necessarily optimal, so the electricity bill resulting in the CCRM would be less than or equal to that of the PSM.

Our problem is defined over a set *T*= (1,..,T^{max}) the time interval of equidistant periods with a time step Δt of 15 mins (0.25 h). The price of electricity p_t (€/KWh) is given at every time $t \in T$, where the day is divided into different intervals of different prices based on smart pricing strategies for the peak, shoulder, and off-peak demands. The neighborhood consists of a set *V* of electric vehicles (EVs) that could be charged daily, assuming that each EV *v* corresponds to one house and that every house owns one EV. At any time $t \in T$, the (non-EV) typical power consumption of each house of vehicle *v* is given as $l_{t,v}$, that is the normal power demand of each house such that the power consumption of EVs is excluded (kW). M_t is the neighborhood's household power consumption at time *t* that is either equal to the sum of the parameters $l_{t,v}$ over the set *V* if the houses' number is the same as the number of EVs or greater when some houses have no EV.

Each EV $v \in V$ requires to be charged with a given amount of energy e_v (KWh) estimated based on the available energy in the battery and the travel distance as a sum of the route destinations specified by the EV user for the next day. The arrival time a_v to the house and the departure time d_v from the house are given for each EV. The SOC for each vehicle *v* at the arrival time is defined with the input parameter $SOC_v^{arrival}$. Each EV $v \in V$ is characterized by an energy capacity QE_v (kWh), an output battery voltage $U_v^{battery}$, a charge capacity represented by the parameter Q_v (Ah), and equipped with an onboard charger of a power capacity defined as L_v. We define the state of charge (SOC) of a battery as the amount of charge it contains divided by its charge capacity Q_v.

All EVs are subjected to a charging interruption parameter N for battery health reasons resulting in a longer battery life cycle. Like the model in chapter 4, we set a maximum and a minimum value of SoC defined as the input parameters SOC^{max} and SOC^{min} for battery health reasons. Each house of EV v is subjected to a maximum contract power denoted by the parameter P_v that is agreed on by both the user and the energy supplier. In the garage of each EV house *v*, we assume that a level 2 single-phase 230V-32A smart charger with a power capacity of up to 7.3 kW defined by the parameter G is installed.

Just like in section 4.1 and based on the battery model presented in section 3.3.2, we approximate a linear piecewise function for the discretized CC-CV charging process of the batteries, which consists of several breakpoints $q_v + 1$ fitted to the real CC-CV concave charging function of the battery of vehicle v. The linear approximation of the battery's charging function of vehicle v assumes that the charging current $I_{v,b}^{max}$ represents a ceiling to the actual current to be retrieved between breakpoints b and $b-1$ for $b \in B_v$ having B_v as the set of breakpoints fitted to the actual CC-CV charging process of the battery of vehicle v. Let $SOC_{v,b}^{break}$ be the SoC associated with the breakpoint $b \in B_v$ of the charging function of vehicle v. Finally, we set a minimum current $I_{v,b}^{min}$ applied to EFV v between two consecutive breakpoints b and $b-1$ of the battery's charging function for battery protection purposes.

5.2 PEAK SHAVING MODEL FORMULATION

Five sets of decision variables are required for the formulation of PSM. Binary variables $z_{t,v}^{b}$ take a value of 1 if vehicle v is retrieving current while being plugged into the EVSE during period *t* that lies in the time interval between a_v the arrival time to the site and $d_v - 1$ the period before departure time from the site between breakpoints SOC_{b-1}^{break} and SOC_{b}^{break} and take a value of 0 otherwise. While $y_{t,v}$ are binary variables that depend on the values of $z_{t,v}^{b}$. They take a value of 1 for any interruption that occurs in the charging process of vehicle v between periods $t-1$ and t and takes a value of 0 otherwise.

Real and positive variables $i_{t,v}$ refer to the charging current applied to vehicle v during the entire period t. Real and positive variables $soc_{t,v}$ refer to the state of charge of vehicle v at the beginning of time t. Finally, Real and positive variable X^{max} that corresponds to the maximum charging power retrieved from the grid by all the neighborhood houses during the planning interval. To sum up, our problem is presented in the following mathematical model and the mixed-integer linear programming formulation (MILP), respectively:

Sets:

- T: The set of time in the scheduling horizon $(T = \{1, \dots, T^{max}\}, (t \in T)$
- V: Set of EVs. $(v \in V)$
- B_v: Set of breakpoints used in the piecewise linear approximation of the CC-CV charging function of the battery of vehicle v. $(b \in B_v)$

Parameters:

- M_t: The neighborhood household total power consumption at time t.
- $l_{t,v}$: non-flexible consumption profile (non-EV) of each house of EV v at time t. (kW)
- Q_v: The charge capacity of the battery of EV v. (Ah)
- QE_v: The energy capacity of the battery of EV v. (kWh)
- L_v: The onboard power capacity of the charger of EV v. (kW)
- N_v: The maximum number of cuts allowed for the battery of EV v.
- a_v: The arrival time of EV v to the house.
- d_v: The departure time of EV v from the house.
- e_v: Energy needed by EV v. (KWh)
- $SOC_v^{arrival}$: The state of charge associated with the arrival time for each EV $v \in V$.
- P_v The Grid power capacity of the house of EV v at any time(kW)
- $U_v^{battery}$: The rated voltage of the battery of EV v. (V)
- l_v^{max} : Power supply limit of the EVSE installed at the house of EV v (Charger specification). (kW)
- $I_{v,b}^{max}$: The maximum current that could be withdrawn in the piecewise linear approximation of the CC-CV charging function of the charger of EV v between the breakpoints b and $b-1$ with $b \in B_v$, $b > 0$. (A)
- $I_{v,b}^{min}$: The minimum current that could be withdrawn in the piecewise linear approximation of the CC-CV charging function of the charger of EV v between the breakpoints b and $b-1$ with $b \in B_v$, $b > 0$. (A)
- $SOC_{v,b}^{break}$: The state of charge associated with breakpoints $b \in B_v$ of the piecewise linear approximation of the CC-CV charging function of the charger of EV v.
- SOC^{max}: The maximum state of charge that any vehicle could reach while charging.

- SOC^{min}: The minimum state of charge that any vehicle could reach during the discharging process while performing its route the next day.
- q: The average weighted power loss factor due to the AC-DC conversion.
- Δt: Timestep in (h).

Variables:

- $i_{t,v} \geq 0$: current withdrawn by EV v at time t. (A)
- $soc_{t,v} \geq 0$: The state of charge of EV v at time t.
- $z_{t,v}^{b} \in \{0,1\}$: 1 if EV v is charging at time t with a state of charge between $SOC_{,b-1}^{break}$ and $SOC_{v,b}^{break}$.
  0 otherwise.
- $y_{t,v} \in \{0,1\}$: 1 if EV v stops charging at time period t.
  0 otherwise
- $\bar{X} \geq 0$: The maximum total household power consumption of the neighborhood withdrawn from the grid along the planned horizon.

Formulation:

$$\text{minimize} \qquad \text{Maximum power} = \bar{X} \tag{40}$$

subject to:

$$\left(M_t + \sum_{v \in V} \frac{i_{t,v}}{Q_v} QE_v\right) \leq \bar{X} \qquad \forall t \in T \tag{41}$$

$$l_{t,v} + \frac{i_{t,v}}{Q_v} QE_v \leq P_v \qquad \forall\, t \in T, v \in V \tag{42}$$

$$\sum_{t=1}^{a_v - 1} \sum_{v \in V} \sum_{b \in B_v \setminus \{0\}} z_{t,v}^{b} + \sum_{t=d_v}^{T^{max}} \sum_{v \in V} \sum_{b \in B_v \setminus \{0\}} z_{t,v}^{b} = 0 \tag{43}$$

$$soc_{t,v} = SOC_v^{arrival} \qquad \forall v \in V, t \in \{1, \dots, a_v\} \tag{44}$$

$$soc_{d_{v+1},v} = soc_{d_v} - \frac{e_v}{QE_v} \qquad \forall v \in V \tag{45}$$

$$soc_{d_v,v} = soc_{a_v} + \frac{e_v}{QE_v} \qquad \forall v \in V \tag{46}$$

$$\sum_{t \in T} \frac{i_{t,v} \Delta t (1-q)}{Q_v} + SOC_v^{arrival} - SOC^{min} = \frac{e_v}{QE_v} \qquad \forall v \in V \tag{47}$$

$$soc_{t,v} = soc_{t-1,v} + \frac{i_{t-1,v} \Delta t (1-q)}{Q_v} \qquad \forall t \in \mathrm{T} \backslash \{1, d_v, d_v + 1\}, v \in V \tag{48}$$

$$soc_{t+1,v} \leq SOC_{v,b}^{break} + 1 - z_{t,v}^b \qquad \forall t \in \{a_v, \dots, d_v - 1\}, v \in V, b \in B_v \backslash \{0\} \tag{49}$$

$$soc_{t,v} \leq SOC_{v,b-1}^{break} - 1 + z_{t,v}^b \qquad \forall t \in \{a_v, \dots, d_v\}, v \in V, b \in B_v \backslash \{0\} \tag{50}$$

$$SOC^{min} \leq soc_{t,v} \leq SOC^{max} \qquad \forall t \in T, v \in V \tag{51}$$

$$i_{t,v} \leq \sum_{b \in B_v \backslash \{0\}} I_{v,b}^{max} z_{t,v}^b \qquad \forall t \in T, v \in V \tag{52}$$

$$i_{t,v} \leq \sum_{b \in B_v \backslash \{0\}} I_{v,b}^{min} z_{t,v}^b \qquad \forall t \in T, v \in V \tag{53}$$

$$\sum_{b \in B_v \backslash \{0\}} z_{t-1,v}^b - \sum_{b \in B_v \backslash \{0\}} z_{t,v}^b \leq y_{t,v} \qquad \forall t \in \{a_v + 1, \dots, d_v\}, v \in V \tag{54}$$

$$\sum_{b \in B_v \backslash \{0\}} z_{\mathrm{t},v}^b \geq y_{\mathrm{t},v} \qquad \forall t \in \mathrm{T} \backslash \{a_v + 1, \dots, d_v\}, v \in V \tag{55}$$

$$\sum_{t \in T} y_{t,v} \leq N_v + 1 \qquad \forall v \in V \tag{56}$$

$$i_{t,v} \leq \frac{l_v^{max}}{U_v^{battery}} \cdot 1000 \cdot \sum_{b \in B_v \backslash \{0\}} z_{t,v}^b \qquad \forall t \in T, v \in V \tag{57}$$

$$i_{t,v} \leq \frac{L_v}{U_v^{battery}} \cdot 1000 \cdot \sum_{b \in B_v \setminus \{0\}} z_{t,v}^b \qquad \forall t \in T, v \in V \tag{58}$$

$$z_{t,v}^b \in \{0,1\} \qquad \forall v \in V, t \in T, b \in B_v \tag{59}$$

$$y_{t,v} \in \{0,1\} \qquad \forall v \in V, t \in T \tag{60}$$

The objective function (40) minimizes the maximum total household power consumption of the neighbourhood withdrawn from the grid along the planning horizon $\bar{X}$ to reduce the impact of the increasing EVs' charging demand. Specifically, $\bar{X}$ represents the maximum value of the sum of the normal power consumption M_t of all the houses in the neighborhood and the power retrieved by all the EVs at any period t over the planned time interval.

Constraints (41) calculates the maximum charging power retrieved from the grid throughout the entire planned interval. Constraints (42) ensure that the instantaneous total power consumption of each house would never exceed the contract power limit P_v at any time t. Constraints (43) ensure that no charging events take place while the EVs are performing their routes such that variables $z_{t,v}^b$ take the value of 0. Constraints (44) and (45) assign the discharging process of each vehicle v to its departure period d_v and that its SOC remains constant until the arrival period.

Constraints (46) and (47) ensure for each vehicle v to be charged the exact amount of the predefined needed energy e_v between the departure d_v and the arrival a_v periods from and to the house, respectively. Constraints (48) define the SOC of vehicle v at the beginning of time t as the sum of its SoC at the beginning of the previous period $t-1$ and the SoC gained equivalent to the charge current retrieved during the entirety of period $t-1$. Constraints (49) and (50) bound the SoC of vehicle v between two consecutive breakpoints depending on the specific piecewise linear function of the CC-CV process that corresponds to the charger installed in the house of vehicle v. Constraints (51) set limits for the SoC of each vehicle during the charging and discharging processes between the predefined parameters SOC^{max} and SOC^{min} for longer battery life.

Constraints (52)-(53) set a range for the variation of the charge current applied to vehicle v between the maximum and minimum current values $I_{v,b}^{max}$ and $I_{v,b}^{min}$ that are associated with the segment of the CC-CV charger-specific linear piecewise linear function to prevent undercharging and overcharging effects. Constraints (54)-(56) set a limit N_v for the maximum number of cuts allowed for each EV along the planning horizon to minimize the effects of battery degradation resulting in longer battery life. Constraints (57) ensure that the charging current applied on vehicle v would not exceed the charging station's power capacity. Constraints (58) force the power retrieved by vehicle v from the charging station to respect its onboard charger's power capacity. Constraints (59) and (60) define the domains of the variables that were not appropriately bounded by the other constraints.

5.3 CHARGING COST REDUCTION MODEL FORMULATION

The CCRM is a cost minimization model and is a subsequent submodel dependent on the primary optimization model PSM. The CCRM aims to provide EV users a degree of freedom in choosing their charging schedule for electricity bill reduction while not violating the maximum power constraint established in the primary model. This model depends mainly on the results of the PSM such that we generate slack parameters calculated through the difference between the obtained value of $\bar{X}$ and the total power retrieved by all the houses, which is estimated using the output decision variables $\overline{\iota_{t,v}}$ at each time t that represent the charge current applied to each vehicle *v* at time t. This model is applied individually to each house of the neighbourhood that owns an EV.

CCRM is designed with the same sets created in the PSM: set of time T, set of EVs *V*, and the set of breakpoints B_v that corresponds to the CC-CV charging process of each vehicle. The input parameters are considered the same as those used in the primary model but with slight changes. Because CCRM is applied to each house of EV v individually, then the total household power consumption of the neighbourhood isn't needed and is replaced with only the normal power consumption $l_{t,v}$ (kW) of every house *v* at time t. The basic power and the slack parameters of the power allowed to be withdrawn by EV v at time t are defined by $\overline{u_{t,v}}$ (kW) and $\overline{s_{t,v}}$ (kW), respectively. The parameters $\overline{u_{t,v}}$ correspond to the decision variable of the charge current $\overline{\iota_{t,v}}$ applied to each vehicle v at time *t* as an output of the first optimization stage performed in PSM. We define $\overline{u_{t,v}}$ (kW) as the power retrieved by vehicle v at time t and is estimated by dividing the product of the charge current $\overline{\iota_{t,v}}$ (A) and the energy capacity QE_v (kWh) by the total charge capacity Q_v (Ah) for each vehicle *v* as shown in Eq. (61).

$$\overline{u_{t,v}} = \frac{i_{t,v}}{Q_v} Q E_v \quad \forall t \in T, v \in \mathrm{V} \tag{61}$$

The slack parameters $\overline{s_{t,v}}$ are the additional power allowed to be retrieved by vehicle v at time t compared to $\overline{u_{t,v}}$. The combination of both parameters $\overline{u_{t,v}}$ and $\overline{s_{t,v}}$ represent the grid limit during the charging process of vehicle *v* at any time *t,* which replace the constraints **(41)** in the PSM. $\overline{s_{t,v}}$ estimation is done in two steps where we first calculate the total power slack parameters S_t (kW) for all the houses in the neighbourhood and then divide these total slack parameters among EV users based on a particular method. S_t is estimated as the difference between the grid's peak power value $\bar{X}$ (kW) and the total power retrieved by all the neighbourhood's houses at every time *t* as in Eq. (62) such that both the normal consumption of all houses M_t and the EVs' power consumption are included.

$$\bar{S_t} = \bar{X} - \left(M_t + \sum_{v \in V} \overline{u_{t,v}} \right) \quad \forall t \in T \tag{62}$$

$\bar{S_t}$ is distributed among EV users with different proportions where each EV gets an additional power value of $\overline{s_{t,v}}$ (kW) on top of its original power limit $\overline{u_{t,v}}$ based on two different approaches. At each period t, the slack parameters are assigned only to the EVs that comply with the following conditions:

- Each vehicle v must be physically plugged into its charging point such that t lies between its arrival and departure periods a_v and d_v, respectively.
- The total power consumption of the house of vehicle v ($l_{t,v} + \overline{u_{t,v}}$) (kW) should be less than the contract power limit P_v.
- The power retrieved $\overline{u_{t,v}}$ must be less than the charging power capacity expressed by the minimum value among the onboard charger capacity L_v and the EVSE capacity l_v^{max}.
- Each vehicle *v* must be relatively empty such that the cumulative charged energy stored in its battery packs should be smaller than 90% of the energy needed e_v (kWh) by vehicle v to travel its route the next day. This condition prevents the EVs that get almost fully charged at early periods and not in need of slack parameters from lowering the chances of the empty EVs benefiting from higher slack parameters for a more efficient model of higher cost reductions to the largest possible number of EVs.

We define C_t as the subset of V that consists of all the eligible EVs to be given complementary slack parameters $\overline{s_{t,v}}$ according to the previously mentioned conditions at every period t. After knowing the number of vehicles in C_t, we distribute the total power slack parameters $\overline{S_t}$ among these vehicles in a fair way to make sure that each vehicle v take the most advantage of $\overline{s_{t,v}}$. In Eqs. (63)-(65), we present the mathematical approach we follow to estimate the suitable slack value for each vehicle *v* at any time *t*.

$$x_{t,v} = \begin{cases} \min\left(L_v, l_v^{max}, P_v - l_{t,v}\right) - u_{t,v} & \forall v \in C_t,\ C_t \subset V \\ 0 & \forall v \in V \backslash \{C_t\},\ C_t \subset V \end{cases} \qquad \forall t \in T \tag{63}$$

$$F_t = \sum_{v \in V} x_{t,v} \qquad \forall t \in T \tag{64}$$

$$s_{t,v} = \begin{cases} \frac{x_{t,v}}{F_t} \cdot S_t & if\ F_t > S_t \\ x_{t,v} & if\ F_t \leq S_t \end{cases} \qquad \forall v \in V, \forall t \in T \tag{65}$$

$$s_{t,v} = \begin{cases} \frac{S_t}{|C_t|} & \forall v \in C_t,\ C_t \subset V \\ 0 & \forall v \in V \backslash \{C_t\},\ C_t \subset V \end{cases} \qquad \forall t \in T \tag{66}$$

First, and using Eq. (63), we estimate how much additional power to $\overline{u_{t,v}}$ each vehicle $v \in C_t$ at every time *t* can retrieve before reaching the power capacity of its onboard charger, the capacity of the EVSE, or the contract power limit P_v after excluding the household power consumption $l_{t,v}$ and it's denoted by the parameter $\overline{x_{t,v}}$. For the EVs that don't respect the previously mentioned conditions, then they don't belong to the subset C_t and that $x_{t,v}$ take the value of 0. In Eq. (64), we calculate F_t the sum of all the parameters $x_{t,v}$ at every time *t* which is necessary for the fair distribution of S_t based on a percentage approach.

Finally, and through Eqs. (65) and (66), we determine the exact slack parameter $\overline{s_{t,v}}$ suitable for each vehicle v at any time t. Eq. (65) refers to the percentage slack distribution approach such that $\overline{s_{t,v}}$ equal to $\overline{x_{t,v}}$ if the total allowed additional power of all the EVs $\overline{F_t}$ is less than or equal to the total slack parameter $\overline{S_t}$. However, if $\overline{F_t}$ is greater than $\overline{S_t}$ which means that the total slack parameter is not enough to provide $\overline{x_{t,v}}$ to each vehicle v, then we consider giving it a weighted $\overline{s_{t,v}}$ equals to a fraction of $\overline{S_t}$ equivalent to the percentage of the individual required power$\overline{x_{t,v}}$ for vehicle v out of the total required power value $\overline{F_t}$ for all EVs.

On the other hand, Eq. (66) corresponds to the even slack distribution approach where $\overline{S_{t,v}}$ equal to the ratio of $\overline{S_t}$ the total slack parameter over the number of vehicles that belong to the subset $\overline{C_t}$ for every vehicle $v \in C_t$ at every time t. Only one equation of the two Eqs. (65) and (66) will be used in our optimization model depending on whether we choose to follow the percentage distribution approach or the even one for calculating the slack parameters.

Four sets of decision variables are required to formulate CCRM that represent a correction of the similar decision variables used in the PSM. Binary variables $z_{t,v}^{b}$ take a value of 1 if vehicle v is retrieving current while being plugged into the EVSE during period t that lies in the time interval between a_v the arrival time to the site and $d_v - 1$ the period before departure time from the site between breakpoints SOC_{b-1}^{break} and SOC_{b}^{break} and take a value of 0 otherwise. While $y_{t,v}$ are binary variables that depend on the values of $z_{t,v}^{b}$ and take a value of 1 for any interruption that occurs while charging vehicle v between periods $t-1$ and t and takes a value of 0 otherwise.

Real and positive variables $i_{t,v}$ refer to the charging current applied to vehicle *v* during the entire period t. Finally, real and positive variables $soc_{t,v}$ refer to the state of charge of vehicle *v* at the beginning of time t. To sum up, our problem is presented in the following mathematical model and the mixed-integer linear programming formulation (MILP), respectively:

Sets:

- T: The set of time in the scheduling horizon ($T = \{1, \dots, T^{max}\}, t \in T$)
- V: Set of EVs. ($v \in V$)
- B_v: Set of breakpoints used in the piecewise linear approximation of the CC-CV charging function of the battery of vehicle v. ($b \in B_v$)

Parameters:

- $l_{t,v}$: non-flexible consumption profile (non-EV) of each house of EV v at time t. (kW)
- p_t: Electricity price at time t. ($€/kWh$)
- Q_v: The charge capacity of the battery of EV v. (Ah)
- QE_v: The energy capacity of the battery of EV v. (kWh)
- L_v: The onboard power capacity of the charger of EV v. (kW)
- N_v: The maximum number of cuts allowed for the battery of EV v.
- a_v: The arrival time of EV v to the house.
- d_v: The departure time of EV v from the house.

- e_v: Energy needed by EV v. (KWh)
- $SOC_v^{arrival}$: The state of charge associated with the arrival time for each EV $v \in V$.
- P_v The Grid power capacity of the house of EV v at any time(kW)
- $U_v^{battery}$: The rated voltage of the battery of EV *v*. (V)
- l_v^{max} : Power supply limit of the EVSE installed at the house of EV *v* (Charger specification). (kW)
- $I_{v,b}^{max}$: The maximum current that could be withdrawn in the piecewise linear approximation of the CC-CV charging function of the charger of EV *v* between the breakpoints *b* and *b-1* with $b \in B_v$, $b > 0$. (A)
- $I_{v,b}^{min}$: The minimum current that could be withdrawn in the piecewise linear approximation of the CC-CV charging function of the charger of EV *v* between the breakpoints *b* and *b-1* with $b \in B_v$, $b > 0$. (A)
- $SOC_{v,b}^{break}$: The state of charge associated with breakpoints $b \in B_v$ of the piecewise linear approximation of the CC-CV charging function of the charger of EV *v*.
- SC^{max}: The maximum state of charge that any vehicle could reach while charging.
- SOC^{min}: The minimum state of charge that any vehicle could reach during the discharging process while performing its route the next day.
- $u_{t,v}$: The power retrieved by EV v at time t as an output from the PSM. (kW)
- $s_{t,v}$**:** The power slack parameter is given to each vehicle v at time t for more flexibility in the charge schedule. (kW)
- q: The average weighted power loss factor due to the AC-DC conversion.
- Δt: Timestep in (h).

Variables:

- $i_{t,v} \geq 0$: current withdrawn by EV *v* at time *t*. (A)
- $soc_{t,v} \geq 0$: The state of charge of EV *v* at time *t*.
- $z_{t,v}^b \in \{0,1\}$: 1 if EV *v* is charging at time *t* with a state of charge between $SOC_{v,b-1}^{break}$ and $SOC_{v,b}^{break}$.
  0 otherwise.
- $y_{t,v} \in \{0,1\}$: 1 if EV *v* stops charging at time period *t*.
  0 otherwise

Mathematical Formulation of $\mathbf{CCRM}_v$ $\forall v \in V$:

$$\text{minimize:} \qquad \sum_{t \in t} p_t \Delta t \left(l_{t,v} + \frac{i_{t,v}}{Q_v} QE_v \right) \tag{67}$$

subject to:

$$\frac{i_{t,v}}{Q_v} QE_v \leq \overline{u_{t,v}} + \overline{s_{t,v}} \qquad \forall\, t \in T \tag{68}$$

$$l_{t,v} + \frac{i_{t,v}}{Q_v} QE_v \leq P_v \qquad \forall\, t \in T \tag{69}$$

$$\sum_{t=1}^{a_v - 1} \sum_{b \in B_v \backslash \{0\}} z_{t,v}^b + \sum_{t=d_v}^{T^{max}} \sum_{b \in B_v \backslash \{0\}} z_{t,v}^b = 0 \tag{70}$$

$$soc_{t,v} = SOC_v^{arrival} \qquad \forall t \in \{1, \dots, a_v\} \tag{71}$$

$$soc_{d_v+1,v} = soc_{d_v,v} - \frac{e_v}{QE_v} \tag{72}$$

$$soc_{d_v,v} = soc_{a_v,v} + \frac{e_v}{QE_v} \tag{73}$$

$$\sum_{t \in T} \frac{i_{t,v} \Delta t (1-q)}{Q_v} + SOC_v^{arrival} - SOC^{min} = \frac{e_v}{QE_v} \tag{74}$$

$$soc_{t,v} = soc_{t-1,v} + \frac{i_{t-1,v} \Delta t (1-q)}{Q_v} \qquad \forall t \in \mathrm{T} \backslash \{1, d_v, d_v + 1\} \tag{75}$$

$$soc_{t+1,v} \leq SOC_{v,b}^{break} + 1 - z_{t,v}^b \qquad \forall t \in \{a_v, \dots, d_v - 1\}, b \in B_v \backslash \{0\} \tag{76}$$

$$soc_{t,v} \leq SOC_{v,b-1}^{break} - 1 + z_{t,v}^b \qquad \forall t \in \{a_v, \dots, d_v\}, b \in B_v \backslash \{0\} \tag{77}$$

$$SOC^{min} \leq soc_{t,v} \leq SOC^{max} \qquad \forall t \in T \tag{78}$$

$$i_{t,v} \leq \sum_{b \in B_v \setminus \{0\}} I_{v,b}^{max} z_{t,v}^{b} \qquad \forall t \in T \tag{79}$$

$$i_{t,v} \leq \sum_{b \in B_v \setminus \{0\}} I_{v,b}^{min} z_{t,v}^{b} \qquad \forall t \in T \tag{80}$$

$$\sum_{b \in B_v \setminus \{0\}} z_{t-1,v}^{b} - \sum_{b \in B_v \setminus \{0\}} z_{t,v}^{b} \leq y_{t,v} \qquad \forall t \in \{a_v + 1, \dots, d_v\} \tag{81}$$

$$\sum_{b \in B_v \setminus \{0\}} z_{t,v}^{b} \geq y_{t,v} \qquad \forall t \in \mathrm{T} \setminus \{a_v + 1, \dots, d_v\} \tag{82}$$

$$\sum_{t \in T} y_{t,v} \leq N_v + 1 \tag{83}$$

$$i_{t,v} \leq \frac{l_v^{max}}{U_v^{battery}} \cdot 1000 \cdot \sum_{b \in B_v \setminus \{0\}} z_{t,v}^{b} \qquad \forall t \in T \tag{84}$$

$$i_{t,v} \leq \frac{L_v}{U_v^{battery}} \cdot 1000 \cdot \sum_{b \in B_v \setminus \{0\}} z_{t,v}^{b} \qquad \forall t \in T \tag{85}$$

$$z_{t,v}^{b} \in \{0,1\} \qquad \forall t \in T, b \in B_v \tag{86}$$

$$y_{t,v} \in \{0,1\} \qquad \forall t \in T \tag{87}$$

The objective function (67) minimizes cost_v the total electricity bill over the planning horizon for each house of vehicle $v \in V$. The $CCRM_v$ is applied individually to each house owning an EV by creating a loop over the set V. cost_v (€) is the product of the energy cost p_t ($€/\mathrm{kWh}$), the duration of time Δt (hours), and the total power retrieved by the house, including both $l_{t,v}$ (kW) the household power and the EV charging power retrieved by house v at every period t then summed up over the planning horizon of set T. The power retrieved while charging vehicle v at every time t is determined based on Eq. (61), similar to the calculation of $\overline{u_{t,v}}$. Constraints (68) set a limit to the power retrieved by vehicle v at every time t using the slack parameters $\overline{s_{t,v}}$ such that their combination with the parameters $\overline{u_{t,v}}$ represent a weighted grid limit for each vehicle v at every time t. Constraints (69)-(87) do the same job as the constraints (42)-(60) used in modeling the PSM; however, in the $CCRM_v$, they are all applied to only one vehicle v for the entire planning horizon.

5.4 SIMPLE EXAMPLE OF SEVERAL OPTIMAL SOLUTIONS

This section aims to help the reader better understand the functionality of the RNS and the correlation between both models, the PSM and CCRM, by presenting a small instance with different parameters that give other optimal solutions. We design this example with a time interval of 24 equidistant periods with a time step of one hour, resulting in a full-day instance. The planning horizon starts from 16:00 and lasts until 15:00 the next day, such that we have a whole night charging problem. We discretize our planning horizon with 24 equidistant periods with period lengths of one hour (i.e., $\delta = 1\ h$), where 16:00 is set to 1 and 15:00 is denoted by 24. We consider having a set of 3 EVs such that each vehicle represents a house in the neighbourhood.

The cost of energy p_t is assumed to be as follows: 0.25 ($€/\mathrm{kWh}$) during the peak hours from periods 1 to 3 and 21 to 24 (12:00-18:00), 0.05 ($€/\mathrm{kWh}$) during the off-peak hours from periods 9 to 17 (00:00-8:00), and 0.15 ($€/\mathrm{kWh}$) during the shoulder hours the rest of day. The total household power consumption parameters M_t (kW) of all the houses in the neighbourhood and the individual household power consumption $l_{t,v}$ (kW) of each house of an EV user *v* are given at every period *t*. The EV's specifications-related parameters and all the routes data for every vehicle $v \in V$ are shown in Table 18.

Table 18: The design specifications and route parameters for the simple numerical example

V	EV model	Q (Ah)	QE (kWh)	L (kW)	$U^{battery}$ (V)	l^{max} (kW)	P (kW)	$SOC^{arrival}$	N	a	d	e (kWh)
1	BMW i3	120	42.24	11	352	7.36	10	0.05	2	4	22	31.68
2	RAV4	108	41.8	10	386	7.36	10	0.05	2	8	17	31.35
3	NISSAN LEAF	66	24	6.6	360	7.36	6	0.05	2	6	19	18

For simplification, we set only three breakpoints associated with the linear approximation CC-CV charging process of the battery of each vehicle *v* using a level 2 fast charger of 7.36 (kW) power capacity and a charge current of 32 (A) such that $B_v = \{0,1,2\}$. The values of the maximum current $I_{v,b}^{max}$ and the minimum current $I_{v,b}^{min}$And the SOC breakpoint $SOC_{v,b}^{break}$ that correspond to the breakpoints specified to each vehicle *v* are summarized in Table 19. We assume having an average weighted charging loss that is constant at any state of charge or any current charge value, and it is equal to 6.5%. We set a minimum and a maximum SOC value of 0.05 and 0.99, respectively.

Table 19: The design parameters associated with the linear approximation breakpoints of the charging process of different vehicles' models

B_v	EV 1 (BMW i3)			EV 2 (RAV4)			EV 3 (NISSAN LEAF)		
	$SOC_{1,b}^{break}$	$I_{1,b}^{max}$ (A)	$I_{1,b}^{min}$ (A)	$SOC_{2,b}^{break}$	$I_{2,b}^{max}$ (A)	$I_{2,b}^{min}$ (A)	$SOC_{3,b}^{break}$	$I_{3,b}^{max}$ (A)	$I_{3,b}^{min}$ (A)
0	0	0	0	0	0	0	0	0	0
1	0.923	21	2	0.92	19.1	2	0.882	18.5	2
2	0.99	10.5	1	0.99	10	1	0.99	10.5	1

This example consists of two cases with two different solutions, where case one is based on distributing the slack parameters evenly among all eligible EVs at every time *t* as in Eq. (66). However, case two considers estimating specific weighted slack parameters to each vehicle *v* at every period *t* using the Eqs. (63), (64), and (65).

Table 20: Optimal solution of the PSM

T	1	2	3	4	5	6	7	8	9	10	11	12	13	14	15	16	17	18	19	20	21	22	23	24	
M_t (kW)	9.86	10.84	11.07	12.06	9.36	10.99	9.83	4.85	1.38	0.90	1.01	0.92	1.02	3.34	0.94	2.01	8.04	6.85	5.17	4.25	5.10	5.69	5.41	5.71	
p_t (€/kWh)	0.25	0.25	0.25	0.15	0.15	0.15	0.15	0.15	0.05	0.05	0.05	0.05	0.05	0.05	0.05	0.05	0.05	0.15	0.15	0.15	0.25	0.25	0.25	0.25	$cost_v$ (€)
Vehicle: 1																									
$l_{t,1}$ (kW)	3.03	3.34	3.41	3.71	2.88	3.38	3.03	1.49	0.42	0.28	0.31	0.28	0.31	1.03	0.29	0.62	2.47	2.11	1.59	1.31	1.57	1.75	1.66	1.76	
$i_{t,1}$ (A)	0	0	0	0	3.98	0	0	0	0	32	0	0	0	0	0	0	0	0	0	32	30.23	0	0	0	
$u_{t,1}$ (kW)	0	0	0	0	0.91	0	0	0	0	7.36	0	0	0	0	0	0	0	0	0	7.36	6.95	0	0	0	10.70
$soc_{t,1}$	0.05	0.05	0.05	0.05	0.05	0.07	0.07	0.07	0.07	0.07	0.23	0.23	0.23	0.23	0.23	0.23	0.23	0.23	0.23	0.23	0.40	0.55	0.05	0.05	
$z^b_{t,1}$	0	0	0	0	1	0	0	0	0	1	0	0	0	0	0	0	0	0	0	1	1	0	0	0	
$y_{t,1}$	0	0	0	0	0	1	0	0	0	0	1	0	0	0	0	0	0	0	0	0	0	1	0	0	
Vehicle: 2																									
$l_{t,2}$ (kW)	3.64	4.00	4.09	4.45	3.46	4.06	3.63	1.79	0.51	0.33	0.37	0.34	0.38	1.23	0.35	0.74	2.97	2.53	1.91	1.57	1.88	2.10	2.00	2.11	
$i_{t,2}$ (A)	0	0	0	0	0	0	0	22.75	32	0	10.18	0	0	0	0	32	0	0	0	0	0	0	0	0	
$u_{t,2}$ (kW)	0	0	0	0	0	0	0	5.25	7.38	0	2.35	0	0	0	0	7.38	0	0	0	0	0	0	0	0	10.47
$soc_{t,2}$	0.05	0.05	0.05	0.05	0.05	0.05	0.05	0.05	0.17	0.33	0.33	0.38	0.38	0.38	0.38	0.38	0.55	0.05	0.05	0.05	0.05	0.05	0.05	0.05	
$z^b_{t,2}$	0	0	0	0	0	0	0	1	1	0	1	0	0	0	0	1	0	0	0	0	0	0	0	0	
$y_{t,2}$	0	0	0	0	0	0	0	0	0	1	0	1	0	0	0	0	1	0	0	0	0	0	0	0	
Vehicle: 3																									
$l_{t,3}$ (kW)	3.18	3.50	3.58	3.90	3.02	3.55	3.18	1.57	0.44	0.29	0.33	0.30	0.33	1.08	0.30	0.65	2.60	2.21	1.67	1.37	1.65	1.84	1.75	1.85	
$i_{t,3}$ (A)	0	0	0	0	0	4.59	9.56	8.44	0	16.34	0	0	0	0	0	0	0	16.3	0	0	0	0	0	0	
$u_{t,3}$ (kW)	0	0	0	0	0	1.07	2.22	1.96	0	3.80	0	0	0	0	0	0	0	3.79	0	0	0	0	0	0	9.27
$soc_{t,3}$	0.05	0.05	0.05	0.05	0.05	0.05	0.09	0.18	0.25	0.25	0.40	0.40	0.40	0.40	0.40	0.40	0.40	0.40	0.55	0.05	0.05	0.05	0.05	0.05	
$z^b_{t,3}$	0	0	0	0	0	1	1	1	0	1	0	0	0	0	0	0	0	1	0	0	0	0	0	0	
$y_{t,3}$	0	0	0	0	0	0	0	0	1	0	1	0	0	0	0	0	0	0	1	0	0	0	0	0	
X_t (kW)	9.86	10.84	11.07	12.06	10.28	12.06	12.06	12.06	8.76	12.06	3.36	0.92	1.02	3.34	0.94	9.39	8.04	10.64	5.17	11.61	12.06	5.69	5.41	5.71	
S_t (kW)	2.20	1.22	0.99	0	1.78	0	0	0	3.30	0	8.70	11.13	11.04	8.72	11.11	2.67	4.01	1.42	6.89	0.45	0	6.36	6.65	6.34	
$\bar{X}$ (kW)	12.06																								

Table 21: Optimal solution of the CCRM using the percentage weighted algorithm for calculating the complementary slack parameters.

T	1	2	3	4	5	6	7	8	9	10	11	12	13	14	15	16	17	18	19	20	21	22	23	24	
p_t(€/kWh)	0.25	0.25	0.25	0.15	0.15	0.15	0.15	0.15	0.05	0.05	0.05	0.05	0.05	0.05	0.05	0.05	0.05	0.15	0.15	0.15	0.25	0.25	0.25	0.25	
S_t (kW)	2.20	1.22	0.99	0	1.78	0	0	0	3.30	0	8.70	11.13	11.04	8.72	11.11	2.67	4.01	1.42	6.89	0.45	0	6.36	6.65	6.34	$cost_v$ (€)
Vehicle: 1																									
$l_{t,1}$ (kW)	3.03	3.34	3.41	3.71	2.88	3.38	3.03	1.49	0.42	0.28	0.31	0.28	0.31	1.03	0.29	0.62	2.47	2.11	1.59	1.31	1.57	1.75	1.66	1.76	
$s_{t,1}$ (kW)	0	0	0	0	1.78	0	0	0	1.88	0	3.55	4.01	3.98	3.27	4.01	1.55	2.75	1.42	6.89	0	0	0	0	0	
$\overline{i_{t,1}}$ (A)	0	0	0	0	0	0	0	0	5.34	20.91	10.08	11.40	11.32	5.13	0	0	0	0	0	0	0	0	0	0	
$\overline{u_{t,1}}$ (kW)	0	0	0	0	0	0	0	0	1.88	7.36	3.55	4.01	3.98	1.81	0	0	0	0	0	0	0	0	0	0	8.48
$\overline{soc_{t,1}}$	0.05	0.05	0.05	0.05	0.05	0.05	0.05	0.05	0.05	0.09	0.25	0.33	0.42	0.51	0.55	0.55	0.55	0.55	0.55	0.55	0.55	0.55	0.05	0.05	
$\overline{z_{t,1}^b}$	0	0	0	0	0	0	0	0	1	1	1	1	1	1	0	0	0	0	0	0	0	0	0	0	
$\overline{y_{t,1}}$	0	0	0	0	0	0	0	0	0	0	0	0	0	1	1	0	0	0	0	0	0	0	0	0	
Vehicle: 2																									
$l_{t,2}$ (kW)	3.64	4.00	4.09	4.45	3.46	4.06	3.63	1.79	0.51	0.33	0.37	0.34	0.38	1.23	0.35	0.74	2.97	2.53	1.91	1.57	1.88	2.10	2.00	2.11	
$s_{t,2}$ (kW)	0	0	0	0	0	0	0	0	0	0	2.42	4.01	3.98	3.27	4.01	0	0	0	0	0	0	0	0	0	
$\overline{i_{t,2}}$ (A)	0	0	0	0	0	0	0	0	19.07	0	12.31	10.37	10.30	5.72	0	0	0	0	0	0	0	0	0	0	
$\overline{u_{t,2}}$ (kW)	0	0	0	0	0	0	0	0	7.38	0	4.76	4.01	3.98	2.21	0	0	0	0	0	0	0	0	0	0	9.94
$\overline{soc_{t,2}}$	0.05	0.05	0.05	0.05	0.05	0.05	0.05	0.05	0.05	0.22	0.22	0.32	0.41	0.50	0.55	0.55	0.55	0.05	0.05	0.05	0.05	0.05	0.05	0.05	
$\overline{z_{t,2}^b}$	0	0	0	0	0	0	0	0	1	0	1	1	1	1	0	0	0	0	0	0	0	0	0	0	
$\overline{y_{t,2}}$	0	0	0	0	0	0	0	0	0	1	0	0	0	1	1	0	0	0	0	0	0	0	0	0	
Vehicle: 3																									
$l_{t,3}$ (kW)	3.18	3.50	3.58	3.90	3.02	3.55	3.18	1.57	0.44	0.29	0.33	0.30	0.33	1.08	0.30	0.65	2.60	2.21	1.67	1.37	1.65	1.84	1.75	1.85	
$s_{t,3}$ (kW)	0	0	0	0	0	0	0	0	1.42	0	2.73	3.11	3.07	2.19	3.10	1.12	1.27	0	0	0	0	0	0	0	
$\overline{i_{t,3}}$ (A)	0	0	0	0	0	0	0	0	0	8.79	7.52	8.55	8.44	2.00	0	0	0	0	0	0	0	0	0	0	
$\overline{u_{t,3}}$ (kW)	0	0	0	0	0	0	0	0	0	3.20	2.73	3.11	3.07	0.73	0	0	0	0	0	0	0	0	0	0	8.36
$\overline{soc_{t,3}}$	0.05	0.05	0.05	0.05	0.05	0.05	0.05	0.05	0.05	0.05	0.17	0.28	0.40	0.52	0.55	0.55	0.55	0.55	0.55	0.05	0.05	0.05	0.05	0.05	
$\overline{z_{t,3}^b}$	0	0	0	0	0	0	0	0	0	1	1	1	1	1	0	0	0	0	0	0	0	0	0	0	
$\overline{y_{t,3}}$	0	0	0	0	0	0	0	0	0	0	0	0	0	1	1	0	0	0	0	0	0	0	0	0	
X_t^{CCRM} (kW)	9.86	10.84	11.07	12.06	9.36	10.99	9.83	4.85	10.64	11.45	12.06	12.06	12.06	8.08	0.94	2.01	8.04	6.85	5.17	4.25	5.10	5.69	5.41	5.71	

Table 22: Optimal solution of the CCRM using the even distribution algorithm for estimating the complementary slackness parameters.

T	1	2	3	4	5	6	7	8	9	10	11	12	13	14	15	16	17	18	19	20	21	22	23	24	
p_t(€/kWh)	0.25	0.25	0.25	0.15	0.15	0.15	0.15	0.15	0.05	0.05	0.05	0.05	0.05	0.05	0.05	0.05	0.05	0.15	0.15	0.15	0.25	0.25	0.25	0.25	
S_t (kW)	2.20	1.22	0.99	0	1.78	0	0	0	3.30	0	8.70	11.13	11.04	8.72	11.11	2.67	4.01	1.42	6.89	0.45	0	6.36	6.65	6.34	$cost_v$ (€)
Vehicle: 1																									
$l_{t,1}$ (kW)	3.03	3.34	3.41	3.71	2.88	3.38	3.03	1.49	0.42	0.28	0.31	0.28	0.31	1.03	0.29	0.62	2.47	2.11	1.59	1.31	1.57	1.75	1.66	1.76	
$s_{t,1}$ (kW)	0	0	0	0	1.78	0	0	0	1.65	0	2.90	3.71	3.68	2.91	3.70	1.33	2.01	1.42	6.89	0	0	0	0	0	
$\overline{i_{t,1}}$ (A)	0	0	0	0	0	0	0	0	4.69	11.47	8.23	10.54	10.45	8.26	10.52	0	0	0	0	0	0	0	0	0	
$\overline{u_{t,1}}$ (kW)	0	0	0	0	0	0	0	0	1.65	4.04	2.90	3.71	3.68	2.91	3.70	0	0	0	0	0	0	0	0	0	8.48
$\overline{soc_{t,1}}$	0.05	0.05	0.05	0.05	0.05	0.05	0.05	0.05	0.05	0.09	0.18	0.24	0.32	0.40	0.47	0.55	0.55	0.55	0.55	0.55	0.55	0.55	0.05	0.05	
$\overline{z_{t,1}^b}$	0	0	0	0	0	0	0	0	1	1	1	1	1	1	1	0	0	0	0	0	0	0	0	0	
$\overline{y_{t,1}}$	0	0	0	0	0	0	0	0	0	0	0	0	0	0	1	1	0	0	0	0	0	0	0	0	
Vehicle: 2																									
$l_{t,2}$ (kW)	3.64	4.00	4.09	4.45	3.46	4.06	3.63	1.79	0.51	0.33	0.37	0.34	0.38	1.23	0.35	0.74	2.97	2.53	1.91	1.57	1.88	2.10	2.00	2.11	
$s_{t,2}$ (kW)	0	0	0	0	0	0	0	0	0	0	2.90	3.71	3.68	2.91	3.70	0	0	0	0	0	0	0	0	0	
$\overline{i_{t,2}}$ (A)	0	0	0	0	0	0	0	0	19.07	0	13.55	9.59	9.51	6.04	0	0	0	0	0	0	0	0	0	0	
$\overline{u_{t,2}}$ (kW)	0	0	0	0	0	0	0	0	7.38	0	5.25	3.71	3.68	2.34	0	0	0	0	0	0	0	0	0	0	9.94
$\overline{soc_{t,2}}$	0.05	0.05	0.05	0.05	0.05	0.05	0.05	0.05	0.05	0.22	0.22	0.33	0.42	0.50	0.55	0.55	0.55	0.05	0.05	0.05	0.05	0.05	0.05	0.05	
$\overline{z_{t,2}^b}$	0	0	0	0	0	0	0	0	1	0	1	1	1	1	0	0	0	0	0	0	0	0	0	0	
$\overline{y_{t,2}}$	0	0	0	0	0	0	0	0	0	1	0	0	0	1	1	0	0	0	0	0	0	0	0	0	
Vehicle: 3																									
$l_{t,3}$ (kW)	3.18	3.50	3.58	3.90	3.02	3.55	3.18	1.57	0.44	0.29	0.33	0.30	0.33	1.08	0.30	0.65	2.60	2.21	1.67	1.37	1.65	1.84	1.75	1.85	
$s_{t,3}$ (kW)	0	0	0	0	0	0	0	0	1.65	0	2.90	3.71	3.68	2.91	3.70	1.33	2.01	0	0	0	0	0	0	0	
$\overline{i_{t,3}}$ (A)	0	0	0	0	0	0	0	0	0	10.44	7.97	10.20	6.68	0	0	0	0	0	0	0	0	0	0	0	
$\overline{u_{t,3}}$ (kW)	0	0	0	0	0	0	0	0	0	3.80	2.90	3.71	2.43	0	0	0	0	0	0	0	0	0	0	0	8.36
$\overline{soc_{t,3}}$	0.05	0.05	0.05	0.05	0.05	0.05	0.05	0.05	0.05	0.05	0.20	0.31	0.46	0.55	0.55	0.55	0.55	0.55	0.55	0.05	0.05	0.05	0.05	0.05	
$\overline{z_{t,3}^b}$	0	0	0	0	0	0	0	0	0	1	1	1	1	0	0	0	0	0	0	0	0	0	0	0	
$\overline{y_{t,3}}$	0	0	0	0	0	0	0	0	0	0	0	0	1	1	0	0	0	0	0	0	0	0	0	0	
X_t^{CCRM}	9.86	10.84	11.07	12.06	9.36	10.99	9.83	4.85	10.41	8.74	12.06	12.06	10.80	8.58	4.65	2.01	8.04	6.85	5.17	4.25	5.10	5.69	5.41	5.71	

Tables 20, 21, and 22 illustrate two solutions of the simple instance explained above to reduce the EV charging impact on the grid and show different strategies of providing the EV users a degree of freedom in charging their EVs with the least cost. Table 20 presents the optimal solution of the PSM that is the first stage of the main problem TSREV-CSP. This solution focuses on charging all EVs with the required energy no matter the energy cost while keeping the grid power as low as possible. We observe that the peak power demand $\bar{X}$ obtained by the PSM has a value of 12.06 (kW) that is equal to the maximum household power consumption of the building. Whereas the solutions in Tables 21 and 22 refer to the CCRM optimal solutions and focus on the effect of the slack parameters obtained in the PSM for minimizing the electricity bill of each house in the neighbourhood. The solution in Table 20 is common for both cases one and two because of having fixed input parameters in both cases and its independence from the slack parameters. Tables 21 and 22 illustrate the results of the first and the second case based on the weighted percentage distribution algorithm and the even distribution algorithm of $s_{t,v}$, respectively.

The energy cost of each house in the specified neighbourhood is determined using Eq. (67) for all three tables. We find that the total energy cost of house 1 reduces from €10.7 obtained by the PSM down to €8.84 when applying the CCRM, while that of house 2 reduces from €10.47 down to €9.94 and house 3 from €9.27 to €8.36. By comparing all the solutions together, it's evident that both the energy supplier and EV users' goals were achieved using the optimization model of TSREV-CSP in both cases. That is because we see the maximum grid power obtained in the PSM being always respected at a value of 12.06 kW over the planned horizon. In addition to the apparent electricity bill reduction of each house when applying the CCRM in each of the two cases. However, the resultant energy cost for all houses has been constant when using the CCRM in both cases. The Energy cost reduction over the two stages of the optimization model TSREV-CSP is clearly illustrated in Figure 40, where the electricity bill for house 1 registered the highest reduction rate of around 20%. In comparison, the least cost reduction happens to be for house 2 with a rate of 5%.

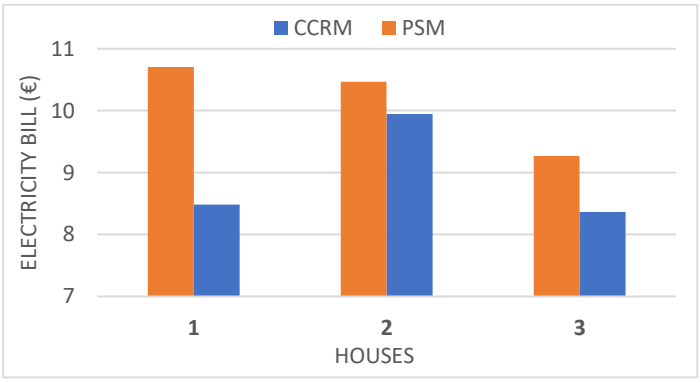

Figure 40: A comparison of the electricity bills of all the houses obtained in the PSM and the CCRM.

a)

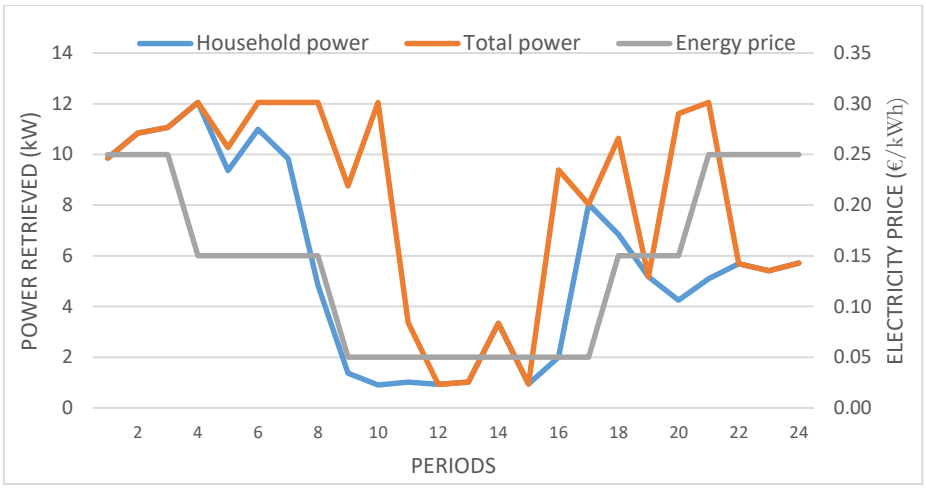

b)

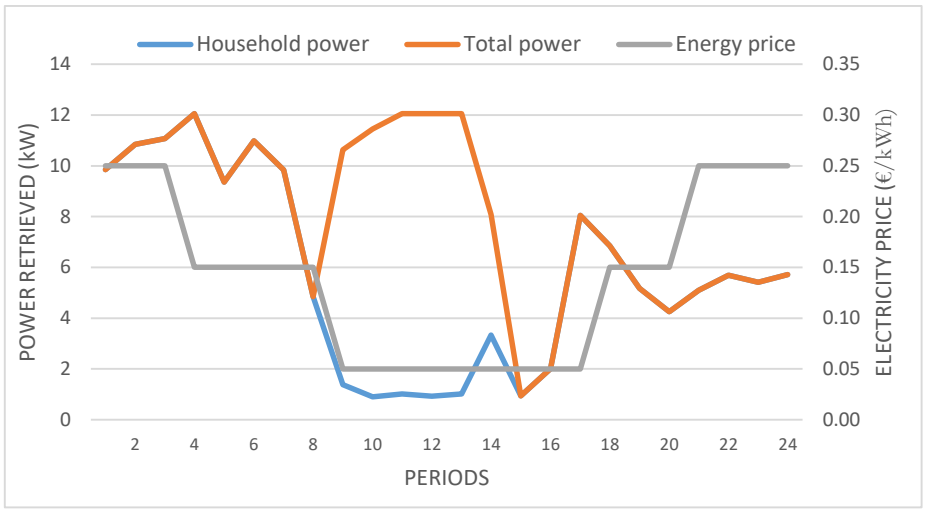

c)

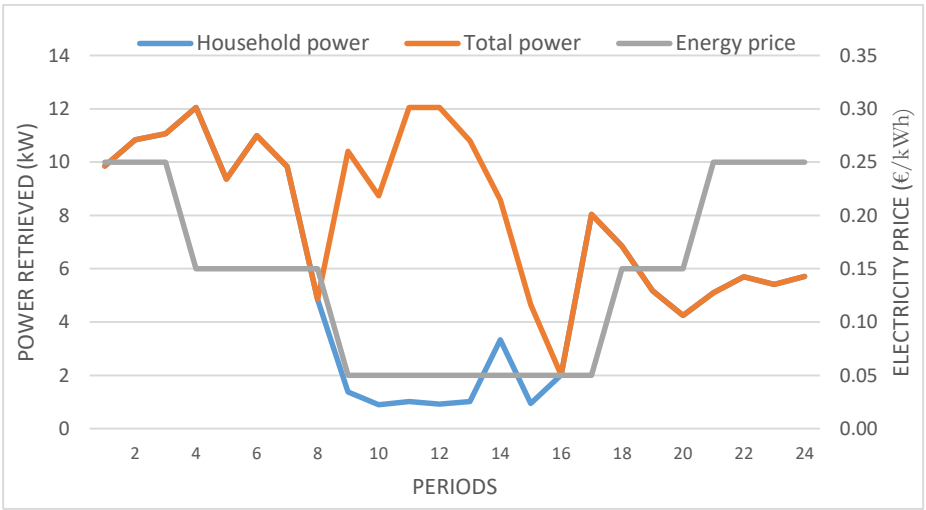

Figure 41: The power retrieved by all the houses in the neighbourhood: (a) optimal solution of the PSM, (b) optimal solution of the CCRM with % slack distribution algorithm, (c) optimal solution of the CCRM with even slack distribution algorithm.

a)

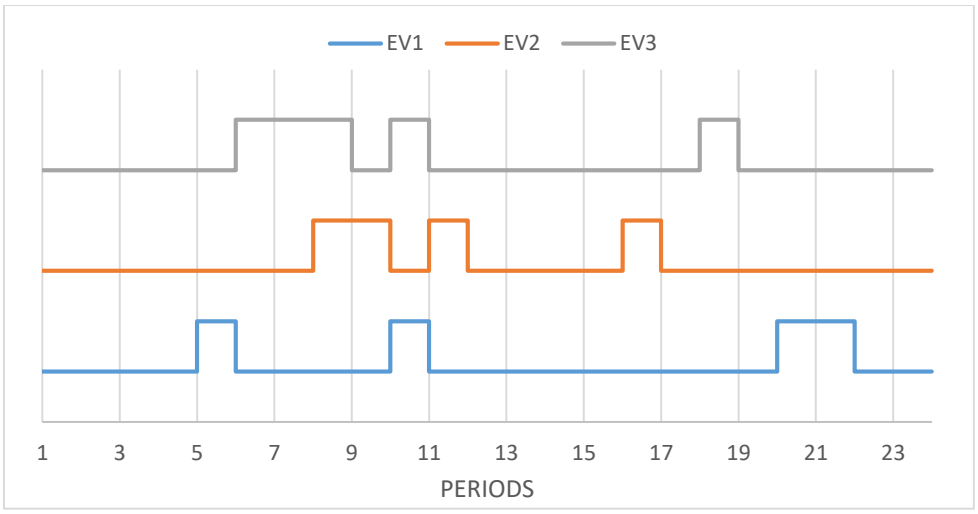

b)

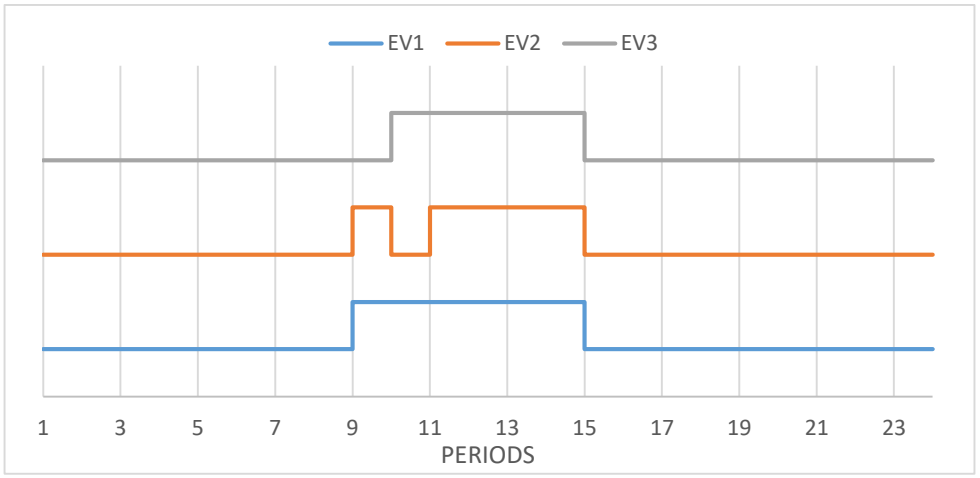

c)

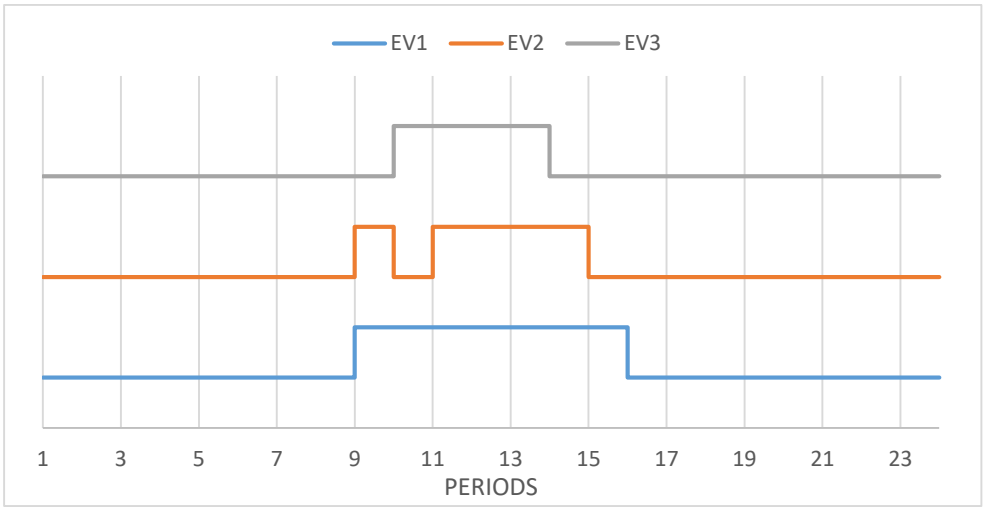

Figure 42: The charging schedule of all the EVs in the neighbourhood: (a) optimal solution of the PSM, (b) optimal solution of the CCRM with % slack distribution algorithm, (c) optimal solution of the CCRM with even slack distribution algorithm.

The solutions in Tables 20, 21, and 22 are illustrated in Figures 41 and 42, where graph (a) in both figures corresponds to the optimal solution of the PSM, while graphs (b) and (c) refer to the optimal solutions of cases one and two, respectively. Figure 41 shows the total power retrieved by all the houses in the neighbourhood over the planning interval of the optimal solutions in both cases. The orange curve represents the sum of the total power retrieved, including both the household power consumption and the EV charging power, while the blue one corresponds to the household power consumption only. By looking at graph (a), we observe that EV charging impact on the grid capacity is negligible because the maximum power obtained in the PSM equals exactly the maximum household power consumption of all the houses combined of 12.06 kW at period 4. Then when applying the CCRM on each house in the neighbourhood as in graphs (b) and (c) of both cases, we see the effect of the intelligent pricing techniques on reducing the electricity bill represented in shifting the EV charging loads towards the periods of the day with the lowest household power consumption and the least energy costs that lie between the periods 9 to 15 (00:00-06:00).

Figure 42 presents the optimized charging schedule of all the EVs in the neighbourhood for the three cases. By comparing chart (a) with charts (b) and (c), we can say that the charging schedule obtained from CCRM in both cases is more efficient from the battery health perspective as it reduces the charging interruptions automatically when charging all EVs on the off-peak periods of the day at the same time of reducing charging costs and respecting the grid power capacity. We observe slight changes in the charging behavior of EVs when using the two different approaches in CCRM, as shown in charts (b) and (c). The reduction in the values of the slack parameters given to vehicle 1 using the even distribution algorithm leads to a longer charging period of an additional hour. In contrast, the charging time of vehicle 3 is reduced by an hour when gaining higher slack parameters under the same distribution approach. However, the charging schedule of vehicle 2 didn’t change for having insignificant variations in the slack parameters between cases one and two.

6 RESULTS, DISCUSSIONS, AND MANAGERIAL INSIGHTS

This chapter presents the results of all the test instances we generate for both models under different scenarios. This chapter aims to validate the proposed smart charging strategies of the models discussed in chapters 4 and 5, analyze the grid impact under various scenarios, investigate the parameters that affect the total electricity bill and its breakdown components, and derive some managerial insights from the presented outcomes. All the experiments were executed using a machine with an operating system of Microsoft Windows 10 (64 bits and equipped with an 8 GB RAM processor. We use Python 3.7.3 as an open-source programming language to implement the formulations, generate some plots and figures, and process the results. We optimize the models using IBM ILOG CPLEX Optimization Studio V12.9.0.0, and it was necessary to create an interface between Python and the CPLEX solver by using Pyomo. Pyomo is a python optimization modeling object that contains a rich set of supporting libraries that simplify the formulation's presentation.

In section 6.1, we present the main datasets that are common for all the test instances of the EFV-CCSP proposed in chapter 4, and we provide a description of the base case scenario and some of its results. Moreover, we analyze the impact of different parameters by analyzing the results of the corresponding test instances and compare them with the base case scenario. Similarly, we present in section 6.2 the base case description of the TSREV-CSP discussed in chapter 5 with its corresponding results and analyze the impact of different parameters. A total of 629 experiments were performed with a total runtime of about five days such that 405 experiments refer to the EFV-CCSP and 224 correspond to the TSREV-CSP. All the experiments of the EFV-CCSP were subjected to a time limit of 1200 seconds (20 minutes). Similarly, we set the same time limit for each stage of the TSREV-CSP which means a 20 minutes time limit is applied to the PSM but in the CCRM, each house is subjected to this time limit.

There are two reasons for setting a time limit to our optimization model. The first is mainly to have a more practical optimization model for the users. However, the second reason goes back to some technical limitations of the machine used to perform these tests. Moreover, we set a minimum optimality gap of 0.5% for the solutions generated by all the tests within the specified time limit. Our experiments for both problems are planned over a one-day interval for a single overnight charging event assumed to be from 15:15 till 15:00 of the other day with a 15 mins time step which results in 97 equidistant periods.

6.1 RESULTS OF THE COMMERCIAL AND INDUSTRIAL PROBLEM

In this section, we present the results of the experiments performed for the commercial and industrial problem besides analyzing the impact of some parameters on the obtained optimal solutions. We generate three instances for three homogeneous fleet sizes n of 8, 12, and 16 medium-duty EFV. The three instances represent different travel behaviors that require different energy values and various arrival and departure periods for each vehicle of the fleet. We generate the instances as follows: instance (1) represents a case of average energy demand e_v represented by a range of 70%-80% of the battery's capacity equivalent to 60-65 miles as recommended by Feng & Figliozzi,(2013) for higher utilization efficiency of electric trucks. The overnight charging period of instance (1) is 15-16 hours, equivalent to an 8-9 hours working interval. Instance (2) refers to a case of low energy demand in the range of 60%-70% of the battery's capacity and a longer charging period equal to 16-17 hours. Finally, instance (3) is the case of a long travel behavior equivalent to 80%-90% of the battery's SoC and 10-11 hours charging period, and it represents an example of the worst-case scenario. We randomly generate the arrival and departure periods for each vehicle in all three instances where the arrival periods lie in the range of 15:30-18:00 equivalent to periods range of 2-12, whereas the departure periods are generated between 7:00 and 9:30 equivalent to periods range of 64-74. The nine main instances are summarized in Table 23.

Table 23: The nine main instances of the commercial and industrial scenario.

instance	Number of EVs	Range of SoC needed	Charging period range
1_8V	8	70%-80%	14-15 hours
2_8V	8	60%-70%	15-16 hours
3_8V	8	80%-90%	10-11 hours
1_12V	12	70%-80%	14-15 hours
2_12V	12	60%-70%	15-16 hours
3_12V	12	80%-90%	10-11 hours
1_16V	16	70%-80%	14-15 hours
2_16V	16	60%-70%	15-16 hours
3_16V	16	80%-90%	10-11 hours

The EFVs are considered to be a homogeneous fleet of medium-duty electric trucks like Mitsubishi Fuso,(2019) that are equipped with six large battery packs and capable of driving a range of 80 miles. These battery packs together consist of approximately 606 3.6 V-38 Ah lithium ion battery cells that are assembled in a special configuration of series and parallel connections to produce a total energy capacity of 82.8 kWh, an output voltage of 360 V, and a total charge capacity of 120 Ah. These EFVs are equipped with an onboard charger of 11 kW power capacity when using AC power supplies.

We consider having a non-refrigerated warehouse as a commercial building type, and we generate full day normal power demand data in the form of 15mins-average power consumption based on the hourly energy consumption dataset presented by Miller & Meggers,(2017). The prices of electricity that vary during the day are assumed similar to those of the summer scenario proposed in (Pelletier et al., 2018), where we consider 0.25 $€/kWh$ during the peak hours (12:00-18:00), 0.05 $€/kWh$ during the off-peak hours (00:00-08:00), and 0.15 $€/kWh$ during the shoulder hours that represent the rest of the day. We set the maximum and minimum SoC as 0.99 and 0.05 respectively that are fixed for all the test instances and we consider that the minimum SoC itself is the SoC of all the EFVs at their arrival periods at the beginning of the planning horizon.

6.1.1 Base Case Scenario Description

The base case represents a scenario of using only an AC single-phase single-socket level-2 smart EVSE that is characterized by a 7.36 kW power capacity, a current up to 32 A, and a 230 V output voltage (pod POINT, n.d.-a). By referring to the battery charging process illustrated in section 3.3.1, we notice that this EVSE can charge the battery up to a SoC of 95% in a maximum of 11.5 hours entirely in the CC phase without any breakpoint. This implies the unnecessity of so many breakpoints, so we approximate the battery's charging process with only three breakpoints 0.05, 0.95, and 0.99, and having maximum DC values of 0, 3.4 A, and 1.75 A respectively excluding the charging losses. We estimate the battery charging losses independently of the SoC by 6.75% which is fixed for the other test instances. We define the minimum current that must be retrieved by the battery as 10% of the corresponding maximum current at the same breakpoint. We set the grid power for the value of 500 kW to neglect its effects which we present in previous chapters. The FRD fees are considered higher than the electricity price with a value of 11 $€/kW$ taken from Pelletier et al.,(2018) as well. Finally, we allow each EFV to go through a maximum of two charging interruptions by setting the parameter N to the value of two.

6.1.2 Base Case Results

Table 24: The results of all instances in the base case scenario.

	Electricity Bill (€)					Gap (%)	
instance	FRD	E	total	P_max	Time(s)	initial	final
1_8V	786.33	206.13	992.46	71.48	13.61	27.47	0
2_8V	706.66	202.74	909.40	64.24	9.25	20.84	0
3_8V	893.51	208.06	1101.57	81.23	8.58	34.65	0.05
1_12V	980.28	234.58	1214.86	89.12	443.77	78.92	0.5
2_12V	848.84	229.29	1078.13	77.17	77.27	33.23	0
3_12V	1139.88	238.44	1378.32	103.63	963.06	75.99	0
1_16V	1159.24	263.46	1422.70	105.39	160.05	49.4	0.1
2_16V	997.83	256.80	1254.63	90.71	217.92	42.62	0
3_16V	1382.92	267.52	1650.44	125.72	942.91	71.39	0

Table 24 shows the results of the nine different instances under the base case scenario where it consists of the total energy cost of the building defined as "total" $(€)$, its breakdown into FRD charges $(€)$ and normal energy cost "E" $(€)$, peak power demand "P_max" (kW), solution time (s), and the intial and final gaps $(\%)$. We notice that we got an optimal solution for all the instances and with acceptable run time for almost all the cases with a maximum run time of 443.7 s while only "3_12V" and "3_16" needed more than double the run time of the other cases to get an optimal solution. Moreover, all the final gaps are reported within a maximum of 0.1 $\%$.

Figure 43 presents the total electricity bill and the peak power demand for all the charging behaviours of the commercial base case. By looking at both the total energy cost and the peak power demand in all instances, we notice that when the number of EVs increases, the peak power demand and the total energy cost increase as well. Similarly, both the maximum power retrieved and the total electricity bill of the building are higher for the cases of higher energy demand and shorter charging time as in "3_8V", "3_12V", and "3_16V" than the cases of lower energy demands and longer charging periods like "2_8V", "2_12V", and "2_16V".The least power demand and the cheapest energy cost were reported for the instance "2_8V" by 64.24 (kW) and € 909.4 respectively, while the highest ones were reported for the instance "3_16V" by 125.72 (kW) and €1382.92 respectively. We explain these increases by the limited charging capacity of the EVSE that might be forced to work the whole charging period at its rated power to satisfy the energy demand. This provides a low degree of freedom in choosing cheaper periods of the day to charge the EVs, which is clearly shown in instances "3_8V", "3_12V", and "3_16V".

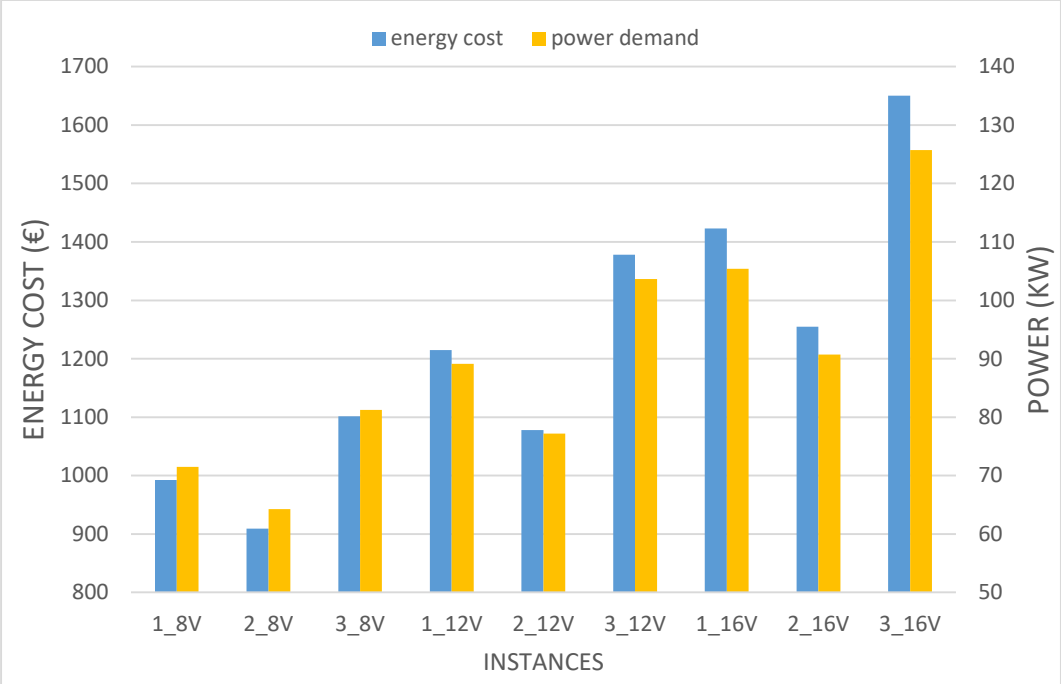

Figure 43: The total electricity bill and the peak power demand for all the charging behaviours of the commercial base case.

The combined effects of the number of EVs and their energy demands can be understood by comparing the instance of a few EFVs and high energy demand "3_8V" with the instance of more EFVs at low energy demand "2_12V". We can say that the additional four EFVs didn't impact the power system since lower energy demands mean a more flexible charging schedule. It allows the EFVs' owner to reduce both the electricity bill from €1101.57 at "3_8V" to €1078.32 at "2_12V" which hasn't been affected by the increase in the EV energy costs from about €208 at "3_8V" to €229.29 at "2_12V". In addition to reducing the peak power demand from around 81.23 (kW) at "3_8V" down to 77.17 (kW) at "2_12V". The same exactly applies to the instances "3_12V" and "2_16V".

Figure 44 presents the percentage contribution of the FRD charges and energy costs to the electricity bill. It shows that as the number of EFVs rises, the share of FRD charges increases at the expense of the normal energy costs due to the increase in the peak power demand, and this rate of increase is higher for larger energy demand scenarios. Thus, the higher the number of EFVs with critical energy demands means more chargers functioning at their rated power which leads to additional power demands.

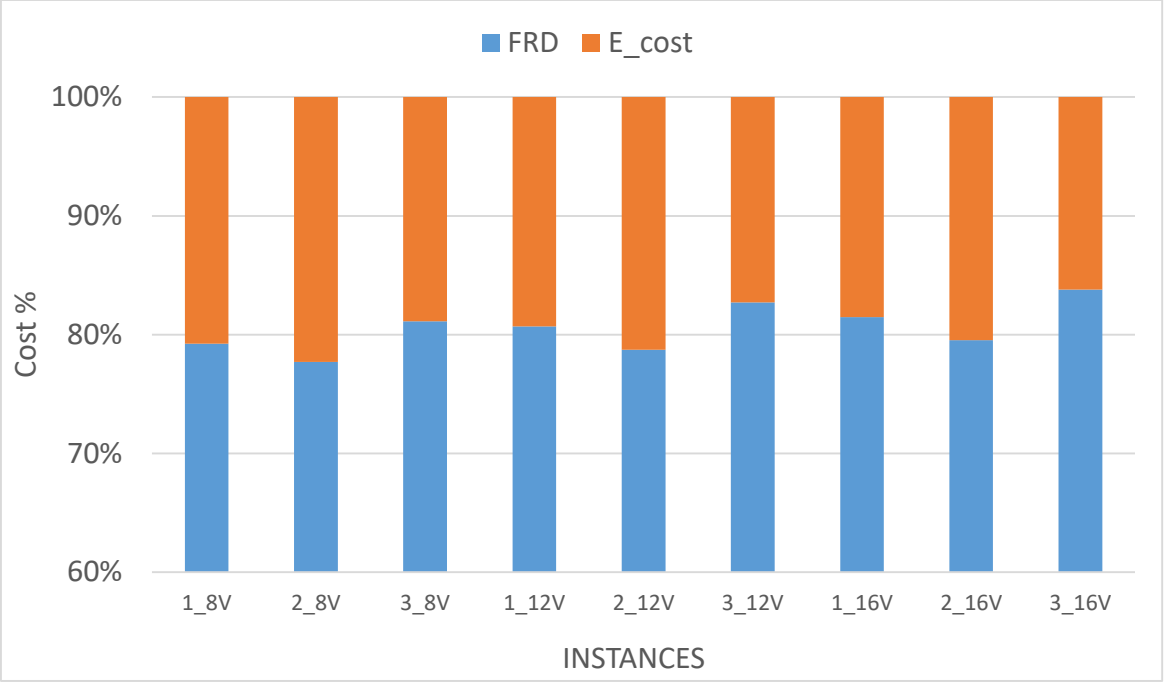

Figure 44: The FRD charges and energy cost contributions in the total electricity bill of the building for all the instances.

6.1.3 Multi-Criteria Analysis for The Commercial Charging Problem

In this section, we conduct extensive experiments of multiple scenarios similar to the one generated in the base case to analyze the effect of different parameters on the validation of our model and to identify better smart charging approaches. **Table 25** presents a summary of all the experiments performed under the various scenarios in terms of the solution time of the optimality condition reached. Our analysis considers having eight types of charging clusters that replace the predefined single-phase single-socket EVSE used in the base case scenario to study the impact of the clustered charging techniques on the energy cost and the peak power. These eight types of clusters are represented by the columns' names in each of the subtables shown in **Table 25** that we explain in the following section. We consider having two main types of three-phase charging clusters in terms of power levels, where one is characterized by a maximum power capacity of 11 kW while the other has a power capacity of 22 kW. For each scenario of the eight ones mentioned previously, we use several identical clusters with an equal number of charging points defined as sockets.

The name of each cluster type is defined by "$\alpha S\_\beta kW$" where "α" represents the number of sockets available in the cluster, S stands for the word socket, β specifies the maximum power capacity of the cluster and kW stands for the unit of power. For example, the seventh column in Table 25 that is named "3S_22kW", represents the case of using charging clusters of a 22 kW power capacity and each consists of three charging sockets. In case the number of the sockets available in all clusters is odd compared to an even number of EFVs, then we use the 7.36 kW single-socket charger used in the base case to make up the difference in the number of chargers and EVs. Each section of Table 25 refers to a different scenario by changing one parameter concerning the base case to identify its impact on the optimization model and the cost of energy.

Our multi-criteria analysis consists of three main affecting parameters classified as follows: FRD fees scenarios where the first subtable corresponds to the base case with high FRD charges assumed to be 11 $(€/kW)$ while the second one refers to the case of having lower FRD charges compared to the electricity prices with a value of 0.1 $(€/kW)$. The second one is the introduction of grid restrictions by changing the value of P from 500 (kW) in the base case to 110 kW as we see in the third subtable. Finally, the fourth and the fifth subtables correspond to the cases of and charging interruption control by changing the charging interruption limitations from two $(N = 2)$ in the base case to zero $(N = 0)$ and $(N = 1)$ one interruption respectively.

The colors used in Table 25 represent the feasibility level of the test instances performed. The cells with orange color refer to an infeasible problem. The yellow and blue cells are indicators of the optimization model's termination because of reaching the preset time limit. The main difference between these two colors is that the yellow one refers to a feasible problem with an integer optimal solution found upon the occurrence of the model's termination. However, the blue-colored cell represents the test instance with no solution found when reaching the preset time limit. The optimal solution found might be of a high optimality gap, as we can see in Table 26 that presents the final optimality gap of the solutions found for each test instance based on all scenarios where the colors used are similar to those in Table 25. Using Tables 25 and 26 together, we simplify our analysis in the coming sections by eliminating some charging technologies that obtain in the majority of the test instances either infeasible solutions (i.e., in orange and blue) or feasible and optimal solutions with poor final gap values of above 2%.

Table 25: The solution time of all the tests of the commercial charging problem under the five main scenarios.

Solution Time (s) (1200 s time limit)									
				High FRD (F = 11 $(€/kW)$)					
Instance	Base	1S_11	2S_11	3S_11	2S_22	3S_22	4S_22	5S_22	6S_22
1_8V	13.6	30.2	52.6		61.6	39.8	22.6	31.8	
2_8V	9.3	50.8	59.1	42.0	99.7	114.3	27.1	31.6	24.8
3_8V	8.6	187.9	1200.1		102.5	45.8	183.0		
1_12V	443.8	1200.2	20.0		208.5	140.1	111.3	183.8	
2_12V	77.3	112.1	20.7	265.6	282.8	117.3	105.8	118.1	63.7
3_12V	963.1	561.9	1200.1		436.9	378.9	1200.2		
1_16V	160.1	1200.3	1200.1		1200.1	394.6	376.3	318.1	
2_16V	217.9	1200.4	1200.1	716.4	80.6	368.9	218.7	172.0	217.5
3_16V	942.9	1200.2	1200.1		1114.4	670.3	1200.1		
				Low FRD (F = 0.1 $(€/kW)$)					
Instance	Base	1S_11	2S_11	3S_11	2S_22	3S_22	4S_22	5S_22	6S_22
1_8V	13.0	22.7	47.4		41.1	104.0	17.9	24.6	
2_8V	11.2	34.5	45.6	82.7	40.2	30.1	17.4	24.1	54.4
3_8V	9.0	66.6			113.3	106.0	110.2		
1_12V	158.0	394.5	20.1		22.0	156.5	89.3	1200.1	
2_12V	61.3	129.7	294.0	223.1	27.8	103.5	83.9	484.0	47.8
3_12V	163.5	273.7	1200.1		326.6	311.2	1200.1		
1_16V	198.3	296.7	639.3		672.0	879.4	262.7	1200.1	
2_16V	229.3	381.5	1071.8	1200.1	77.0	386.9	206.8	663.3	746.8
3_16V	423.4	700.9	1205.7		675.3	1200.1	1200.5	1200.2	
				P= 110 kW					
Instance	Base	1S_11	2S_11	3S_11	2S_22	3S_22	4S_22	5S_22	6S_22
1_8V	16.0	27.9	50.5		155.1	52.1	21.0	21.6	
2_8V	11.9	61.8	66.6	38.0	81.0	84.6	38.3	21.1	23.5
3_8V	8.8	249.8			71.9	82.6	124.3		
1_12V	1200.1	1009.0	21.1		24.8	175.2	222.3	162.7	
2_12V	79.7	138.5	19.7	247.0	32.2	100.2	100.8	95.1	60.3
3_12V									
1_16V									
2_16V	209.2	380.7	1200.1	916.4	753.7	437.3	234.4	270.0	213.6
3_16V									
				No interruption (N = 0)					
Instance	Base	1S_11	2S_11	3S_11	2S_22	3S_22	4S_22	5S_22	6S_22
1_8V	17.1	174.7	54.9		82.1	30.6	60.2	41.4	
2_8V	15.6	276.3	141.1	62.2	168.9	87.1	54.2	43.2	140.4
3_8V	8.9	242.6			231.1	102.0	278.6		
1_12V	897.0	1083.5	265.1		181.6	190.4	87.8	319.8	
2_12V	68.4	1200.1	571.2	443.7	201.5	267.0	104.1	103.3	135.4
3_12V	625.1	1200.2	1200.1		1200.1	252.7	1200.1		
1_16V	171.1	1200.5	1200.1		1200.5	485.5	1137.8	1202.0	
2_16V	243.6	1200.3	1200.1	1200.1	859.4	489.6	339.0	301.7	658.8
3_16V	870.6	1200.1	1204.3		1200.1	1200.2	1200.1		
				One interruption (N = 1)					
Instance	Base	1S_11	2S_11	3S_11	2S_22	3S_22	4S_22	5S_22	6S_22
1_8V	12.8	235.8	50.2		54.8	31.2	44.3	22.8	
2_8V	15.8	42.8	105.8	90.6	108.7	66.1	26.3	46.6	49.9
3_8V	9.9	209.0			256.4	100.7	119.5		
1_12V	477.6	1200.1	16.5		166.1	161.3	125.7	266.6	
2_12V	63.5	1140.3	20.6	471.1	29.5	85.8	109.1	152.6	103.1
3_12V	441.6	823.2	1200.1		1186.1	248.3	1200.2		
1_16V	166.7	1200.2	1200.1		1200.1	667.9	920.7	398.4	
2_16V	228.1	322.1	1200.1	1200.1	1200.1	802.8	475.7	263.4	267.7
3_16V	656.3	1200.2	1200.1		1200.1	716.2	1200.1		

Table 26: The Optimality gap of all the tests of the commercial charging problem under the five main scenarios.

Optimality Final Gap (%)						
			high FRD			
Case	Base	1S_11	2S_11	2S_22	3S_22	4S_22
1_8V	0	0.04	0.39	0.33	0.22	0
2_8V	0	0.25	0.02	0	0	0
3_8V	0.05	0.03		0.11	0.22	0.47
1_12V	0.5	14.83	0.43	0	0	0
2_12V	0	0	0.28	0.44	0.03	0
3_12V	0	0.11		0.46	0.1	
1_16V	0.1		1.24	2.11	0.33	0.03
2_16V	0		78.24	0.09	0	0.14
3_16V	0			0.12	0.41	
			Low FRD			
Case	Base	1S_11	2S_11	2S_22	3S_22	4S_22
1_8V	0	0.14	0.33	0.04	0.21	0
2_8V	0.16	0.12	0	0	0	0
3_8V	0	0.05		0.17	0.5	0.16
1_12V	0	0	0	0.31	0	0
2_12V	0.16	0.19	0	0.16	0.06	0.24
3_12V	0	0.11		0.49	0.37	
1_16V	0	0.26	0	0	0.33	0
2_16V	0.17	0.24	0.24	0.23	0	0
3_16V	0	0.12		0.29	0.72	
			P= 110 kW			
Case	Base	1S_11	2S_11	2S_22	3S_22	4S_22
1_8V	0.05	0.05	0.39	0	0	0
2_8V	0.02	0.37	0.32	0	0	0
3_8V	0.02	0.03		0.1	0.21	0.49
1_12V	9.23	0	0.4	0.03	0.1	0
2_12V	0.01	0.29	0.37	0.11	0.03	0
3_12V						
1_16V						
2_16V	0	0.1		0.02	0	0.14
3_16V						
			No interruption (N = 0)			
Case	Base	1S_11	2S_11	2S_22	3S_22	4S_22
1_8V	0	0	0.39	0.02	0.22	0.02
2_8V	0	0	0	0	0.24	0
3_8V	0	0.03		0.33	0.47	0.47
1_12V	0	0	0.44	0	0.1	0.45
2_12V	0		0.26	0.03	0	0.13
3_12V	0	76.23		0.38	0.32	
1_16V	0	75.5	75.5	75.5	0.33	0.37
2_16V	0		0.44	0.02	0	0.14
3_16V	0.03			10.44	3.25	
			One interruption (N = 1)			
Case	Base	1S_11	2S_11	2S_22	3S_22	4S_22
1_8V	0	0	0.39	0.02	0.22	0
2_8V	0.2	0.36	0.1	0	0.15	0.02
3_8V	0.01	0.03		0.05	0.05	0.48
1_12V	0	79.06	0.25	0	0.1	0.45
2_12V	0	0	0.26	0.03	0.03	0.44
3_12V	0	0.11		0.16	0.15	
1_16V	0		1.24	75.51	0.02	0.02
2_16V	0	0.04	78.22	78.25	0	0.05
3_16V	0			0.15	0.5	

6.1.4 Impacts of the Clustered Charging Technology

The breakpoints associated with the linear approximation of the discretized charging process presented in section 3.3.1 are considered to be kind of the same value since the onboard charger capacity applies a power limit while charging, allowing the EFVs to withdraw a maximum power of 12 kW that is almost equivalent to the socket power of "1S_11Kw". That's the reason why we consider at least two sockets for the cluster's type "2S_22 kW". The charging breakpoints are set for four since the CV stage is entered at a SoC of 0.935 and earlier than 0.95. The breakpoints for the 11 kW clusters are as follows: 0.05, 0.935, 0.95, and 0.99 that correspond to charging currents of 5.1 A, 3.4 A , and 1.7 A. For the 22 kW clusters, we apply the same breakpoints on its charging process but with current values of 5.6 A, 3.5 A, and 1.7 A. By referring to Table 25, we see that instances "3S_11kW", "5S_22kW", and "6S_22kW" got so many infeasibilities to the level of ignoring them in our test instances.

Table 27: The peak power demand in (kW) using different types of clusters.

Case	Base	1S_11kW	2S_11kW	2S_22kW	3S_22kW	4S_22kW
1_8V	71.49	71.04	71.44	71.2	71.17	70.95
2_8V	64.24	64.22	64.04	64	64	64
3_8V	81.23	80.66		80.68	80.8	92.29
1_12V	89.12	106.09	88.42	87.84	87.84	87.84
2_12V	77.18	76.93	77.24	77.43	76.91	76.88
3_12V	103.63	102.28		102.65	102.15	
1_16V	105.39		106.12	107.31	104.58	104.1
2_16V	90.71		123.12	90.54	90.45	90.65
3_16V	125.72			123.98	124.4	

Table 27 presents the peak power demand of 63 test instances that were performed on the predefined nine charging behaviors. In each instance, we use only one cluster type to charge the EVs. The peak power values that correspond to the instances using the single-phase EVSE are the highest on many instances with few exceptions that are mainly due to the optimization model termination when reaching the time limit before giving the optimal solution and are colored with yellow. All the power values are reported in the range of about 64 (kW) up to approximately 125 (kW). Figure 45 illustrates a summary of the results presented in Table 27 that helps to easily allocate the variations among the different instances. In general, the charging clusters of 22 (kW) showed better results in terms of the peak power demand than the other charging types for the majority of the test instances.

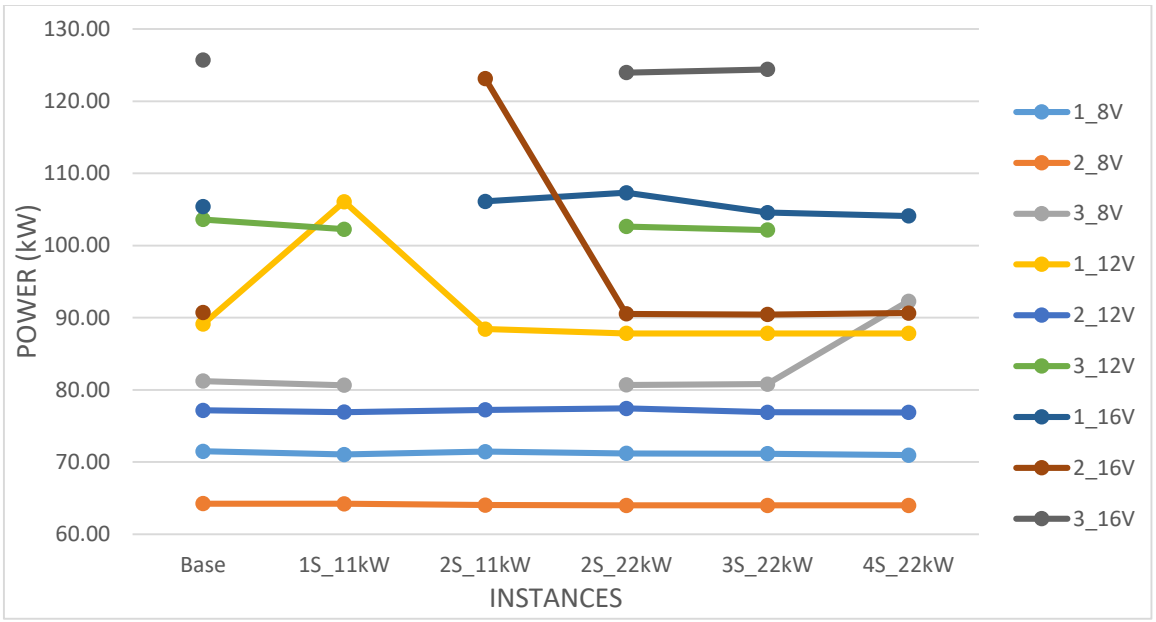

Figure 45: Peak power demand variation based on the different charging clusters used for all charging behaviors.

"3S_22kW" clusters give optimal solutions within the time limit and show peak power reduction for all the test instances performed compared to the base case. Each "3S_22kW" cluster type replaces three 7.36 (kW) chargers used in the base case. By looking at "4S_22kW", we notice that the peak power values are the lowest for most of the instances except for the two instances "3_12V" and "3_12V" that are colored in blue which need more time to reach the optimal solution. The peak power reduction reflects the decrease of the FRD fees and might reduce the total electricity bill based on the flexibility of the charging schedule during the periods of the cheapest electricity prices over the planning horizon.

Table 28 presents the total electricity bill of the building for all the test instances presented in Table 27, besides showing the percentage contributions of the FRD fees and energy costs in each electricity bill. Similar to the peak power, the energy costs follow the same trend in which the charging clusters with a capacity of 22 (kW) show better results than those of 11 (kW) capacity. This is clearly shown in the percentage of instances with either acceptable optimal solutions having relatively low final gaps less than 2% for each charging type where almost 50% of the instances using both charging types "1S_11kW" and "2S_11kW" give higher energy cost or no solution at all when reaching the preset time limit. However, 100% of the test instances of "3S_22kW" show cost reduction compared to the base case nad around 85% of those of "2S_22kW" and "4S_22kW" charging techniques result in cost reduction.

Table 28: The cost analysis of the different charging technologies and their effect on the total energy cost and its contributions.

	Instance	1_8V	2_8V	3_8V	1_12V	2_12V	3_12V	1_16V	2_16V	3_16V
Base	FRD (%)	79.23	77.71	81.11	80.69	78.73	82.70	81.48	79.53	83.79
	E_cost (%)	20.77	22.29	18.89	19.31	21.27	17.30	18.52	20.47	16.21
	total (€)	992.46	909.40	1101.57	1214.86	1078.13	1378.32	1422.70	1254.63	1650.44
1S_11kW	FRD (%)	79.07	77.65	80.95	82.59	78.65	82.44			
	E_cost (%)	20.93	22.35	19.05	17.41	21.35	17.56			
	total (€)	988.29	909.78	1096.05	1412.92	1075.88	1364.71			
2S_11kW	FRD (%)	79.24	77.62		80.48	78.75		81.68	84.15	
	E_cost (%)	20.76	22.38		19.52	21.25		18.32	15.85	
	total (€)	991.76	907.63		1208.52	1078.86		1429.13	1609.36	
2S_22kW	FRD (%)	79.07	77.60	80.94	80.34	78.85	82.52	81.97	79.47	83.52
	E_cost (%)	20.93	22.40	19.06	19.66	21.15	17.48	18.03	20.53	16.48
	total (€)	990.49	907.19	1096.56	1202.58	1080.21	1368.26	1440.13	1253.18	1632.93
3S_22kW	FRD (%)	79.13	77.60	80.97	80.34	78.65	82.40	81.33	79.46	83.56
	E_cost (%)	20.87	22.40	19.03	19.66	21.35	17.60	18.67	20.54	16.44
	total (€)	989.34	907.19	1097.69	1202.58	1075.75	1363.61	1414.47	1252.10	1637.75
4S_22kW	FRD (%)	79.04	77.60	83.03	80.34	78.64		81.20	79.52	
	E_cost (%)	20.96	22.40	16.97	19.66	21.36		18.80	20.48	
	total (€)	987.44	907.19	1222.60	1202.58	1075.46		1410.34	1253.90	

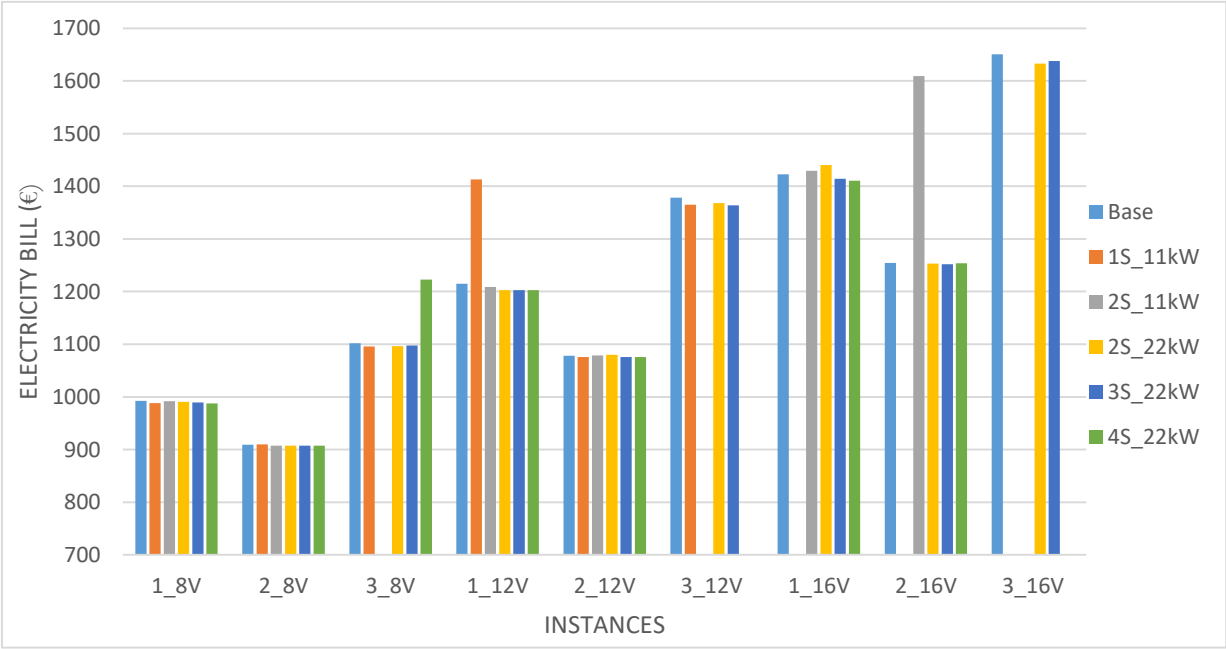

Figure 46: The total electricity bill of the building for all the instances using different charging technologies.

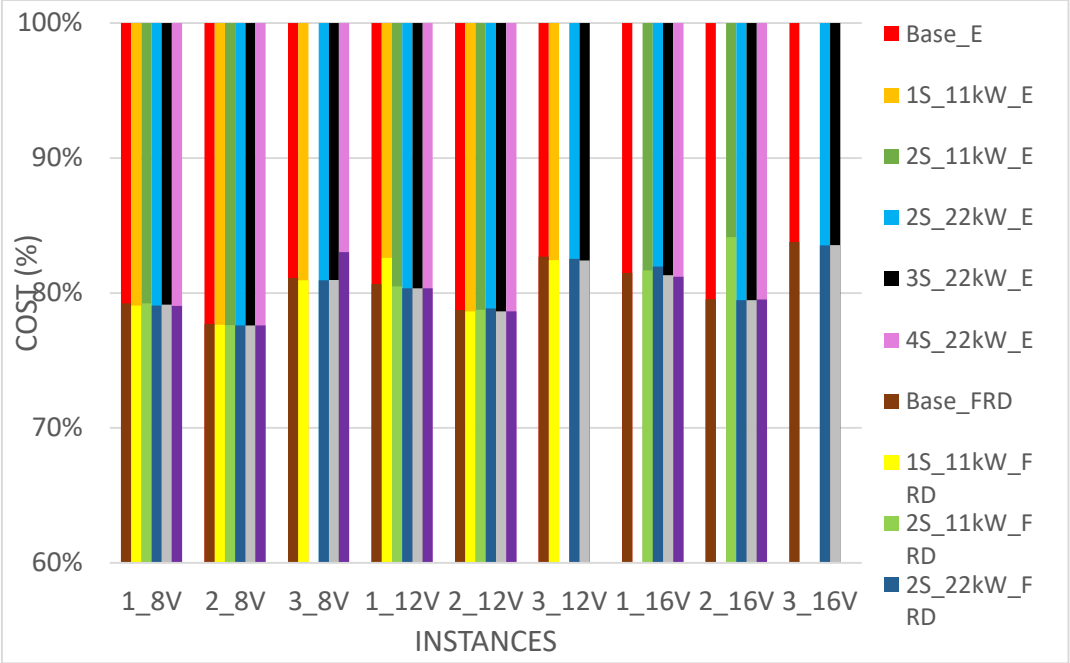

Figure 47: The percentage contributions of the FRD fees and energy costs in the electricity bill of different test instances using multiple charging techniques.

Figure 46 illustrates the total electricity bill of the building for the various test instances of different charging techniques presented in **Table 28**. The charging costs for the normal charging behaviors "1_8V", "1_12V", and "1_16V" in the base case scenario are around €992, €1215, and €1423 respectively. The costs are the most compared to the costs of the other clustered charging technologies with ignoring the poor optimal solution of "1S_11kW" for instance "1_12V", and "2S_11kW" and "2S_22kW" for instance "1_16V". The least charging costs are around €987 and €1410 for instances "1_8V" and "1_16V" respectively using the clustered charging technology "4S_22kW" and around €1203 for instance "1_12V" using the clustered charging technologies "2S_22kW", "3S_22kW", and "4S_22kW".

Figure 47 shows the percentage contributions of the electricity bill's components for each test instance using the different charging technologies. We see that the FRD fees generally contribute to around 80% in all the test instances and their percentages increase with the increase of peak power demand. This is clear in the instances "3_8V" and "1_12V" using clusters "4S_22kW" and "1S_11kW" respectively where the peak power increase rises the FRD fees by around 3% compared to other charging technologies. Similarly, the charging cluster "2S_11kW" increases the FRD contribution by 5% in test instance "2_16V" due to the additional peak power demands.

6.1.5 Effects of the FRD Charges

In this section, we study the impact of FRD charges on the peak power demand of the building besides its effect on the breakdown of the total electricity bill of the building. We repeat the same experiments performed in the previous section 6.1.4 by reducing the FRD charges to 0.1$(€/kW)$ while fixing the other parameters. **Figure 48** shows the peak power demand for all instances under both scenarios of high and low FRD charges. We see that the FRD charges reduction imposes higher power demand on the grid for all the test instances. By looking at the base case, we notice that the peak power demand increases by a minimum of about 19 (kW) in instance "3_8V" and a maximum of around 63 (kW) in instance "1_16V". The charging power demand when using clusters with a high power capacity per socket like "1S_11kW", "2S_22kW" appears to be much higher than other charging technologies. In many instances like "3_16V", we find a difference of around 40 (kW) higher compared to the power obtained by the base case charging technology of 80 (kW).

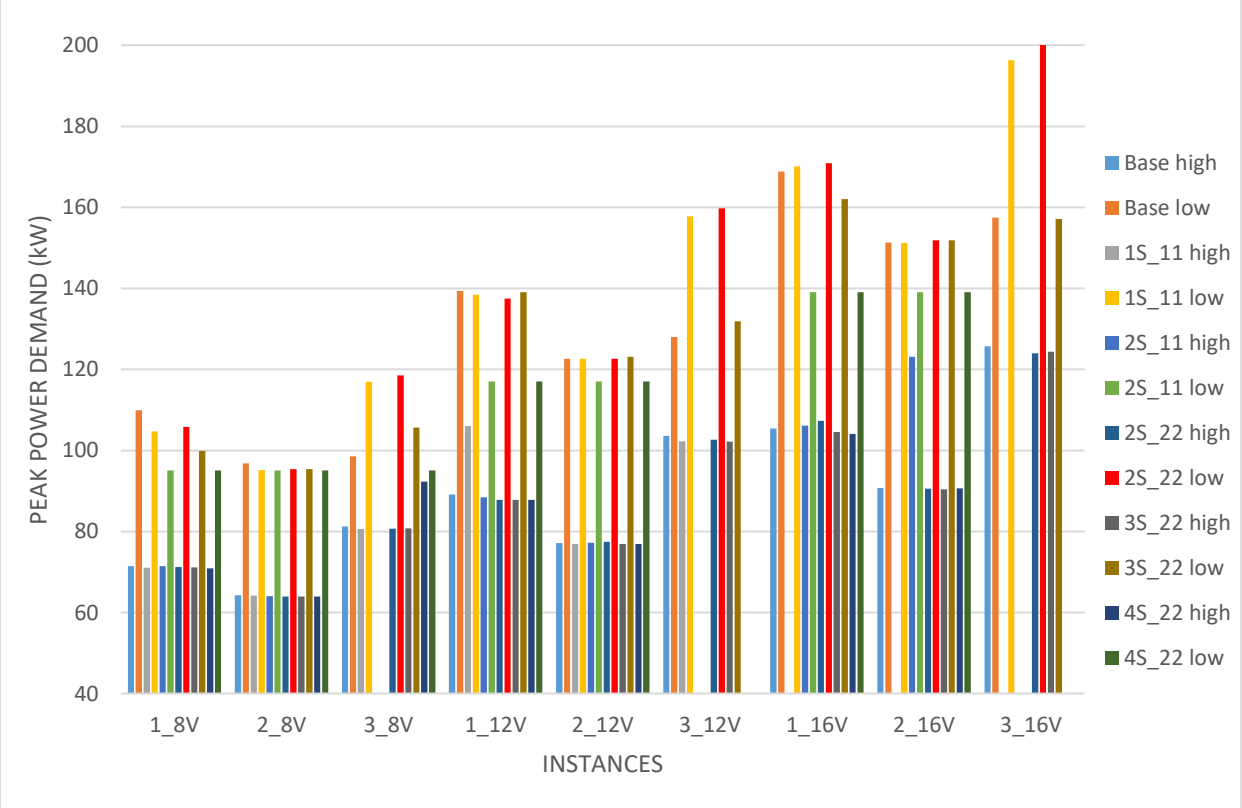

Figure 48: A comparison between the peak power demand in the instances of high FRD charges and the ones with low FRD charges using different charging technology.

Table 29: The total electricity bill of the building, the percentage contribution of the FRD fees in the total cost, and the energy cost reduction rate for different test instances using multiple charging technologies under the low and high FRD charges scenario.

Charging Technology	FRD Scenario		Instance								
			1_8V	2_8V	3_8V	1_12V	2_12V	3_12V	1_16V	2_16V	3_16V
Base	high	FRD	79.23%	77.71%	81.11%	80.69%	78.73%	82.70%	81.48%	79.53%	83.79%
		E (€)	206.1	202.7	208.1	234.6	229.3	238.4	263.5	256.8	267.5
		total (€)	992.46	909.40	1101.57	1214.86	1078.13	1378.32	1422.70	1254.63	1650.44
	low	FRD	5.75%	5.37%	4.78%	6.61%	6.30%	5.46%	7.35%	7.23%	6.03%
		E (€)	180.0	170.8	196.3	196.9	182.2	221.8	212.9	194.2	245.5
		total (€)	191.04	180.43	206.13	210.88	194.50	234.57	229.78	209.32	261.27
1S_11	high	FRD	79.07%	77.65%	80.95%	82.59%	78.65%	82.44%			
		E . red.	-0.34%	-0.31%	-0.37%	-4.86%	-0.17%	-0.52%			
		total	988.29	909.78	1096.05	1412.92	1075.88	1364.71			
	low	FRD	5.66%	5.28%	6.11%	6.85%	6.31%	7.43%	7.76%	7.22%	8.45%
		E . red.	2.98%	0.05%	8.46%	4.47%	-0.01%	11.38%	5.02%	-0.04%	13.33%
		total	185.16	180.18	191.36	201.97	194.52	212.30	219.21	209.39	232.43
2S_11	high	FRD	79.24%	77.62%		80.48%	78.75%		81.68%	84.15%	
		E . red.	0.12%	-0.21%		-0.56%	0.01%		0.62%	0.68%	
		total	991.76	907.63		1208.52	1078.86		1429.13	1609.36	
	low	FRD	4.69%	5.01%		5.16%	5.62%		5.53%	6.09%	
		E . red.	-7.18%	-5.63%		-9.35%	-7.82%		-11.53%	-10.45%	
		total	202.49	189.88		227.06	208.20		251.36	228.40	
2S_22	high	FRD	79.07%	77.60%	80.94%	80.34%	78.85%	82.52%	81.97%	79.47%	83.52%
		E . red.	-0.57%	-0.22%	-0.47%	-0.77%	0.35%	-0.29%	1.42%	-0.18%	-0.62%
		total	990.49	907.19	1096.56	1202.58	1080.21	1368.26	1440.13	1253.18	1632.93
	low	FRD	5.72%	5.30%	6.21%	6.79%	6.31%	7.55%	7.82%	7.25%	8.67%
		E . red.	3.14%	0.20%	8.82%	4.12%	0.02%	11.78%	5.33%	-0.01%	14.14%
		total	184.98	179.96	190.81	202.58	194.47	211.60	218.63	209.39	230.84
3S_22	high	FRD	79.13%	77.60%	80.97%	80.34%	78.65%	82.40%	81.33%	79.46%	83.56%
		E . red.	-0.17%	-0.22%	-0.38%	-0.77%	-0.18%	-0.63%	-0.25%	-0.15%	-0.66%
		total	989.34	907.19	1097.69	1202.58	1075.75	1363.61	1414.47	1252.10	1637.75
	low	FRD	5.30%	5.30%	5.26%	6.59%	6.34%	5.67%	7.07%	7.27%	6.14%
		E . red.	0.77%	0.20%	3.03%	-0.13%	0.15%	1.11%	0.01%	0.25%	2.20%
		total	188.65	179.96	200.88	211.11	194.29	232.48	229.08	208.89	255.83
4S_22	high	FRD	79.04%	77.60%	83.03%	80.34%	78.64%		81.20%	79.52%	
		E . red.	-0.42%	-0.22%	0.30%	-0.77%	-0.19%		-0.66%	0.01%	
		total	987.44	907.19	1222.60	1202.58	1075.46		1410.34	1253.90	
	low	FRD	4.71%	5.01%	4.39%	5.16%	5.61%		5.53%	6.10%	
		E . red.	-6.82%	-5.63%	-5.53%	-9.35%	-8.09%		-11.53%	-10.17%	
		total	201.83	189.88	216.62	227.06	208.70		251.36	227.85	

However, when the number of sockets per cluster increases with a simultaneous decrease in the power capacity of each socket at the time all sockets are being used, then the impact of FRD charges is negligible compared to other charging technologies. This is clearly shown in all instances using clusters "2S_11kW" and "4S_22kW" that could deliver a maximum of 5.5 (kW) per socket when all sockets are occupied. This power impact for both charging technologies is recorded with a maximum of 40 (kW) in instance "2_12V" using cluster "2S_11kW" and 50 (kW) in instance "2_16V" using cluster "4S_22kW" which is way less than that of other charging technologies.

Table 29 presents a comparison of the building's total electricity bill in different test instances using the six previously discussed charging technologies under the two scenarios of high and low FRD charges. It also shows the energy costs in all test instances as obtained in the base case "E" and the percentage contribution of the FRD fees in the total cost "FRD" and the energy cost reduction rate "$E.red.$" in each instance using the various charging technologies compared to the base case. We see that the total electricity bill of the building in all instances reduces by an average of 82% when applying the low FRD charges scenario. Applying the low FRD charges reduces the FRD fees contribution to the total electricity bill from an average of 80% down to a maximum of 8.5%. We notice wider variations in the energy costs E when using different charging technologies after applying the low FRD charges.

The negative values of "$E.red.$" represent the increase rate in the energy costs compared to the base case. By comparing the values of "$E.red.$" obtained by the different clusters, we observe that clusters "1S_11kW", "2S_22kW", and "3S_22kW" show an increase in energy costs in the majority of the test instances in the range of 0.01% and up to 4.86% when applying the high FRD charge. On the contrary, applying the low FRD charges results in energy cost reduction in most of the instances with rates that can reach a value of 14.4% using those three clusters. However, the cluster "2S_11kW" shows the other way around of energy cost increase in the case of low FRD charges ranging from 5.63% and up to 11.53% and meager reduction rates in the case of high FRD charges that reaches a maximum of 0.68% in the best case. However, we find that cluster "4S_22kW" shows increased energy costs between 0.19% and 11.53% for both cases of low and high FRD charges in all test instances compared to the base case scenario. The increased energy costs could be explained by the lower impact of the total FRD fees resulted from lower FRD charges that provide the EFVs with a bigger degree of freedom to charge at any time without any power restrictions and only depending on the minimum electricity prices.

Figure 49 illustrates a comparison of the total electricity bill of the building under the high and low FRD scenarios in the different test instances presented in Table 29. while Figure 50 represents only the charging energy cost in the same tests. By looking at both figures, we can see the cost reduction in both the total electricity bill and the EFV charging energy cost when applying the low FRD charges. Moreover, we notice that the base case's charging technology that has a power capacity of 7.36 (kW) shows better results than the clusters with lower charging capacity. "2S_11kW" and "4S_22kW" are examples of these clusters that can deliver a maximum power of 5.5 (kW) per socket when all are being used simultaneously and cause an average additional energy cost of around €16 compared to the base case technology. On the contrary, the clusters of type "3S_22kW" that can deliver a minimum of 7.36 (kW) per socket equivalent to the power capacity of the chargers used in the base case scenario show remarkable energy cost reduction compared to that of the base case. So far, the cluster type of "3S_22kW" show better results in terms of peak power and electricity bills when applying both the high and low FRD charges.

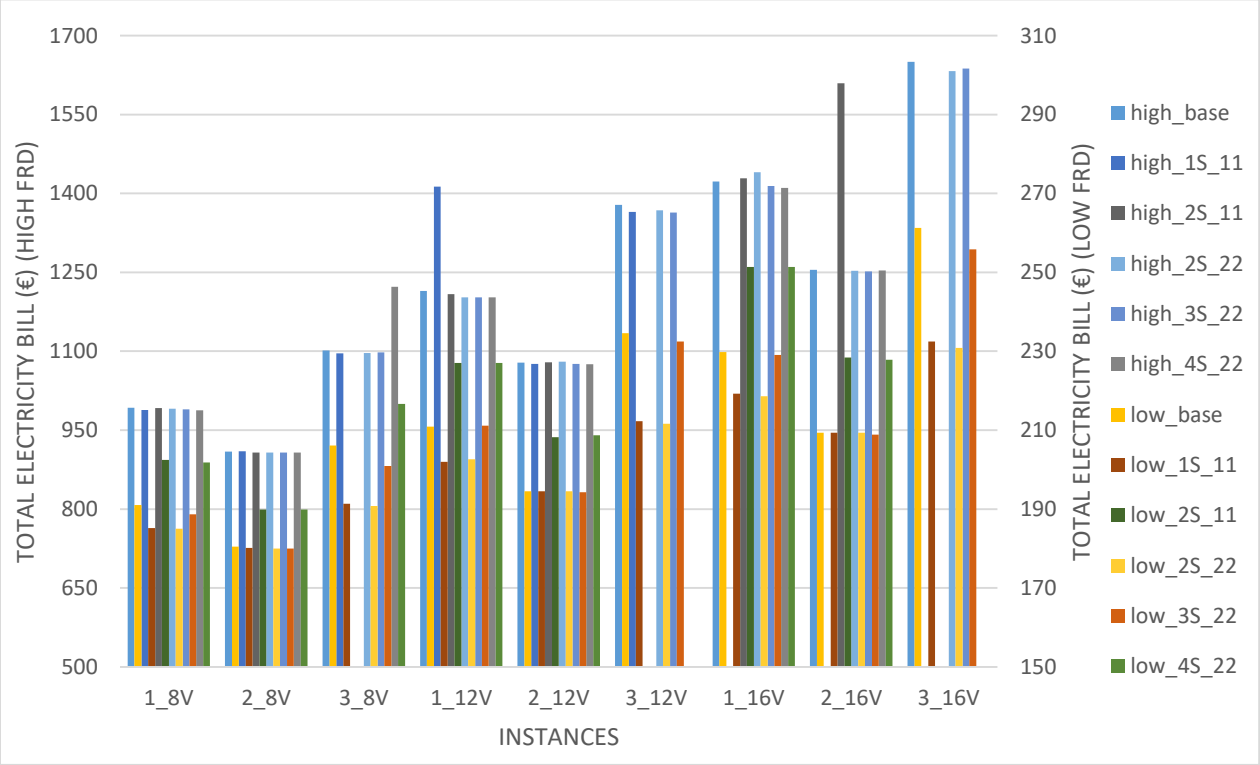

Figure 49: The total electricity bill of the building for different test instances using multiple charging technologies under the low and high FRD charges scenario.

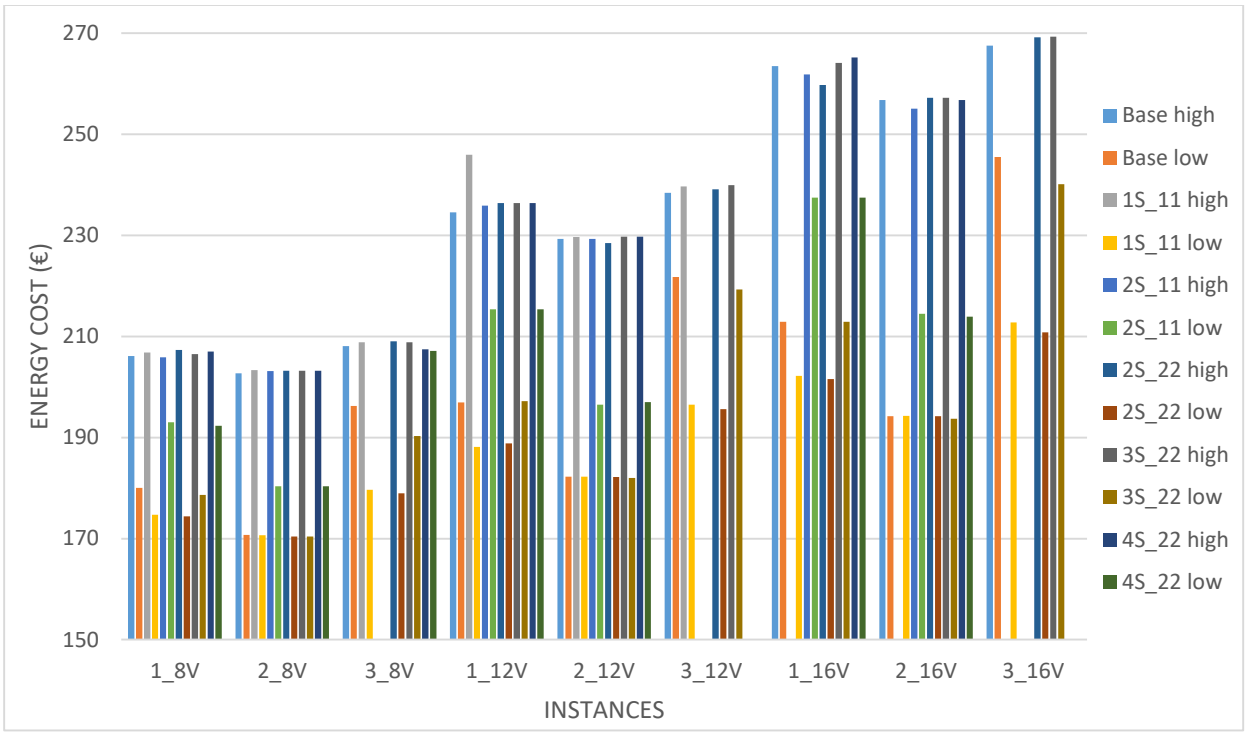

Figure 50: The charging energy cost for different test instances using multiple charging technologies under the low and high FRD charges scenario.

6.1.6 Impact of Grid's Power Limit

In this section, we investigate the effects of imposing a power limit on the building's peak power retrieved from the grid. We repeat the same experiments performed in section 6.1.4 by changing the grid power from 500 (kW) to 110 (kW) while fixing the other parameters. By referring to **Table 25**, we see that no feasible solutions were found for instances "3_12V", "1_16V", "2_16V", and "3_16V" when applying the grid power limit, so we'll exclude all the related test instances of all charging technology from our analysis.

Figure 51 presents the peak power demand for different test instances using multiple charging technologies with setting a power limit on the grid's capacity. We see that there are no significant changes in the peak power after applying the power limit except for the base case charging technology in instance "1_12V", where the peak power increases by about 11 (kW) due to the poor solution reached on the optimization model's time limit. On the other hand, the power limit helps the chargers "1S_11kW" to improve their power demand by a reduction of 18 (kW) and give an optimal charging schedule within 1009 seconds less than the time limit of the optimization model as shown in **Table 25**.

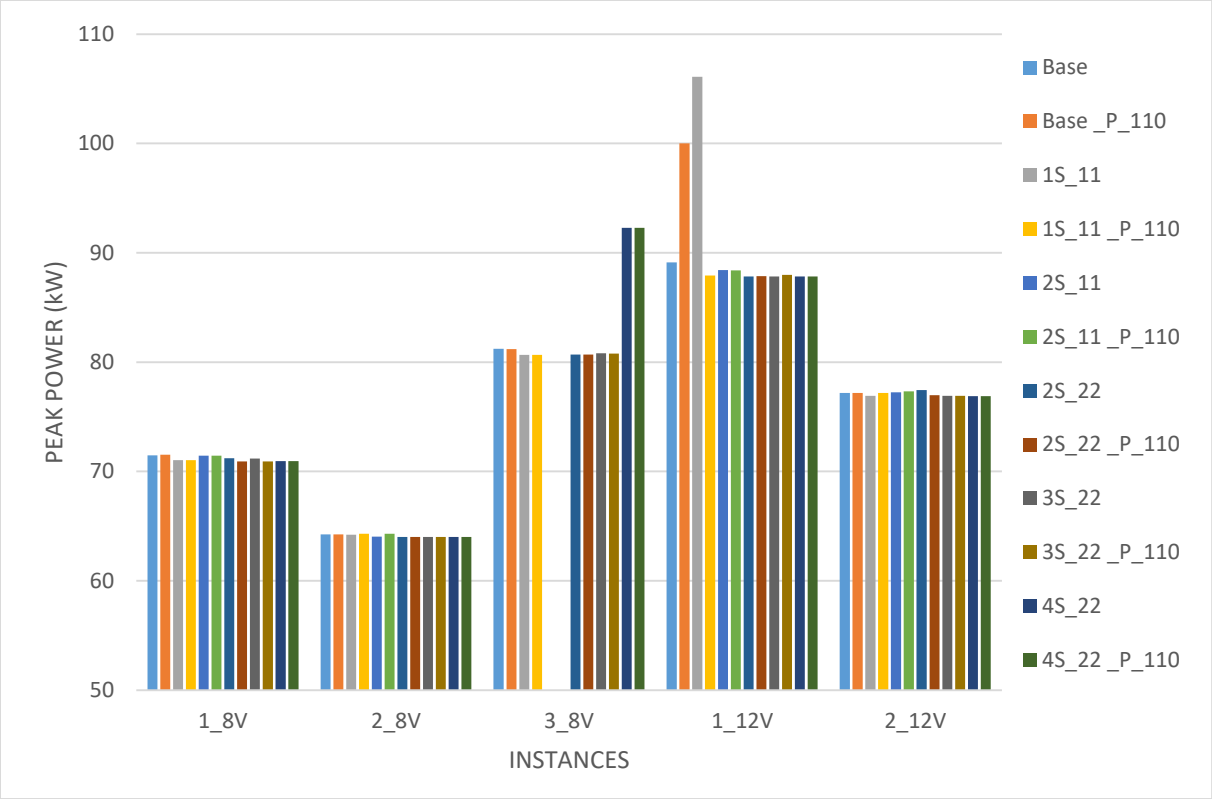

Figure 51: The peak power demands of the building for different test instances after applying a grid's power limit.

Figures 52 and 53 present the impact of the grid's power limit on the building's total electricity bill and the EFVs' charging energy cost respectively, in different test instances and using various charging technologies. By looking at both figures, we notice that the results are similar to those of the peak power where no significant changes are shown except for instance "1_12V" for both the base case charging technology and cluster "1S_11kW". By looking at the base case in instance "1_12V", we see that the total electricity bill increases by around €120 when applying the power limit even though the charging energy costs are reduced by about €4. That is due to the rise of peak power that maximizes the effects of FRD fees. However, using the charger "1S_11kW" in instance "1_12V" reduces the building's total electicity bill along with the reduction of the charging energy costs, which is explained by the significant reduction in the peak power demand as shown in Figure 51.

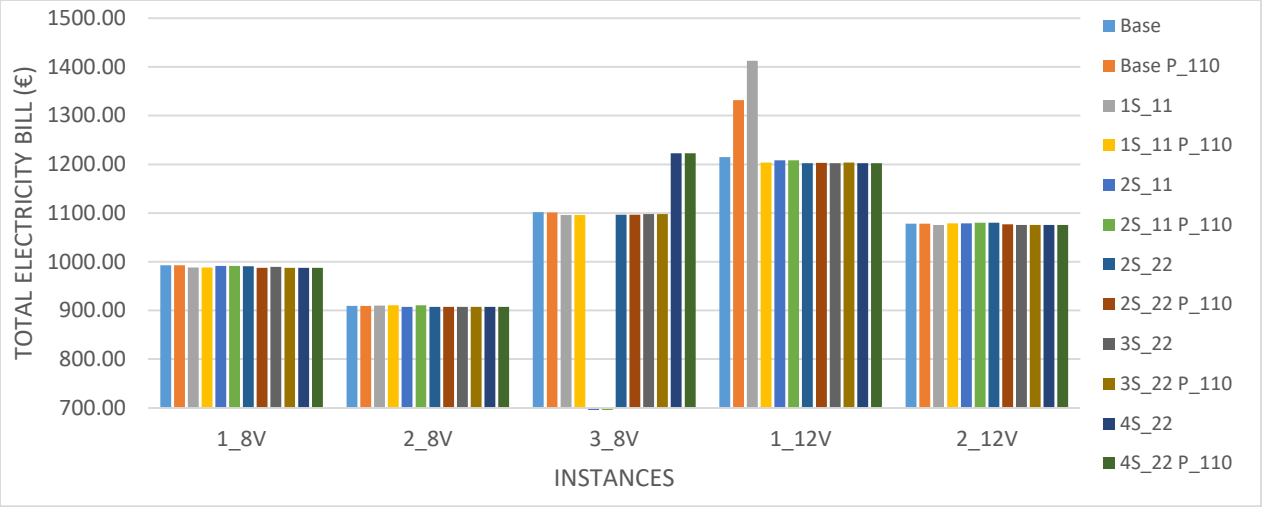

Figure 52: A comparison of the building's total electricity bill in different test instances under the effects of the grid's power limit.

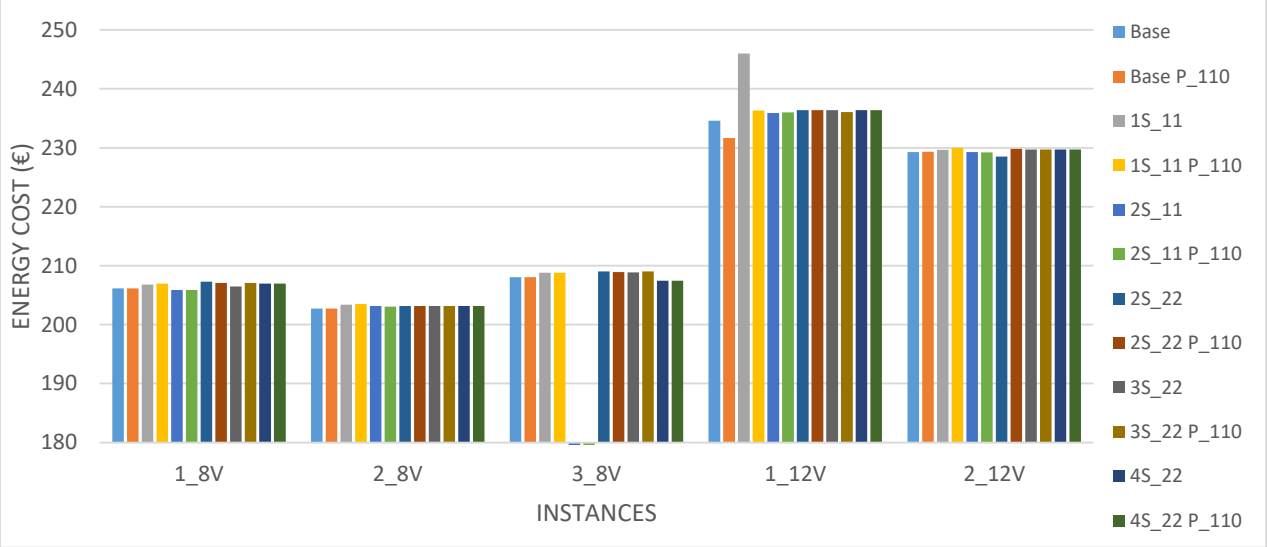

Figure 53: A comparison of the charging energy cost in different test instances under the effects of the grid's power limit.

6.1.7 Effects of Charging Interruptions

In this section, we investigate the impact of charging interruptions on the solutions resulted in section 6.1.4 through running the same test instances after changing only the number of charging interruptions N from two in the base case to one $(N = 1)$ and zero $(N = 0)$. By referring to Tables 25 and 26, we notice that these two scenarios of one and zero charging interruption increase the runtime of the optimization model for most test instances but keep the final gap within the acceptable range.

(a)

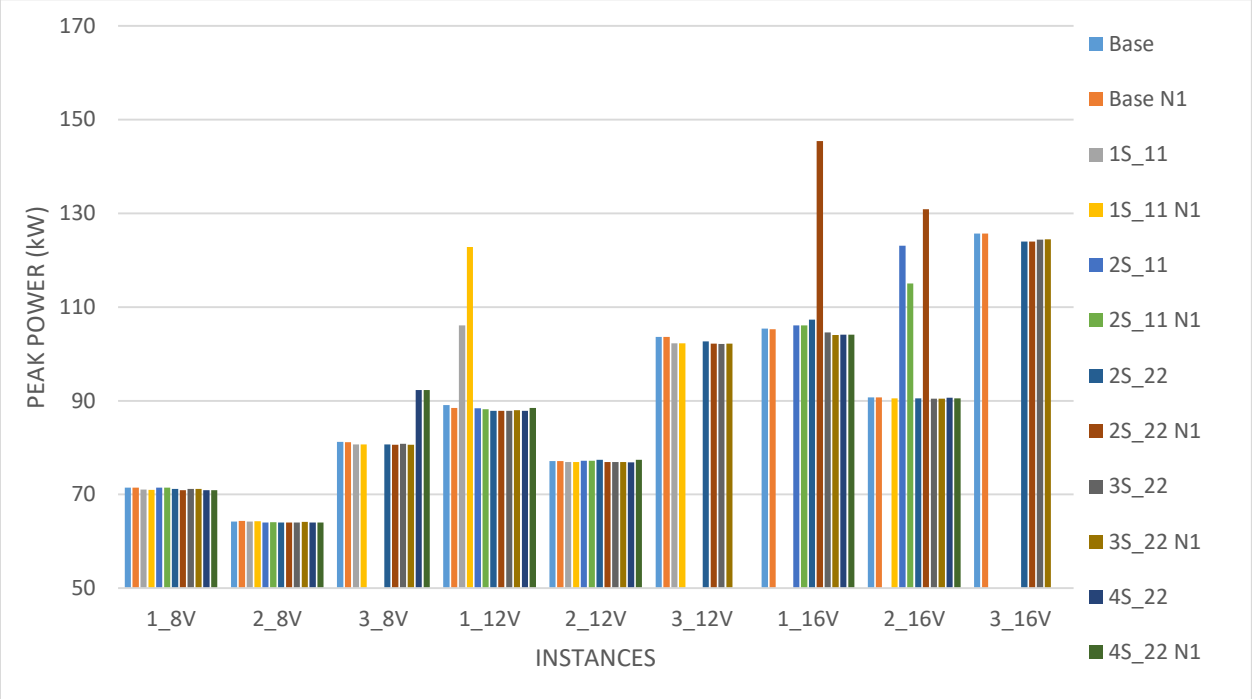

(b)

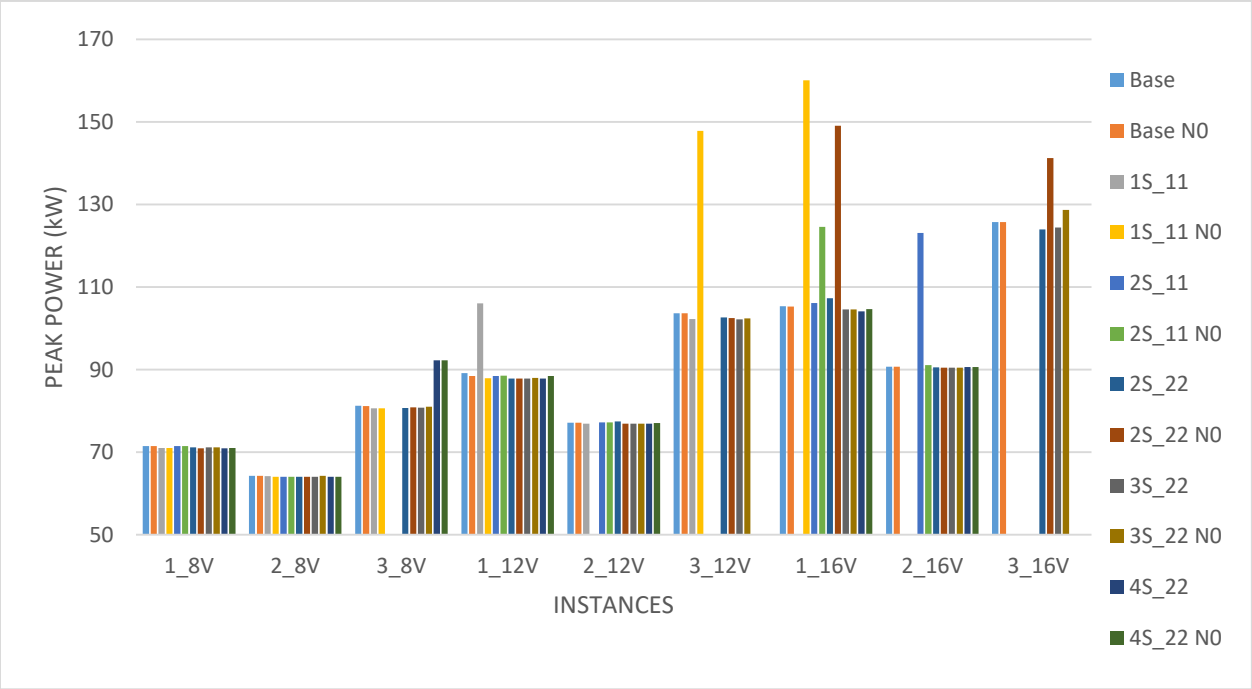

Figure 54: A comparison of the peak power demand in different test instances using the multiple charging technologies: (a) refers to the scenario of $N = 1$, (b) refers to the scenario of $N = 0$.

(a)

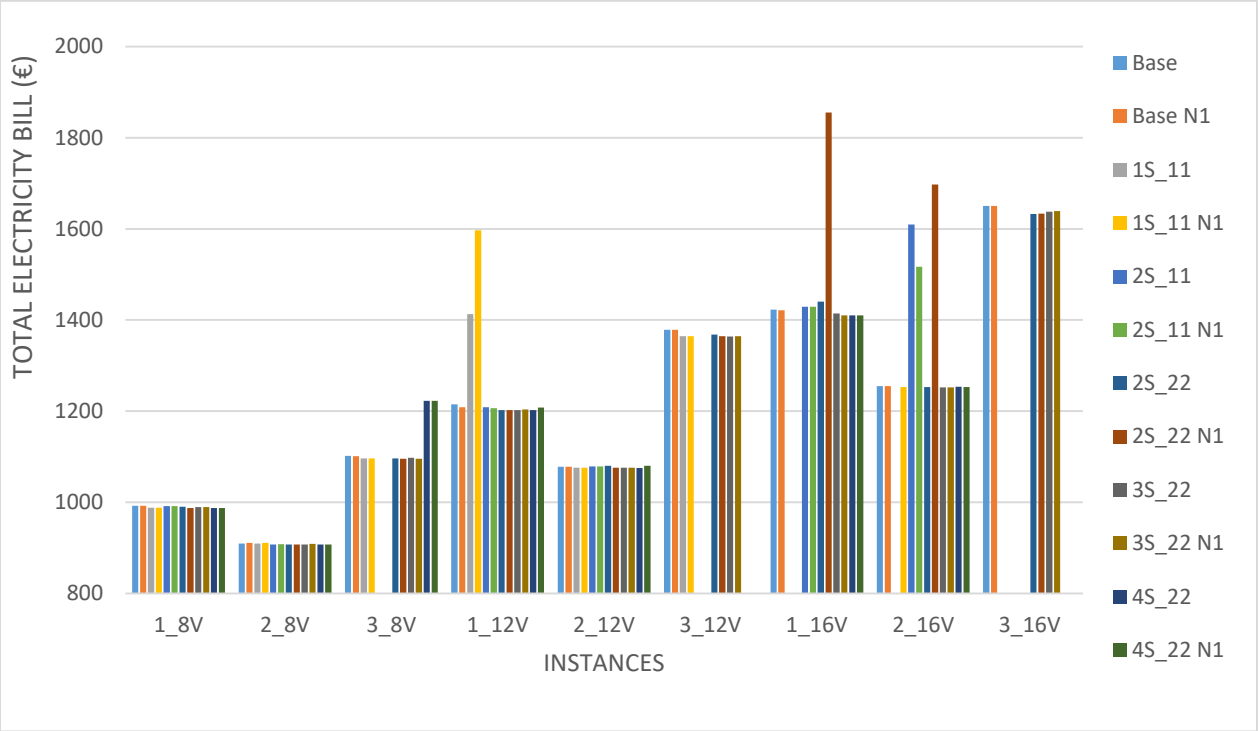

(b)

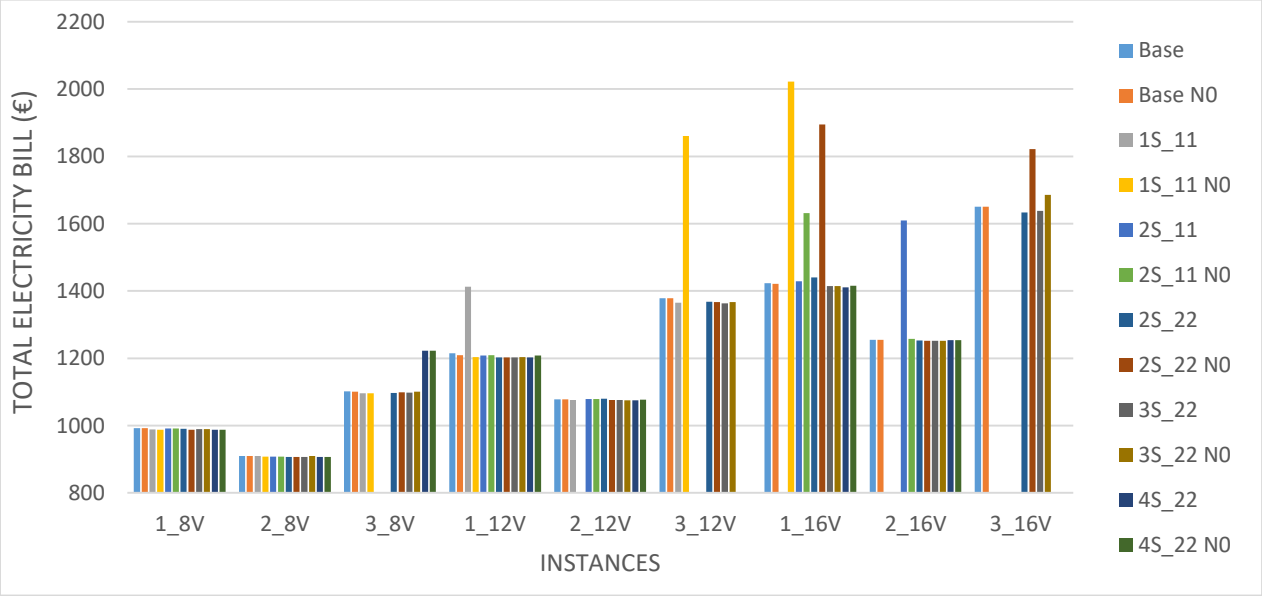

Figure 55: A comparison of the building's total electricity bill in different test instances using multiple charging technologies under two scenarios: (a) One charging interruption, (b) zero charging interruptions.

Figure 54 presents a comparison between the building's peak power demand in different test instances and using various charging technologies. (a) refers to a comparison between the base scenario and the "N1" scenario of two and one allowed charging interruptions respectively, while (b) corresponds to a similar comparison but with "N0" zero charging interruptions allowed instead of "N1". By comparing all charging technologies for both scenarios, we see that no significant changes take place for both scenarios in almost all the test instances using all charging technologies except for clusters "1S_11kW", "2S_11kW", and "2S_22kW" in some instances that correspond to 12V and 16V.

In general, the base scenario of two charging interruptions shows better results of lower peak power than the other two cases. This is also clear in Figure 55 that presents a comparison of the building's total electricity bill between the base scenario of two charging interruptions allowed and (a) of one charging interruption and (b) of zero charging interruption for different test instances using various charging technologies. The results of the total electricity bill show the same trend of the peak power demand in Figure 54 since the FRD charges contribute to around 80% of the total bill, which increases and decreases proportionally with the peak power value in all instances.

6.2 RESULTS OF THE RESIDENTIAL NEIGHBOURHOOD PROBLEM

In this section, we present the results of the experiments performed for the residential neighborhood problem, besides analyzing the impact of some parameters on the obtained optimal solutions. Similar to what we did in section 6.1, we generate four instances for a neighbourhood of four sizes m of 30, 40, 50, and 60 heterogenous EVs. The travel and charging behaviors of residential EVs are more random than the commercial ones and their arrival and departure periods are more unpredictable.

We generate the four instances as follows: instance (1) represents a case of relatively low energy demand e_v represented by a range of 50%-65% of the battery's energy capacity and with a long overnight charging period of 17-19. Instance (2) refers to a case of normal energy demand in the range of 65%-80% of the battery's energy capacity and an average charging period in the range of 14-17 hours. Instance (3) is the case of a long travel behavior equivalent to 80%-90% of the battery's SoC and a charging period of 11-13 hours, and it represents an example of the worst-case scenario.

Finally, we generate instance (4) as a random combination of all three instances together for a more realistic case study. We randomly generate the arrival and departure periods for each EV in all instances where the arrival periods lie in the range of 15:30-23:00 equivalent to periods range of 2-32, whereas the departure periods are generated between 6:00 and 11:00 equivalent to periods range of 60-80. The sixteen main instances are summarized in Table 30.

Table 30: The main instances of the residential neighbourhood problem.

instance	Number of EVs	Range of SoC needed	Charging period range
1-30V	30	50%-65%	17-19 hours
2-30V	30	65%-80%	14-17 hours
3-30V	30	80%-90%	11-13 hours
4-30V	30	65%-90%	11-19 hours
1-40V	40	50%-65%	17-19 hours
2-40V	40	65%-80%	14-17 hours
3-40V	40	80%-90%	11-13 hours
4-40V	40	65%-90%	11-19 hours
1-50V	50	50%-65%	17-19 hours
2-50V	50	65%-80%	14-17 hours
3-50V	50	80%-90%	11-13 hours
4-50V	50	65%-90%	11-19 hours
1-60V	60	50%-65%	17-19 hours
2-60V	60	65%-80%	14-17 hours
3-60V	60	80%-90%	11-13 hours
4-60V	60	65%-90%	11-19 hours

We perform our experiments based on a full day normal power demand data in the form of 15mins-averaged power consumption in (kW). Our dataset is generated based on a minute-averaged individual household power consumption dataset by Hebrail & Berard,(2012), where their data were measured using several submeters installed inside a house near Paris. We assume that all the houses in the neighbourhood have a similar retrieved power pattern for the sake of simplicity all over the day. We set the maximum and minimum SoC as 0.99 and 0.05 respectively that are fixed for all the test instances, and we consider that the minimum SoC itself is the SoC of all EVs at their arrival periods at the beginning of the planning horizon.

We consider having only three models of passenger EVs distributed randomly among all the houses in the neighbourhood, where each house is assumed to have only one EV. The EV models used in our experiments and their technical specifications like the charge and energy capacities, battery output voltage, onboard charger's power capacity, number of battery packs, and the house's EVSE power capacity are summarized in Table 31. We assume that all the houses in the neighbourhood are equipped with only one type of EVSE that is an AC single-phase single-socket level-2 smart power supply characterized by a 7.36 (kW) power capacity, a current up to 32 A, and a 230 V output voltage (pod POINT, n.d.-a).

Table 31: Technical specifications of different EVs of residential users.

EV model	Charge capacity (Ah)	Energy capacity (kWh)	Onboard charger capacity (kW)	Battery voltage (V)	EVSE power capacity (kW)	Number of battery packs	source
BMW i3	120	42.24	11	352	7.36	3	(BMW, 2018)
Toyota RAV4	108	41.8	10	386	7.36	3	(Toyota, 2013)
NISSAN Leaf	66	24	6.6	360	7.36	2	(Nissan, 2017)

By referring to section 3.3.2, we approximate the battery's charging process for all EV models with the same number of breakpoints assumed to be five but having different values of $SOC_{v,b}^{break}$, ${I_{v,b}}^{max}$, and ${I_{v,b}}^{min}$ depending on the charging profile of the EV's battery, as shown in Table 32. We define the minimum current that must be retrieved by the battery as 10% of the corresponding maximum current at the same breakpoint. We assume the battery charging loss factor to be 6.75% of the input power retrieved from the EVSE independently of the SoC and input current value, just like in the experiments of the commercial problem.

Table 32: The parameters corresponding to the breakpoints that are approximated for the charging process of a Lithium-ion battery cell for each EV model.

B_v	BMW i3			Toyota RAV4			NISSAN LEAF		
	$SOC_{v,b}^{break}$ (%)	${I_{v,b}}^{max}$ (A)	${I_{v,b}}^{min}$ (A)	$SOC_{v,b}^{break}$ (%)	${I_{v,b}}^{max}$ (A)	${I_{v,b}}^{min}$ (A)	$SOC_{v,b}^{break}$ (%)	${I_{v,b}}^{max}$ (A)	${I_{v,b}}^{min}$ (A)
0	5.0%	0	0	5.0%	0	0	5.0%	0	0
1	92.3%	7	0.7	92.0%	6.4	0.64	88.1%	9.25	1
2	94.9%	3.5	0.35	94.6%	3.4	0.34	92.6%	5.25	0.53
3	95.7%	2.5	0.25	95.3%	2	2	94.2%	3.25	0.33
4	99.0%	1.5	0.15	99.0%	0.15	0.15	99.0%	2	0.2

6.2.1 Base Case Scenario Description

The base case scenario includes the sixteen test instances presented in Table 30 with the assumption of some parameters that will be changed in later sections to analyze the feasibility of our model besides the common parameters discussed above. We assume a smart pricing strategy of three electricity prices that vary during the day depending on the power consumption intensity on a zonal scale (Limmer, 2019). We consider the same pricing strategy of the summer scenario proposed in (Pelletier et al., 2018). We set an energy price of 0.25 $(€/kWh)$ during the peak hours (12:00-18:00), 0.05 $€/kWh$ during the off-peak hours (00:00-08:00), and 0.15 $€/kWh$ during the shoulder hours that represent the rest of the day.

We assume that each house in the neighbourhood possesses an EV where its arrival and departure periods and the energy needed are predefined by the EV user, as explained before. We set the grid contract power implied on each house to a value of 20 (kW) such that its effect is neglected. We allow for each EV an interruption parameter of two cuts during the entire charging process. Each test instance is optimized based on both the even and percentage slack variables' distribution approaches of the CCRM.

6.2.2 Base Case Results

In this section, we present the results of the base case scenario and interpret some indications of its remarkable data. Tables 33 and 34 show the numerical outcomes of the sixteen main test instances presented before and present a comparison between the solutions obtained by following both the percentage and even distribution approaches. Table 33 mainly shows the obtained results of the running time of both optimization stages, the output peak power demand from the optimization model of PSM, and the final gap. The columns "$\bar{X}\ (kW)$" and "$max\ M_t\ (kW)$" represent the peak power demand of the neighbourhood that is the main objective function of PSM and the input maximum household power consumption of the neighbourhood along the entire day respectively. We notice that the power retrieved by the neighbourhood while charging the EVs during the whole day periods never exceeded its non-EV maximum household power consumption for all test instances except for instance "1-50V" of a minor increase. Looking at the final gap of all solutions, we see that only instance "1-50V" obtained a solution with a gap higher than zero with a value of 0.04% that is still below our preset minimum gap. Column "PSM time" represents the solution time of only the optimization model of PSM where the maximum run time is around 67 secs and that the run time increases with more EVs and higher energy demands.

Table 33: The results obtained for the base case scenario, including peak power demand of, run time, and final gap comparisons.

instance	PSM final gap (%)	$\bar{X}$ (kW)	max M_t (kW)	PSM time (s)	CCRM-%		CCRM-E	
					max time (s)	total time (s)	max time (s)	total time (s)
1-30V	0	131.43	131.43	9.48	0.52	8.26	0.42	8.54
2-30V	0	131.43	131.43	8.17	0.40	7.47	0.55	7.31
3-30V	0	131.43	131.43	16.25	0.49	7.44	0.53	7.23
4-30V	0	131.43	131.43	18.38	0.55	8.25	0.41	7.49
1-40V	0	175.71	175.71	12.03	0.35	9.20	0.52	10.23
2-40V	0	175.71	175.71	16.94	0.34	9.34	0.51	10.64
3-40V	0	175.71	175.71	28.53	1.64	11.54	0.48	9.91
4-40V	0	175.71	175.71	14.73	0.43	11.59	1.04	12.35
1-50V	0.04	220.08	219.99	13.91	0.64	14.69	0.40	13.85
2-50V	0	219.99	219.99	18.84	0.50	12.31	0.59	13.90
3-50V	0	219.99	219.99	33.20	2.86	15.21	0.48	11.88
4-50V	0	219.99	219.99	28.33	0.39	12.46	0.38	11.31
1-60V	0	263.47	263.47	41.84	0.48	14.27	2.27	19.82
2-60V	0	263.47	263.47	25.09	0.33	13.44	0.44	12.57
3-60V	0	263.47	263.47	67.31	0.51	12.61	0.64	13.40
4-60V	0	263.47	263.47	29.30	0.34	13.51	0.42	13.28

However, the last four columns show the run time of the optimization model of "CCRM" where the first two refer to "CCRM-%" the case of the percentage slack distribution approach among the houses in the neighbourhood, while the last two correspond to the even approach "CCRM-E". "max time" represents the time value of the house with highest CCRM's run time on the entire neighbourhood while "total time" is the sum of the CCRM's run time of all the houses in the neighbourhood. By summing the "PSM time" with each "total time" of the CCRM cases, we see that the total run time of the TSREV-CSP in all test instances is highly acceptable where the maximum time is recorded by around 80 seconds in instance "3-60V". We also notice that the individual maximum run time of the CCRM model for all houses in all instances has an average value of 0.5 (s), with some exceptions having a maximum value of 2.86 (s).

Table 34: Cost analysis and a comparison between the results of the CCRM's even and percentage approaches in the base scenario.

instance	CCRM-% (%)							CCRM-E (%)						
	Z	R	I	avg r.	min r.	max r.	max i.	Z	R	I	avg r.	min r.	max r.	max i.
1-30V	0	96.67	3.33	7.91	1.98	17.67	0	3.33	96.67	0	7.96	1.98	17.67	0
2-30V	3.33	96.67	0	5.11	1.23	10.83	0	3.33	96.67	0	5.10	1.18	10.83	0
3-30V	26.67	66.67	6.67	0.94	0.01	6.91	0.17	23.33	70	6.67	0.88	0	6.81	0.17
4-30V	0	93.33	6.67	5.29	0.60	19.18	0	3.33	93.33	3.33	5.28	0.60	19.18	0
1-40V	0	100	0	8.43	2.53	17.63	0	0	100	0	8.51	2.53	17.63	0
2-40V	0	100	0	5.53	0	14.55	0	2.50	97.50	0	5.66	0.90	14.55	0
3-40V	62.50	17.50	20	3.42	0	5.18	0	62.50	17.50	20	3.45	0	5.26	0
4-40V	0	95	5	4.71	0.25	19.45	0	0	95	5	4.72	0.60	19.30	0
1-50V	2	98	0	8.91	2.78	19.32	0	2	98	0	8.98	3.29	19.32	0
2-50V	0	100	0	5.15	0.40	14.82	0	0	100	0	5.16	0.37	14.82	0
3-50V	38	58	4	1.74	0	9.51	0	38	58	4	1.76	0	9.51	0
4-50V	2	96	2	5.67	0.23	19.63	0	2	96	2	5.65	0.22	19.63	0
1-60V	0	100	0	10.05	4.03	20.03	0	0	100	0	10.09	4.03	20.03	0
2-60V	0	98.33	1.67	7.11	0.38	15.16	0	1.67	98.33	0	7.08	0.36	15.16	0
3-60V	15	80	5	1.89	0	11.32	0	15	80	5	1.88	0	11.32	0
4-60V	3.33	96.67	0	5.95	0.02	24.07	0	3.33	96.67	0	5.93	0.04	23.61	0

Table 34 shows a comparison and cost analysis between the electricity bills of all houses in the neighbourhood obtained from the PSM, CCRM-%, and CCRM-E in all test instances. All the values are represented as percentages where "Z", "R", and "I" refer to the percentage of houses in the neighbourhood that have no changes, reduction, or increase in their electricity bill when comparing the cost in PSM with either CCRM-% or CCRM-E. The reduction percentage for each house in the neighborhood is calculated using Eq. (88), in which a positive result corresponds to "R" while a negative one refers to "I". The same equation is used for both comparisons of CCRM by simply replacing $Bill_v^{CCRM-\%}$ with $Bill_v^{CCRM-E}$. The electricity bill of each house in the PSM could be calculated in the same way as CCRM using Eq. (67). For both CCRM approaches, the column "avg r" represents the average value of the reduced bills among all houses in the neighbourhood. However, the last three columns, "min r", "max r", and "max i", refer to the reduction percentage of the houses with the minimum and maximum reduction rate and the increasing percentage of the houses with the maximum increasing rate respectively.

$$red(\%)_v = \frac{Bill_v^{PSM} - Bill_v^{CCRM-\%}}{Bill_v^{PSM}} \times 100 \tag{88}$$

Both CCRM approaches show almost the same results except for some minor variations in the average, minimum, and maximum reduction rates. We also find that at least 93% of the houses in the neighbourhood have cost reductions in their electricity bill compared to that of the PSM in all the test instances except those of worst-case scenarios like "3-40V" where only 17.5% of the houses reduced their energy cost. Moreover, in the test instances (3) of the highest energy demands for different EV sizes show the least values of the average and maximum reduction rates, besides having the only remarkable value of the cost increase rate of around 0.17%.

On the contrary, It is always the case that the test instances with the lowest energy demands have the highest average reduction rate as well all test instances with relatively low energy demands like (1) and (2) for all EV sizes result in a higher percentage of houses with cost reduction. That could be explained by higher flexibility in shifting the charging schedule towards the periods of lower energy prices. Even though some test instances show substantial percentages of houses with increased electricity bills compared to those in the PSM, but the cost increased rates are found to be less than 0.01%, so they will be neglected and set to zero.

6.2.3 Effects of Smart Pricing Strategies

In this section, we study the effects of smart pricing strategies on our optimization model by repeating the sixteen test instances generated in the previous section 6.2.1 with changing only the electricity pricing strategy from 3 periods of 3 different prices per day to only two like the case in Italy (Terna, 2018) while fixing all parameters. The 2-prices strategy divides the entire day into only two periods, mainly peak hours that are from 8:00 until 20:00 and an off-peak period that includes the rest hours of the day. We assume an energy price of 0.25 $(€/kWh)$ for the peak period while a value of 0.15 $(€/kWh)$ is assumed for the off-peak period. Since only the electricity price parameters are changed and having mentioned that the optimization formulation of the PSM is independent of the prices and costs, then the output decision variables of PSM are not going to change and would be excluded from our analysis.

Figure 56 illustrates the runtime values of the houses with the maximum solution time and the total runtime of the CCRM following both the "%" and "E" slack distribution approaches under the base case scenario and the 2-prices one. We notice that the 2-prices strategy imposes additional runtime in almost all test instances, especially in instances "2-30V" and "4-60V", but the highest recorded time for the entire run is registered around 24 (s) which is still highly acceptable. In instances "2-30V" and "4-60V", the runtime values of the houses with the maximum solution time using the "even" approach increased by around 12 (s) and 8 (s) respectively.

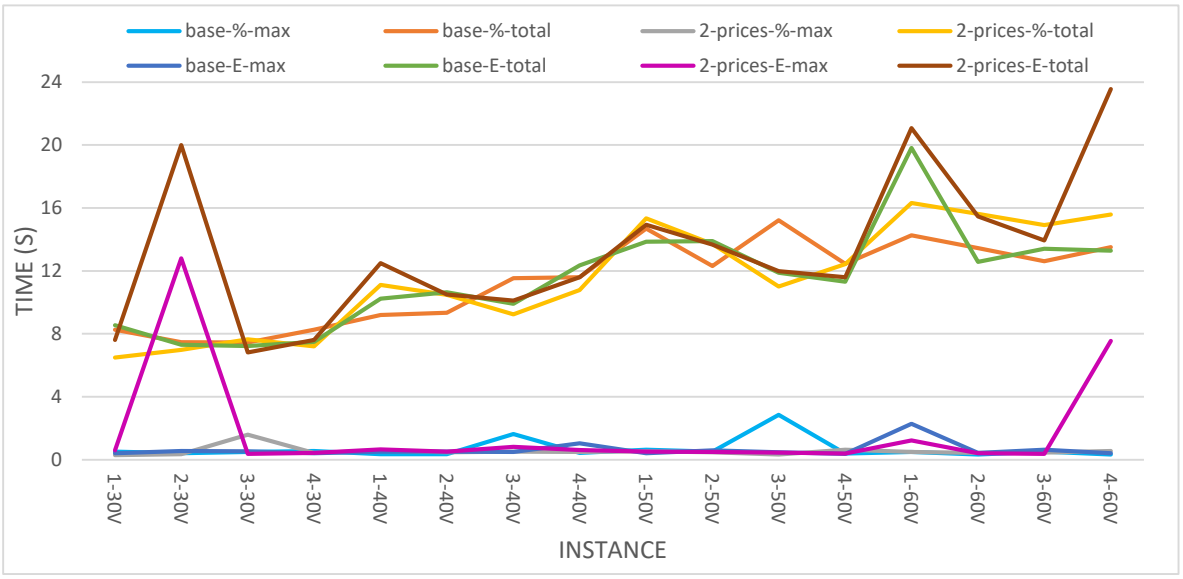

Figure 56: Comparison between the run time of the optimization models using the "CCRM-E" and the "CCRM-%" approaches under both scenarios of the base case and Two-price.

Figures 57 and 58 illustrate a comparison between the cost analysis results presented in Table 34 of the base case scenario and the ones obtained from the 2-prices scenario. Figure 57 shows the percentages of the houses in the neighbourhood that have no changes, reduction, or increase in their electricity bill. We see that there are huge declinations by a minimum rate of 24% and up to 57% in the number of houses that had energy cost reductions when comparing "base_%_R" with "2-prices_%_R" and "base_E_R" with "2-prices_E_R". On the other hand, both "Z" and "I" show a remarkable increase by average increase rates of around 20% and 15% respectively.

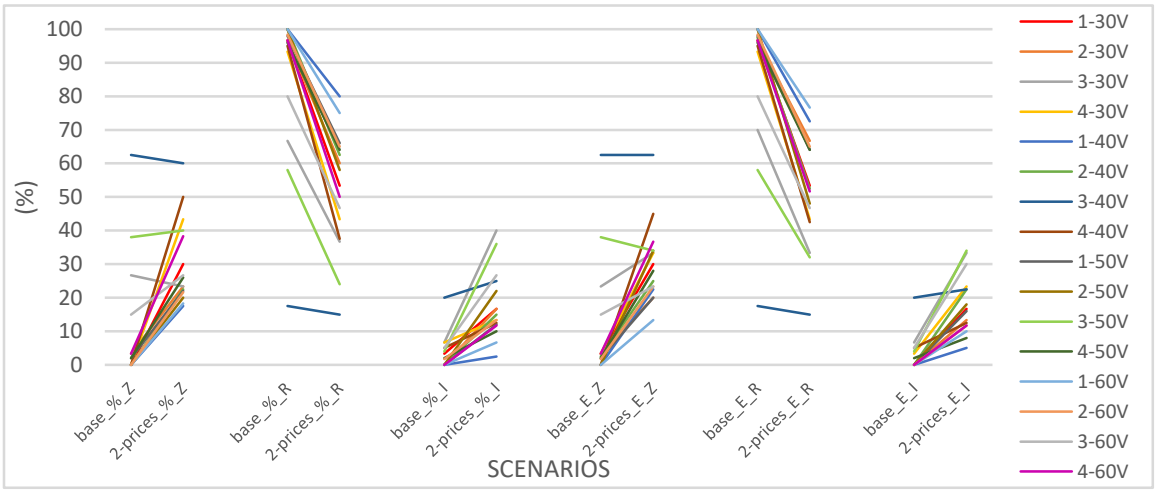

Figure 57: Comparison between the percentages of houses in the neighbourhood with no changes, reduction, or increase in their energy bills under the base case and 2-prices scenarios.

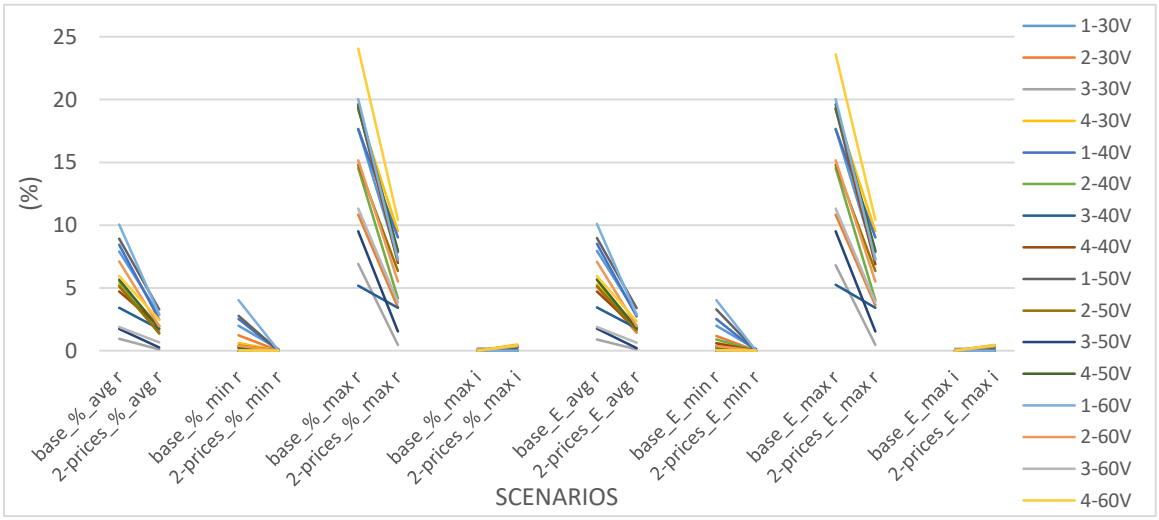

Figure 58: Comparison between the average reduction rates and the reduction increase percentages of the houses with the maximum and minimum rates under both the base case and 2-prices scenarios.

Figure 58 shows the average reduction rates and the reduction percentages of the houses, and the maximum and minimum reduction rates besides those of the top increase rates. We notice the same descending trend for the three reduction rates up to 24% in some test instances like "4-60V". The maximum average reduction rate for both "%" and "E" decreases from 10% to around 3.3%, while we see slight increases in the percentages of the maximum increase rates up to 0.5%. That proves the advantages of smart pricing strategies to improve the efficiency of smart charging technologies.

6.2.4 Impacts of Charging Interruptions

The work performed in this section is very similar to that in section 6.1.7, where we repeat twice the same test instances in the base case scenario after changing only the charging interruption parameter N_v from two to one (N1) and then zero (N0) while fixing all the other parameters. Figure 59 illustrates a comparison of the runtime between the three scenarios of the base case, "N1" and "N0" applied to all test instances of the base case and using both the "CCRM-%" and "CCRM-E" approaches. We see that the "N1" scenario shows relatively lower solution timings in many test instances for both the PSM and the total runtime of TSREV-CSP that reaches a maximum of 50 (s) compared to the base case scenario. However, the optimization runtime is negatively influenced by the "N0" scenario for both the PSM one and the total solution time in all test instances where the maximum runtime gets doubled from 80 (s) for instance "3-60V" in the base case to almost 160 (s) for instance "1-60V".

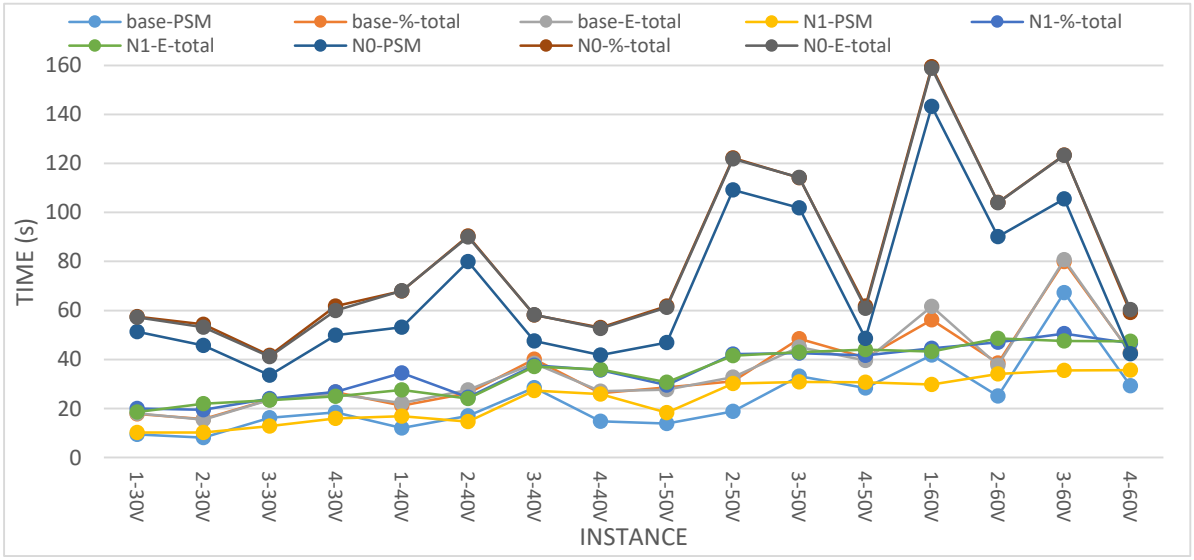

Figure 59: The runtime analysis of the optimization models following the "CCRM-%" and the "CCRM-E" under different charging interruption scenarios compared to the base case.

Figure 60 presents a comparison between the peak power demand obtained from the PSM under three different scenarios of the base case, "N1", and "N0" discussed before. We see that no changes occur when applying the three scenarios in all the test instances except for a minor power increase of around $1(kW)$ in test instances "3-30V" and "4-60V" when applying the "N0" scenario. This proves that the number of charging interruptions does not affect the objective function of the PSM. But that's not the case when applying the CCRM-% and CCRM-E, as shown in Figures 61 and 62. They present the percentage distribution of the houses based on the reduction rates in their electricity bills and the corresponding average, maximum, and minimum reduction rates and the maximum increase rate among all houses in the entire neighbourhood respectively.

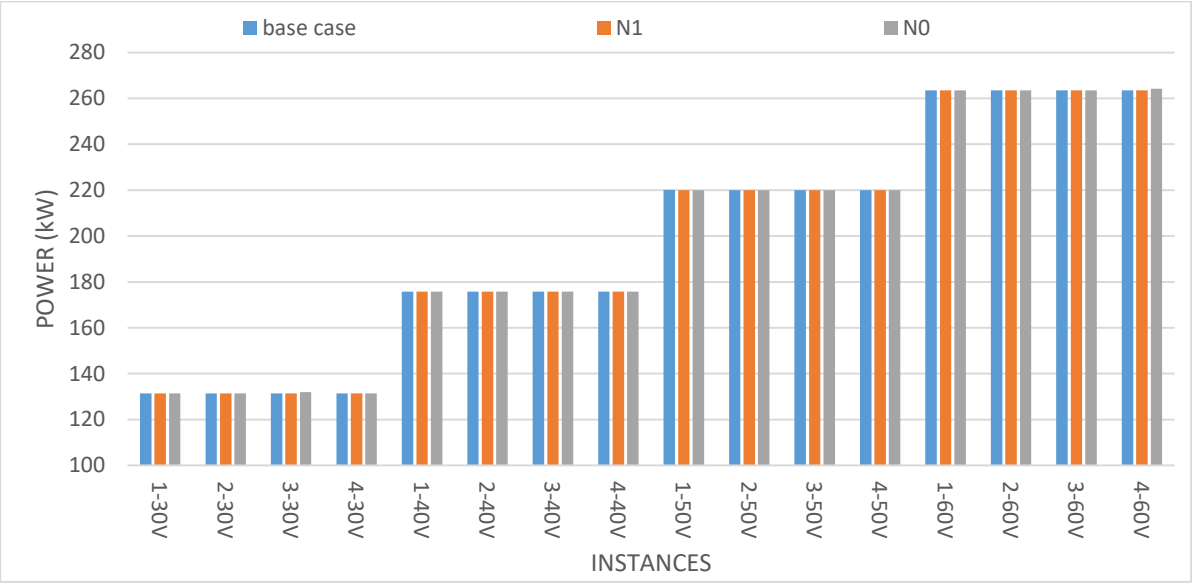

Figure 60: The peak power demands obtained by the PSM for two different charging interruption scenarios and compared to the base case one.

By looking at Figure 61, we see that "N1" shows the best results for all percentage distribution parameters among all three scenarios in the majority of the test instances and using both the "%" and "E" approaches of CCRM. "N1" improves the percentages of houses with reduced energy costs "R" in all test instances. The least value of "R" is found for instance "1-30V" of 90% when applying both CCRM approaches of "N1" at the time of having four values of "R" with a maximum of 80% in the base case scenario that correspond to instances "3-30V", "3-40V", "3-50V", and "3-60V". However, by looking at "N0_%_R", we notice that "N0" brings down the same percentages in all test instances to a maximum of 80%, except in instance "1-30V", which is kept at 90% compared to "N1". The complete opposite takes place for the houses with a non-changed electricity bill "Z" and those with an increased one "I".

The percentage distributions of the houses of "Z" in almost all test instances decline to a maximum of about 7% under the "N1" scenario when it was 60% in the base case while it rises to the value of 43% with the majority of "Z" percentages lie in the range of 15% to 43% when applying the "N0" scenario. Similarly, the values of "I" for most of the test instances decrease from a maximum of 20% under the base case scenario to around 7% when applying "N1" to restore much worse values than those in the base case when applying "N0" reaching a maximum of approximately 18% but with an average increase rate of 7% for all test instances.

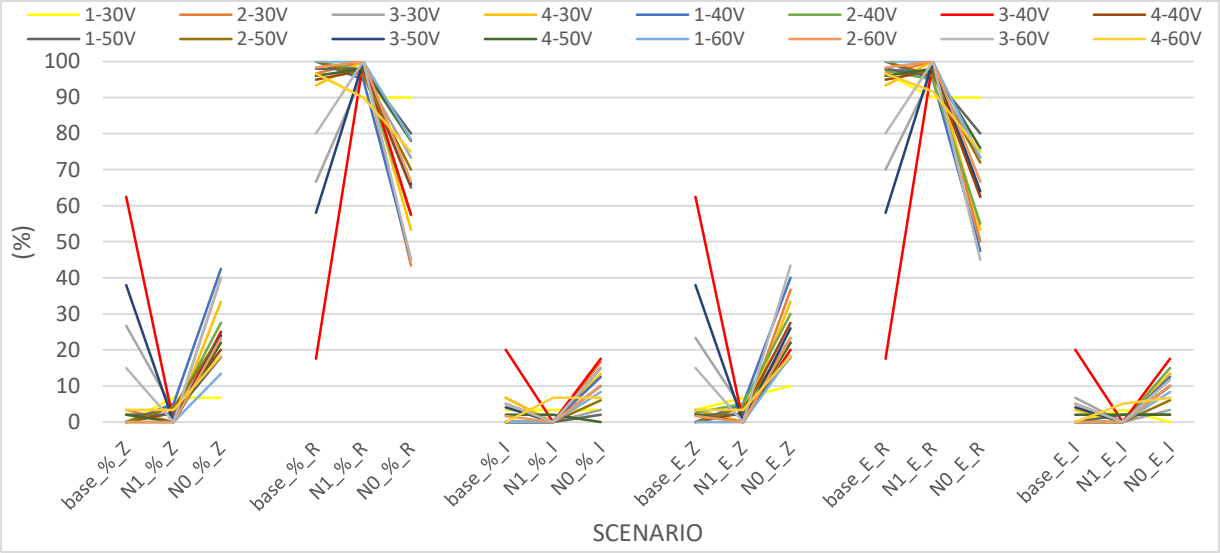

Figure 61: The percentage distribution of the houses in the neighbourhood based on the reduction rate in their energy bills for different charging interruption scenarios compared to the base case.

Figure 62 shows and compares the average reduction rates (avg r) of all the houses with reduced costs in the neighbourhood in all test instances besides the corresponding percentage values of the houses with the maximum (max r) and minimum (min r) reduced cost rates and those of the maximum rate of the increased bill (max i) for the scenarios of the base case, N1, and N0. We observe that the average reduction rates obtained by "N1" for 40% of the test instances are less than those resulting from the base case. However, the other 60% of the test instances show an increase of at least 2% and up to 6% in their "avg r" compared to those in the base case scenario. Still, the values of "avg r" in all test instances under the "N1" scenario are higher than those of the "N0" scenario by a value of at least 2% and up to 5%. Even though the percentages of "max r" for the "N0" scenario are higher than those of the "N1" and the base case scenarios, but its smaller percentages of the houses with reduced costs in all test instances explain the reasons behind showing the least rates of "avg r".

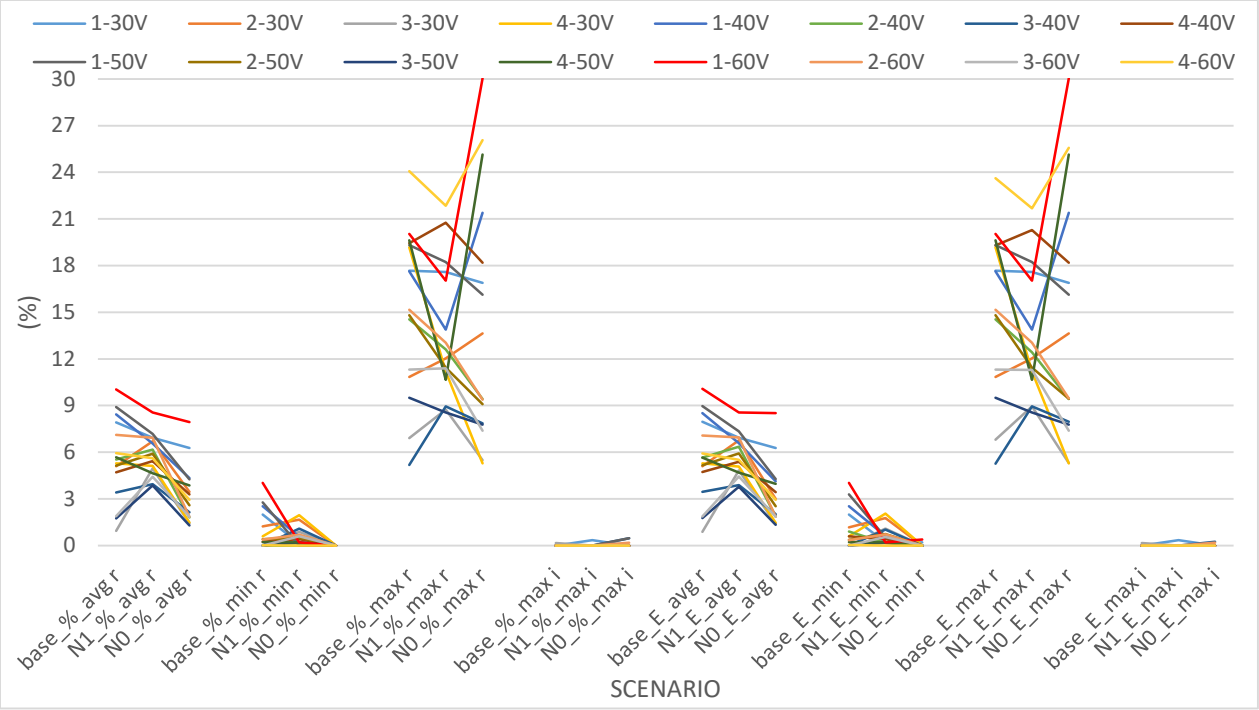

Figure 62: The average, maximum, and minimum reduction rates and the maximum increase rate in electricity bills among all houses in the entire neighbourhood under the base case and two different charging interruption scenarios.

6.2.5 Effects of the Grid Power Restrictions

In this section, we study the effects of the contract power agreed on by each EV-user and the DSO denoted by P_v by simply repeating the same test instances of the base case three times in which each one corresponds to a new scenario with a specific value of P_v. We assume having a scenario (P10) with a value of 10 (kW) assigned to the contract power for each house in the neighbourhood, then another scenario (P6) with a value of 6 (kW), and the third one (P-mix) with a random mix of both 6 and 10 (kW). **Figure 63** illustrates the runtime of the PSM as well as the total runtime of the TSREV-CSP model in all test instances and for all the power limit scenarios compared to the base case. Under all the proposed scenarios, we find that the total runtime in all test instances reaches a maximum of 70 (s) except for "3-60V" that takes around 139 (s) due to the long runtime of the PSM while the total runtime in the base case is only 80 (s). However, the peak power demands of the neighbourhood in all test instances for the three power limit scenario show no changes at all compared to their values in the base case scenario, as shown in **Figure 64**. We explain this by the effect of the PSM on reducing the power consumption of each house to its minimum.

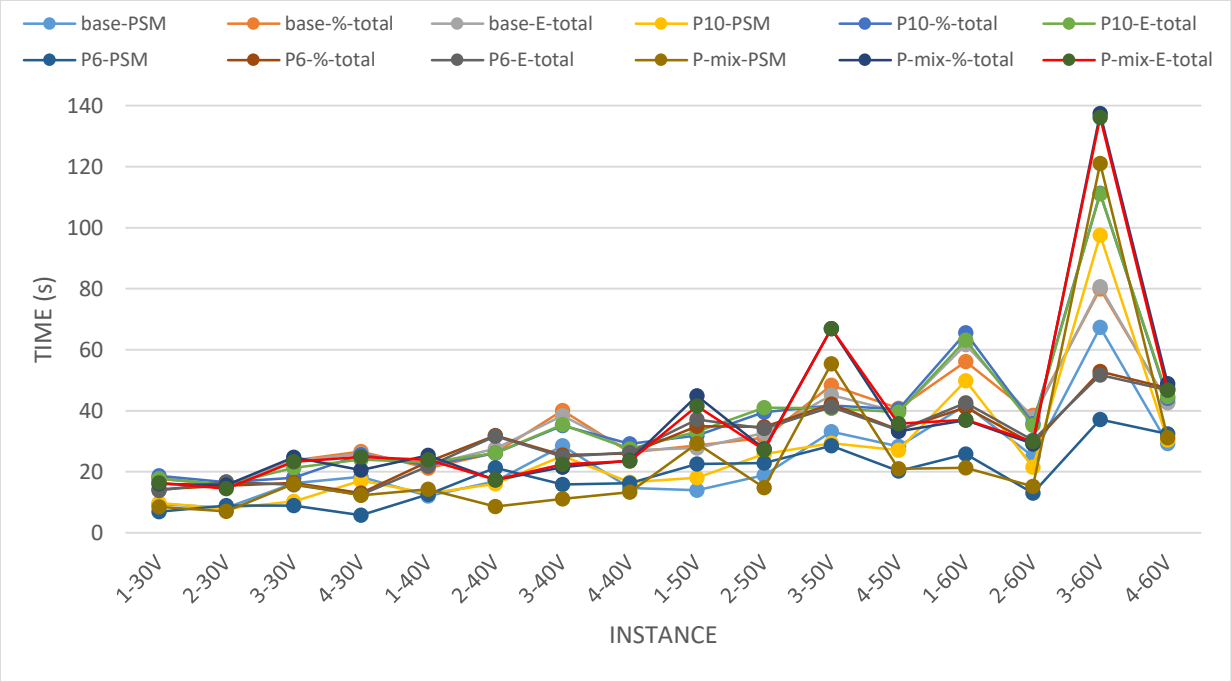

Figure 63: The runtime comparison of the optimization model following the "CCRM-%" and the "CCRM-E" between different scenarios of power grid restrictions compared to the base case in all test instances.

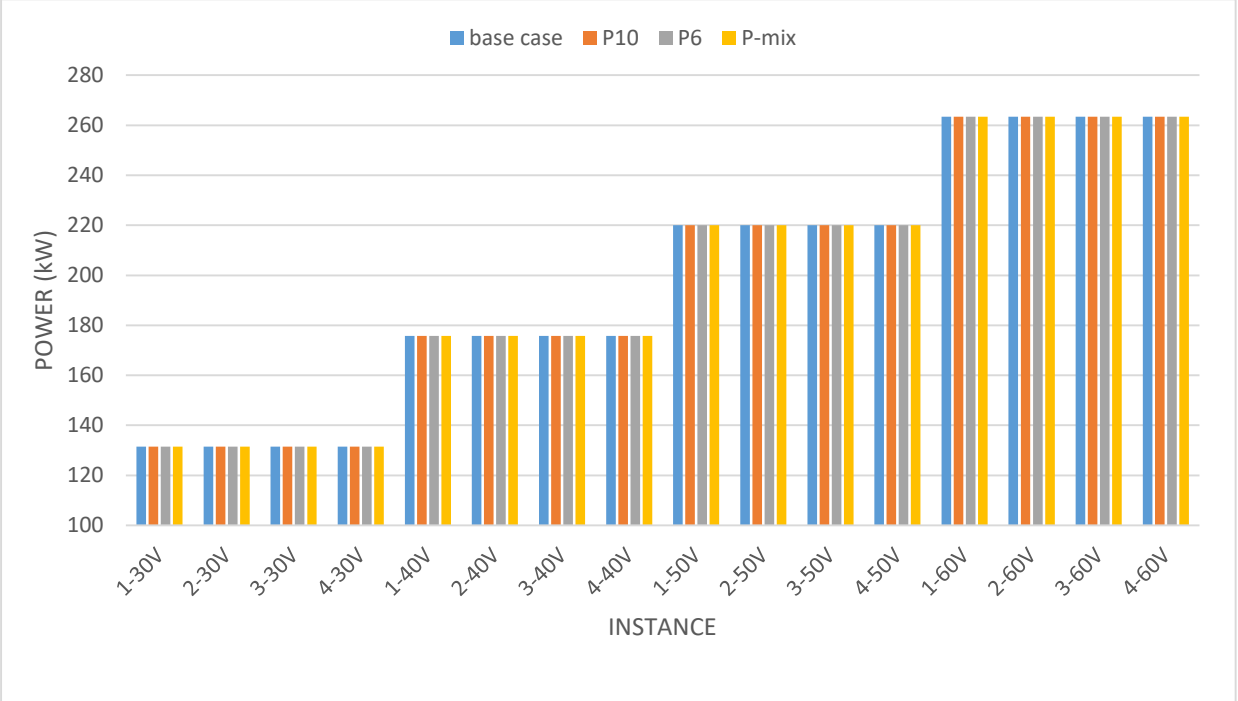

Figure 64: The peak power demands obtained by the PSM for two different scenarios of various power grid restrictions compared to the base case one.

Figure 65 illustrates the percentage distribution of the houses based on the reduction rates in their electricity bills for the entire neighbourhood in all test instances under the effects of different power limit scenarios. We notice that the values of "R" under the "P10" and "P-mix" scenarios are not that different from those of the base case wherein the majority of the test instances, there are at least 92% of the houses in the neighbourhood with a reduction rate. But when applying the "P6" scenario, we find that more than 50% of the test instances show a lower number of houses with energy cost reductions that reach a maximum of 87% compared to those of the base case and the other two scenarios. This makes the electricity contracts with a 10 (kW) power limit more efficient in our case study.

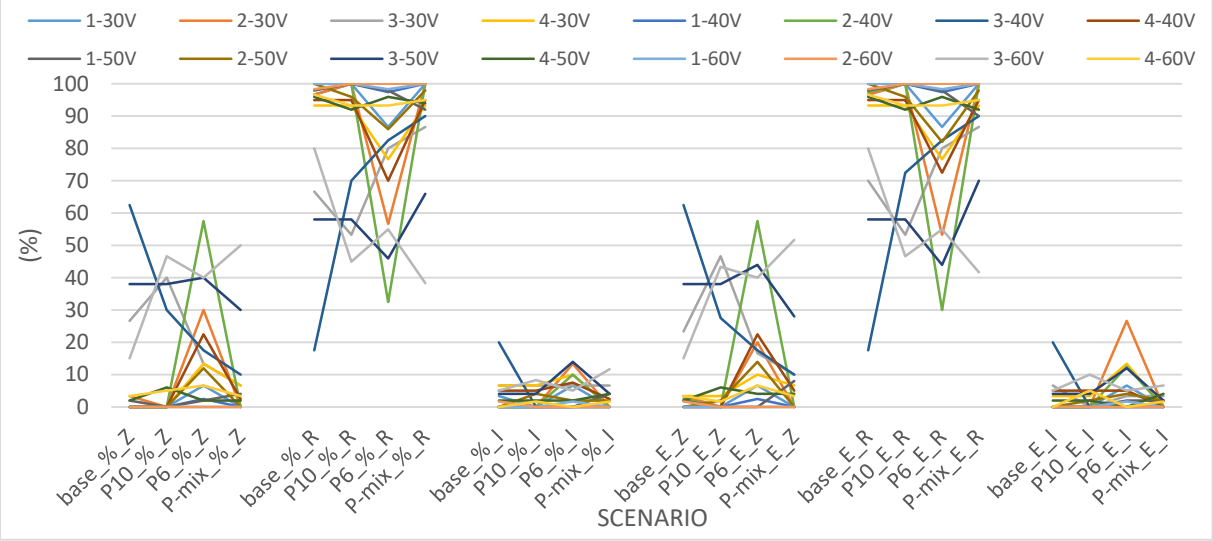

Figure 65: The percentage distribution of all the houses in the neighbourhood in all test instances based on the reduction rate in their energy bills for different scenarios, each of a different power restriction value per house compared to the base case.

That's also obvious through the results shown in Figure 66 that present the average, maximum, and minimum reduction rates and the maximum increase rate among all houses in the neighbourhood. We also find that all the values of "avg r", "max r" and "min r" obtained by "P10" in all test instances are slightly less than those of the base case but remarkably higher than all the values obtained by "P6" except for "max i". We notice that all the values of "max i" obtained by all scenarios in all test instances are lower than 0.3%. This enhances the feasibility of our model even when applying power limits on all the houses in the neighbourhood.

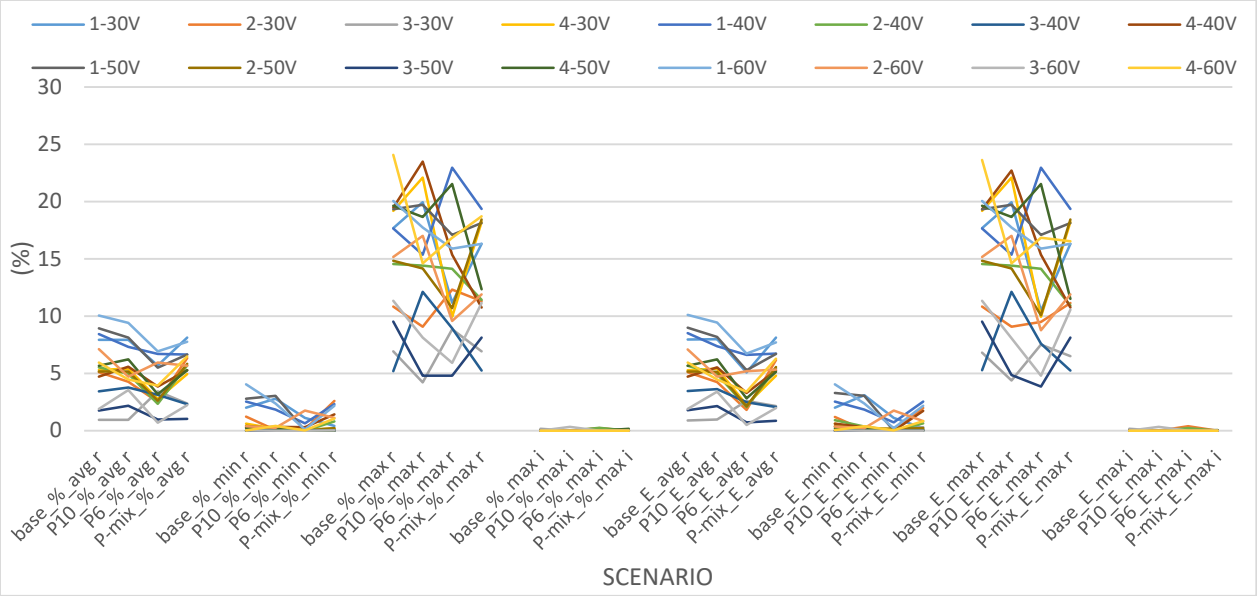

Figure 66: The average, maximum, and minimum reduction rates and the maximum increase rate in the electricity bills among all houses in the entire neighbourhood under the base case and three other scenarios, each of different power grid limit values.

6.2.6 Impacts of EV Penetration Level

This section aims to prove the feasibility of TSREV-CSP for different types of residential neighbourhoods, each of a different percentage of EV users. For this reason, we redo the test instances generated in the base case under three new scenarios “M1/2”, “M2/3”, and “M3/4”. “M1/2” refers to the scenario of having a neighbourhood with half the houses as EV-users owning only one EV while “M2/3” and “M3/4” correspond to two different scenarios similar to “M1/2” but with two third and three fourth the houses in the neighbourhood are EV-users of only one EV respectively. Figure 67 demonstrates a comparison between the runtime of the PSM and TSREV-CSP model using both the “%” and “E” CCRM approaches under the three scenarios of EV users’ sizes. We notice that the maximum total runtime among all test instances is around 81 (s) which is relatively low compared to that of the scenarios discussed in the previous sections. We also see that the runtime of both the PSM and the total one increases gradually with the increase of the number of EVs in the neighbourhood and with higher energy demand. However, as the percentage of EV users in the neighbourhood increases with the rise of the number of EVs, then the optimization model starts taking more time to obtain an optimal solution, and that’s clear, and the low runtime of “M1/2” for the majority of test instances.

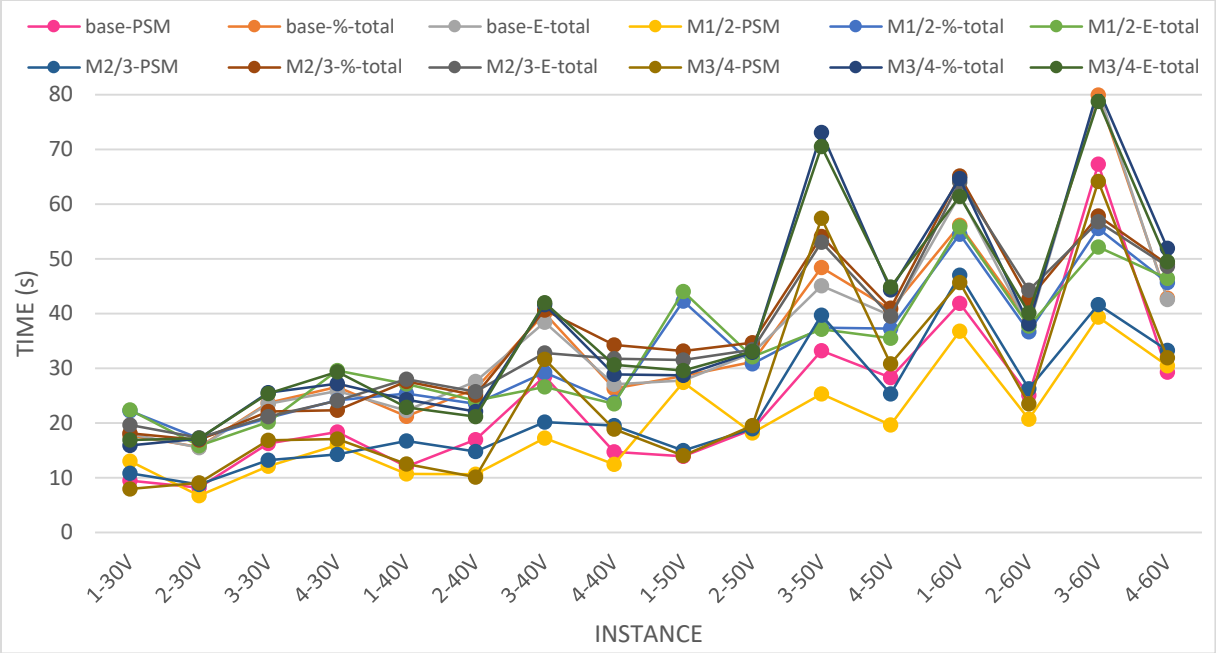

Figure 67: Comparison of the PSM and the TSREV-CSP model's total runtime between different scenarios of EV penetration levels compared to the base case in all test instances.

Figure 68 shows a comparison of the peak power demands obtained by the PSM in each instance for the different scenarios of EV users' percentage with the maximum household power consumption of all the houses and the peak power retrieved by EV users together in the entire neighbourhood. We notice that the optimized peak power is always less than or equal to that of the fixed household power consumption in all test instances and for the four different scenarios. This proves the role of PSM in reducing the uncertainty about the increasing energy demand for charging EVs due to their higher penetration levels. However, we see that as the percentage of EV users in the neighbourhood rises, the peak power demand of all the EV users' houses decreases significantly. That's obvious when comparing the values of the base case scenario having all houses as EV users with those of the other scenarios in all test instances. For instance, the peak power in instance "1-50V" reduces from 237.33 (kW) under the scenario "M3/4" to 220.08 (kW) for the base case scenario recording the least reduction rate of around 7%. The power reduction reaches its maximum in instance "3-50V" with a rate of 41% where the peak power demand of all EV users decreases from around 373 (kW) for "M1/2" to a value of 220 (kW) for the base case scenario. By comparing the peak power of EV users only in all test instances for all the four scenarios, including the base case, we find that the values of "Xmax" under the base case scenario are at an average of 22.3% less than those of "EVmax" obtained by the other scenarios.

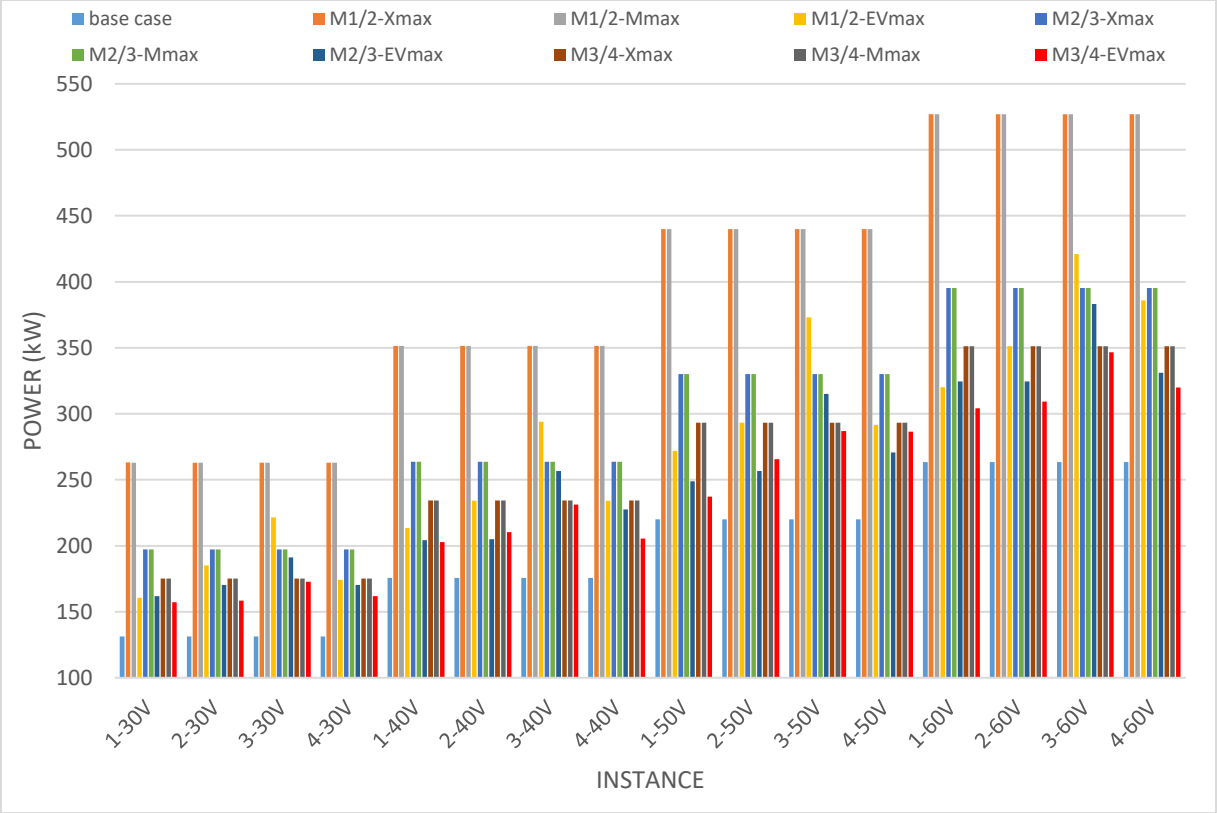

Figure 68: Comparison between the peak power demand of the neighbourhood and the peak power demand of EV users only in the same neighbourhood obtained by the PSM for three scenarios of different EV sizes compared to the base case one.

Moreover, Figures 69 and 70 demonstrate a cost analysis and comparison among the four presented scenarios by showing the percentage distribution of the houses based on the reduction rates in their electricity bills and the corresponding average, maximum, and minimum reduction rates and the maximum increase rate among all houses in the entire neighbourhood respectively. We notice that the test instances with the worst-case scenario "3-30V", "3-40V", "3-50V", and "3-60V" always show the lowest percentages of houses with reduced electricity bills and the worst average reduction rates as well as the highest ones of the houses with non-changes or increased bills. If we ignore these four test instances, we observe that all scenarios show satisfying results regarding the percentages distribution of the houses in the neighbourhood with at least 94% of "R", and a maximum of 6% for both "Z" and "I" except for some test instances like "4-30V" and "4-60V" that obtained poor values of "R". We note that "M1/2" results in at least 50% of the test instances with reduced electricity bills for all the houses in the neighbourhood.

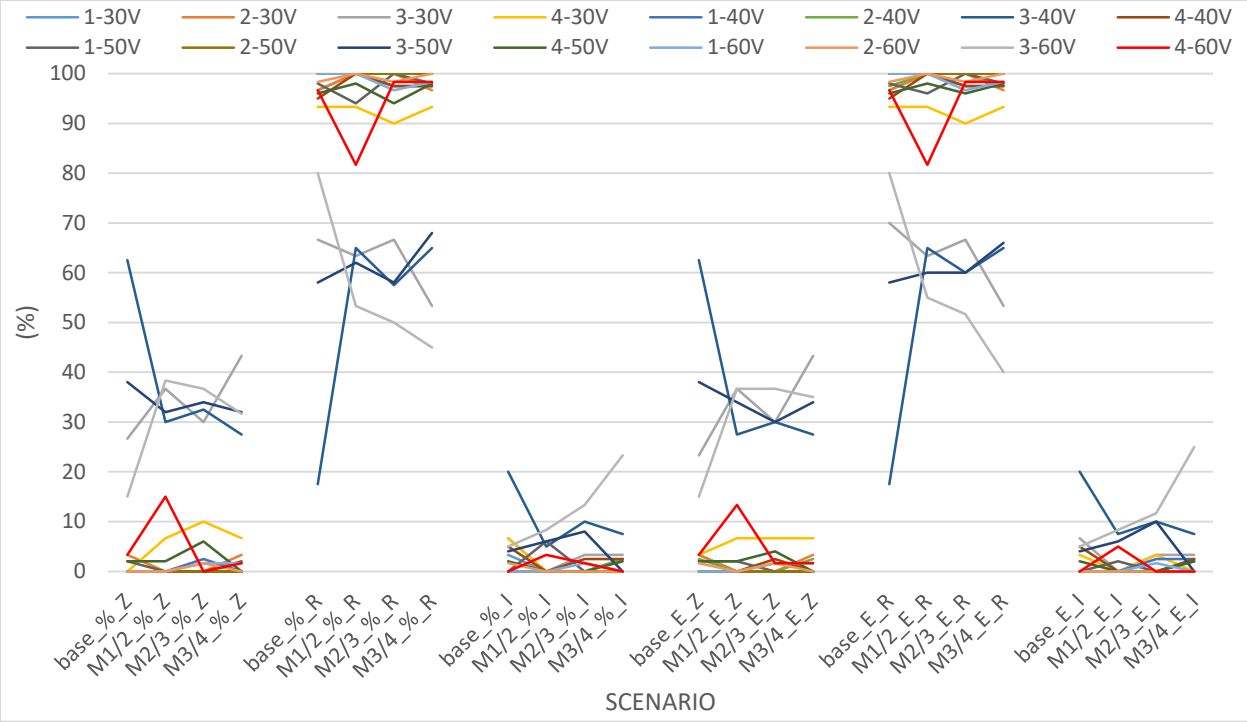

Figure 69: The percentage distribution of all the houses in the neighbourhood in all test instances based on the reduction rate in their energy bills for different cases EV users' percentages compared to the base case.

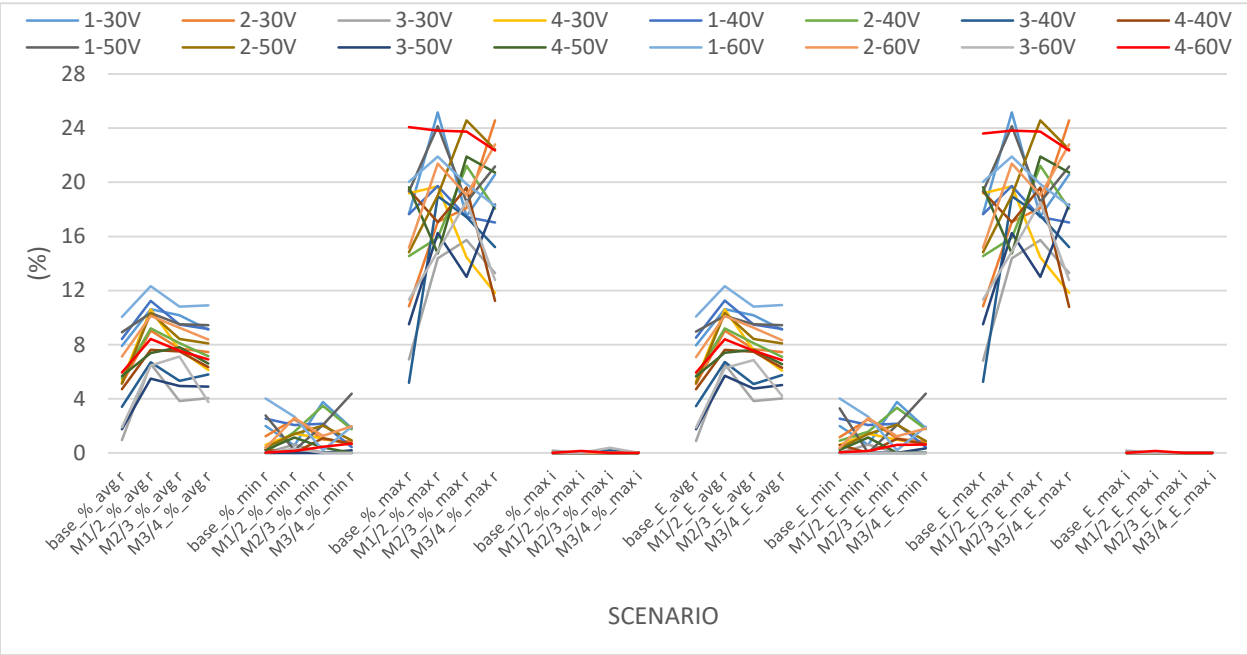

Figure 70: The average, maximum, and minimum reduction rates and the maximum increase rate in the electricity bills among all houses in the entire neighbourhood under the base case and three other scenarios, each of a different percentage of EV users in the same neighbourhood.

Figure 70 shows a privilege for "M1/2" over the other scenarios in the percentages of the average reduction rates in all test instances for both CCRM approaches the "%" and "E". We notice that the values of "avg r" decrease with the increase of the percentage of EV users in the neighbourhood in all test instances where the "avg r" at each instance reduces by 2% to 5% as moving from the scenario of 50% EV users "M1/2" to the base case of 100%. Similarly, the best value of the maximum reduction rate in most test instances is obtained by "M1/2" compared to those obtained by other scenarios. In general, the results obtained by the scenarios of EV penetration level less than 100% are relatively better than those of the base case.

6.2.7 Significance of The Peak Shaving Model

In this section, we analyze the importance of the PSM in reducing the peak power demand of the neighbourhood and help to normalize the power consumption profile to reduce uncertainty in the power retrieved values throughout the day. To do so, we formulate two optimization models with single-stage objective functions and independent from that of the PSM. "Cost" refers to one of the two new models and is characterized by only one objective function of a cost minimization problem for the electricity bill of each house in the neighbourhood individually. It shares the same mathematical formulation as the one of CCRM presented in section 4.3 except for removing the constraint (68) to neglect the effect of PSM. This model is applied to the sixteen test instances under the base case scenario as well as being applied to the two scenarios of different contract power values "P10" and "P6" presented in section 6.2.5 that are referred to as "Cost-base", "Cost-P10", and "Cost-P6" respectively. The second optimization model is a heuristic one based on the concept of adding FRD fees in the objective function as in Eq. (12). The mathematical formulation is identical to that of the CCRM but with replacing the objective function (67) with Eq. (89) and replacing constraint (68) with Eq. (90) where "x" in both equations is a new decision variable to calculate the peak power demand. This model is denoted by "Cost-peak" and is applied only to the base case scenario to compare results with those obtained in section 6.2.2.

$$\text{minimize:} \qquad \sum_{t \in t} p_t \Delta t \left(l_{t,v} + \frac{i_{t.v}}{Q_v} Q E_v \right) + x \cdot 10 \tag{89}$$

$$l_{t,v} + \frac{i_{t.v}}{Q_v} Q E_v \leq x \qquad \forall\, t \in T \tag{90}$$

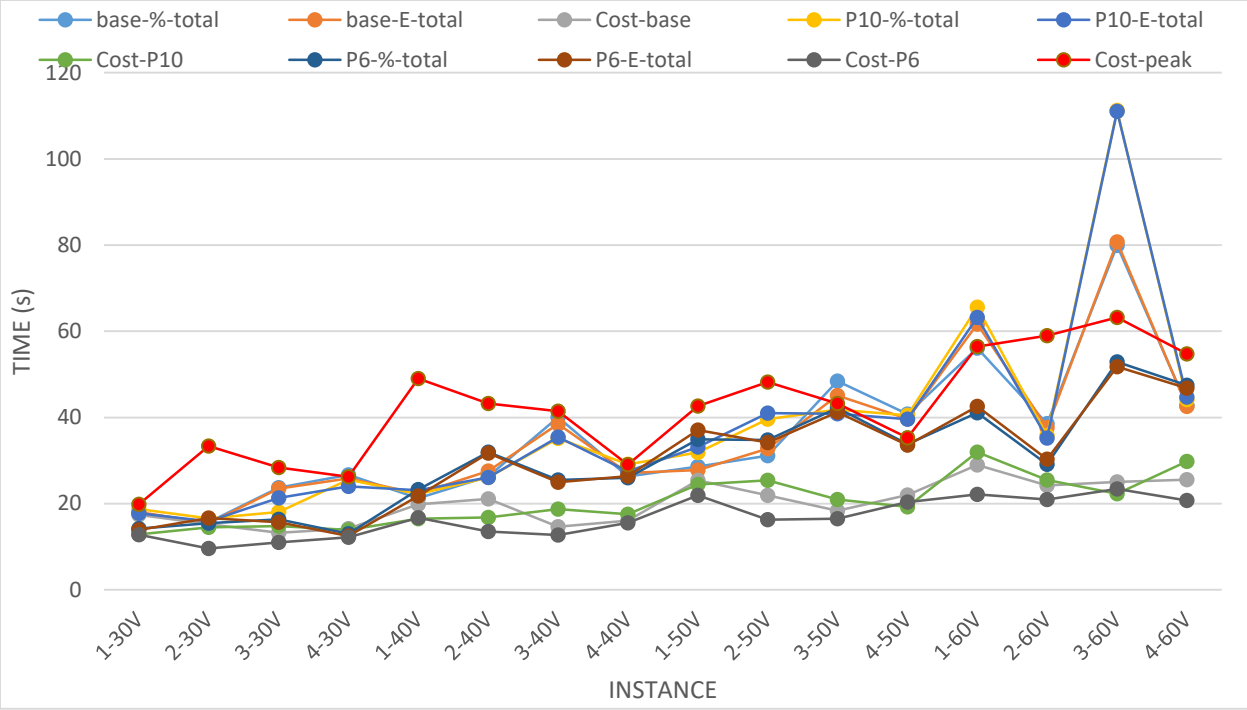

Figure 71: Comparison of the overall runtime of the optimization models between the TSREV-CSP and the Cost model.

Figure 71 shows the overall runtime needed by the optimization models of the TSREV-CSP and "Cost" to obtain an optimal solution in each instance under different scenarios of the grid's power limit. We find that the "Cost" model applied to the base case, P10, and P6 so far takes the least time to obtain an optimal solution in all test instances compared to the time taken by TSREV-CSP under the same scenarios. Moreover, the highest runtime is shown for the "Cost-peak" model in 80% of the test instances but recording a maximum runtime of 63 (s) which is around 20 (s) less than that needed by the TSREV-CSP in the base case scenario.

The comparison between the peak power values obtained by the models of both the TSREV-CSP and "Cost" under the base case, P10, and P6 scenarios are presented in **Figure 72**. We notice a considerable peak power values increase in all test instances that vary from at least 37% in all the instances of the size of "30V" for the "Cost-P6" scenario and up to around 130% in instances "1-40V", "1-50V", and "1-60V" for the "Cost-P10" case. When using the "Cost" model, the maximum power rises from around 264 (kW) in instance "1-60V" under the TSREV-CSP base case to a maximum value of around 600 (kW). However, the "Cost-peak" scenario that uses the "Cost" model shows no significant changes for the peak power demand in all test instances, which proves the capability of such an optimization approach to substitute our TSREV-CSP.

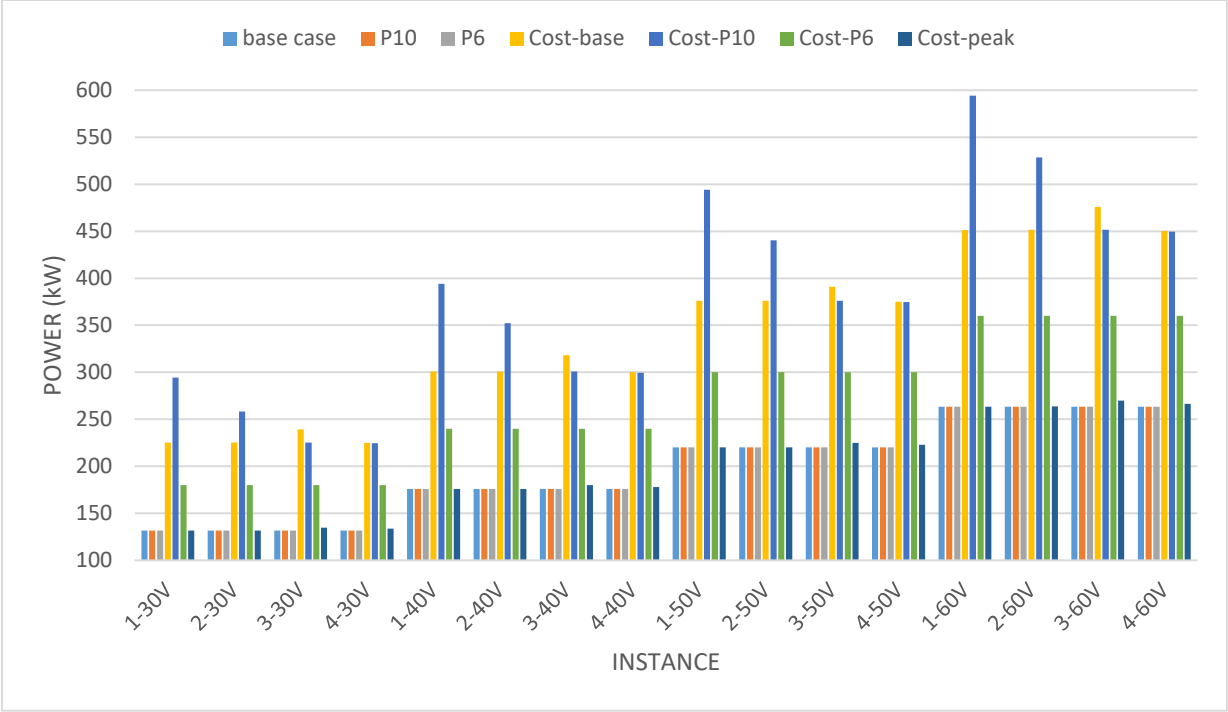

Figure 72: Comparison between the peak power demand obtained by the PSM and that obtained by the "Cost" model in the same neighbourhood under different scenarios.

The cost analysis is presented in figures **73** and **74** that show the percentage distribution values of all the houses in the entire neighbourhood based on their reduction rate in the electricity bill and the percentages of cost reduction and increase corresponding to the houses with the maximum reduction and increase rates respectively. It is pretty apparent the improvements in the percentage of houses that had energy cost reductions which goes along with the positive declination in the portion of houses with no changes or even increase in their electricity bill when applying the "Cost" model compared to the TSREV-CSP one. "Cost-base", "Cost-P10", and "Cost-P6" show the best results in both figures with 100% of the houses having cost reductions in more than 80% of the test instances and a minimum of 94% in the worst case, besides the highest average reduction rate of at least 7.5% and negligible "max I" values. But the fact that "Cost" doesn't satisfy the objectives of the DSO with the lowest power demand and power system relief, then these results would be neglected. However, the "Cost-peak" model still shows a good record with at least 97% and a maximum of 6% of the houses with cost reduction and increase in their electricity bills respectively, after ignoring the worst-case test instances like "3-30V", "3-40V", "3-50V" and "3-60V". This makes its average reduction rates in all test instances way better than that of the base case with a minimum of 6.5%, but its maximum increase rates are slightly worse with a maximum of around 2%.

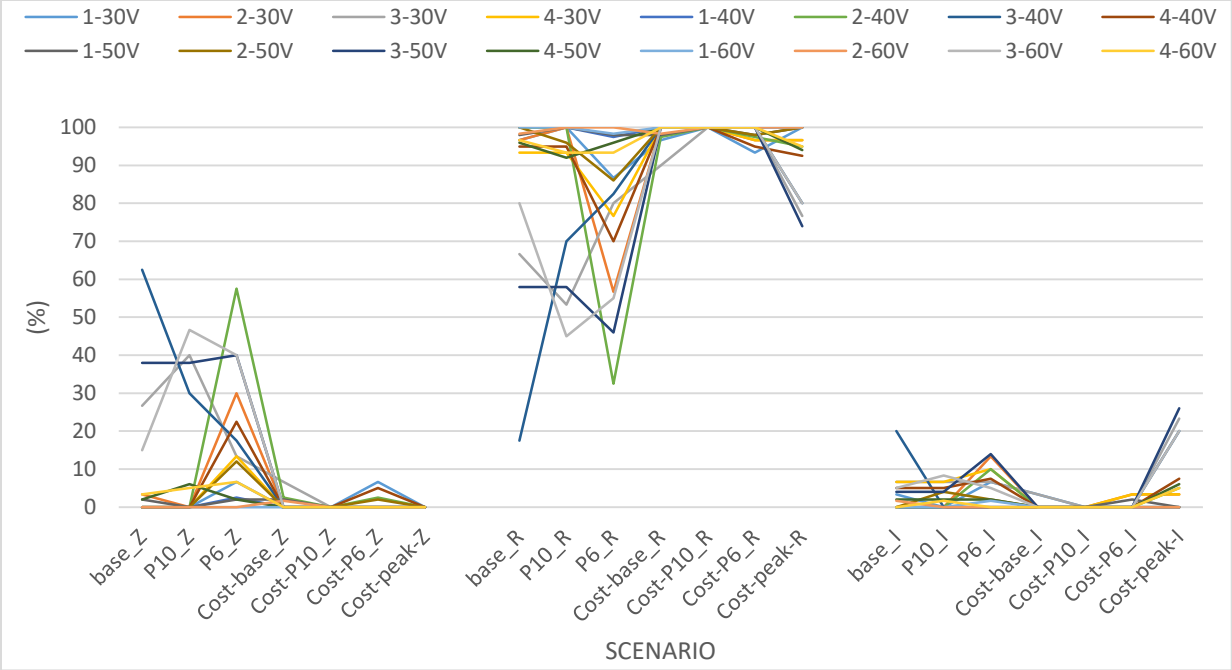

Figure 73: The percentage distribution of all the houses in the neighbourhood in all test instances based on the reduction rate in their energy bills for different cases of the grid's power limit compared to the base case and using both models of the TSREV-CSP and "Cost".

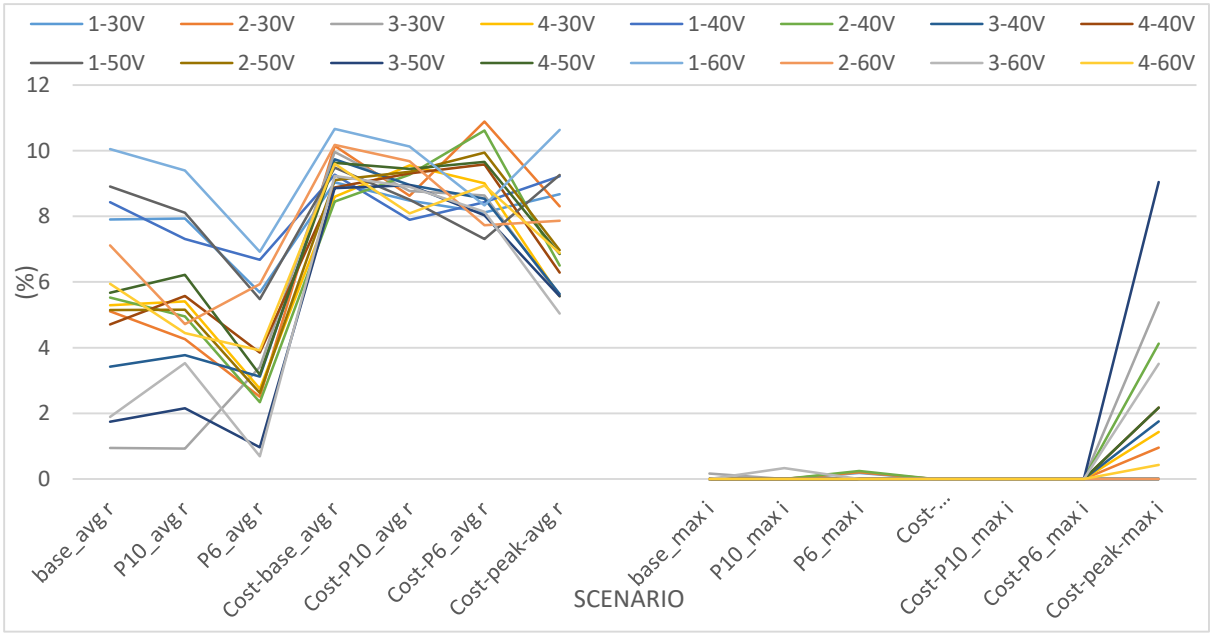

Figure 74: The average reduction and the maximum increase rates in the electricity bills of all houses in the entire neighbourhood obtained from the optimization models of the "Cost" and TSREV-CSP under the base case and different scenarios each of various grid's power limit values.

7 CONCLUSIONS

This research highlighted a few of the most critical challenges that EV adoption is still facing nowadays and explored opportunities for new technologies and strategies to prove EVs' credibility and help to overcome some of its drawbacks that represent barriers to higher adoption rates. We shed light on problems related to high charging costs, poor charging accessibility, and the uncertainty in charging power demands due to the increasing level of EV penetration with uncontrolled charging behaviors, which negatively impacts the power grid. Two case studies of two different scenarios were presented where one considers minimizing the total electricity bill of a commercial facility by optimizing the charging schedule of its medium-duty electric freight vehicles on periods of low energy costs. Moreover, we proposed a new technology of three-phase smart charging clusters where each could replace up to four single-phase smart chargers for better charging accessibility and some economic benefits. We formulate a mathematical model for a cost minimization problem, and we apply it to different cases of different input parameters, using several clustered charging technologies.

The second scenario considers a residential neighbourhood problem supplied with electric energy by a DSO that aims to reduce and normalize the peak power demand of the entire neighbourhood for higher grid efficiency and better frequency balance. At a residential scale, the DSO considers EVs as a remarkable load on the grid and relates the peak power reduction to the optimization of the charging schedule of EVs to shift their charging profile towards periods with the lowest energy demands. This requires a replacement of the conventional EV chargers installed in each house with smart ones, which cause additional costs on EV users that might be solved with some incentives.

We proposed a two-stage optimization model that consists of two submodels. The first is a peak shaving model (PSM) that aims to minimize the peak power demand of the neighbourhood by optimizing the charging schedule of EVs during low energy periods independently of the energy prices. However, the second model is a subsequent one that is charging cost reduction model (CCRM) performed individually on each house of the neighbourhood to minimize its total electricity bill by rescheduling the charging periods obtained by the PSM based on the low electricity prices during the day. It depends on the optimized peak power demand of the neighbourhood obtained by the PSM to evaluate an average weighted grid power limit specific to each house to ensure the respect of the obtained global power limit.

We generated several test instances of different travel behaviors and various energy demands that represent the base case scenario for both models of the commercial and residential problems. Then we repeated the same test instances under several scenarios of different charging interruption parameters, different values of power grid restrictions, new energy smart pricing strategies, and multiple cases of EV users' sizes in the residential neighbourhood. Moreover, we performed all the tests on the commercial problem using several proposed charging technologies. Finally, we generated an optimization model similar to the one in the commercial problem with the same concept of FRD charges applied to the peak power demand of each house individually, and then we compared its results with those obtained by the PSM. All the instances under all scenarios resulted in 629 experiments.

By comparing all the results obtained from both problems, we could say that the optimization models of both problems have proven their feasibility. Concerning the proposed cluster charging technologies, we found that the clusters with a power capacity of 22 (kW) and equipped with three (3S-22kW) and up to four sockets (4S-22kW) showed better results than those of the base case and other charging technologies in most of the test instances. However, "3S-22kW" which can replace three single-phase chargers used in the base case scenario of one charging point having a maximum power of 7.36 (kW) appeared to be the most efficient among all. When applying low FRD charges, which means the possibility of retrieving higher power at low cost, the base scenario was limited in retrieving higher power at periods of the lowest prices. In contrast, "3S-22kW" gave EVs a higher possibility to reduce their charging cost by shifting their charging schedule towards periods of low prices with a power capacity above 7.36 (kW) and up to 12 (kW). Most of the test instances obtained an optimal solution with a relatively short time using "3S-22kW" just like in the base case.

The results obtained in the residential neighbourhood problem were quite attractive compared to the ones of the commercial problem. Even though peak power reduction means a lower charging cost in most cases compared to uncontrolled charging strategies, but using the CCRM for each house in the neighbourhood helped in further reducing the electricity bills. In the majority of the proposed scenarios and almost all test instances, an average of 85% of the houses in the neighbourhood were able to reduce their energy costs with an average reduction of 7%, which reached a maximum of 25% in some cases.

The base case scenario has shown improved results than that of the two-prices smart pricing strategies, where more variable prices during the day give EV users a better degree of freedom for choosing their charging schedule at lower costs. Moreover, we obtained the best results for the case of 10 (kW) power restrictions applied to each house as well for the scenarios of allowing EVs to have only one charging interruption. The final task was the comparison between the results of both optimization models of the two-stage and the cost-based ones. The comparison showed that the cost minimization problems without power restrictions might cause the same effects as uncontrolled charging strategies in terms of power impacts on the grid. Having the lowest prices of electricity during the night, cost minimization models would charge all EVs at the same periods of the lowest energy prices that might result in extremely high power demand from the grid to unbalance. However, the heuristic cost minimization model with penalized peak power in the objective function showed a high potential of substituting the two-stage model but with slightly higher peak power values and caused some houses to have increased energy costs compared to the ones obtained by the two-stage model.

All in all, we proposed new charging technologies and strategies and proved their technical feasibilities, but some of the poor obtained results require furthermore studies. Further research goals may be aimed at exploring more parameters and constraints to improve the obtained results. More heuristic models would help in reducing the solution time for cases of higher EV capacities. It could also be interesting to explore more clustering methods for EV chargers and apply them on larger scales and different case studies like public parks and daytime commercial buildings, e.g., shopping centers and office buildings. An economic analysis in the long run for the proposed clustered charging technology might be necessary to enhance their feasibility level over the traditional charging methods, especially in the case of commercial scenarios.

8 BIBLIOGRAPHY

Ahmad, F., Alam, M. S., Alsaidan, I. S., & Shariff, S. M. (2020). Battery swapping station for electric vehicles: Opportunities and challenges. *IET Smart Grid*, *3*(3), 280–286. https://doi.org/10.1049/iet-stg.2019.0059

Apostolaki-Iosifidou, E., Codani, P., & Kempton, W. (2017). Measurement of power loss during electric vehicle charging and discharging. *Energy*, *127*, 730–742. https://doi.org/10.1016/j.energy.2017.03.015

ASME. (n.d.). *Top 10 Growing Smart Cities*. https://www.asme.org/topics-resources/content/top-10-growing-smart-cities

Aurora. (2018). *Opportunities in Electric Vehicle Charging at Commercial and Industrial Sites*. https://www.auroraer.com/wp-content/uploads/2018/10/Aurora-Report-Full-Opportunities-in-EV-charging-at-CI-sites-October-2018.pdf

Bañol Arias, N., Hashemi, S., Andersen, P. B., Træholt, C., & Romero, R. (2020). Assessment of economic benefits for EV owners participating in the primary frequency regulation markets. *International Journal of Electrical Power and Energy Systems*, *120*(September 2019), 105985. https://doi.org/10.1016/j.ijepes.2020.105985

Barone, G., Brusco, G., Menniti, D., Pinnarelli, A., Polizzi, G., Sorrentino, N., Vizza, P., & Burgio, A. (2020). How smart metering and smart charging may help a local energy community in collective self-consumption in presence of electric vehicles. *Energies*, *13*(6). https://doi.org/10.3390/en13164163

Bedogni, L., Bononi, L., Borghetti, A., Bottura, R., D'Elia, A., & Cinotti, T. S. (2015). Integration of traffic and grid simulator for the analysis of e-mobility impact on power distribution networks. *2015 IEEE Eindhoven PowerTech, PowerTech 2015*. https://doi.org/10.1109/PTC.2015.7232662

Berkeley, N., Bailey, D., Jones, A., & Jarvis, D. (2017). Assessing the transition towards Battery Electric Vehicles: A Multi-Level Perspective on drivers of, and barriers to, take up. *Transportation Research Part A: Policy and Practice*, *106*(June), 320–332. https://doi.org/10.1016/j.tra.2017.10.004

BMW. (2018). *Technical specifications. BMW i3 (120 Ah).* https://www.press.bmwgroup.com/global/article/attachment/T0284828EN/415571

Chaim, A., Sprei, F., Samaras, C., & Sean, Z. (2016). Effectiveness of incentives on electric vehicle adoption in Norway. *Transportation Research Part D*, *46*, 56–68. https://doi.org/10.1016/j.trd.2016.03.011

Chau, K. T., Wong, Y. S., & Chan, C. C. (1999). Overview of energy sources for electric vehicles. *Energy Conversion and Management*, *40*(10), 1021–1039. https://doi.org/10.1016/S0196-8904(99)00021-7

Cho, I. H., Lee, P. Y., & Kim, J. H. (2019). Analysis of the effect of the variable charging current control method on cycle life of Li-ion batteries. *Energies*, *14*(15). https://doi.org/10.3390/en12153023

Ding, Y., Cano, Z. P., Yu, A., Lu, J., & Chen, Z. (2019). Automotive Li-Ion Batteries: Current Status and Future Perspectives. *Electrochemical Energy Reviews*, *2*(1), 1–28. https://doi.org/10.1007/s41918-018-0022-z

Driving Electric. (n.d.). *How to choose the best home EV charger*. https://www.drivingelectric.com/your-questions-answered/102/how-choose-best-home-ev-charger

Dudin, M. N., Zasko, V. N., Dontsova, O. I., & Osokina, I. V. (2020). The energy politics of the european union and the possibility to implement it in post-soviet states. *International Journal of Energy Economics and Policy*, *10*(2), 409–416. https://doi.org/10.32479/ijeep.9077

Eden Strategy Institute, & Ltd., O. P. (n.d.). *Top 50 Smart City Governments*. Retrieved March 25, 2021, from file:///C:/Users/BOB/Desktop/thesis/documentations/really helpful/smart cities/Top 50 Smart City Governments.html

EDF. (n.d.). *EDF, taking the European lead in smart charging for 2020*. Retrieved March 24, 2021, from https://www.edf.fr/en/the-edf-group/inventing-the-future-of-energy/electric-mobility-for-today-and-tomorrow/smart-charging

enel X. (n.d.). *JuicePole*. enel X. Retrieved March 31, 2021, from https://evcharging.enelx.com/eu/commercial/juicepole

European Environment Agency. (2019). *Electric vehicles in Europe*. *20*, 74. https://www.mckinsey.com/~/media/McKinsey/Locations/Europe and Middle East/Netherlands/Our Insights/Electric vehicles in Europe Gearing up for a new phase/Electric vehicles in Europe Gearing up for a new phase.pdf

ev.energy. (n.d.). *smart home EV charging*. Retrieved March 30, 2021, from https://play.google.com/store/apps/details?id=energy.ev.app&hl=en&gl=US

Falvo, M. C., Sbordone, D., Bayram, I. S., & Devetsikiotis, M. (2014). EV charging stations and modes: International standards. *2014 International Symposium on Power Electronics, Electrical Drives, Automation and Motion, SPEEDAM 2014*, 1134–1139. https://doi.org/10.1109/SPEEDAM.2014.6872107

Feng, W., & Figliozzi, M. (2013). An economic and technological analysis of the key factors affecting the competitiveness of electric commercial vehicles: A case study from the USA market. *Transportation Research Part C: Emerging Technologies*, *26*, 135–145. https://doi.org/10.1016/j.trc.2012.06.007

Ghotge, R., Snow, Y., Farahani, S., Lukszo, Z., & van Wijk, A. (2020). Optimized scheduling of EV charging in solar parking lots for local peak reduction under EV demand uncertainty.

Energies, *13*(5). https://doi.org/10.3390/en13051275

Harrison, C., & Donnelly, I. A. (2011). A theory of smart cities. *Proceedings of the 55th Annual Meeting of the ISSS-2011*, 1–15. http://journals.isss.org/index.php/proceedings55th/article/view/1703

Hebrail, G., & Berard, A. (2012). *Individual household electric power consumption Data Set*. EDF. file:///C:/Users/BOB/Desktop/thesis/provided data/residential_data/UCI Machine Learning Repository_ Individual household electric power consumption Data Set.html

Helmers, E., Dietz, J., & Weiss, M. (2020). *Sensitivity Analysis in the Life-Cycle Assessment of Electric vs . Combustion Engine Cars under Approximate Real-World Conditions*. 1–31.

Hildermeier, J., Kolokathis, C., Rosenow, J., Hogan, M., Wiese, C., & Jahn, A. (2019a). *Smart EV Charging : A Global Review of Promising Practices*. 1–13. https://www.mdpi.com/2032-6653/10/4/80

Hildermeier, J., Kolokathis, C., Rosenow, J., Hogan, M., Wiese, C., & Jahn, A. (2019b). *Start with smart: Promising practices for integrating electric vehicles into the grid*.

Hoke, A., Brissette, A., Maksimović, D., Pratt, A., & Smith, K. (2011). Electric vehicle charge optimization including effects of lithium-ion battery degradation. *2011 IEEE Vehicle Power and Propulsion Conference, VPPC 2011*, *June 2014*. https://doi.org/10.1109/VPPC.2011.6043046

IEA. (2019). Global EV Outlook 2019 to electric mobility. *OECD Iea.Org*, 232. www.iea.org/publications/reports/globalevoutlook2019/

IEA. (2020). *Tracking Transport 2020*. https://www.iea.org/reports/tracking-transport-2020

IRENA. (2019). *Innovation Outlook Charging for Electric*. https://www.irena.org/publications/2019/May/Innovation-Outlook-Smart-Charging

Jiang, L., Huang, Y., Li, Y., Yu, J., Qiao, X., Huang, C., & Cao, Y. (2021). Optimization of Variable-Current Charging Strategy Based on SOC Segmentation for Li-ion Battery. *IEEE Transactions on Intelligent Transportation Systems*, *22*(1), 622–629. https://doi.org/10.1109/TITS.2020.3006092

Kieldsen, A., Thingvad, A., Martinenas, S., & Srensen, T. M. (2016). Efficiency test method for electric vehicle chargers. *EVS 2016 - 29th International Electric Vehicle Symposium*.

Krieger, E. M., Cannarella, J., & Arnold, C. B. (2013). A comparison of lead-acid and lithium-based battery behavior and capacity fade in off-grid renewable charging applications. *Energy*, *60*, 492–500. https://doi.org/10.1016/j.energy.2013.08.029

Kutt, L., Saarijarvi, E., Lehtonen, M., Molder, H., & Niitsoo, J. (2013). A review of the harmonic and unbalance effects in electrical distribution networks due to EV charging. *12th International Conference on Environment and Electrical Engineering, EEEIC 2013*, 556–561. https://doi.org/10.1109/EEEIC.2013.6549577

Lam, L. (2011). A Practical Circuit-based Model for State of Health Estimation of Li-ion Battery Cells in Electric Vehicles. *Online> Http://Www. Eclectic. Eu/Images/ …*, 174. http://repository.tudelft.nl/assets/uuid:a7446a0a-4c29-4c68-bbe2-273f68f85ed7/MScthesis_LongLamv3.pdf

Limmer, S. (2019). Dynamic pricing for electric vehicle charging—a literature review. *Energies*, *12*(18). https://doi.org/10.3390/en12183574

Lin, Q., Wang, J., Xiong, R., Shen, W., & He, H. (2019). Towards a smarter battery management system: A critical review on optimal charging methods of lithium ion batteries. *Energy*, *183*, 220–234. https://doi.org/10.1016/j.energy.2019.06.128

Liu, C., Chau, K. T., Wu, D., & Gao, S. (2013). *Opportunities and Challenges of Vehicle-to-Home , Vehicle-to-Grid Technologies*. *101*(11), 2409–2427.

Liu, M., Mcnamara, P., Shorten, R., & Mcloone, S. (2015). Residential electrical vehicle charging strategies : the good , the bad and the ugly. *Journal of Modern Power Systems and Clean Energy*, *3*, 190–202. https://doi.org/10.1007/s40565-015-0122-2

Loisel, R., Pasaoglu, G., & Thiel, C. (2020). Large-scale deployment of electric vehicles in Germany by 2030 : An analysis of grid-to-vehicle and vehicle-to-grid concepts. *Energy Policy*, *65*(2014), 432–443. https://doi.org/10.1016/j.enpol.2013.10.029

Lund, H., & Kempton, W. (2008). Integration of renewable energy into the transport and electricity sectors through V2G. *Energy Policy*, *36*(9), 3578–3587. https://doi.org/10.1016/j.enpol.2008.06.007

Mahmoudzadeh Andwari, A., Pesiridis, A., Rajoo, S., Martinez-Botas, R., & Esfahanian, V. (2017). A review of Battery Electric Vehicle technology and readiness levels. *Renewable and Sustainable Energy Reviews*, *78*(October 2015), 414–430. https://doi.org/10.1016/j.rser.2017.03.138

Mal, S., Chattopadhyay, A., Yang, A., & Gadh, R. (2013). Electric vehicle smart charging and vehicle-to-grid operation. *International Journal of Parallel, Emergent and Distributed Systems*, *28*(3), 249–265. https://doi.org/10.1080/17445760.2012.663757

Marra, F., Yang, G. Y., Traholt, C., Larsen, E., Rasmussen, C. N., & You, S. (2012). Demand profile study of battery electric vehicle under different charging options. *IEEE Power and Energy Society General Meeting*, 1–7. https://doi.org/10.1109/PESGM.2012.6345063

Michalek, J. J., Chester, M., Jaramillo, P., Samaras, C., Shiau, C. S. N., & Lave, L. B. (2011). Valuation of plug-in vehicle life-cycle air emissions and oil displacement benefits. *Proceedings of the National Academy of Sciences of the United States of America*, *108*(40), 16554–16558. https://doi.org/10.1073/pnas.1104473108

Miller, C., & Meggers, F. (2017). The Building Data Genome Project: An open, public data set from non-residential building electrical meters. *Energy Procedia*, *122*, 439–444. https://doi.org/10.1016/j.egypro.2017.07.400

Mitsubishi Fuso. (2019). *eCanter 1.0 Specifications*. https://www.mitfuso.com/images/manuals/ecanter_specsheet1.pdf

MNP. (2006). *Environmental Balance 2006 Summary*. https://www.pbl.nl/en/publications/EnvironmentalBalance2006-Summary

Montoya, A., Guéret, C., Mendoza, J. E., & Villegas, J. G. (2017). The electric vehicle routing problem with nonlinear charging function. *Transportation Research Part B: Methodological*, *103*, 87–110. https://doi.org/10.1016/j.trb.2017.02.004

Mwasilu, F., Justo, J. J., Kim, E. K., Do, T. D., & Jung, J. W. (2014). Electric vehicles and smart grid interaction: A review on vehicle to grid and renewable energy sources integration. *Renewable and Sustainable Energy Reviews*, *34*, 501–516. https://doi.org/10.1016/j.rser.2014.03.031

Nissan. (2017). *Nissan Leaf, Technical Specifications Brochure*. https://www.nissan-cdn.net/content/dam/Nissan/ireland/Brochures/Leaf Brochure 2017.pdf

Oestreicher, R. (2020). *BRIEF INTRODUCTION INTO E-MOBILITY*. https://scdn.rohde-schwarz.com/ur/pws/dl_downloads/premiumdownloads/premium_dl_brochures_and_datasheets/premium_dl_miscellaneous/Video_6_Automotive_Tech_Day_June_10_Module_6_eMobility_and_BMS.pdf

Pelletier, S., Jabali, O., & Laporte, G. (2018). Charge scheduling for electric freight vehicles. *Transportation Research Part B: Methodological*, *115*, 246–269. https://doi.org/10.1016/j.trb.2018.07.010

Pelletier, S., Jabali, O., Laporte, G., & Veneroni, M. (2017). Battery degradation and behaviour for electric vehicles: Review and numerical analyses of several models. *Transportation Research Part B: Methodological*, *103*, 158–187. https://doi.org/10.1016/j.trb.2017.01.020

Pellicer, S., Santa, G., Andres, L., Maestre, R., Jara, A. J., & Skarmeta, A. G. (2013). A Global Perspective of Smart Cities : A Survey. *2013 Seventh International Conference on Innovative Mobile and Internet Services in Ubiquitous Computing.*, 439–444. https://doi.org/10.1109/IMIS.2013.79

pod POINT. (n.d.-a). *Pod Point Solo Smart Charger- Domestic Datasheet*. https://d3h256n3bzippp.cloudfront.net/PP-D-130042-14-Solo-Smart-Charger-Domestic-Datasheet.pdf

pod POINT. (n.d.-b). *Twin Charger*. pod POINT. https://d3h256n3bzippp.cloudfront.net/PP-D-170091-4-Twin-Charger-Datasheet-3.pdf

Poullikkas, A. (2015). Sustainable options for electric vehicle technologies. *Renewable and Sustainable Energy Reviews*, *41*, 1277–1287. https://doi.org/10.1016/j.rser.2014.09.016

Ros, J., Nagelhout, D., & Montfoort, J. (2009). New environmental policy for system innovation: Casus alternatives for fossil motor fuels. *Applied Energy*, *86*(2), 243–250. https://doi.org/10.1016/j.apenergy.2008.02.019

Schwertner, N., & Macht, G. A. (2018). Energy consumption estimation for routing EVS based on driver behavior. *IISE Annual Conference and Expo 2018*, 1594–1599. https://digitalcommons.uri.edu/cgi/viewcontent.cgi?article=1025&context=mcise_facpubs

Shareef, H., Islam, M. M., & Mohamed, A. (2016). A review of the stage-of-the-art charging technologies, placement methodologies, and impacts of electric vehicles. *Renewable and Sustainable Energy Reviews*, *64*, 403–420. https://doi.org/10.1016/j.rser.2016.06.033

She, Z., Sun, Q., Ma, J., & Xie, B. (2017). What are the barriers to widespread adoption of battery electric vehicles ? A survey of public perception in Tianjin , China. *Transport Policy*, *56*(February), 29–40. https://doi.org/10.1016/j.tranpol.2017.03.001

Skerlos, S. J., & Winebrake, J. J. (2010). Targeting plug-in hybrid electric vehicle policies to increase social benefits. *Energy Policy*, *38*(2), 705–708. https://doi.org/10.1016/j.enpol.2009.11.014

Su, W., Eichi, H., Zeng, W., & Chow, M. (2012). *A Survey on the Electrification of Transportation in a Smart Grid Environment*. *8*(1), 1–10. https://ieeexplore.ieee.org/abstract/document/6051485/

Terna. (2018). Monthly report on the electricity system. In *TERNA GROUP* (Vol. 35, Issue 5). https://doi.org/10.1002/da.22770

Toyota. (2013). *Rav4 EV*. https://nfpa.org/-/media/Files/Training/AFV/Emergency-Response-Guides/Toyota/Toyota-RAV4-EV-2012-2014-ERG.ashx

Tremblay, O., Dessaint, L. A., & Dekkiche, A. I. (2007). A generic battery model for the dynamic simulation of hybrid electric vehicles. *VPPC 2007 - Proceedings of the 2007 IEEE Vehicle Power and Propulsion Conference*, *V*, 284–289. https://doi.org/10.1109/VPPC.2007.4544139

Trippe, A. E., Arunachala, R., Massier, T., Jossen, A., & Hamacher, T. (2015). Charging optimization of battery electric vehicles including cycle battery aging. *IEEE PES Innovative Smart Grid Technologies Conference Europe*, *2015-Janua*(January), 1–6. https://doi.org/10.1109/ISGTEurope.2014.7028735

Turker, H., Pirsan, V., Bacha, S., Frey, D., Richer, J., & Lebrusq, P. (2014). Heuristic strategy for smart charging of Plug-In Electric Vehicle in residential areas: Variable charge power. *3rd International Conference on Renewable Energy Research and Applications, ICRERA 2014*, 938–944. https://doi.org/10.1109/ICRERA.2014.7016524

Un-Noor, F., Padmanaban, S., Mihet-Popa, L., Mollah, M. N., & Hossain, E. (2017). A comprehensive study of key electric vehicle (EV) components, technologies, challenges, impacts, and future direction of development. *Energies*, *10*(8). https://doi.org/10.3390/en10081217

Van Der Burgt, J., Vera, S. P., Wille-Haussmann, B., Andersen, A. N., & Tambjerg, L. H. (2015). Grid impact of charging electric vehicles; Study cases in Denmark, Germany and the

Netherlands. *2015 IEEE Eindhoven PowerTech, PowerTech 2015*. https://doi.org/10.1109/PTC.2015.7232234

Van Vliet, O., Brouwer, A. S., Kuramochi, T., Van Den Broek, M., & Faaij, A. (2011). Energy use, cost and CO2 emissions of electric cars. *Journal of Power Sources*, *196*(4), 2298–2310. https://doi.org/10.1016/j.jpowsour.2010.09.119

Vetter, J., Novák, P., Wagner, M. R., Veit, C., Möller, K. C., Besenhard, J. O., Winter, M., Wohlfahrt-Mehrens, M., Vogler, C., & Hammouche, A. (2005). Ageing mechanisms in lithium-ion batteries. *Journal of Power Sources*, *147*(1–2), 269–281. https://doi.org/10.1016/j.jpowsour.2005.01.006

Wali, K., Koubaa, R., & Krichen, L. (2019). Cost benefit smart charging schedule for V2G applications. *16th International Multi-Conference on Systems, Signals and Devices, SSD 2019*, 34–39. https://doi.org/10.1109/SSD.2019.8893171

Wang, Z., Ching, T. W., Huang, S., Wang, H., & Xu, T. (2021). Challenges Faced by Electric Vehicle Motors and Their Solutions. *IEEE Access*, *9*, 5228–5249. https://doi.org/10.1109/ACCESS.2020.3045716

Warner, J. (2014). Lithium-Ion Battery Packs for EVs. In *Lithium-Ion Batteries: Advances and Applications*. Elsevier. https://doi.org/10.1016/B978-0-444-59513-3.00007-8

White, C. D., & Zhang, K. M. (2011). Using vehicle-to-grid technology for frequency regulation and peak-load reduction. *Journal of Power Sources*, *196*(8), 3972–3980. https://doi.org/10.1016/j.jpowsour.2010.11.010

Wu, Y. A., Ng, A. W., Yu, Z., Huang, J., Meng, K., & Dong, Z. Y. (2021). A review of evolutionary policy incentives for sustainable development of electric vehicles in China: Strategic implications. *Energy Policy*, *148*(PB), 111983. https://doi.org/10.1016/j.enpol.2020.111983

Yilmaz, M., & Krein, P. T. (2013a). Review of battery charger topologies, charging power levels, and infrastructure for plug-in electric and hybrid vehicles. *IEEE Transactions on Power Electronics*, *28*(5), 2151–2169. https://doi.org/10.1109/TPEL.2012.2212917

Yilmaz, M., & Krein, P. T. (2013b). Review of the impact of vehicle-to-grid technologies on distribution systems and utility interfaces. *IEEE Transactions on Power Electronics*, *28*(12), 5673–5689. https://doi.org/10.1109/TPEL.2012.2227500

Yoshimi, K., Osawa, M., Yamashita, D., Niimura, T., Yokoyama, R., Masuda, T., Kondou, H., & Hirota, T. (2012). Practical storage and utilization of household photovoltaic energy by electric vehicle battery. *2012 IEEE PES Innovative Smart Grid Technologies, ISGT 2012*, 1–8. https://doi.org/10.1109/ISGT.2012.6175688

Zhang, P., Qian, K., Zhou, C., Stewart, B. G., & Hepburn, D. M. (2012). A methodology for optimization of power systems demand due to electric vehicle charging load. *IEEE Transactions on Power Systems*, *27*(3), 1628–1636. https://doi.org/10.1109/TPWRS.2012.2186595

Zipf, M., & Most, D. (2016). Cooperation of TSO and DSO to provide ancillary services. *International Conference on the European Energy Market, EEM*, *2016-July*. https://doi.org/10.1109/EEM.2016.7521273

Žitnik, A., & Mehle, B. (2014). Power management for private and semi-private EV charging. *2013 World Electric Vehicle Symposium and Exhibition, EVS 2014*, 1–8. https://doi.org/10.1109/EVS.2013.6914900